Title

Laboratory test of column-foundation moment transfer connection with headed anchors and shear reinforcement

Authors

Worsfold, Benjamin L
Moehle, Jack P

Publication Date

2022-05-01

Report No. UCB/SEMM-2022/01	Structural Engineering Mechanics and Materials

Laboratory Test of Column-Foundation Moment Transfer Connection with Headed Anchors and Shear Reinforcement

By

Benjamin L. Worsfold and Jack P. Moehle

May 2022

Department of Civil and Environmental Engineering
University of California, Berkeley

ABSTRACT

Steel and precast columns are commonly designed to transfer moment loads to concrete foundations through cast-in-place headed anchors. The ACI 318-19 Building Code does not consider the additive effect of both concrete and reinforcing bars when calculating the capacity of the concrete breakout failure mode. Laboratory tests were performed to provide benchmark physical data to determine the applicability of various design methods. The test specimen consisted of a full-scale interior steel-column to concrete-foundation connections located away from foundation edges, with details typical of current construction practice on the West Coast of the United States. Strength was governed by concrete breakout failure. Strategically placed shear reinforcing increased the strength and displacement capacity of anchored connections governed by breakout.

ACKNOWLEDGMENTS

The authors express their gratitude to the ACI Foundation Concrete Research Council, AISC, and the Hilti Corporation for financing this and other ongoing research projects at UC Berkeley relating to concrete anchorage. Special thanks to Ron Klemencic, chairman and CEO of Magnusson Klemencic Associates, Level 10 Constructions, Cascade Steel, and PJ's Rebar Inc. for donations of materials and manual labor. This study was greatly improved through discussions with the following individuals: Rafael Sabelli (director of seismic design at Walter P. Moore), James Malley (senior principal of Degenkolb Engineers), and Dr. Roberto Piccinin (VP for code development and research at Hilti Corporation). The authors would also like to thank the managers and staff of the Structural Engineering Laboratory at UC Berkeley for their support during the design, construction, and testing phases of the project.

CONTENTS

LIST OF FIGURES

LIST OF TABLES

1 INTRODUCTION

This report describes the test results of a steel-column to concrete-foundation connection specimen reinforced with distributed shear reinforcement in the slab.

Connections between structural columns and foundations are common in building construction. Whether the column is cast-in-place concrete, precast concrete, or structural steel, moment transfer at the foundation presents a challenge for designers as little consensus exists regarding what failure modes are relevant or which design provisions apply. The ACI 318-19 Building Code does not consider the additive effect of both concrete and reinforcing bars when calculating the capacity of the concrete breakout failure mode.

The ACI anchoring-to-concrete provisions historically reflect larger safety margins than is common in other parts of the code. This is in part due to the potential for a "single-point fastening" whereby loads can be carried by a connection providing no redundancy and little warning of failure. Various options for reducing conservatism are discussed such as including the beneficial effect of column flexural compression and the use of a median breakout strength rather than a 5-percent fractile value. These measures may allow designers to consider breakout failure in a manner that is more consistent with other methods and may lead to more economical designs, while preserving the overall required reliability.

A full-scale interior steel-column to concrete-foundation connections located away from foundation edges was constructed and tested under reversed-cyclic lateral loading to better understand the failure mechanisms and design requirements of shear reinforcing on concrete breakout failure.

2 LITERATURE REVIEW

A common method for anchoring attachments to concrete is through steel rods with an enlarged bearing surface or head embedded in the concrete. To anchor structural members to concrete foundations, it is common to use threaded bolts with a nut acting as the head, with or without washers. ACI 318-14 Chapter 17 provides building code requirements for the design of such anchors. For single headed bars or groups of headed bars subjected to tensile loads, four failure modes are to be checked:

1. Steel failure
2. Concrete breakout
3. Pull out
4. Concrete side-face blowout

The present research focuses primarily on the concrete breakout failure mode.

When a tensile force is applied to a headed anchor, the load is transferred to the concrete through the bearing surface of the head as normal pressure. This produces tensile stresses locally around the head. When the tensile stresses exceed the tensile capacity of the concrete, cracks initiate around the anchor head. It has been observed experimentally (Eligehausen and Sawade, 1989) that at loads as low as 30% of the ultimate breakout load, discrete cracks have already initiated at the anchor head. As the load increases, the cracks propagate towards the surface in a radially symmetric pattern forming a cone-like segment of concrete. At 90% of the ultimate load, the cracks have traveled only about 30% of the distance from the anchor head to the surface. Figure 2-1 shows the strains along the failure plane at 30% and 90% of the maximum load. If a load is steadily increased until failure, the cracks will travel all the way to the surface and detach the concrete cone. A breakout-type failure is easily identifiable due to the cone-shaped segment of detached concrete.

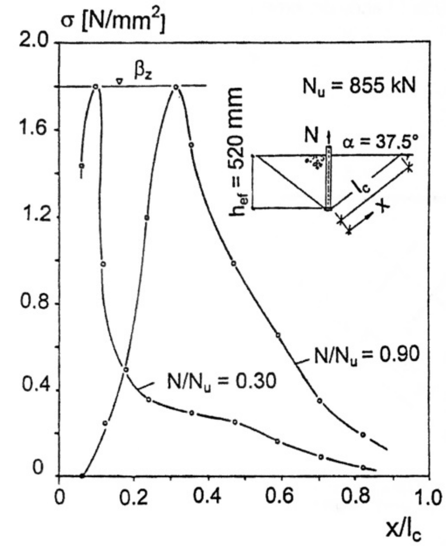

Figure 2-1. Tensile stress distribution perpendicular to the failure cone surface (Eligehausen and Sawade, 1989)

ACI 318-14 breakout equations are based on the so-called CCD-method (Concrete Capacity Design) (Fuchs, et al., 1995). This method assumes a 35° slope for the cone as shown in Figure 2-2 and a uniform stress along the failure surface, which results in the following equation for basic concrete breakout strength of a single anchor in tension in cracked concrete:

$$N_b = k_c\sqrt{f_c'}h_{ef}^{\alpha} \tag{1}$$

Where:

N_b: Basic concrete breakout strength of a single anchor in tension in cracked concrete in lb

k_c: Coefficient k_c = 24 for anchors with h_{ef} < 11 in. and k_c = 16 for anchors with 11 in. $\leq h_{ef} \leq$ 25 in.

f_c': Concrete compressive strength in units of psi

h_{ef}: Effective embedment depth in units of in. (See Figure 2-2)

α: Exponent $\alpha = 1.5$ for anchors with h_{ef} < 11 in. and $\alpha = 5/3$ for anchors with 11 in. $\leq h_{ef} \leq$ 25 in.

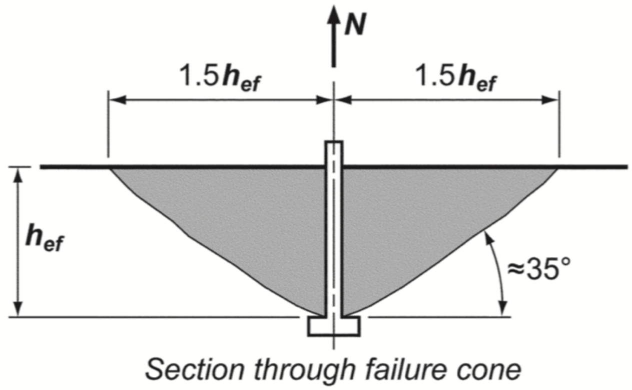

Figure 2-2. Assumed geometry for concrete breakout cone (ACI Committee 318, 2014)

The values of k_c and α in equation (1) were determined from a large database of test results in uncracked concrete at the 5th percent fractile (Fuchs, et al., 1995), which were then adjusted for cracked concrete (Eligehausen, et al., 1995). For anchors with large embedments (11 in. $\leq h_{ef} \leq$ 25 in.), it has been shown that the values of k_c and α developed for small embedment lengths can be overly conservative. Alternate values of k_c and α have been adopted for these larger embedment lengths. To visualize the effect of these new factors, Figure 2-3 plots both models for two values of f_c'. The transition from one model to the next at h_{ef} = 11 in. is clear.

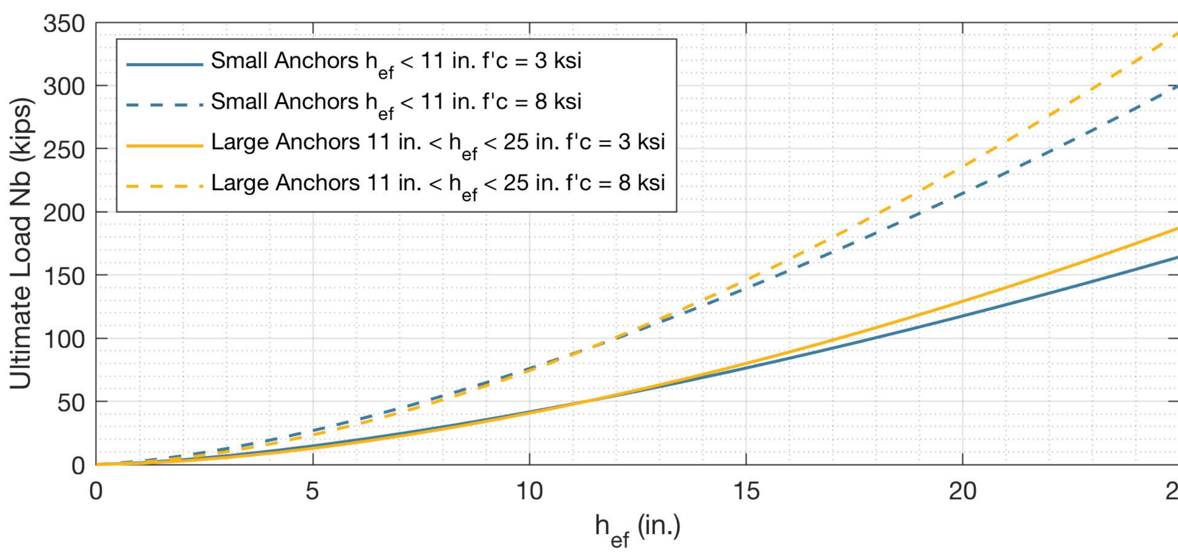

Figure 2-3. ACI 318 Models for basic concrete breakout strength of a single anchor in tension in cracked concrete *N_b*

Equation (1) uses the concrete compressive strength as a proxy for tensile strength, elastic modulus, and other concrete properties. This simplification contributes to scatter in experimental results. Figure 2-4 shows a histogram of the ratio of measured to calculated anchor failure loads for 318 single headed anchor tests. The average value is 0.99 and there is significant scatter.

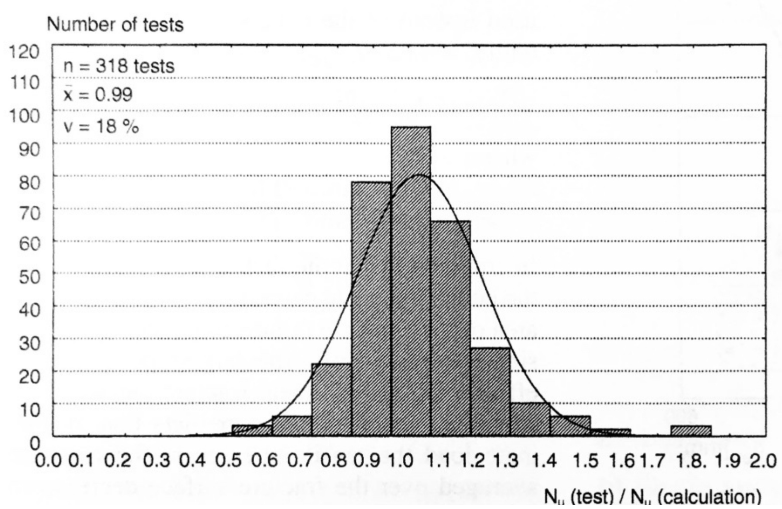

Figure 2-4. Histogram of measured to calculated concrete cone failure loads for headed anchors subjected to concentric tension (Eligehausen, et al., 1992)

Similarly, Figure 2-5 shows the ratio of measured to calculated anchor failure loads for varying concrete compressive strength. Significant scatter is observed. The lower 5% percentile of these results is used in ACI 318. A factor of 1.33 is commonly used to convert from a 5% to the 50% value.

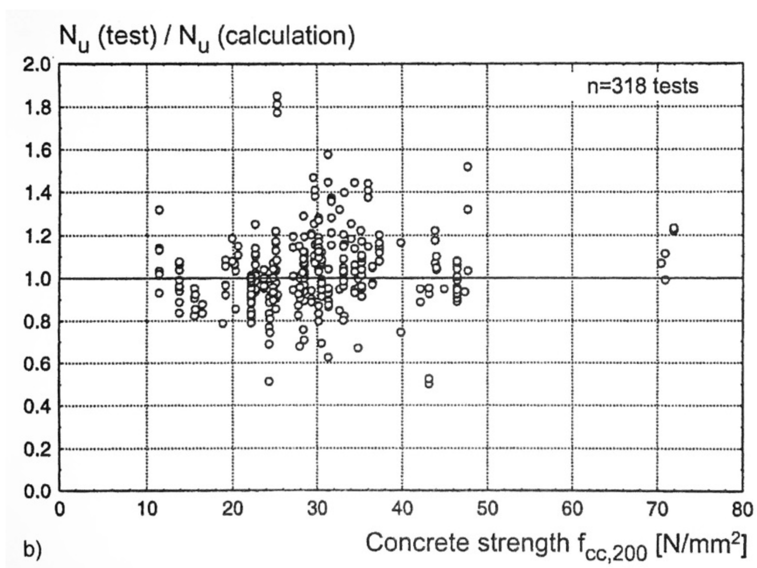

Figure 2-5. Ratio of measured to calculated concrete cone failure loads for headed anchors subjected to tension as a function of concrete compressive strength (Eligehausen, et al., 1992)

Once the basic concrete breakout strength of a single anchor in tension in uncracked concrete is determined (N_b), ACI 318-14 requires that this value be modified to consider group effects, load eccentricity, edge distance, and concrete cracking as follows:

For a single anchor:

$$N_{cb} = \frac{A_{Nc}}{A_{Nco}} \Psi_{ed,N} \Psi_{c,N} \Psi_{cp,N} N_b \tag{2}$$

For a group of anchors:

$$N_{cbg} = \frac{A_{Nc}}{A_{Nco}} \Psi_{ec,N} \Psi_{ed,N} \Psi_{c,N} \Psi_{cp,N} N_b \tag{3}$$

Where:

N_{cb}: Nominal concrete breakout strength in tension of a single anchor

N_{cbg}: Nominal concrete breakout strength in tension of a group of anchors

A_{Nc} : Projected failure area of a single anchor or group in question

$A_{Nco} = 9h_{ef}^2$: Projected concrete failure area of a single anchor if not affected by edges

The term A_{Nc}/A_{Nco} is known commonly as the "group factor" and models the capacity drop due to the presence of multiple anchors with overlapping potential cone failure surfaces. The "group factor" also considers a drop in capacity due to limited edge distance where the potential cone failure surface might intersect a lateral face before reaching the top surface.

The Ψ factors in equations (2) and (3) consider additional modifications. The modification factor for anchor groups loaded eccentrically in tension, $\Psi_{ec,N}$, is calculated as:

$$\Psi_{ec,N} = \frac{1}{\left(1 + \frac{2e'_N}{3h_{ef}}\right)} \tag{4}$$

Where:

$\Psi_{ec,N}$: Modification factor for anchor groups loaded eccentrically in tension

e'_N: Load eccentricity

The modification factor for edge effects of anchor groups in tension, $\Psi_{ed,N}$, is calculated as:

$$\begin{gathered}\text{If } c_{a,min} \geq 1.5h_{ef}\text{, then } \Psi_{ed,N} = 1.0 \\ \text{If } c_{a,min} < 1.5h_{ef}\text{, then } \Psi_{ed,N} = 0.7 + 0.3\frac{c_{a,min}}{1.5h_{ef}}\end{gathered} \tag{5}$$

Where:

$\Psi_{ed,N}$: Modification factor for edge effects of anchors in tension

$c_{a,min}$: Shortest edge distance of any anchor in the group

The modification factor for cracked concrete, $\Psi_{c,N}$, is taken as:

$$\Psi_{c,N} = 1.25 \text{ for uncracked concrete under service loads} \qquad (6)$$
$$\Psi_{c,N} = 1.00 \text{ for cracked concrete under service loads}$$

For cast-in-place anchors, the splitting modification factor is taken as $\Psi_{cp,N} = 1.0$.

Numerical simulations and experimental testing have shown that for the case of a base plate resisting moment and anchored to concrete with multiple anchor groups, equation (3) can be overly conservative. The bearing of the base plate on the surface of the potential concrete breakout cone (see Figure 2-6) apparently increases the anchor group capacity. Figure 2-7 shows multiple proposed modification factors to describe this effect as a function of the joint aspect ratio. The joint aspect ratio serves as a proxy to determine if the compressive bearing force from the column is acting on the potential cone surface or if it is too far away to have a significant effect. Trends in laboratory test data (Mahrenholtz, et al., 2014) are consistent with the modification factor proposed by Herzog (2015).

$$\Psi_M = 2.5 - \frac{z}{h_{ef}} \geq 1.0 \qquad (7)$$

Where:

Ψ_M: Modification factor for compressive bearing force

z: Lever arm. Distance between tension in anchor group and resultants of compressive bearing pressure

h_{ef}: Anchor group effective depth

This factor is not included in ACI 318-14. Similar factors are permitted in some European codes like CEN/TS 1992-4-1:2009.

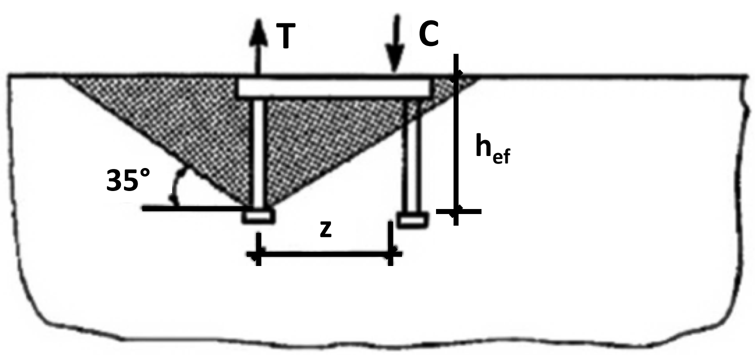

Figure 2-6. Influence of compressive force on concrete cone breakout capacity after Zhao (1993) (Eligehausen, et al., 2006)

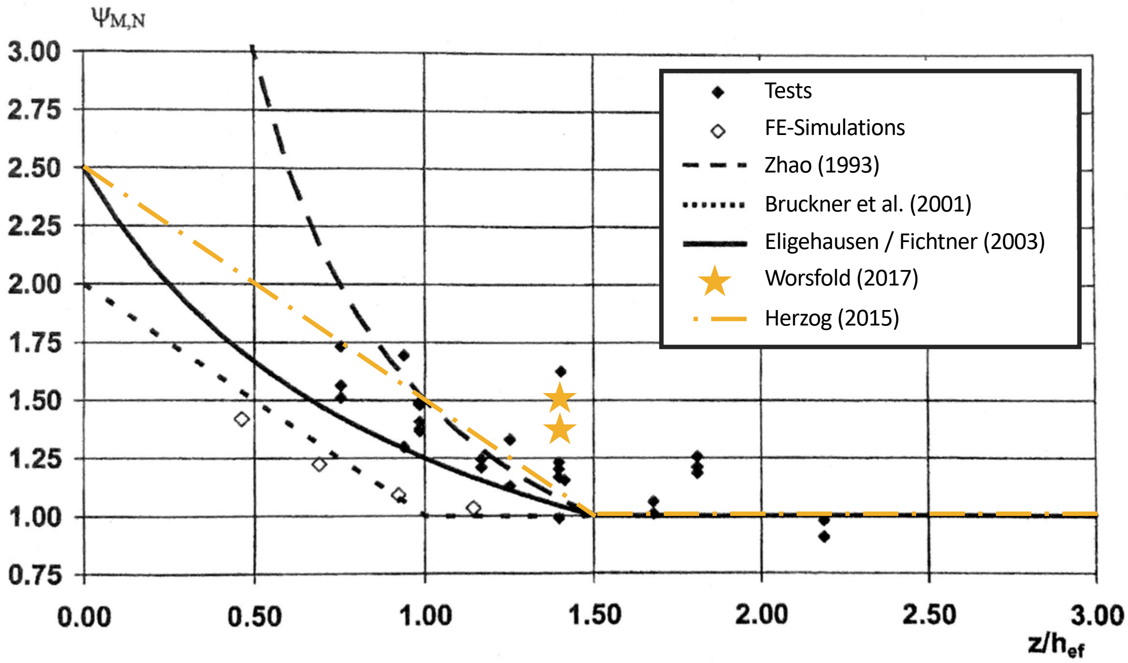

Figure 2-7. Influence of compression force on concrete cone breakout capacity as a function of ratio internal lever arm to embedment depth. Modified from (Eligehausen, et al., 2006)

For the particular case of headed reinforcement terminating in an edge joint, the commentary of ACI 318-14 indicates that if the headed reinforcing bar is developed a distance greater than or equal to $d/1.5$ (see Figure 2-8), then breakout is precluded and it is not required to check for breakout failure using Chapter 17.

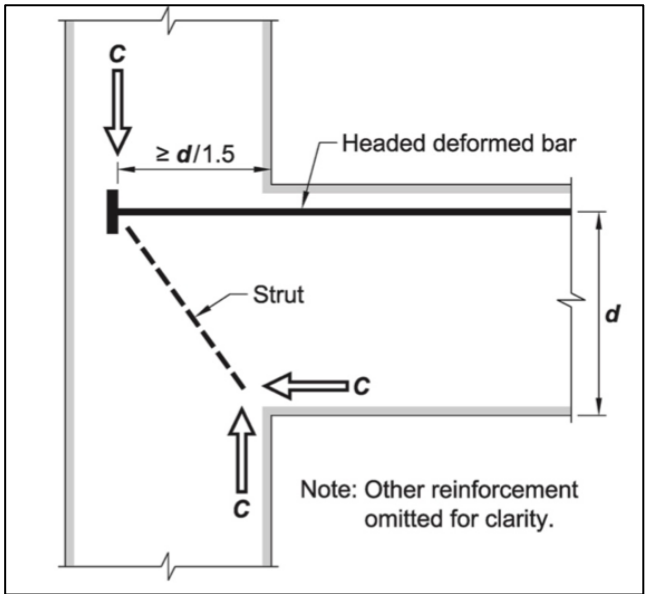

Figure 2-8. Breakout failure precluded in joint by keeping anchorage length greater than or equal to *d / 1.5* (ACI 318-14 R25.4.4.2c)

The ACI 318-19 provisions recognizes some benefits when additional reinforcement is present in the vicinity of anchor groups by defining two categories of reinforcement: anchor reinforcement and supplementary reinforcement. The use of anchor reinforcement is intended as an alternative to explicit calculation of the concrete breakout strength as the concrete strength is ignored. This reinforcement is designed to carry the full force of the anchor group into the member and must be developed on both sides of the assumed breakout plane as per ACI 318 development length provisions. A strength reduction factor of 0.75 is allowed. Research shows (Eligehausen et al., 2009) that anchor reinforcement placed further than $0.5h_{ef}$ from the anchor centerline is not considered effective. Supplementary reinforcement is generally configured and placed similar to anchor reinforcement, but is not designed to carry the full force from the anchor group. This reinforcing is intended to control concrete splitting. When supplementary reinforcement is present, minimum edge, spacing, and thickness provisions need not apply. The use of larger strength reduction factors (Φ) is allowed to recognize increased deformation capacity. Full development of supplementary reinforcement beyond the assumed breakout failure plane is not required.

The Eurocode defines a concept called supplementary reinforcement which is analogous to anchor reinforcement in ACI 318. Supplementary reinforcement in the Eurocode is designed for the full force in the anchor group, disregarding the concrete breakout strength calculation. The strength of the supplementary reinforcement considers explicit calculations for yielding of the reinforcing and bond failure. The reinforcing must be developed on both sides of the assumed failure cone, but less strict requirements are placed on the segment of the bar developed in the concrete cone. A secondary concrete cone failure check is required at the termination of the supplementary reinforcing. The Eurocode allows supplementary reinforcing less than $0.75h_{ef}$ from the anchor centerline to be considered effective.

Papadopoulos et al. (2018) investigated headed reinforcing bars in column-slab connections for bridges through physical testing and finite element simulations. They demonstrated that shear reinforcing in the form of J-bars inside the joint and stirrups outside the joint prevented breakout failure. Additional shear reinforcing bars beyond the first row outside the joint seemed to have no effect. The results led to detailing recommendations adopted by Caltrans in MTD 20-7 (Caltrans 2016).

3 SPECIMEN DESIGN

3.1 SPECIMEN REQUIREMENTS

A main purpose of the test specimen is to determine the effect of shear reinforcing on the moment transfer strength of a column-foundation connection with cast-in-place headed anchors. The main design considerations in designing the test specimen details are as follows:

- All failure modes that are not of interest will be designed to resist the expected yield capacity of the column.
- The specimen design will resemble as closely as possible some aspects of current practice on the West Coast of the United States.
- An ordinary concrete mixture will be used with no special additives. Local materials will be used in accordance with the mixture design in A.6.
- A seismically compact wide-flanged steel column section will be used for the column.
- No axial load will be applied to the column to isolate the effect of moment loading.
- The concrete slab will be large enough to allow for a potential breakout failure to occur without interference of supports or slab edges.
- The specimen will be loaded cyclically and quasi-statically in the longitudinal direction with a displacement driven loading protocol.
- The slab will not rest on the laboratory floor but will be simply supported as this is considered to be a more critical case without soil support.

3.2 SPECIMEN GEOMETRY AND DESIGN

Figure 3-1 is a schematic representation of the test set-up. The footing is prestressed to the laboratory strong floor with nine 1-3/4" 150 ksi Williams Rods loaded to 140 kips each. The prestressing rods and concrete supports are located at opposite ends of the footing in the longitudinal direction (the longitudinal direction is parallel to the column web). Two actuators are attached to the column free end at about 45˚ relative to the principal axis of the column cross section. The actuators are programmed to displace the column in the longitudinal direction only, limiting transverse displacements.

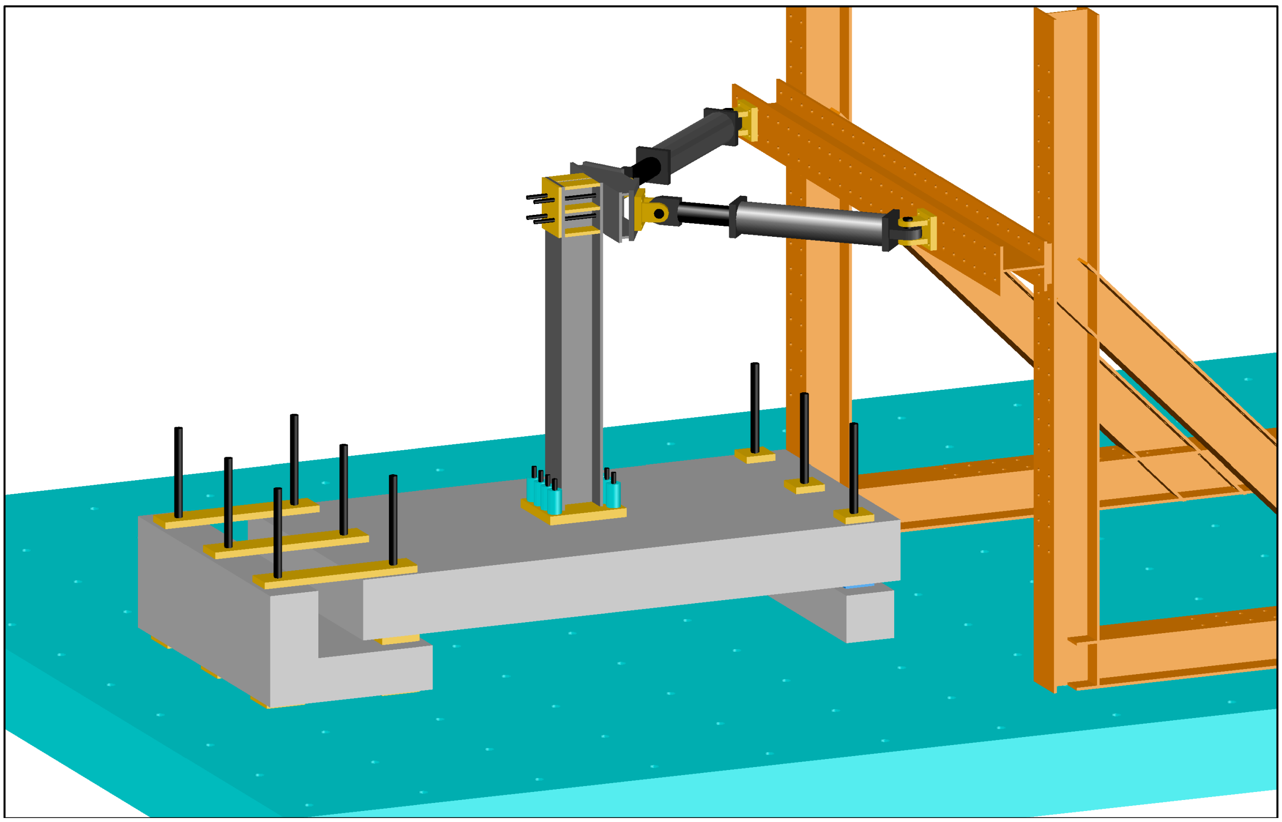

Figure 3-1. Isometric view of specimen and loading frame

Figure 3-2 to Figure 3-9 show the specimen drawings. For complete as-built drawings see APPENDIX B.

As shown in Figure 3-2, Figure 3-3, and Figure 3-4, the column consists of an A992 Grade 50 W12 x 112 steel section. The column is welded to a 24 in. by 21.5 in. by 2-3/4 in. A529 G50 steel base plate with a 5.25 in. by 5.25 in. by 2 in. A529 G50 shear lug (Figure 3-5). The base plate and shear lug are grouted in place to the concrete foundation. Four 1-1/2 in. diameter G105 anchor bolts on each side of the column pass through 1-5/8 in. (Figure 3-6) diameter holes in the base plate and use heavy hex nuts and a plate (1.25 in. x 3.5 in. x 3.5 in.) as heads at an effective depth of 14.3 in. (see Figure 3-7). The anchor bolts extend 10 in. above the base plate to accommodate placement of a load cell on each anchor bolt and to provide additional stretch length.

The foundation slab was designed such that the slab would have sufficient shear and moment strength to resist the expected forces from column yield. Longitudinal reinforcement was designed assuming the reinforcement was Grade 60. However, to ensure that extensive flexural yielding would not occur if moment transfer strength was underestimated, the provided bars are Grade 100. Longitudinal reinforcing mats are provided at both the top and bottom surfaces of the slab. Details are in Figure 3-2.

Shear reinforcing was placed in the region around the anchor groups as seen in Figure 3-8. A larger region was reinforced on the west side of the specimen compared to the east side. The shear reinforcing bars had head on one end and 180-degree hooks on the other (see Figure 3-9). The shear reinforcing bars would hang form the intersections of the longitudinal bars.

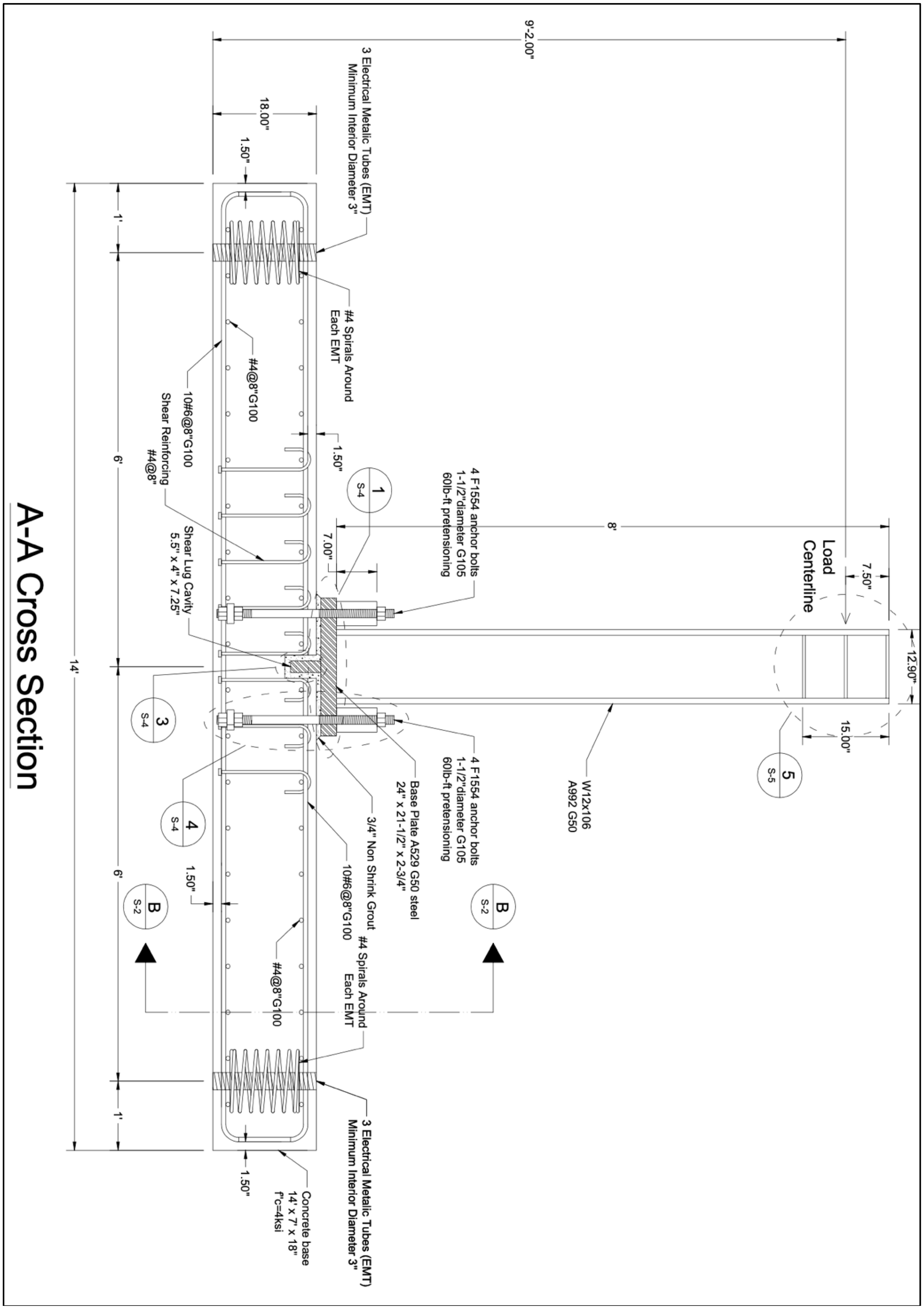

Figure 3-2. Elevation view of longitudinal A-A cross section of specimen

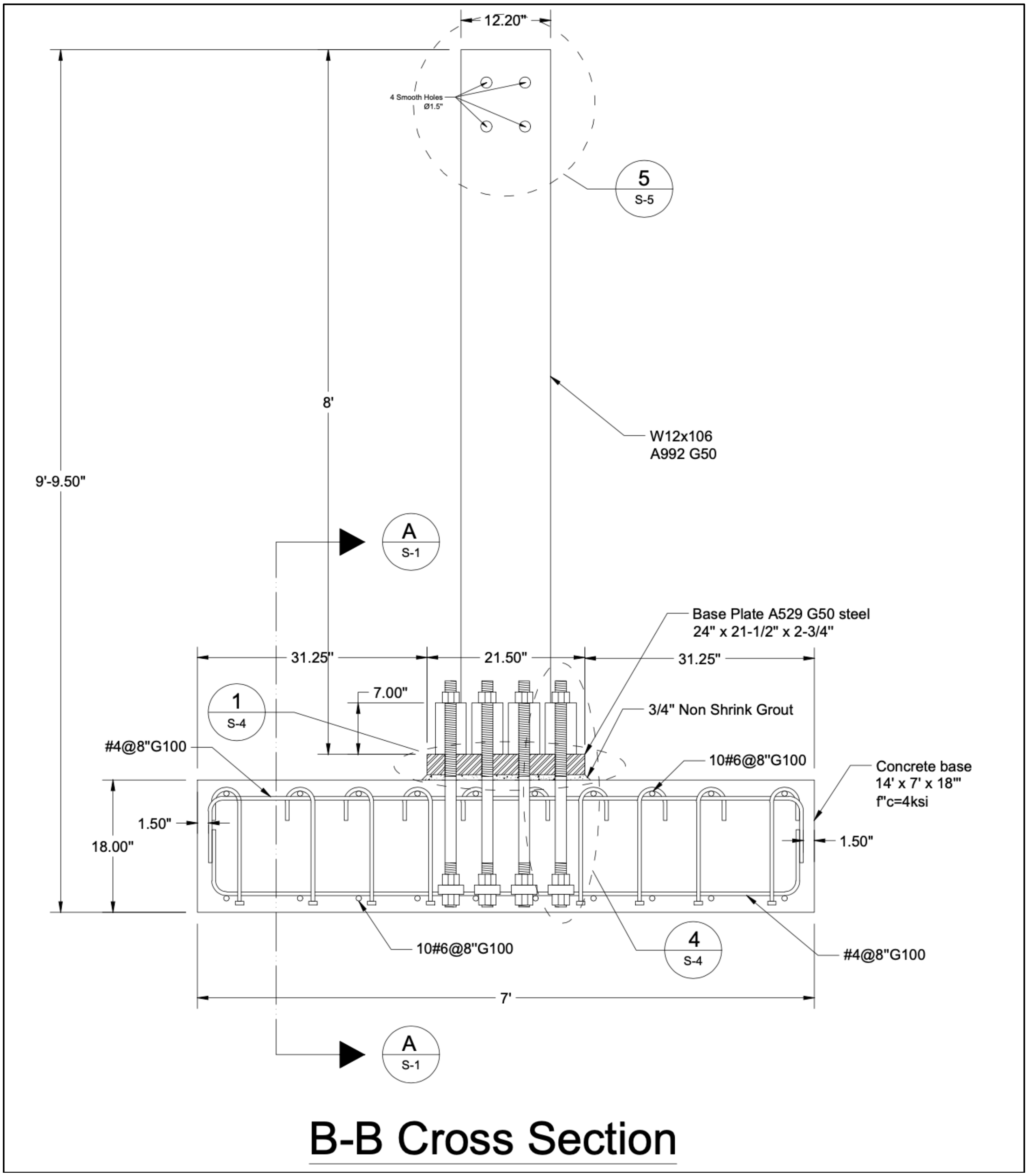

Figure 3-3. Elevation view of transverse B-B cross section of specimen

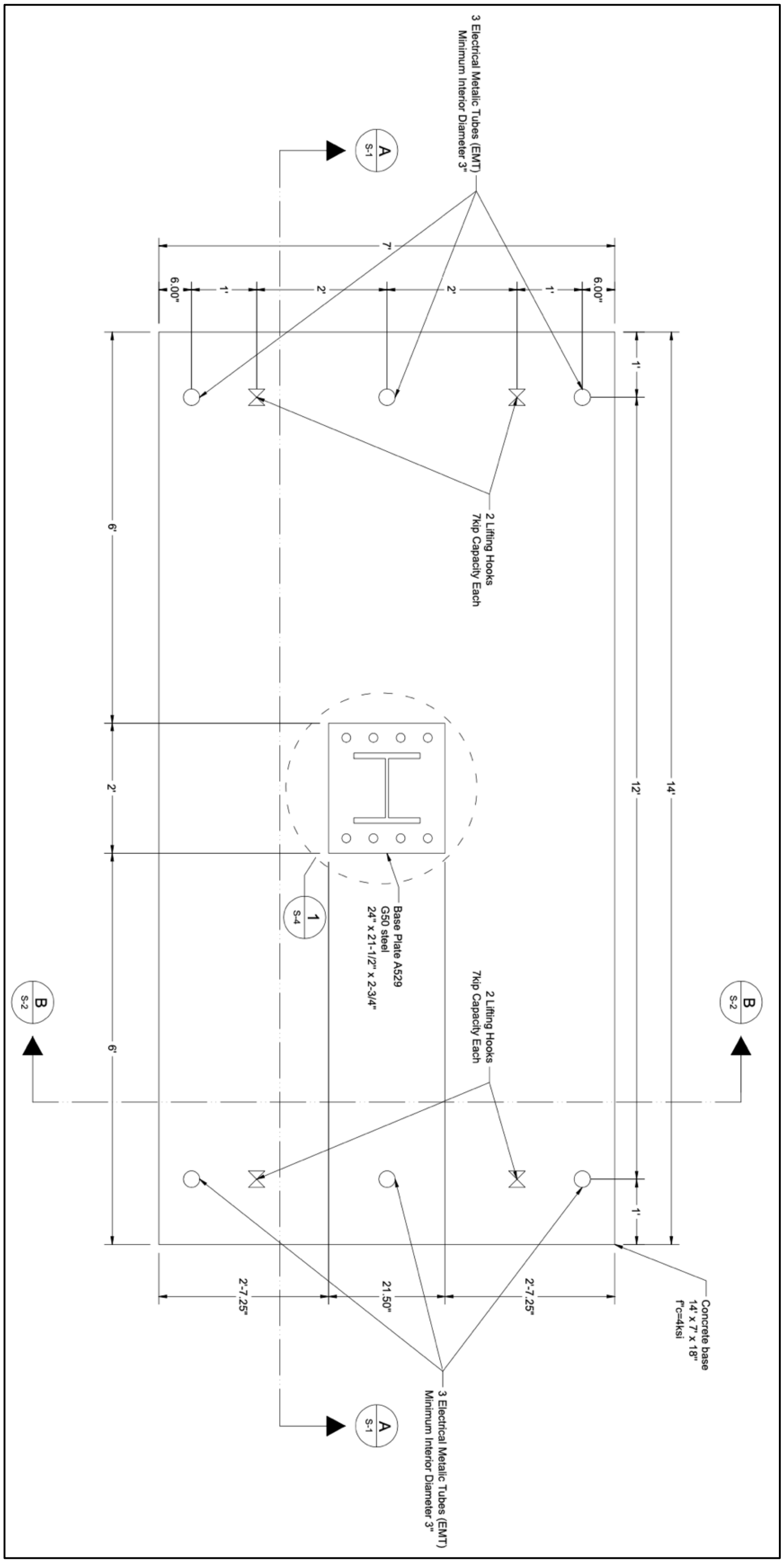

Figure 3-4. Plan view of specimen

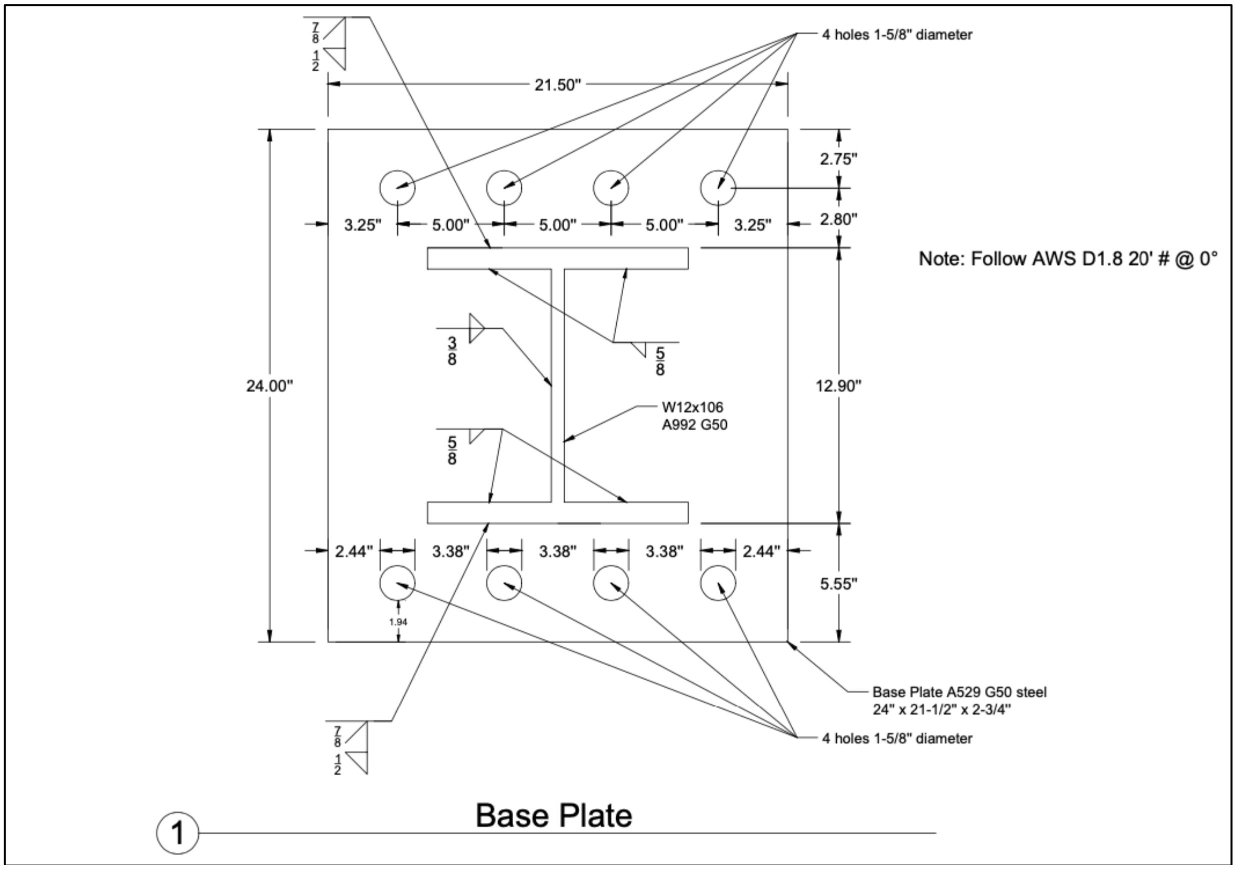

Figure 3-5. Base plate details

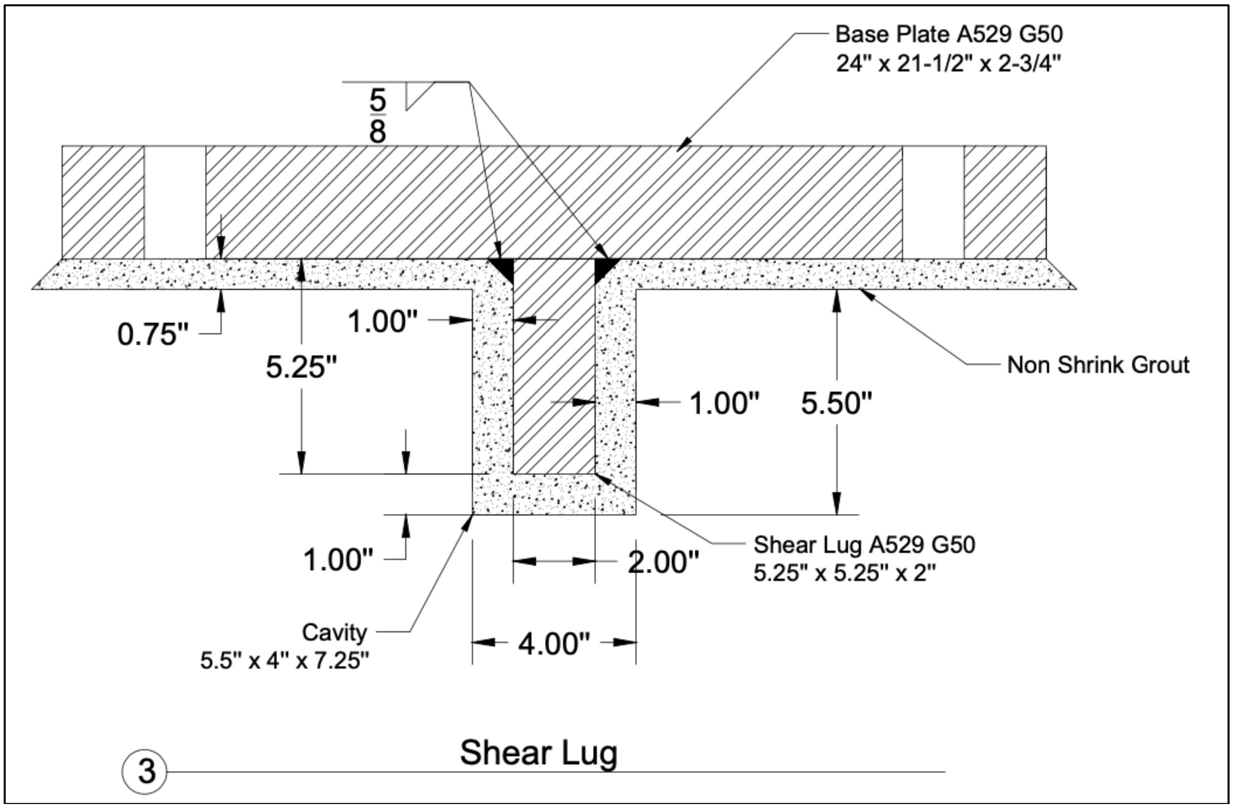

Figure 3-6. Base plate and shear lug details

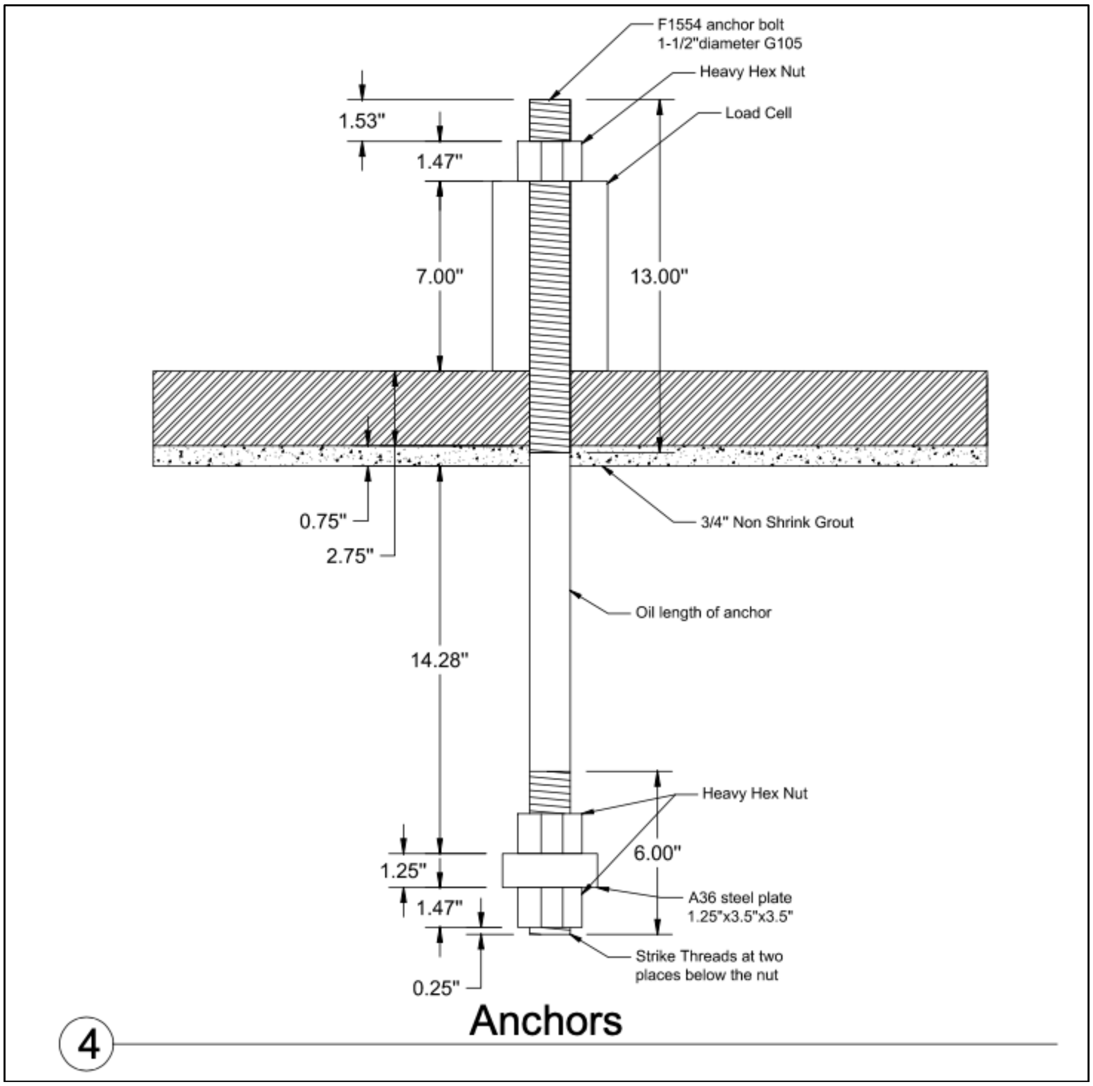

Figure 3-7. Anchor details

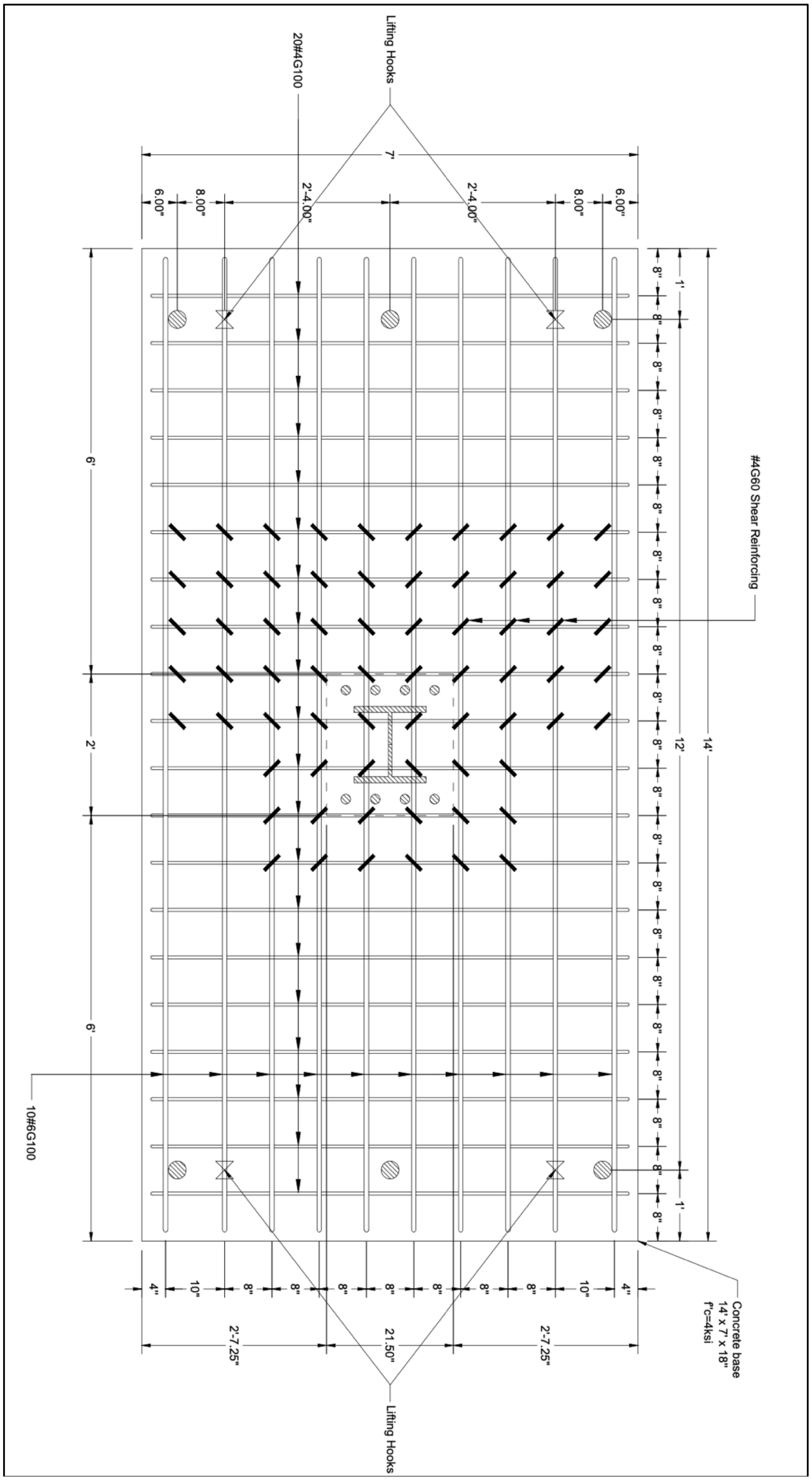

Figure 3-8. Plan view reinforcement location

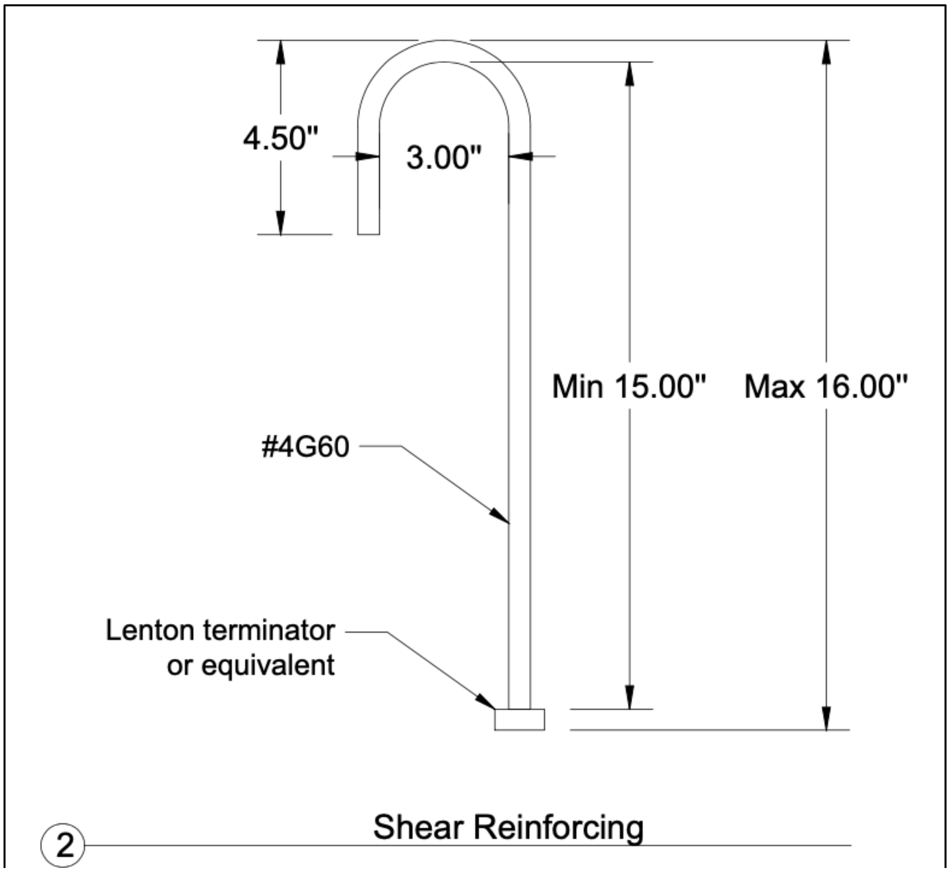

Figure 3-9. Shear reinforcing details

3.3 CALCULATIONS OF CONNECTION STRENGTH

Detailed calculations of the strength of the column-foundation connection are presented below. Mean predictor equations and measured material properties are used. Also, the strength reduction factor for LRFD calculations is set as $\phi = 1$ for all methods shown below. With the exception of moment transfer strength within the column-footing joint, all other strengths (for example, base plate yield, support failure, anchor yield, column failure, etc.) are designed such that the column will yield first. Detailed calculations for all other failure modes are shown in APPENDIX C.

3.3.1 Concrete Breakout Equations (ACI 318-14 Ch.17 Anchoring to Concrete)

3.3.1.1 Unmodified Concrete Breakout Equations

M02 Design: Chap 17 ACI 318-14

2022.04.01

Notation

Input

Output

Condition check

Input Data

$f'c := 3930\ \text{psi}$

$nb := 4$ Number of bolts in tension

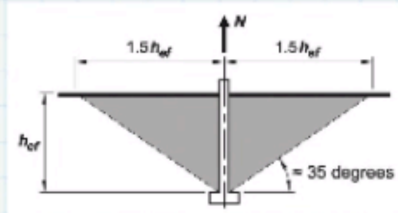

$dia := 1.5\ \text{in.}$ Anchor rod diameter

$hef := 14.28\ \text{in.}$ Anchor rod effective depth

$kc := 24$ Preinstalled rods

$\lambda a := 1$ Normal weight concrete

Group Factor

$$ANco := 9 \cdot hef^2 = \left(1.84 \cdot 10^3\right)\ \text{in.}^2$$

$$ANc := (1.5\ hef \cdot 2) \cdot (1.5\ hef \cdot 2 + 15\ \text{in.}) = \left(2.48 \cdot 10^3\right)\ \text{in.}^2$$

$$\frac{ANc}{ANco} = 1.35$$ Group factor

Single anchor capacity

$$Nb1 := 24\ \lambda a \cdot \sqrt{\frac{f'c}{\text{psi}}} \left(\frac{hef}{\text{in.}}\right)^{1.5} \frac{\text{kips}}{1000} = 81.2\ \text{kips}$$

$$Nb2 := 16\ \lambda a \cdot \sqrt{\frac{f'c}{\text{psi}}} \left(\frac{hef}{\text{in.}}\right)^{\frac{5}{3}} \frac{\text{kips}}{1000} = 84.3\ \text{kips}$$

If 11 in. < hef < 25 in. this equation is allowed

$$Nb := \max(Nb1, Nb2) = 84.3\ \text{kips}$$

ACI318-14 Modification Factors

$\psi ecN := 1.0$ Eccentric loading for rods in tension

$\psi edN := 1.0$ Not close to edge

$\psi cN := 1.25$ Assumed uncracked

$\psi cpN := 1.0$ For post-installed anchor rods only

Breakout Capacity: ACI318-14 without any additional modifications

$$N_{cbg} := \frac{ANc}{ANco} \psi ecN \cdot \psi edN \cdot \psi cN \cdot \psi cpN \cdot Nb = 142 \text{ kips}$$

Breakout Capacity: ACI318-14 mean prediction without additional modification factors

$f_{mean} := 1.33$ Factor to obtain mean predictor

$$N_{cbg'} := \frac{ANc}{ANco} \psi ecN \cdot \psi edN \cdot \psi cN \cdot \psi cpN \cdot Nb \cdot f_{mean} = 189 \text{ kips}$$

In the previous calculation, the factor for uncracked concrete is used ($\psi cN = 1.25$). This factor is based on research by Eligehausen and Balogh (1995). Concrete is considered "uncracked" if service loads applied to the concrete prior to applying the anchor force are insufficient to crack the concrete. It could be argued, however, that the anchors in the test slab provide the main loading for the foundation slab and that these loads are sufficient to crack the concrete in the region of the anchors, and therefore the breakout strength should be based on cracked concrete. The breakout capacity calculation is repeated below considering the concrete to be cracked ($\psi cN = 1.00$).

$$N_{cbg'} := \frac{ANc}{ANco} \psi ecN \cdot \psi edN \cdot \psi cN \cdot \psi cpN \cdot Nb \cdot f_{mean} = 151 \text{ kips}$$

3.3.2 Horizontal Joint Shear Equations (ACI 352R-02 Design of Beam-Column Connections)

The ACI 352-02 (2002) provisions were developed for design of beam-column joints in moment frames. Here we follow an engineering practice of extending the application of the provisions to the design of column-foundation connections in which the flexural tension forces from the column are developed through cast-in-place headed anchors. The ACI 352 design procedure requires definition of the dimensions of the concrete column entering the joint. Here we replace the actual steel column with a pseudo-concrete column. The outer column dimensions are assumed to be the center-to-center distance between the outermost anchors plus an anchor bar diameter plus nominal hoops (0.5 in. diameter) plus twice a nominal cover of 1.5 in., resulting in 24 in. by 20.5 in. nominal column dimensions as shown in Figure 3-10. Detailed calculations of joint nominal strength are shown below.

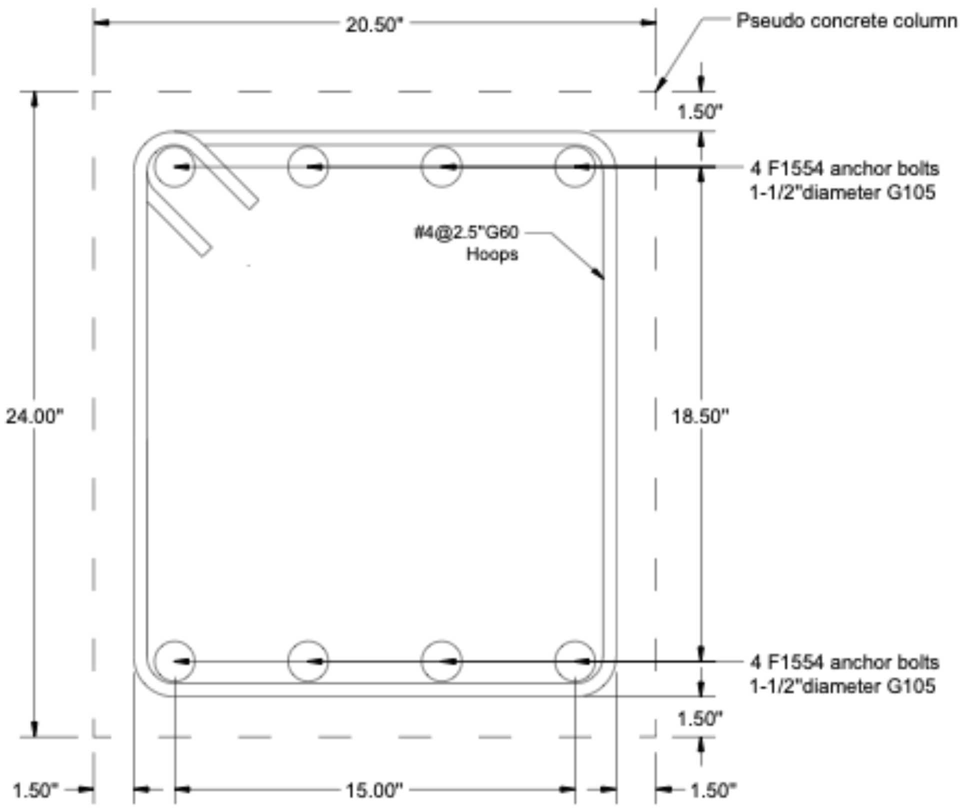

Figure 3-10. Pseudo concrete column dimensions

The nominal horizontal joint shear is calculated below:

Beam-Column Joint (ACI 352)

Column Dimentions — Assumed as center to center of anchors + anchor diameter +confining steel+ 2 covers

$b_c := 15\ in. + 1.5\ in. + 2 \cdot 0.5\ in. + 2 \cdot 1.5\ in. = 20.5\ in.$ — Out of plane width

$h_c := 18.5\ in. + 1.5\ in. + 2 \cdot 0.5\ in. + 2 \cdot 1.5\ in. = 24\ in.$ — In plane horizontal width

Horizontal Joint Capacity

$b_j := b_c = 20.5\ in.$

$\gamma := 15$ — Joint coefficient for roof joint confined on all 4 sides

$V_{nh} := \gamma \cdot \sqrt{\frac{f'c}{psi}} \frac{b_j}{in.} \cdot \frac{h_c}{in.} \frac{kips}{1000} = 463\ kips$ — Nominal horizontal joint shear capacity

The force applied on the column free end (P) can be written as a function of the horizontal joint shear using a moment equilibrium equation from Figure 3-12 and the horizontal equilibrium equation from Figure 3-13(a):

$$P = \frac{V_{nh}}{\frac{1}{0.9dL}\left[(H+t)(L-h_c)-\frac{tL}{2}\right]-\frac{1}{2}} = 89\ kips \tag{8}$$

Where:

P: Force applied on column free end

H: Vertical distance between point of load application and top surface of slab (see Figure 3-11)

L: Horizontal distance between slab supports (see Figure 3-11)

V_{nh}: Nominal horizontal joint shear

t: Slab thickness

h_c: in plane horizontal joint width

Lateral Load (P)

$H := 92\ \text{in.}$ Vertical distance between point of load application and top surface of slab

$L := 144\ \text{in.}$ Horizontal distance between slab supports

$t := 18\ \text{in.}$ Slab thickness

$h_c = 24\ \text{in.}$ In plane horizontal node width

$d := t - 1.5\ \text{in.} - 0.75\ \frac{\text{in.}}{2} = 16.1\ \text{in.}$ Distance from extreme compression fiber to centroid of longitudinal reinforcement

$$l' := \frac{1}{0.9\ d \cdot L}\left((H+t)\ (L-h_c) - \frac{t \cdot L}{2}\right) - \frac{1}{2} = 5.2$$

$P := \frac{V_{nh}}{l'} = 89\ \text{kips}$ Load applied to column free end

The force in the anchor group (T_u) can be calculated using the AISC Design Guide 1 procedure to estimate the distance between the tension and compression resultants form the column (z) as follows:

$$T_u = \frac{PH}{z} = 414\ kips \tag{9}$$

AISC Design Guide 1: P-z-Tu

Uses uniform bearing pressure model to relate lateral load (P), lever arm (z), and Anchor load (Tu).

Input Data

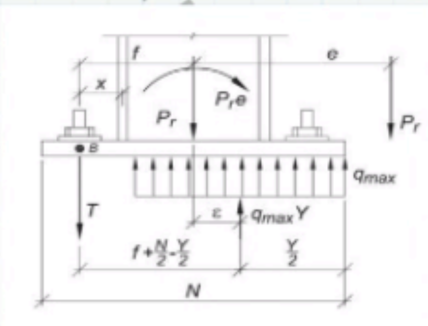

Fig. 3.4.1. Base plate with large moment.

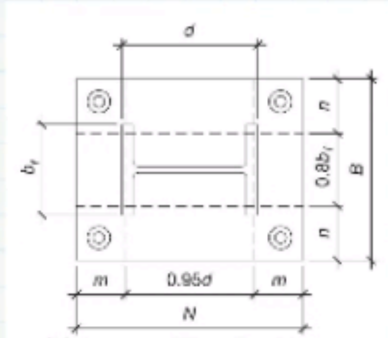

(b) Assumed Bending Lines

$B := 21.5\ \text{in.}$
$N := 24\ \text{in.}$
$f := 9.25\ \text{in.}$

Column: W12x106 A529 G50

Loads

$Pu := 1\ \text{kips}$ Self weight of column and actuator. Some axial load is neccessary or equations do not work

$Vu := P = 89\ \text{kips}$ Lateral load

$Lc := 92\ \text{in}$ Distance from force application to slab surface.

$Mu := Lc \cdot Vu = 8191\ \text{kips} \cdot \text{in.}$

$e := \dfrac{Mu}{Pu} = \left(8.2 \cdot 10^{3}\right)\ \text{in.}$ Almost no axial load so excentricity is very large

Bearing on concrete

ACI 318-14 22.8

A1<<A2 The base plate area is small compared to the concrete pedestal area. Factor of 2 included.

$\varphi_{Bear} := 1$

$f_{pMax} := \varphi_{Bear} \cdot 0.85 \cdot f'c \cdot 2 = 6681 \text{ psi}$

$q_{max} := \varphi_{Bear} \cdot 0.85 \cdot f'c \cdot 2 \cdot B = 144 \dfrac{\text{kips}}{\text{in.}}$

Base plate

$$Y := \left(f + \frac{N}{2}\right) - \sqrt{\left(f + \frac{N}{2}\right)^2 - 2 \cdot \frac{Pu \cdot (e + f)}{q_{max}}} = 2.88 \text{ in.}$$

column yield.

$z := f + \dfrac{N}{2} - \dfrac{Y}{2} = 19.81 \text{ in.}$

Internal lever arm

$Tu := \dfrac{P \cdot H}{z} = 414 \text{ kips}$

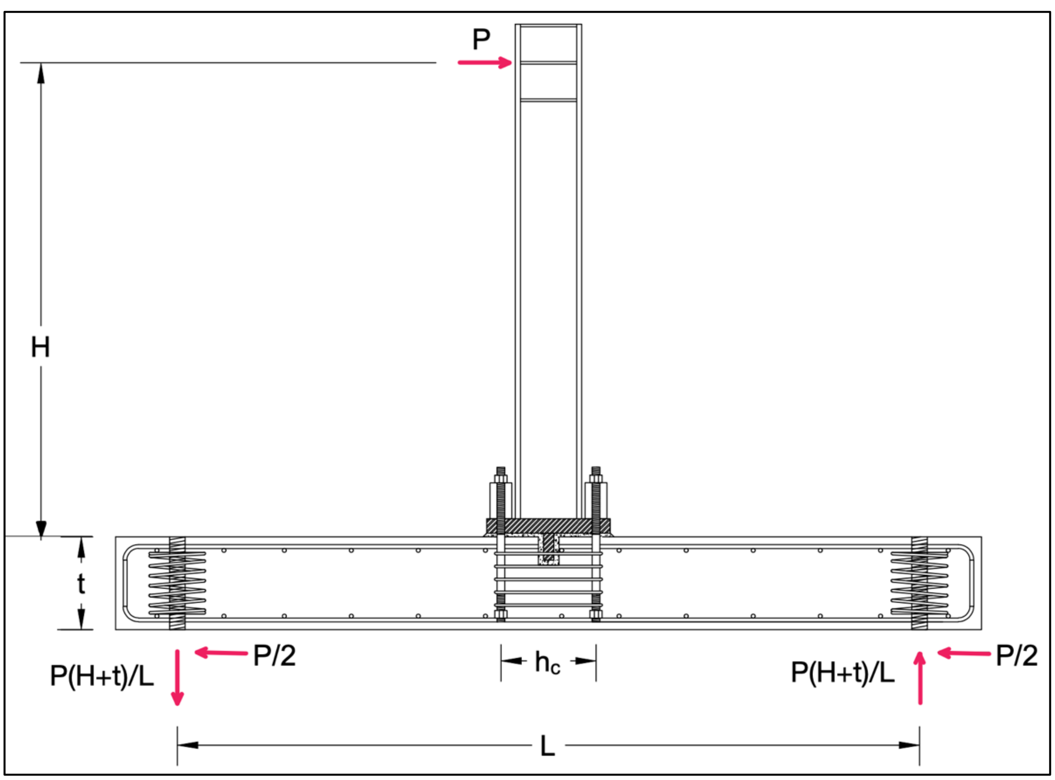

Figure 3-11. Free body diagram complete specimen

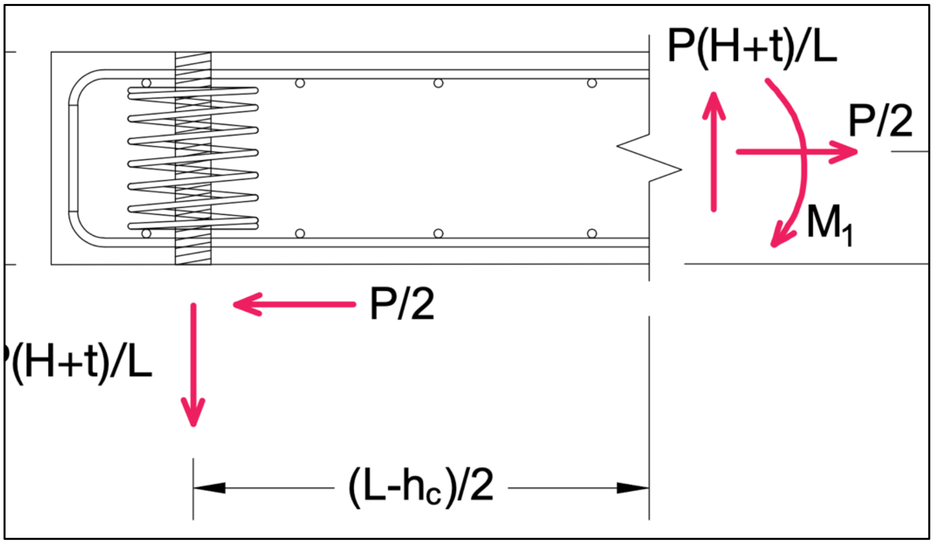

Figure 3-12. Free body diagram internal forces acting on node

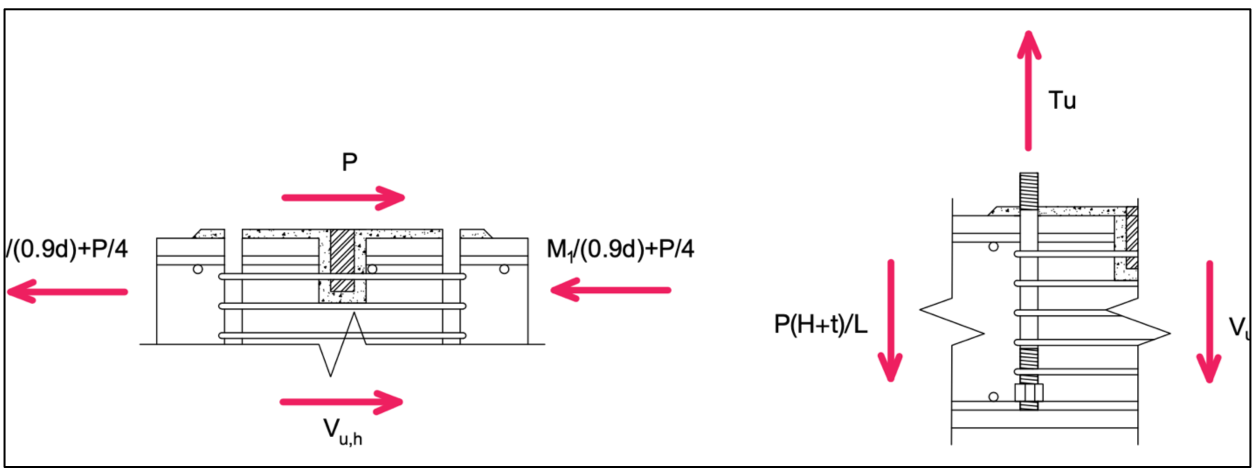

Figure 3-13. Free body diagrams for horizontal (left) and vertical joint shear (right). For clarity, only the horizontal and vertical forces are shown respectively

3.3.3 Secondary Breakout Cones

When a region of distributed shear reinforcement is placed around an anchor group, the potential exists for a secondary breakout cone that engulfs the anchor group and the shear reinforcement. The strength of the secondary breakout cone can be calculated considering the relative increase in the group factor as follows:

$$N_{cbg}^{S} = N_{cbg}^{o}\left(\frac{A_{nc}^{S}}{A_{nc}^{o}}\right) \tag{10}$$

Where:

N_{cbg}^{S}: breakout strength of secondary cone

N_{cbg}^{P}: breakout strength of primary cone

A_{nc}^{S}: tributary area of secondary cone

A_{nc}^{P}: tributary area of primary cone

A summary of the calculations follows:

Secondary Breakout East

The strength of the secondary breakout cone can be calculated considering the relative increase in the group factor.

East anchor group:

$$A_{nc}P := (15\ \text{in.} + 3\ hef) \cdot 3\ hef = (2 \cdot 10^3)\ \text{in.}^2$$

$$A_{nc}S := (15\ \text{in.} + 4.5\ hef) \cdot 3.75\ hef = 4244\ \text{in.}^2$$

$$\frac{A_{nc}S}{A_{nc}P} = 1.71$$

$$N_{cbg}S := N_{cbg} \cdot \left(\frac{A_{nc}S}{A_{nc}P}\right) = 324\ \text{kips}$$

Median breakout strength of east secondary cone.

West anchor group:

$$A_{nc}P := (15\ \text{in.} + 3\ hef) \cdot 3\ hef = (2 \cdot 10^3)\ \text{in.}^2$$

$$A_{nc}S := (15\ \text{in.} + 6.76\ hef) \cdot 4.88\ hef = 7772\ \text{in.}^2$$

$$\frac{A_{nc}S}{A_{nc}P} = 3.14$$

$$N_{cbg}S := N_{cbg} \cdot \left(\frac{A_{nc}S}{A_{nc}P}\right) = 594\ \text{kips}$$

Median breakout strength of west secondary cone.

3.3.4 Summary of Connection Capacities

Table 3-1 lists the median anchor forces in the anchor group according to different failure criteria discussed.

Table 3-1. Median anchor group force using different failure criteria

Failure Mode	Anchor Force (kip)
Breakout (Uncracked)	189
Breakout Secondary East (Uncracked)	324
Breakout Secondary West (Uncracked)	594
Beam-Column Joint	414

4 TEST SET-UP

As can be seen in Figure 4-1, the 18 in. thick foundation slab was placed on concrete supports on both ends. To prevent sliding during the test, the slab was prestressed to the laboratory floor with nine 1-3/4" 150 ksi Williams Rods loaded to 140 kips each. Two actuators were attached to the column near its free end, oriented at approximately 45° from the longitudinal axis and programmed to move the column longitudinally with minimal transverse displacement. Before initiating loading on test day, each anchor was prestressed to 3.5 kip in the following order: one, eight, four, five, two, seven, three, and six (see Figure 4-5 for anchor numbering). The initial load in the anchor groups can be seen in Figure 5-13 before the external loading begins. See Figure 3-1 to Figure 3-6 for detailed drawings of the specimen. See APPENDIX F for photographs of the construction process and testing.

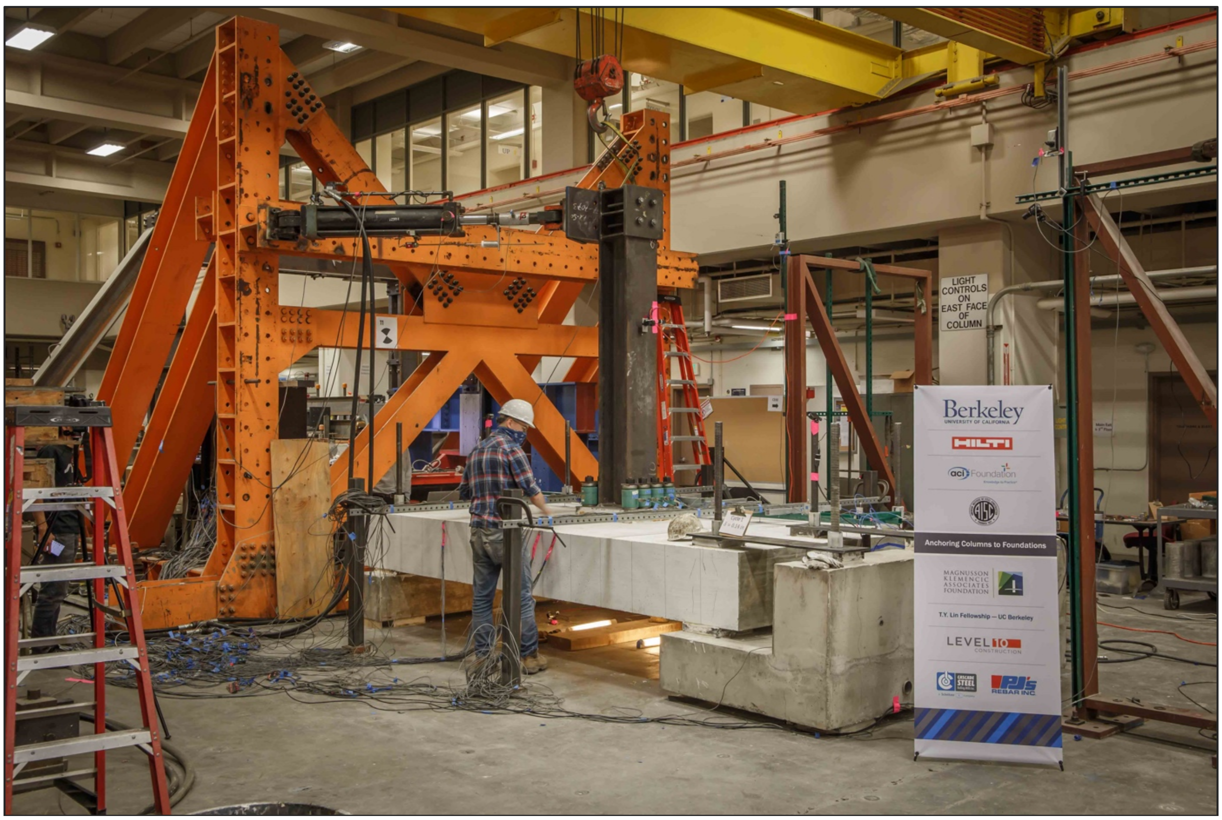

Figure 4-1. Specimen set-up and instrumentation

4.1 INSTRUMENTATION

A total of 91 instruments measuring at a frequency of 2 Hz were used to monitor the specimen behavior during testing. Figure 4-1 shows the final test set-up and instrumentation. The instruments used were:

- 60 strain gages attached to reinforcing steel
- 2 string potentiometers (wire pots)
- 10 load cells
- 17 linear potentiometers

Ten strain gages were placed on longitudinal reinforcing bars. Of these, five were placed on the top layer and five on the bottom layer of the foundation slab as can be seen in the sketches in Figure 4-2. Two strain gages were places on each anchor approximately 3.8” above the anchor bearing surface on opposite sides of the anchor. Finally, one strain gage was placed approximately at mid height (8” from hook end) of each of the 34 “candy cane” reinforcing bars.

Two string potentiometers were used to track the movement of the free end of the column in the North-South and East-West directions (Figure 4-2 and Figure 4-3).

A load cell was placed on each of the eight anchors (Figure 4-5).

Thirteen linear potentiometers were placed on the slab surface to measure the vertical displacements of the concrete and base plate during cyclic loading (Figure 4-6). Finally, four linear potentiometers were used to monitor specimen sliding.

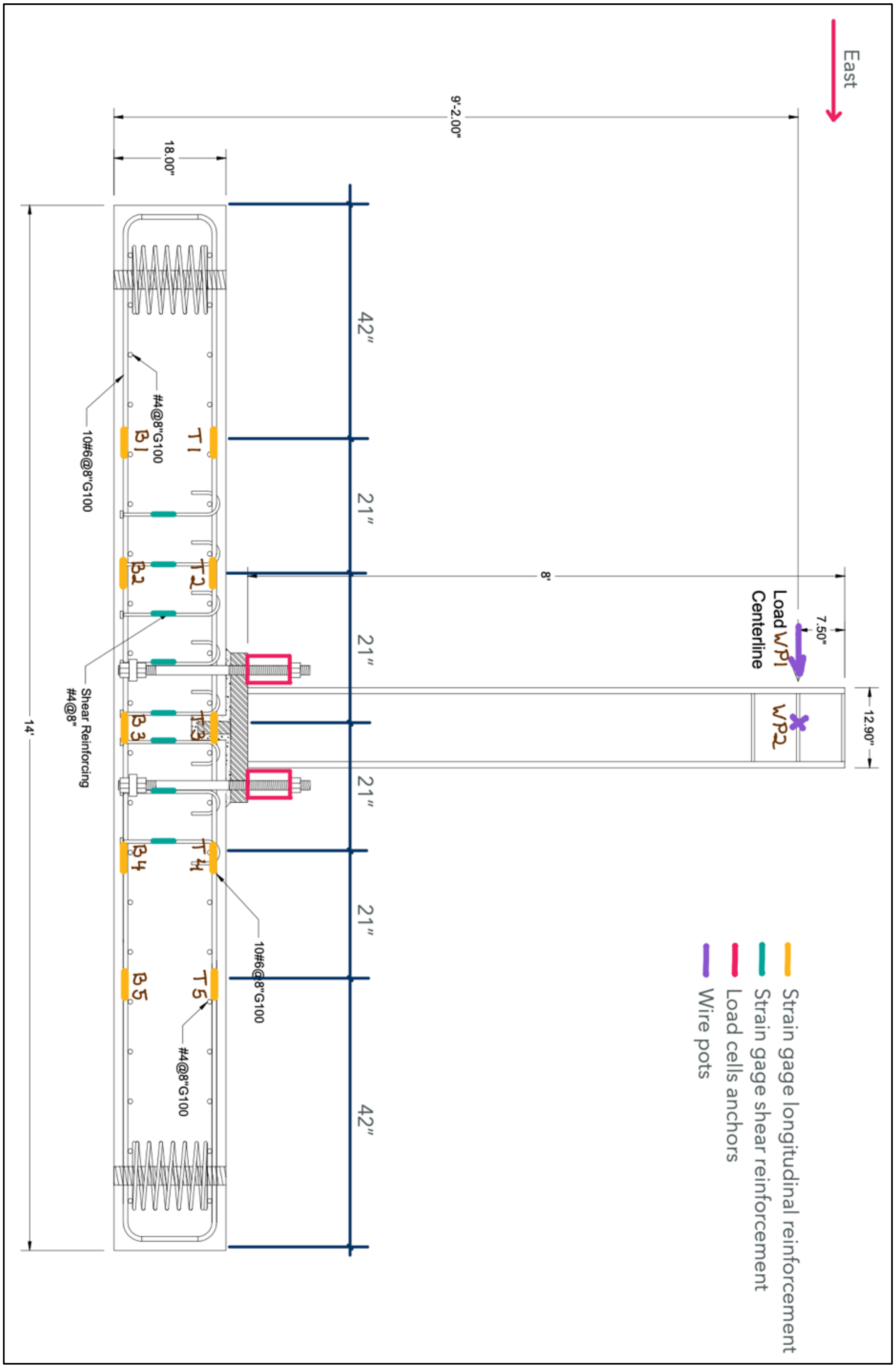

Figure 4-2. Cross section A-A of specimen showing instrumentation

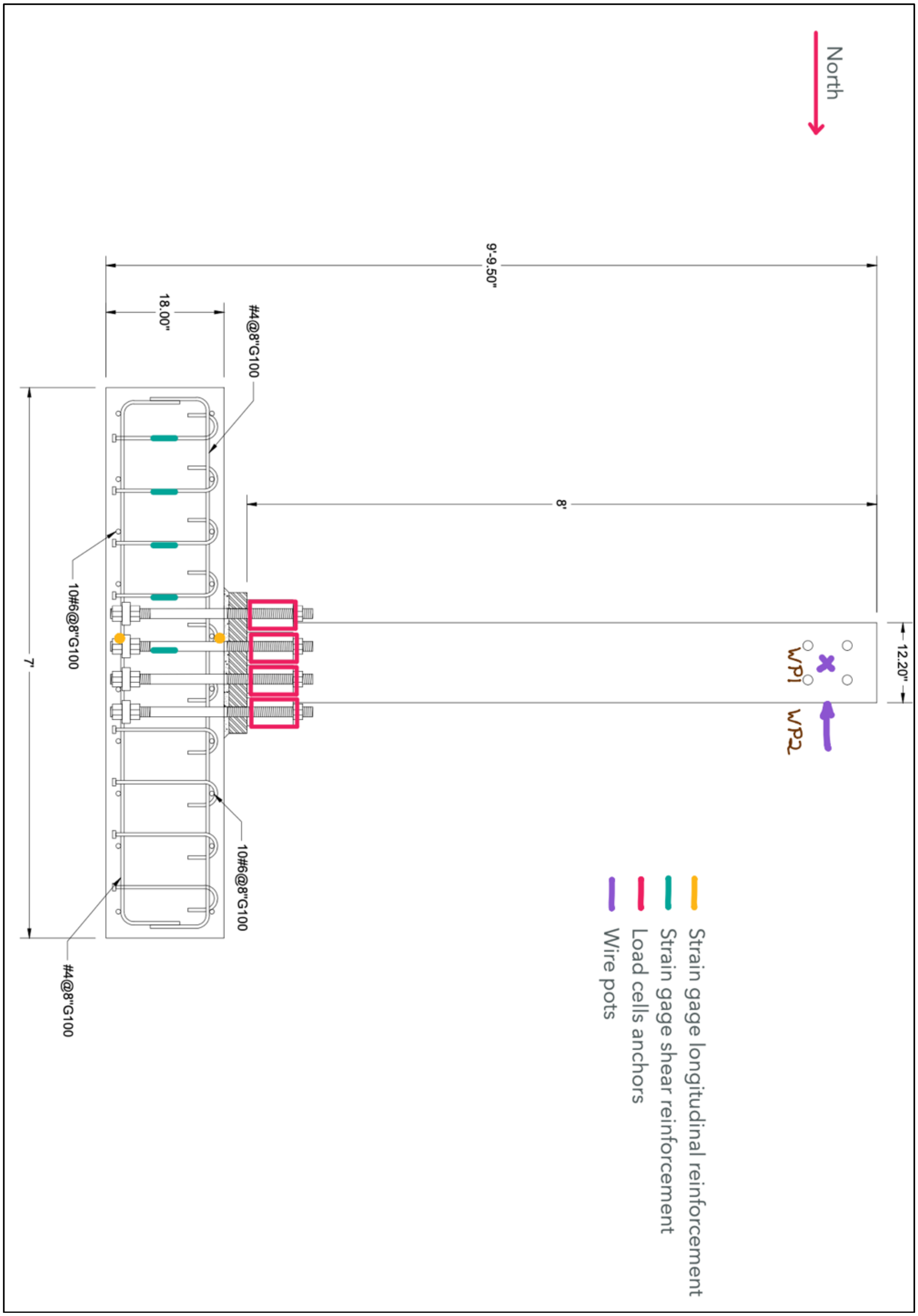

Figure 4-3. Cross section B-B of specimen showing instrumentation

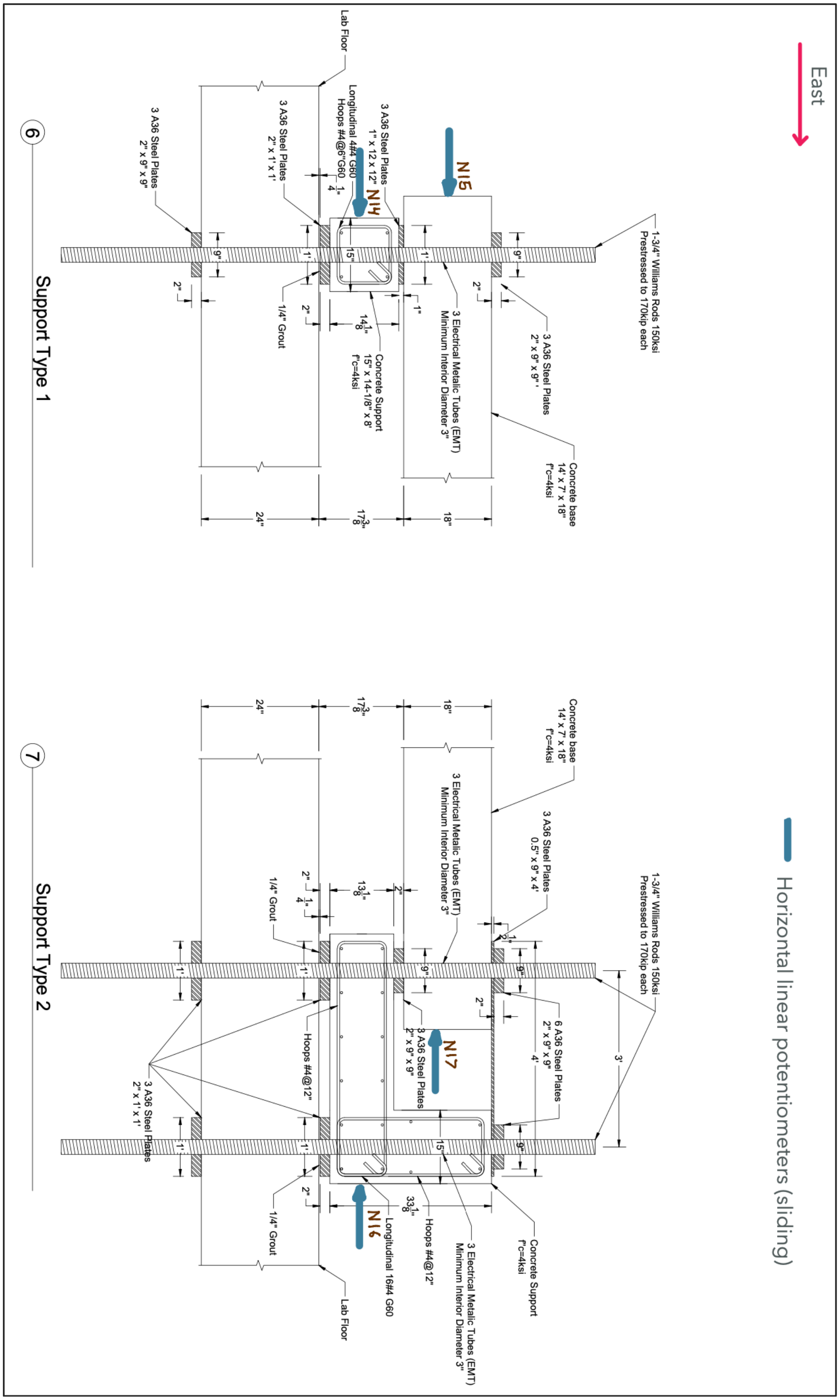

Figure 4-4. Sketch of linear potentiometer location used to measure sliding

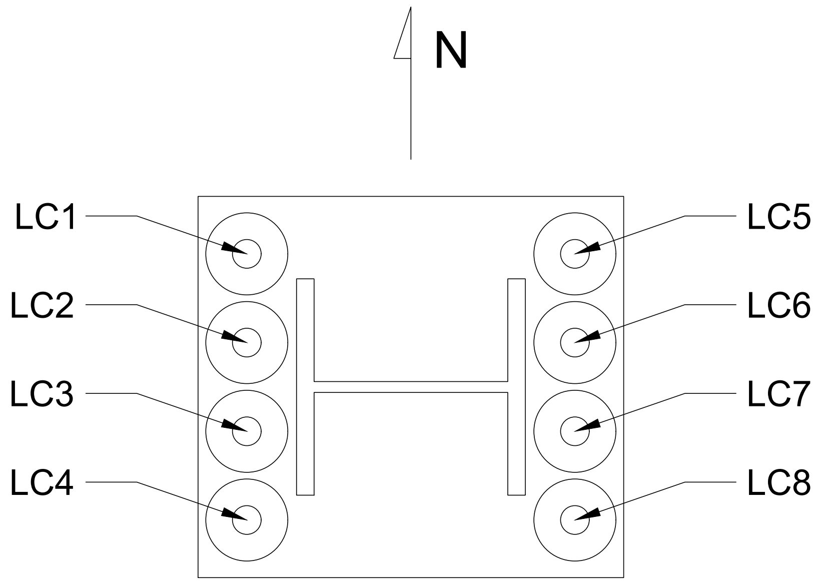

Figure 4-5. Plan view of base plate showing numbering of anchors and load cells

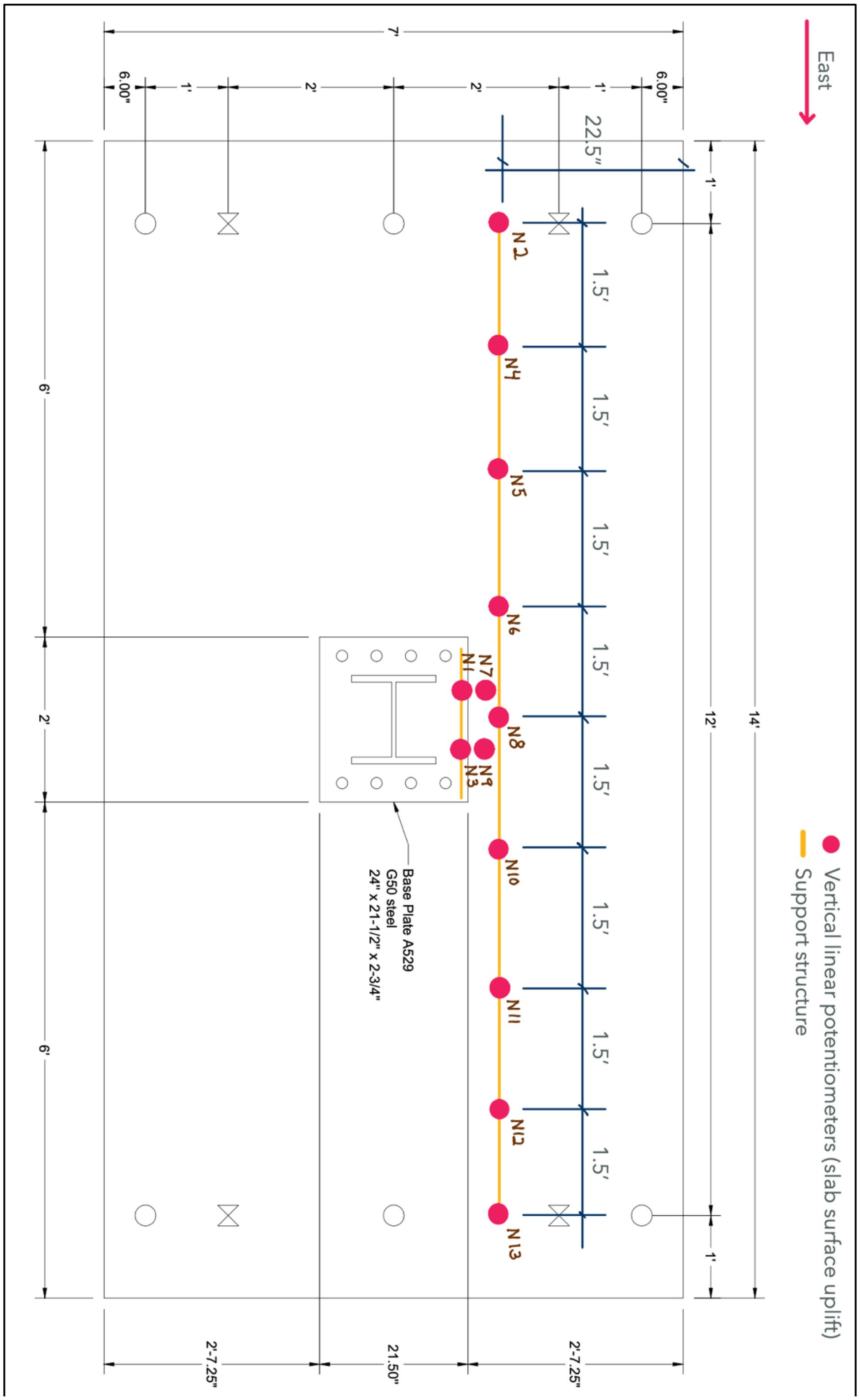

Figure 4-6. Plan view sketch of linear potentiometer location

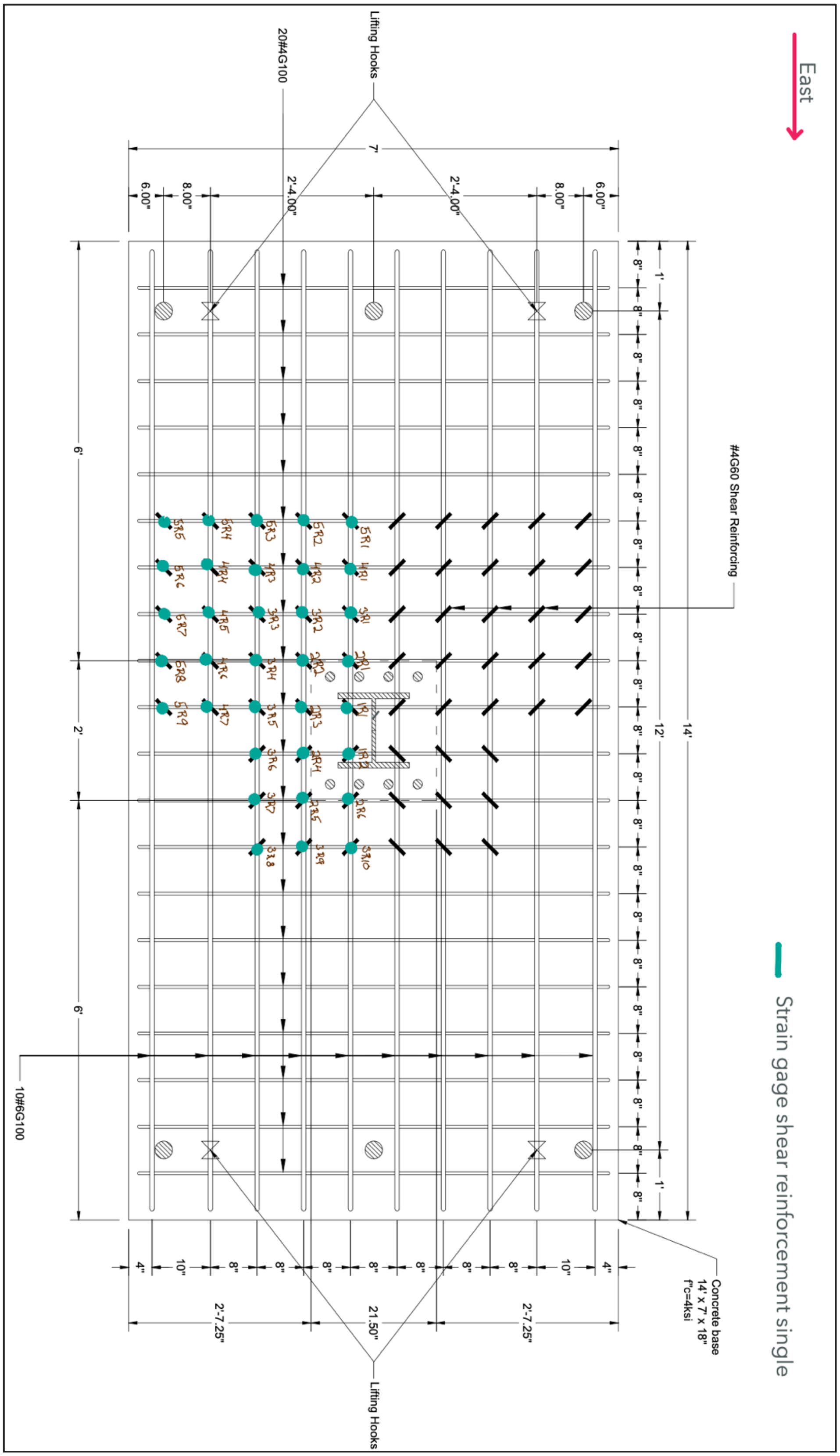

Figure 4-7. Plan view sketch of shear reinforcement strain gage location

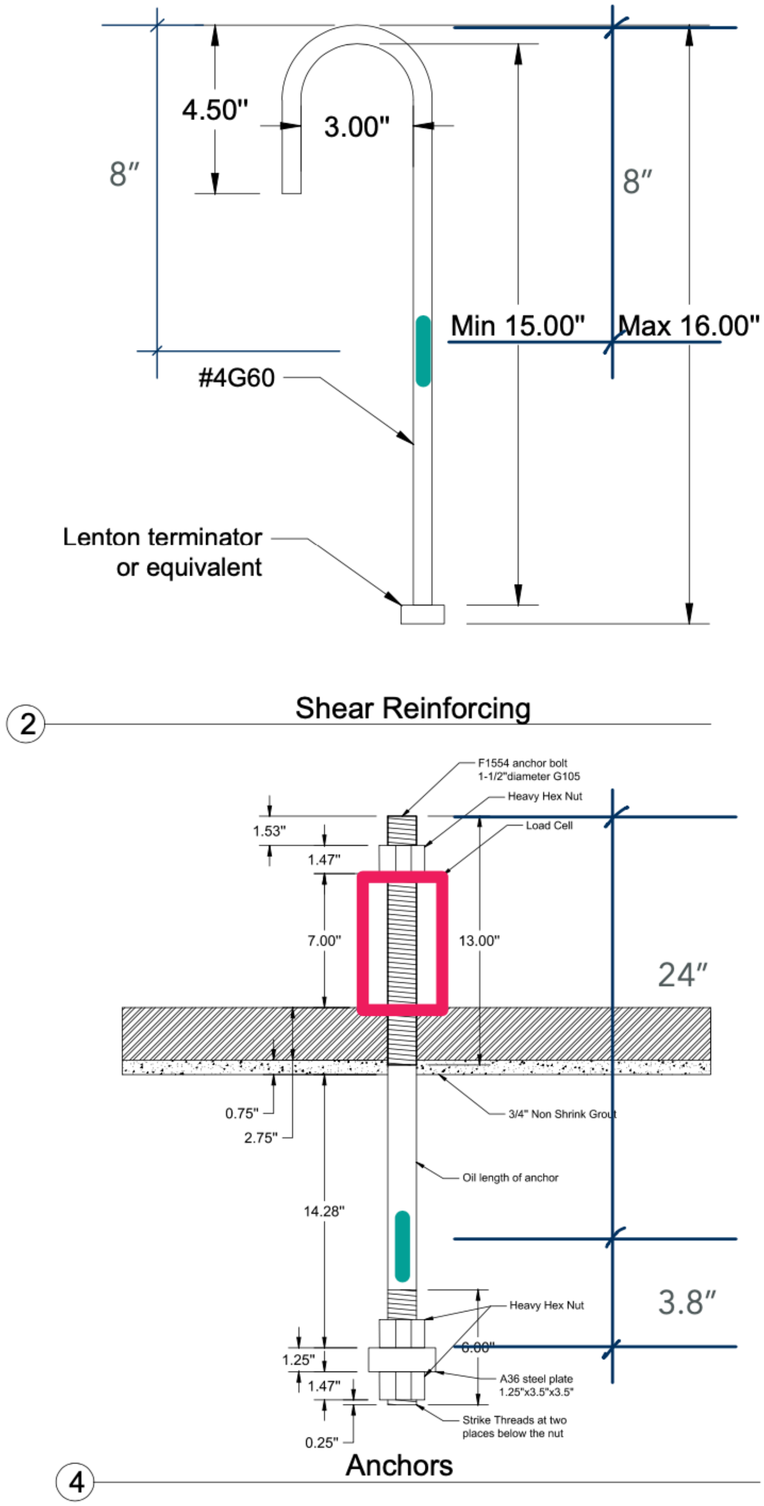

Figure 4-8. Elevation view of strain gage location on shear reinforcing and anchor rods

4.2 LOADING PROTOCOL

The loading protocol was derived from the recommendation of FEMA-461 (2007). The top of the column was subjected to cycles of imposed displacement in the longitudinal direction of increasing amplitudes shown in Table 4-1. Two 45˚ actuators attached to the column were programmed to minimize transverse displacements. Displacements were imposed at a uniform rate, traveling from zero to maximum displacement in 1 min. As can be seen in Figure 4-9, two complete cycles were applied at each amplitude before continuing to the next amplitude. The drift ratio is calculated by dividing the lateral displacement by the vertical distance between the point of load application and the top surface of the slab (92 in.).

Table 4-1. Amplitude of displacement-controlled loading protocol

Cycle	δ (in)	Drift ratio (%)
1	0.14	0.15%
2	0.19	0.21%
3	0.27	0.29%
4	0.38	0.41%
5	0.53	0.58%
6	0.74	0.81%
7	1.04	1.13%
8	1.45	1.58%
9	2.04	2.21%
10	2.85	3.10%
11	3.54	3.85%
12	4.23	4.60%
13	4.92	5.35%
14	5.61	6.10%

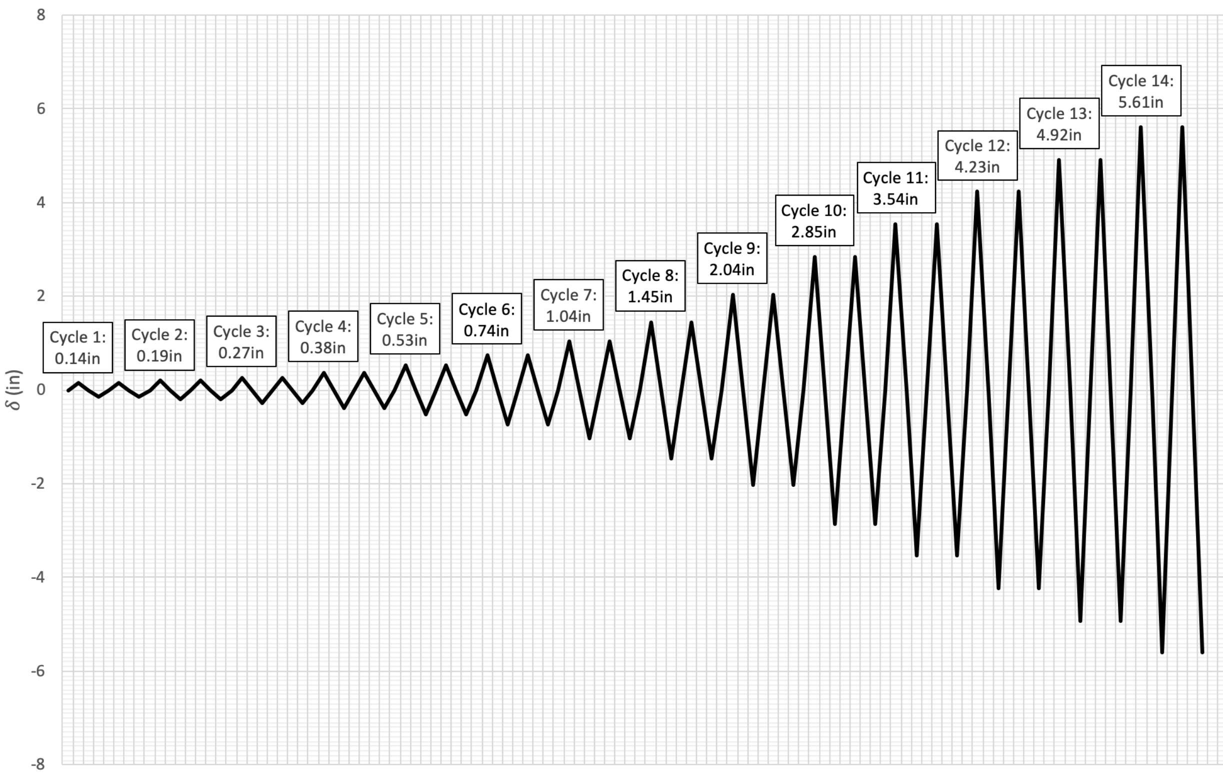

Figure 4-9. Loading protocol imposed to column free end modified from FEMA-461 (2007)

The loading was paused after the first positive and negative peaks of each new displacement target at 50% of the maximum displacement to document crack sizes and propagation.

5 RESULTS

5.1 PICTURES AND VIDEOS

Table 5-1 summarizes the links to one video of the casting and six videos of the testing.

Table 5-1. Links to videos of specimen M02

Video Title	YouTube Link
2020.09.03 M02 Casting column-foundation specimen	https://www.youtube.com/watch?v=yesNQfyEMcs&ab_channel=BenjaminWorsfold
2020.10.07 M02 Column-Foundation Connection Front	https://www.youtube.com/watch?v=KfhxoB9XJ7c&ab_channel=BenjaminWorsfold
2020.10.07 M02 Column-Foundation Connection Diagonal	https://www.youtube.com/watch?v=zF13Uddz-4o&ab_channel=BenjaminWorsfold
2020.10.07 M02 GoPro Column	https://www.youtube.com/watch?v=uKckmjJZGjQ&ab_channel=BenjaminWorsfold
2020.10.07 M02 GoPro Bottom East	https://www.youtube.com/watch?v=X-PtR6-sdyY&ab_channel=BenjaminWorsfold
2020.10.07 M02 GoPro Bottom West	https://www.youtube.com/watch?v=GABp54TcXMA&ab_channel=BenjaminWorsfold
2020.10.07 M02 GoPro Top East	https://www.youtube.com/watch?v=Ou4IBt9YSMk&ab_channel=BenjaminWorsfold
2020.10.07 M02 GoPro Top West	https://www.youtube.com/watch?v=ZSGG9aonAMQ&ab_channel=BenjaminWorsfold

Figure 5-1 shows an elevation view of the specimen at peak displacement in both the west and east directions. Column torsion is observed when the column is loaded in the east direction.

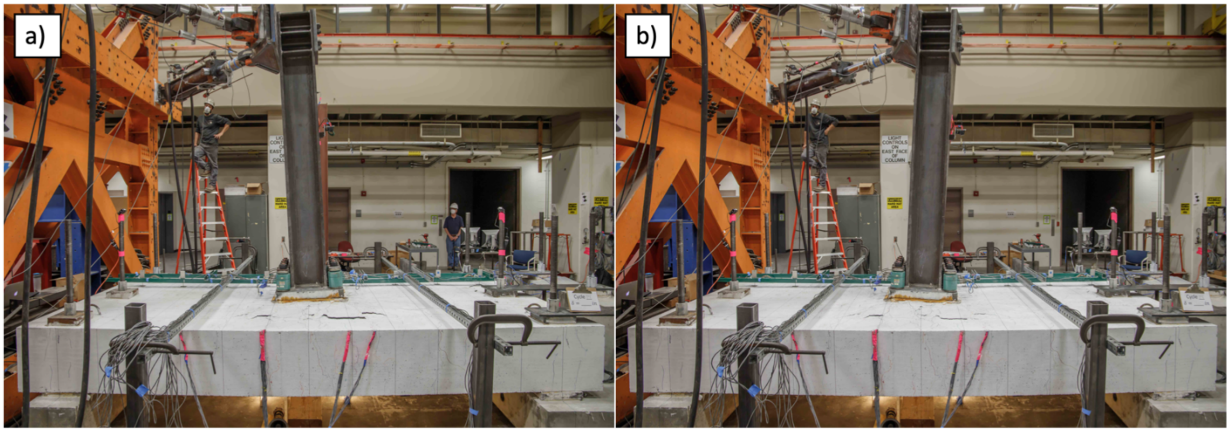

Figure 5-1. Elevation view of specimen at a) maximum westerly displacement and b) maximum easterly displacement

Figure 5-2 shows a plan view of the specimen as seen from a camera attached to the east face of the column. Image a) was taken before the test began, while image b) was taken at the peak easterly displacement. These images show the column free end rotated approximately 7° at the peak easterly displacement. No significant rotation is observed for the peak westerly rotation.

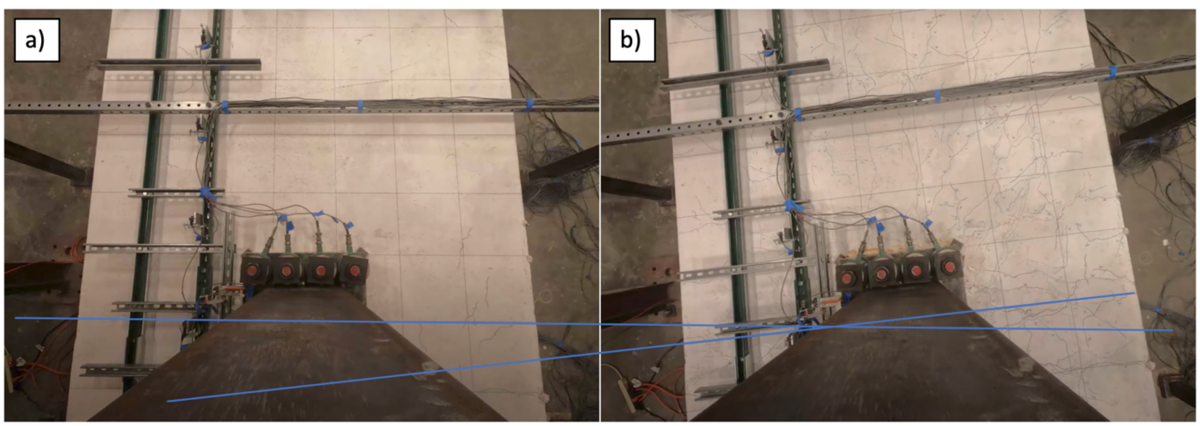

Figure 5-2. Plan view of specimen from the camera attached to east face of column a) before test started and b) at the maximum displacement in the east direction showing approximately an 7° rotation

5.2 CRACK PATTERNS

As was described in section 4.2, the test was paused after each new peak displacement to highlight the emerging crack patterns. The cracks formed at each load cycle were identified with different colors. Figure 5-3 shows the crack patterns at the end of the test on the top surface of the slab and the north and south lateral faces of the slab.

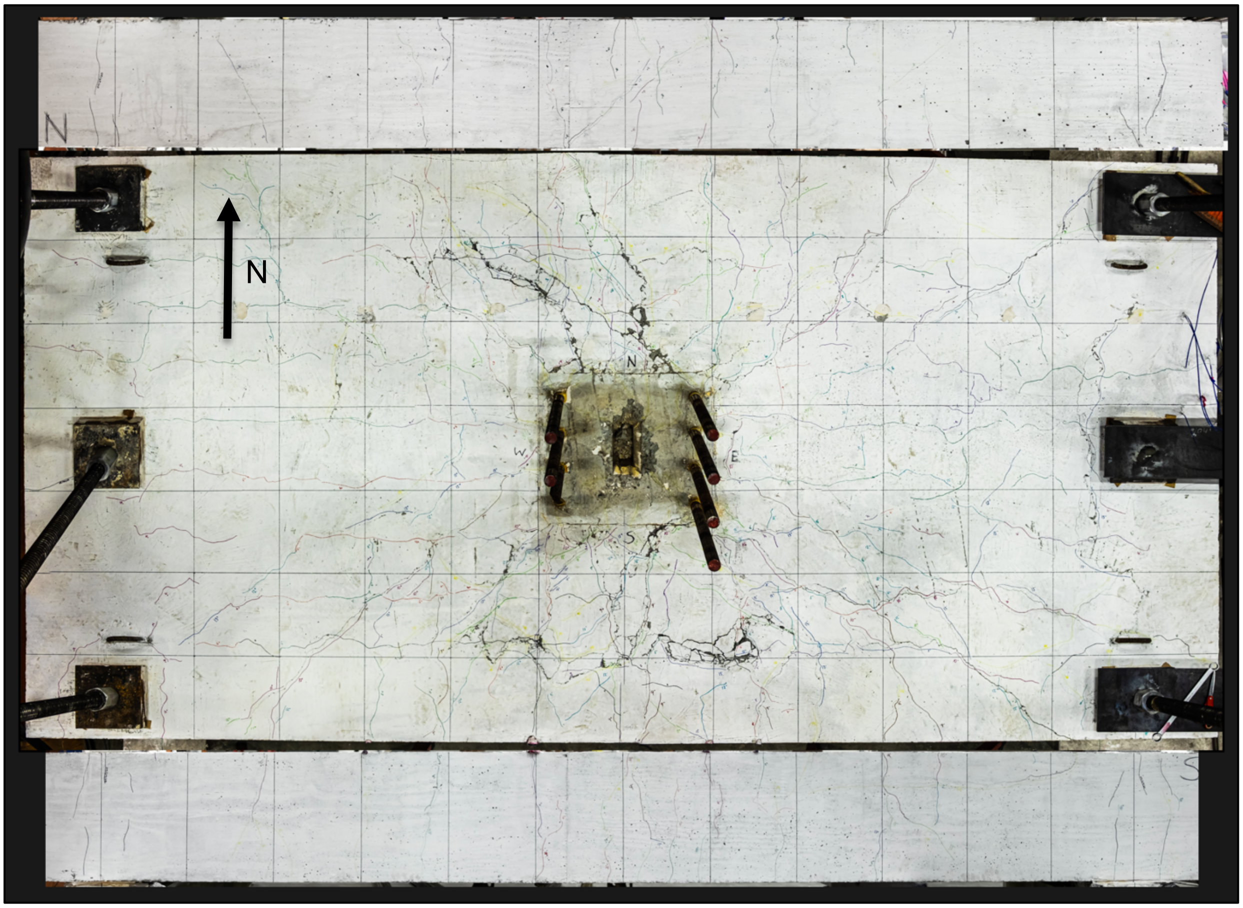

Figure 5-3. Specimen crack pattern after failure, 12 in. x 12 in. grid, top view and two lateral unfolded views

Figure 5-4a) shows a cross section of the test specimen where two failure cones are clearly observed, one per anchor group. Note that the east failure cone is larger than the west. The east side of the specimen had fewer rows of shear reinforcing and they are all contained within the failure cone. The west side had two additional rows of shear reinforcing and the failure cone does not contain all the rows. Figure 5-4b) shows a plan view of the specimen after failure and highlights the regions that sounded hollow when struck. The hollow sound corresponds with the outer edges of the breakout cone. Surface crack patterns indicate a larger failure cone on the east side than on the west.

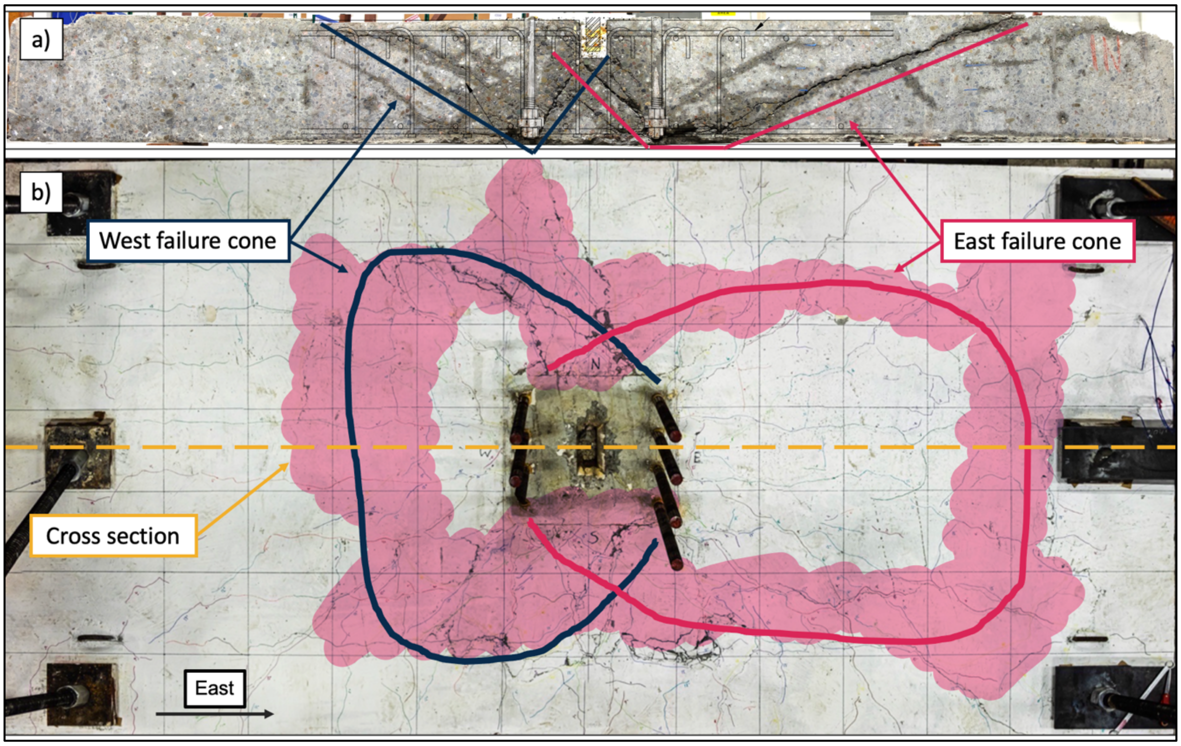

Figure 5-4. a) Specimen cross section and b) plan view highlighting crack patterns and breakout cone geometry, with 12-in. x 12-in. [305 mm x 305 mm] grid for specimen M02. The shaded region produced a hollow sound when knocked.

Cracking was observed on the bottom surface of the specimen as shown in Figure 5-5 and Figure 5-6. Radial cracks were observed to radiate out from the anchor groups. Punching of the anchors through the bottom of the slab was not observed.

Figure 5-5. Damage observed on the bottom surface of the specimen after failure as seen from west to east

Figure 5-6. Damage observed on the bottom surface of the specimen after failure as seen from east to west

5.3 INSTRUMENTATION READINGS

Figure 5-7 plots the force applied to the column free end against the column drift ratio. Each cycle, after cycle 8, is plotted with a different color. The specimen was loaded in the E-W direction. Positive displacement signifies movement towards the east. The E-W and N-S movement of the column free end was triangulated using measurements from two wire pots. The drift ratio was calculated by dividing the E-W displacement by the vertical distance between the point of load application to the top surface of the slab (92 in.). The load was calculated taking the E-W component of the two actuators. No sudden failure was observed. The specimen failed in a ductile manner and was able to achieve more than 4% drift ratio in each direction without a loss in strength.

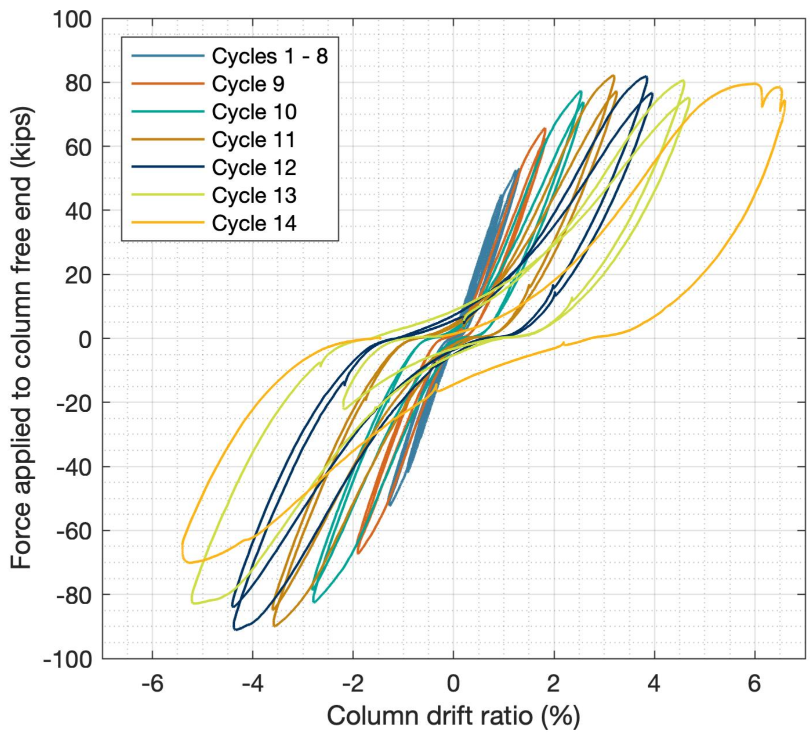

Figure 5-7. Force applied to column free end against column drift ratio (Positive drift ratio is movement to the east)

Figure 5-8 overlays the loading in both directions from Figure 5-7 and shows that the initial stiffness in both directions is similar. The peak load was about 10% larger when loading the east anchor group.

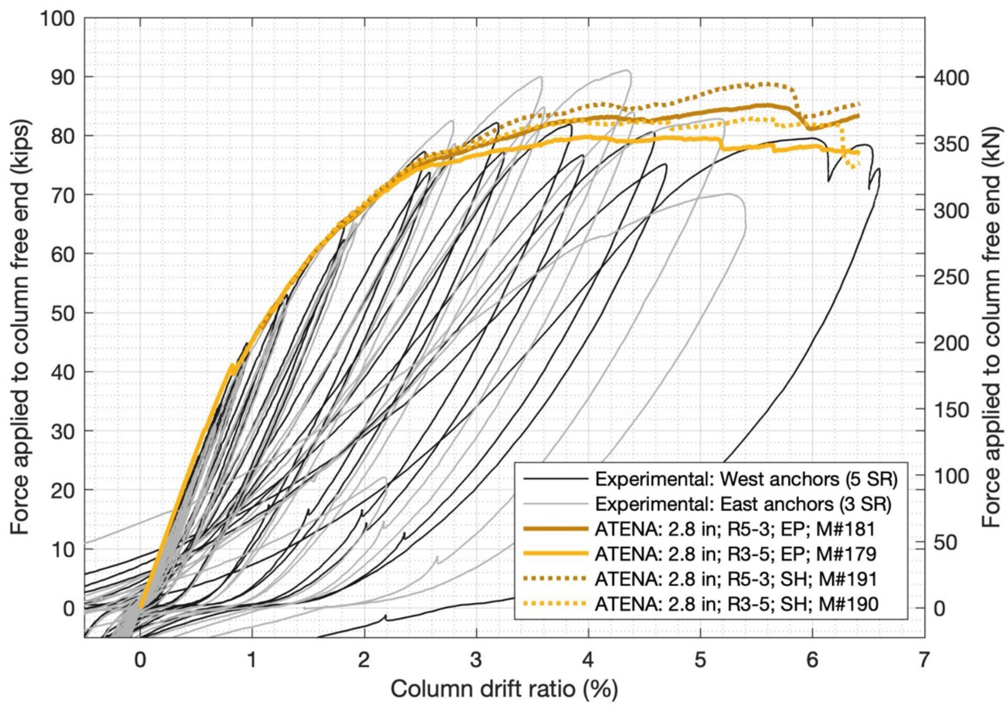

Figure 5-8. Force applied to column free end versus column drift ratio for east and west anchor groups and various ATENA finite element blind predictions

Figure 5-9 plots the column free end displacement over time. The loading was paused after each new displacement goal was passed at about 50% of peak displacement. A pause shows up as a horizontal line.

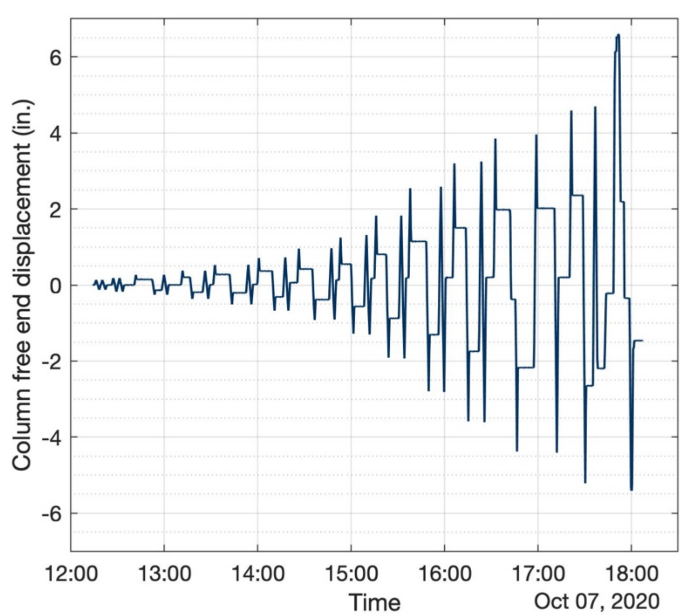

Figure 5-9. Column free end displacement versus time.

Pauses in loading appear as horizontal lines.

Table 5-2 shows the maximum force and drift ratio (DR) for each cycle compared with the displacement goal. The measured DR tends to be lower than the DR goal for each cycle. Figure 5-10 plots the ratio of peak column force and peak DR for each cycle for the west and east loading directions. Up until cycle 8, the peak column force and DR were larger when loading the west anchor group. Between cycles 9 and 13, the peak column force and DR were larger when loading the east anchor group. During cycle 14, the final cycle, the east anchor group had already failed, so the displacement goal was not increased for that loading direction. The displacement goal for the west side was increased. The maximum difference between loading in the east and west directions was about 10% both in terms of column load and DR.

Table 5-2. Maximum displacement and force applied to column free end per cycle

Cycle	DR Goal	West Anchor Group		East Anchor Group	
		Max DR	Max Force (kips)	Max DR	Max Force (kips)
1	0.15%	0.13%	6.7	0.13%	6.4
2	0.21%	0.18%	9.3	0.17%	8.5
3	0.29%	0.27%	13.1	0.26%	12.0
4	0.41%	0.38%	18.5	0.37%	16.9
5	0.58%	0.53%	25.8	0.51%	23.8
6	0.81%	0.73%	34.8	0.67%	31.4
7	1.13%	0.97%	44.9	0.92%	41.9
8	1.58%	1.31%	53.1	1.30%	52.4
9	2.21%	1.82%	65.8	1.93%	67.4
10	3.10%	2.58%	77.3	2.82%	82.5
11	3.85%	3.25%	82.2	3.61%	90.0
12	4.60%	3.96%	81.9	4.41%	91.1
13	5.35%	4.70%	80.6	5.21%	82.8
14	6.10%	6.60%	79.6	5.41%	70.1

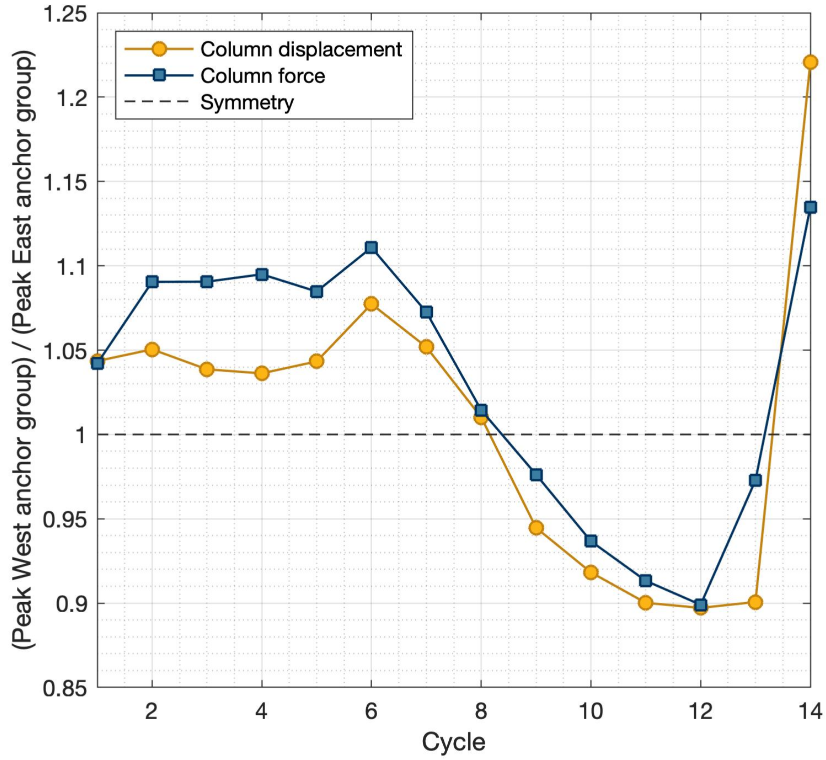

Figure 5-10. Ratio of east and west loading directions for the peak column displacement and peak column force

The specimen begins to leave the elastic region in both loading directions at cycle 8 at an average DR = 1.3%. The specimen reaches a yield plateau in both directions at cycle 11 at an average DR = 3.5%. When loading the east anchor group, the DR was increased to DR = 4.4% without a drop in strength. Then the DR was increased to DR = 5.4% with only a 25% drop in load. When loading the west anchor group, the DR was increased to DR = 6.6% without a drop in strength.

Taking the yield DR as the DR from cycle 11 where the yield plateau is reached and taking the maximum DR as the DR before a drop in strength, an approximate displacement ductility capacity can be calculated as (see Table 5-3):

$$\mu = \frac{DR_{max}}{DR_y}$$

Table 5-3. Approximate ductility capacity calculation per loaded anchor group

Anchor Group	Dry (Cycle 11)	DRmax	μ
West	3.25%	6.60%	2.03
East	3.61%	4.41%	1.22

Figure 5-11 graphs the rotation due to the slab flexure and the anchor extension over time at the slab-column interface. The rotation is calculated from the measurements of four linear potentiometers measuring the vertical displacement of the base plate and the concrete surface. Initially, the slab barely rotates and most of the rotation happens due to extension of the anchors. As the test progresses, damage spreads in the concrete and the slab rotation increases significantly. The rotation due to anchor extension does not increase significantly once the yield strength of the specimen is reached because the load in the anchors does not increase.

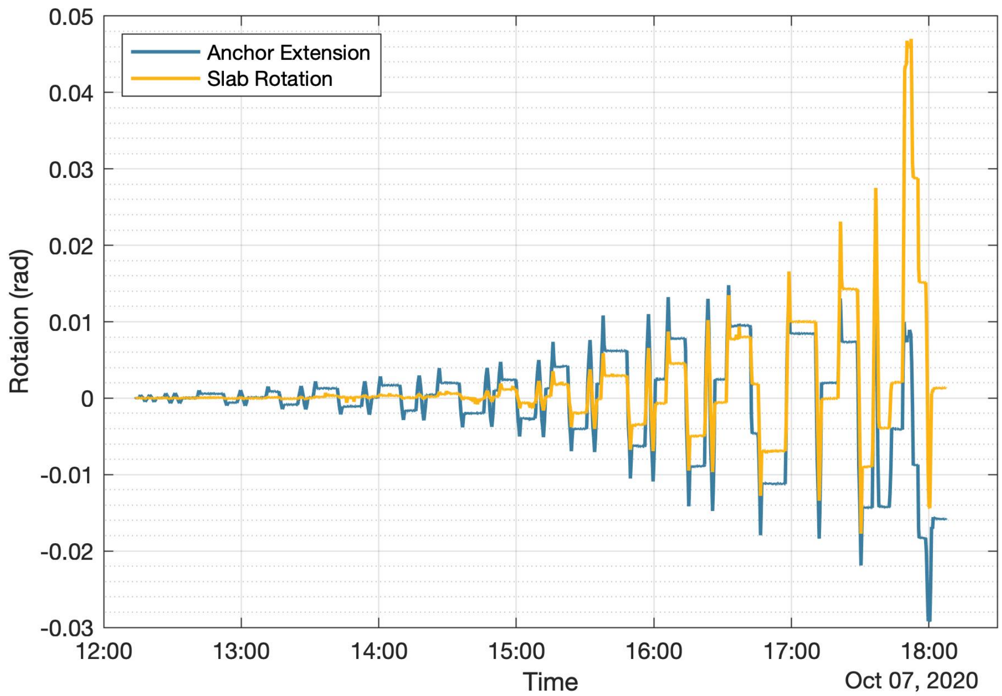

Figure 5-11. Rotation due to slab and anchor extension over time

Figure 5-12 plots the displacement of the column free end versus time and subdivides the displacement into contributions due to slab rotation, anchor extension, elastic column flexure, and elastic column shear. The column elastic deflection is calculated with the elastic theory knowing the load applied to the column free end and the column stiffnesses. The remainder of the displacement is attributed to experimental error. Initially the majority of the displacement is due to the elastic deformation of the column and anchor extension. As damage progresses in the concrete, the contribution of the slab rotation increases while the contribution of the elastic column decreases. The contribution of the anchor extension remains relatively constant once the specimen enters yielding behavior as the load on the specimen does not increase.

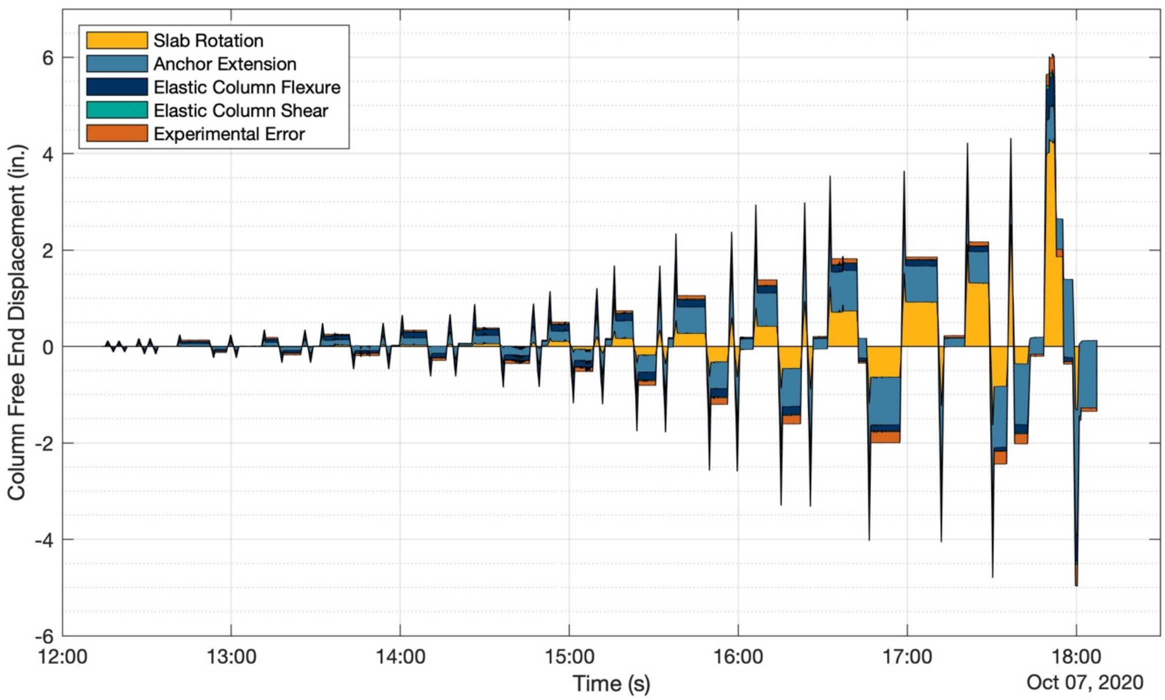

Figure 5-12. Column free end displacement subdivided into contributions from the slab rotation, anchor extension, elastic column flexure, and elastic column shear, and experimental error versus time

Figure 5-13 shows the load in each anchor group versus time as measured by the load cells on each individual anchor. The initial prestress is observed to decrease as loading progresses and disappears completely after about seven cycles. Relaxation of the specimen is not observed when the loading is paused.

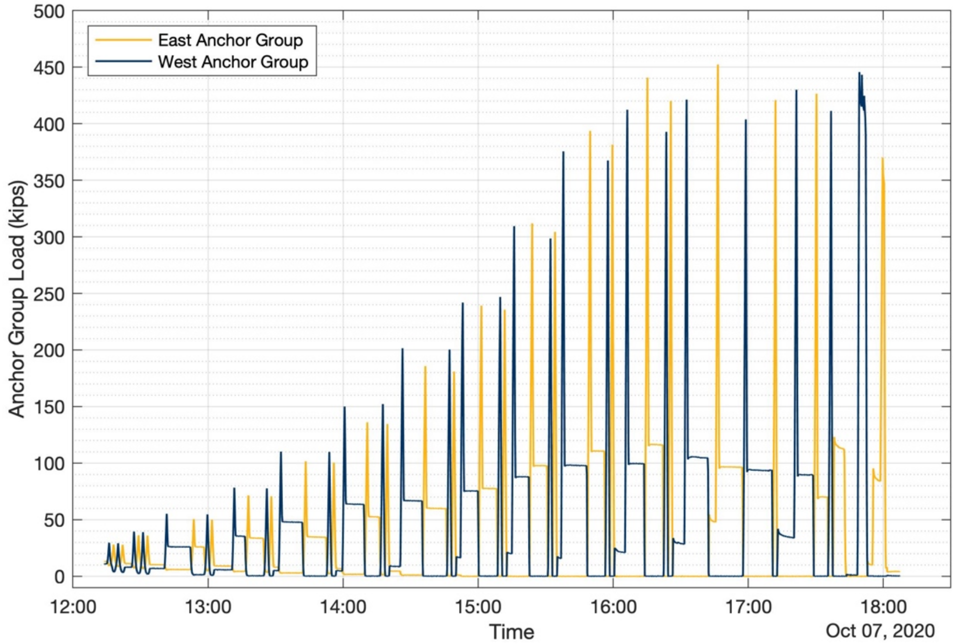

Figure 5-13. Load in each anchor group as measured by load cells on each anchor over time

Figure 5-14 plots the group anchor loads against the column drift ratio for both the east and west groups as well as various ATENA finite element blind predictions. The anchor loads are measured with load cells on each anchor. The initial stiffness is very similar between both loading directions. The peak anchor loads between both loading directions are very similar.
Table ***5-4*** summarizes the maximum loads in each anchor group. Similar to what is observed in Figure 5-8, no sudden drop in strength is observed. The east anchor group shows a very gradual drop in strength.

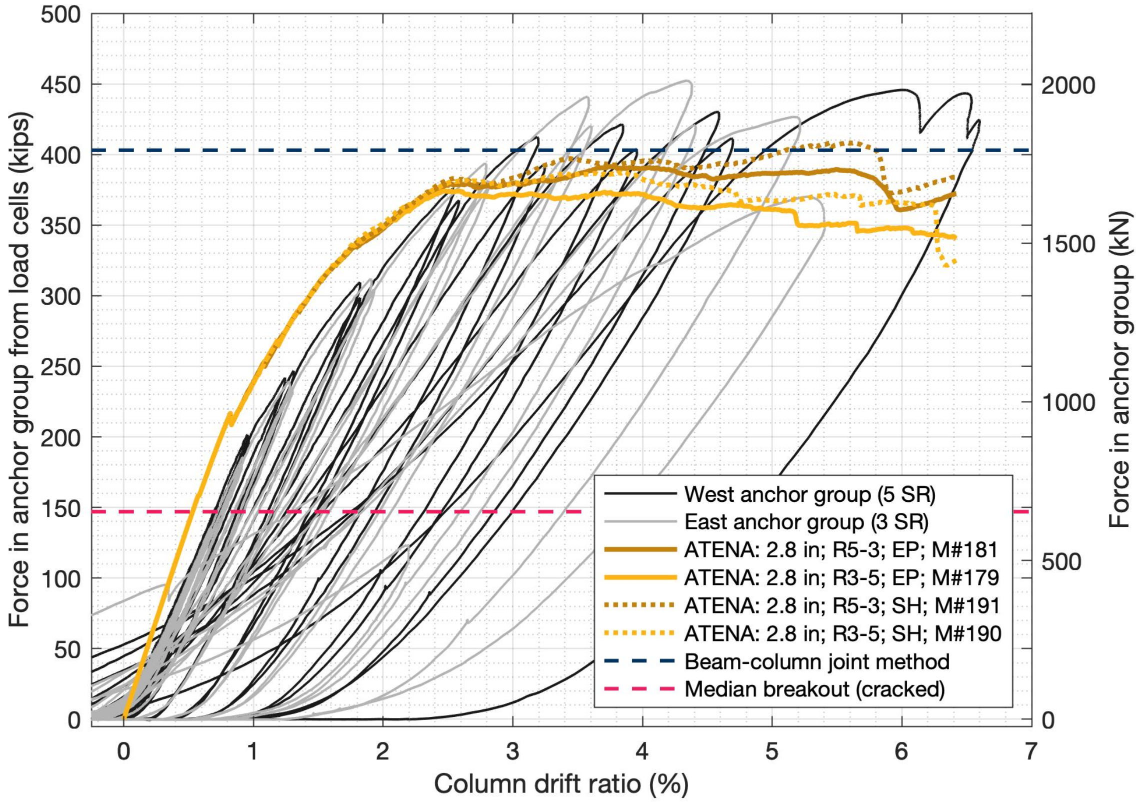

Figure 5-14. Anchor group load versus column drift ratio, experimental data and various ATENA FEM blind predictions (anchor loads from load cells)

Table 5-4. Maximum anchor load for east and west anchor groups as measured by load cells or strain gages

Anchor Group	Max Anchor Load (kips)	
	Load cells	Strain gages
West	446	458
East	452	458

Figure 5-15 plots the same diagram as Figure 5-14 except that the anchor loads are calculated from strain gage measurements on the anchor rods. Before reaching the yield plateau, the loads as measured by the strain gages, are lower than the loads measured by the load cells. This may be because part of the load measured by the load cell is transferred into the concrete through anchor bond. This bond acts on the portion of the anchor rod between the top concrete surface and the strain gage which was placed at mid height (see Instrumentation). Once the yield plateau is reached, the anchor loads measured by these two methods are very similar. The bond between the anchor and the concrete has likely degraded at this point.

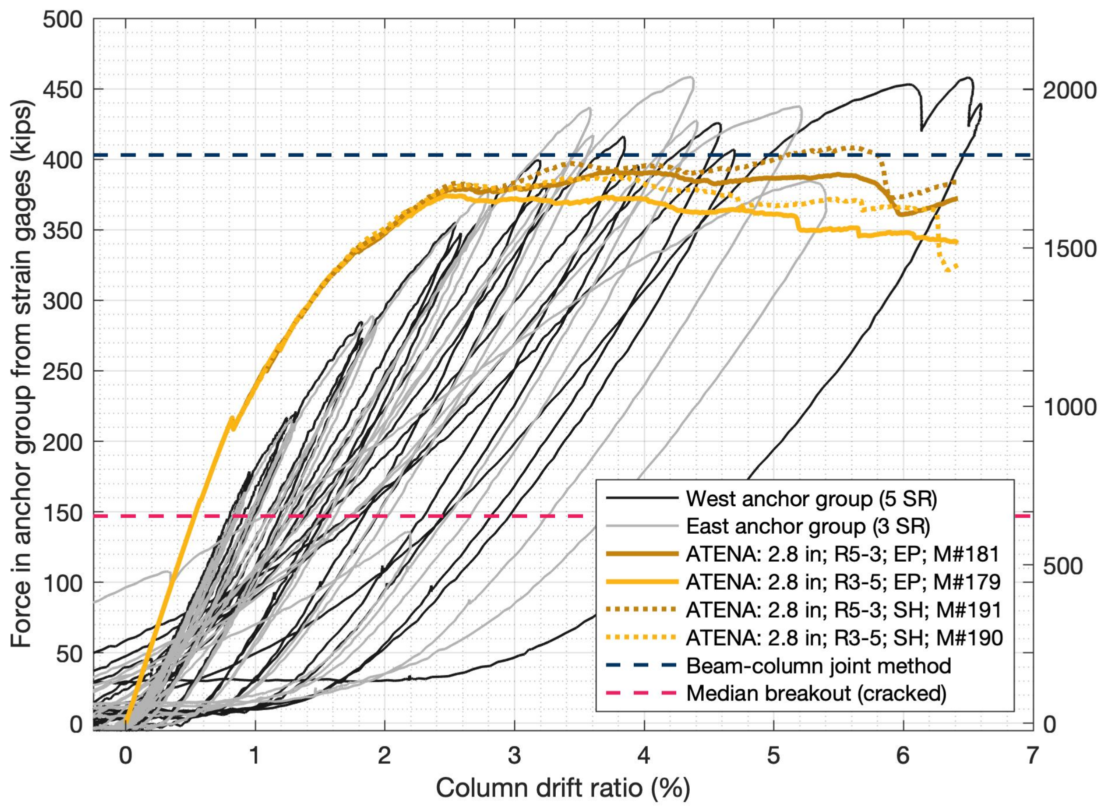

Figure 5-15. Anchor group load versus column drift ratio, experimental data and various ATENA FEM blind predictions (anchor loads from strain gages)

Figure 5-16 and Figure 5-17 plot the anchor group load versus the base plate uplift which serves as a proxy for anchor extension. Figure 5-16 shows the data measured up to cycle 8. Figure 5-17 shows the data for the whole test. The base plate uplift was measured as the difference between the linear potentiometer reading placed vertically on the base plate and slab beside the anchors. Both anchor groups show similar stiffnesses. The graphs originate at (0,0) which indicates that the initial prestressing was successful at eliminating the gap between the base plate and the slab. The east anchor group begins to show some hardening behaviors as loading progresses and the anchor prestressing is lost. Figure 5-17 shows that as loading progresses past cycle 8, the gap between the base plate and the slab increases and the anchor prestressing is lost. A distinct hardening behavior is observed for both anchor groups. The asymmetric behavior during the last load cycle caused the west anchor group to develop a negative gap value.

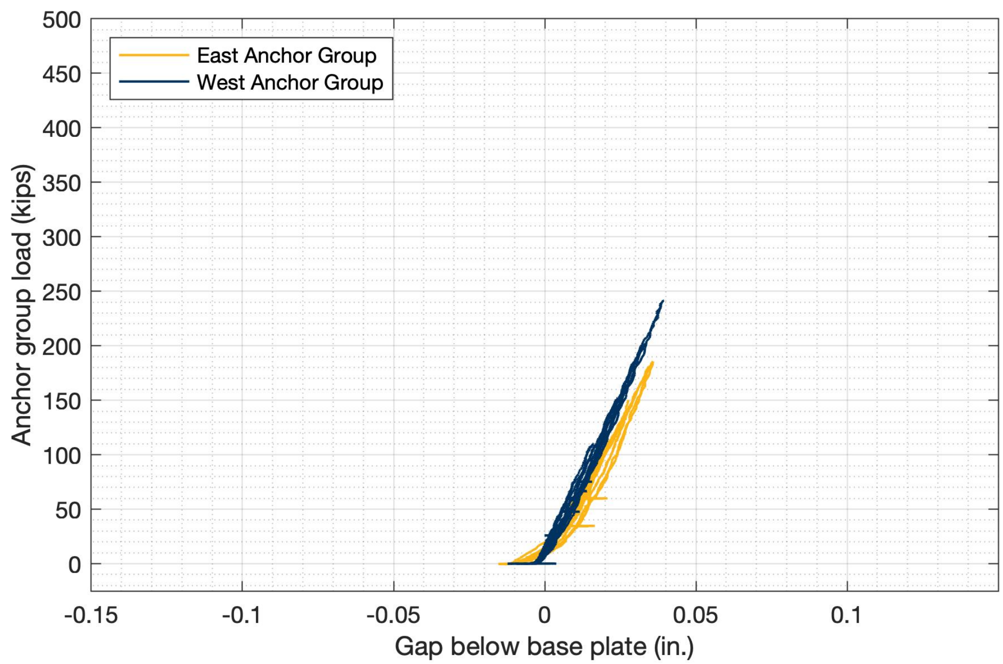

Figure 5-16. Anchor group load against gap below base plate (proxy for anchor extension) as measured by load cells on each anchor and linear potentiometers on base plate and slab (up to cycle 8)

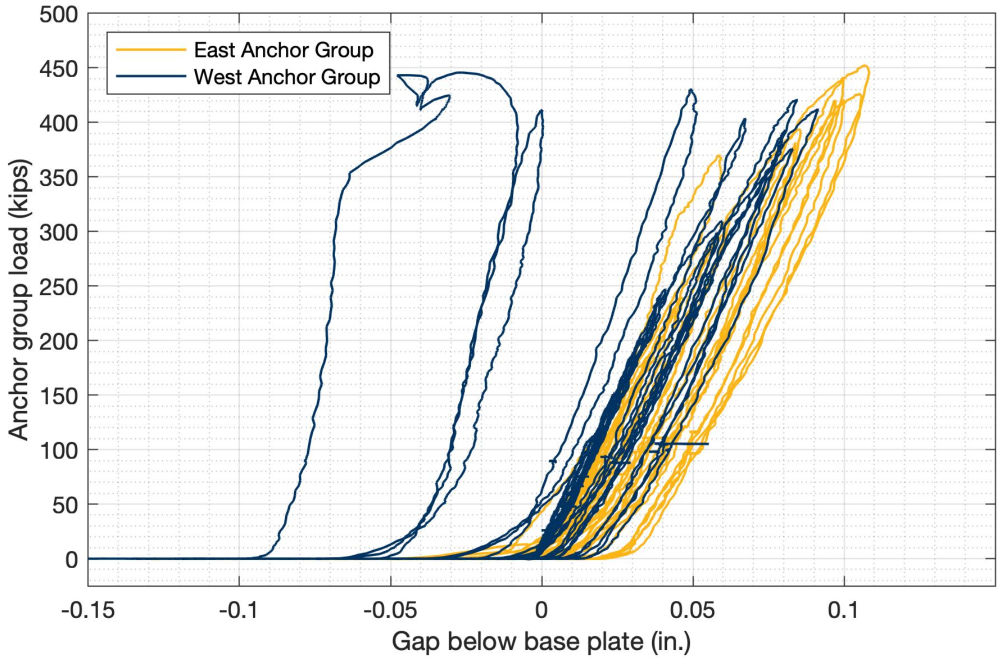

Figure 5-17. Anchor group load against gap below base plate (proxy for anchor extension) as measured by load cells on each anchor and linear potentiometers on base plate and slab (full test)

As described previously, two actuators were attached to the column free end at about 45° to the loading direction and programmed to constrain movement to the longitudinal direction only. Figure 5-18 shows a plan view of the measured displacement of the column free end. When loading towards the west, very little lateral sway was observed. When loading towards the east, some lateral sway towards the south is visible. The pictures in Figure 5-1 show that the actuators are causing torsion in the column and pushing it towards the south. This pattern was also observed in test specimen M01.

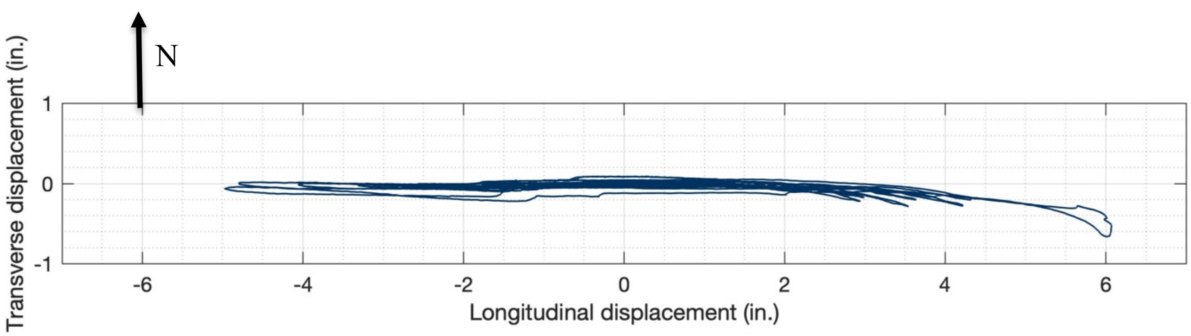

Figure 5-18. Plan view of the displacement of the column free end triangulated with measurements from wire pots 1 and 2 (positive displacement is north and east)

Figure 5-19 plots the force – displacement relationship for the column free end in the transverse Y direction (N-S). The two actuators attached to the column free end were programmed to move the column solely in the longitudinal direction (E-W). For most of the test, the column did not displace significantly in the transverse direction. During the final few cycles, the column began to sway south (negative drift). The actuators applied a force towards the north (positive load) to try to bring the column back to center. This pattern was also observed for test M01.

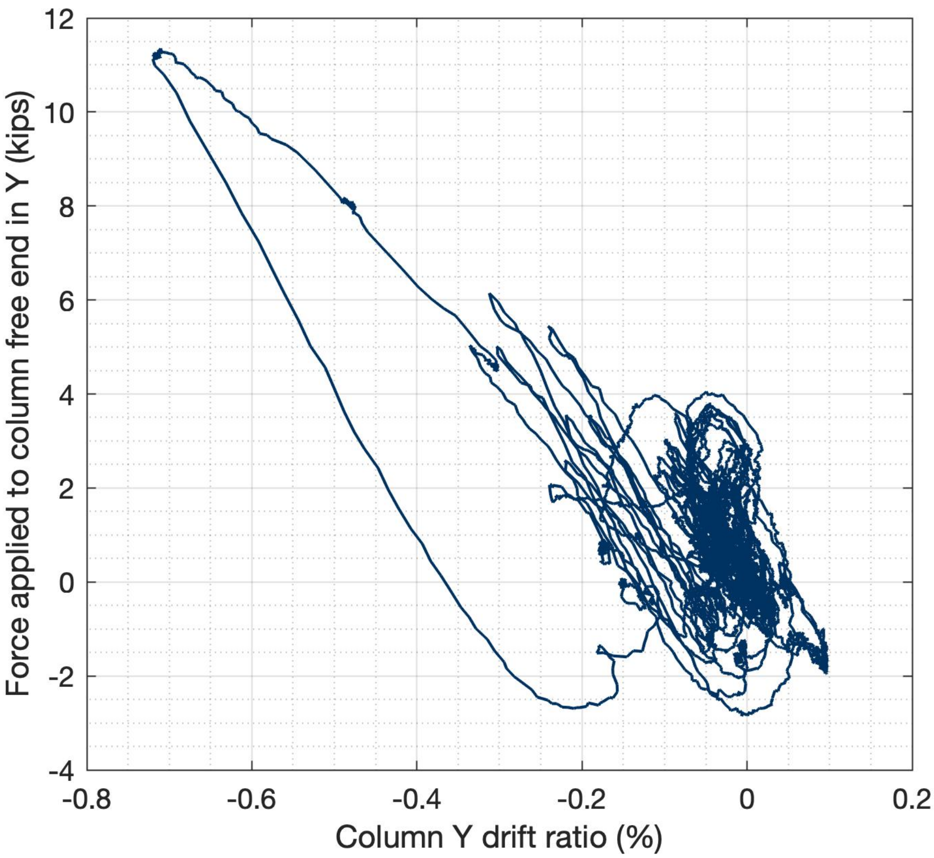

Figure 5-19. Force applied to the column free end in the Y direction (N-S) versus drift ratio in the Y direction (positive load and displacement is towards the north)

If the specimen were perfectly symmetric along the longitudinal axis (creating symmetric north and a south halves), and if the loading were applied perfectly in the longitudinal direction with no transverse loading, then the readings from the north anchor load cells would be identical to the corresponding symmetric south anchors. Figure 5-20 plots the load in each north anchor against the load in the corresponding symmetric south anchor for each anchor group (see Figure 4-5 for anchor numbering). For most of the test no significant asymmetry is observed. Some asymmetry is appears while loading the east anchor groups during post failure cycles.

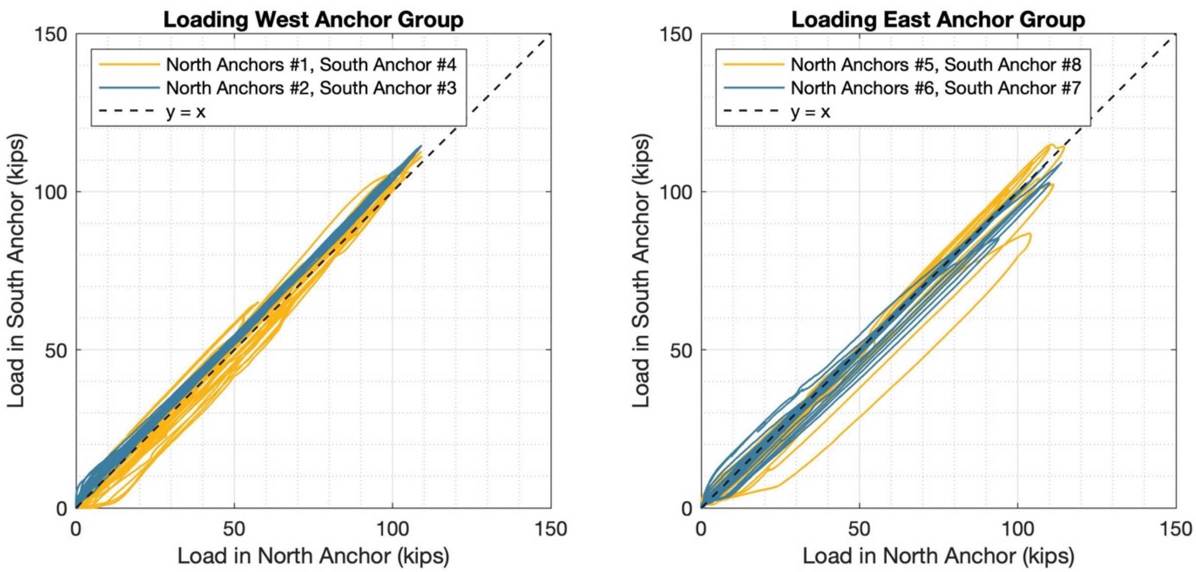

Figure 5-20. Plot of the load in each north anchor versus the load in the corresponding symmetric south anchor for the east and west anchor groups separately

Figure 5-21 plots the loads in the outer anchors number 1, 4, 5, and 8) versus the loads in the inner anchors (number 2, 3, 6, and 7). No significant asymmetry is observed during the test. Both inner and outer anchors seem to carry a similar load. See Figure 4-5 for anchor numbering scheme.

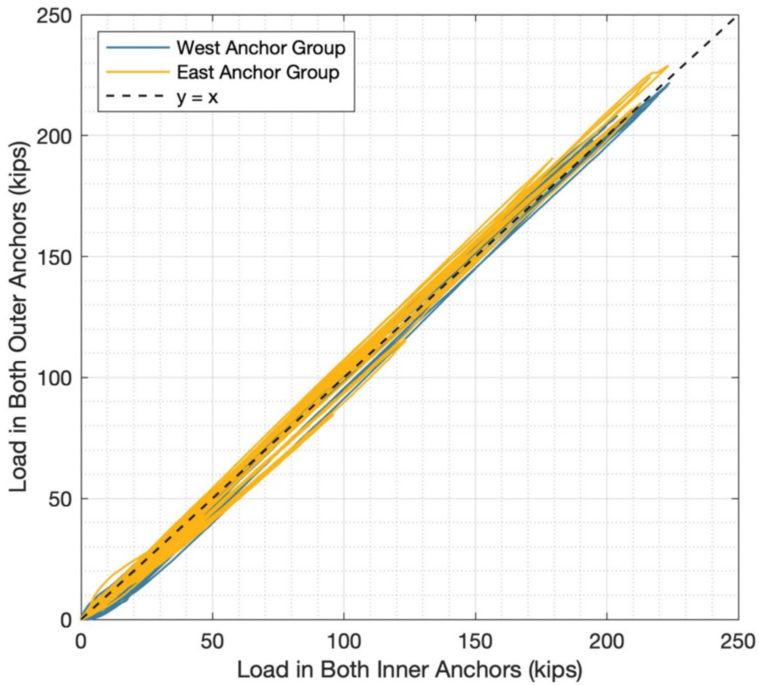

Figure 5-21. Plot of the load in the two inner anchors against the load in the two outer anchors for the east and west anchor groups

Figure 5-22 shows a plan view of the specimen which subdivides the shear reinforcing into five groups / rows. Figure 5-23 shows the maximum strain felt by each shear reinforcing bar. Rows four and five did not yield. Figure 5-25 to Figure 5-29 plot the strain in each shear reinforcing row against the column drift ratio. In these figures the global load – drift ratio plot is also shown to be able to compare the behavior of the shear reinforcement to the specimen global behavior. The first yield of each bar is highlighted. Figure 5-24 shows the moments when each shear reinforcing bar first reaches expected yield strain. Rows one to three all begin to yield during cycle nine at a $DR \approx 1.7\%$. The shear reinforcing in rows four and five did not yield. Yielding begins to happen as the specimen leaves the linear range.

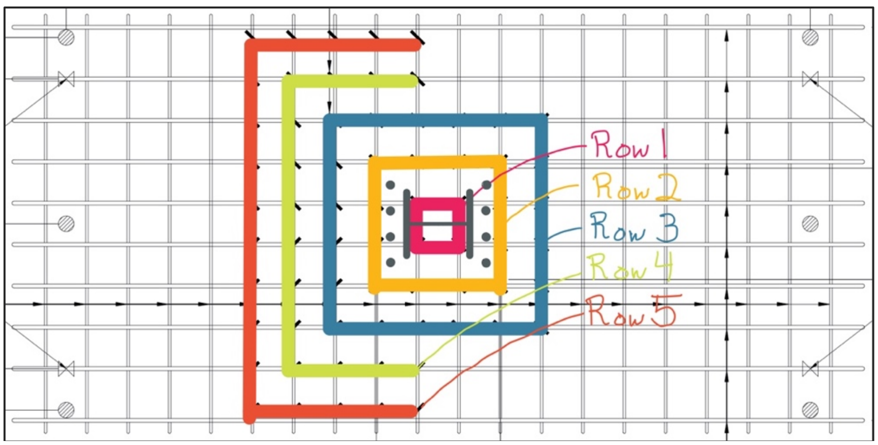

Figure 5-22. Plan view of the specimen separating the shear reinforcing into rows

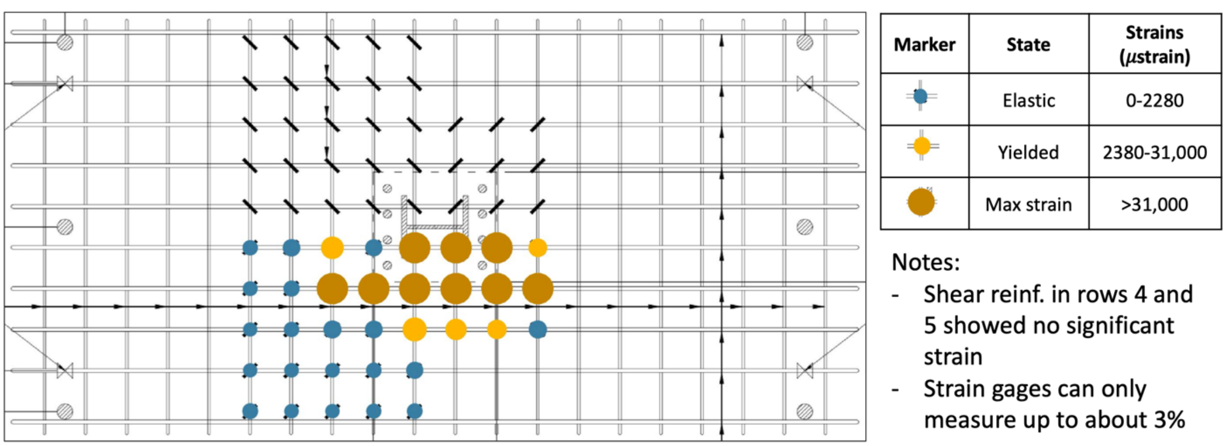

Figure 5-23. Plan view of the specimen showing maximum strain felt by each shear reinforcing bar

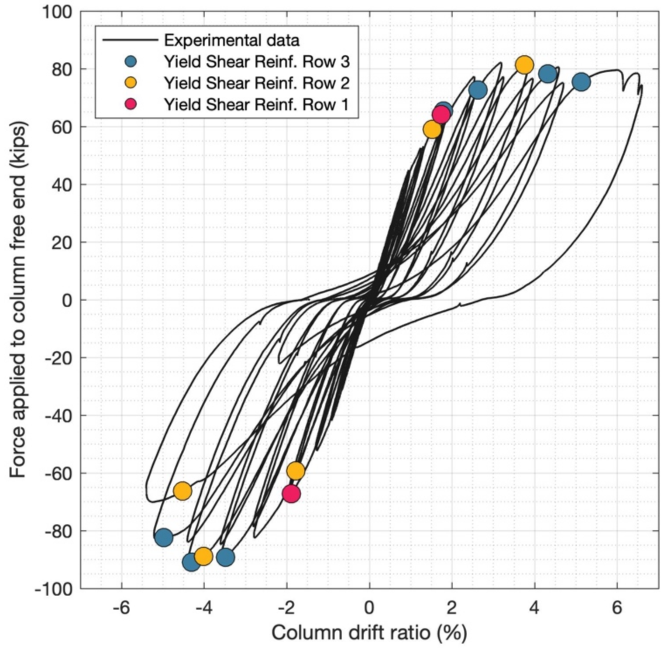

Figure 5-24. Force – drift ratio curve highlighting instances when the shear reinforcing bars first reached the expected yield strain

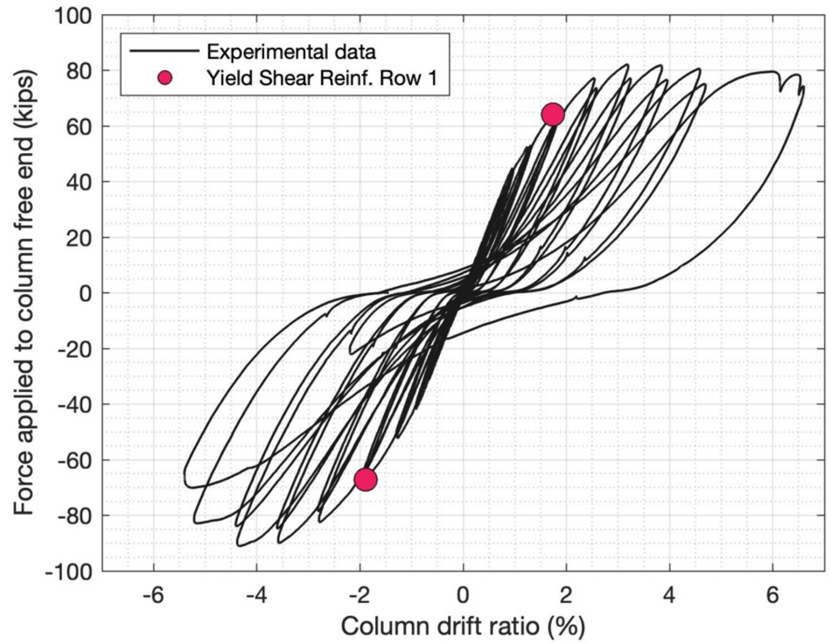

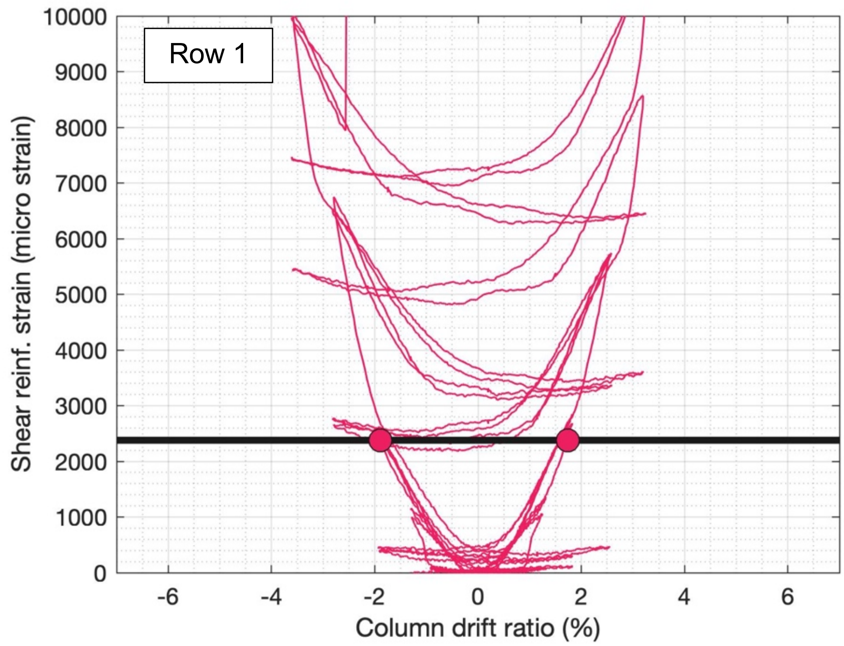

Figure 5-25. Load versus column drift ratio and shear reinforcing strain versus column drift ratio for Row 1. The first yield of each reinforcing bar is shown as a yellow circle. Vertical black lines indicate the first yielding of any reinforcing bar in that row. Expected yield is shown as a horizontal black line

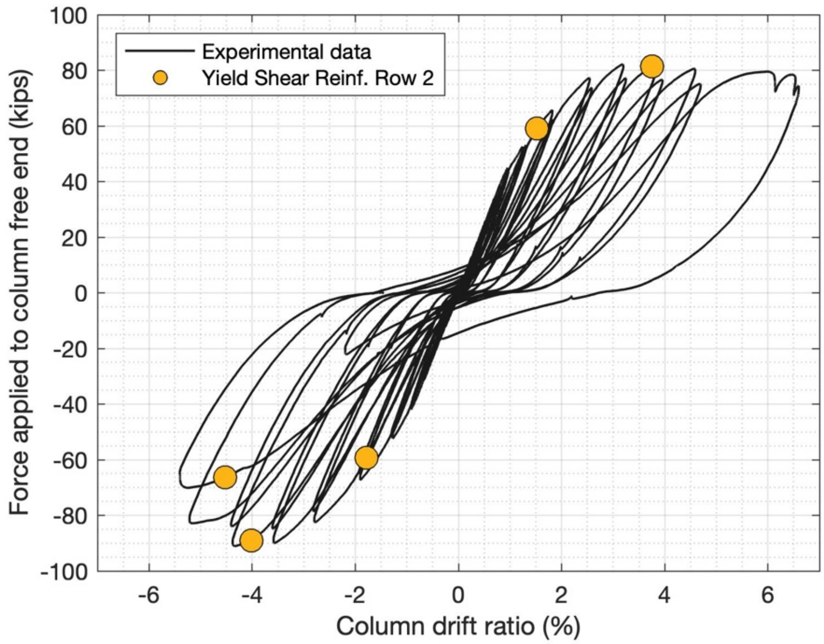

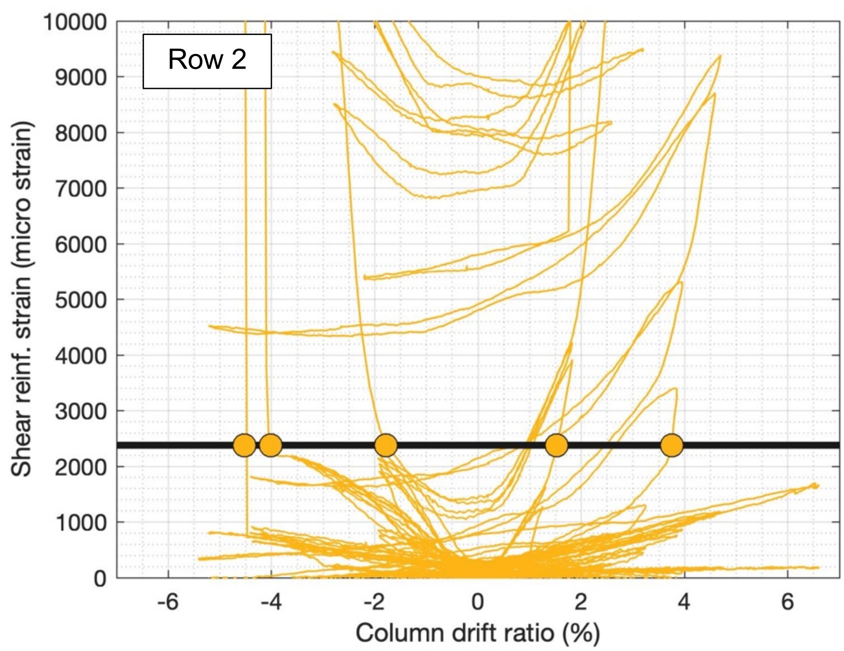

Figure 5-26. Load versus column drift ratio and shear reinforcing strain versus column drift ratio for <u>Row 2</u>. The first yield of each reinforcing bar is shown as a yellow circle. Vertical black lines indicate the first yielding of any reinforcing bar in that row. Expected yield is shown as a horizontal black line

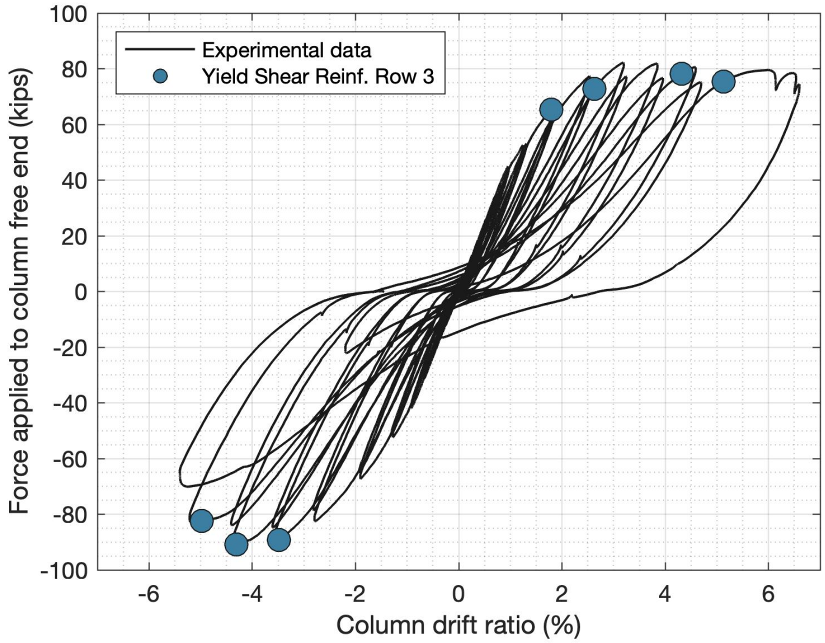

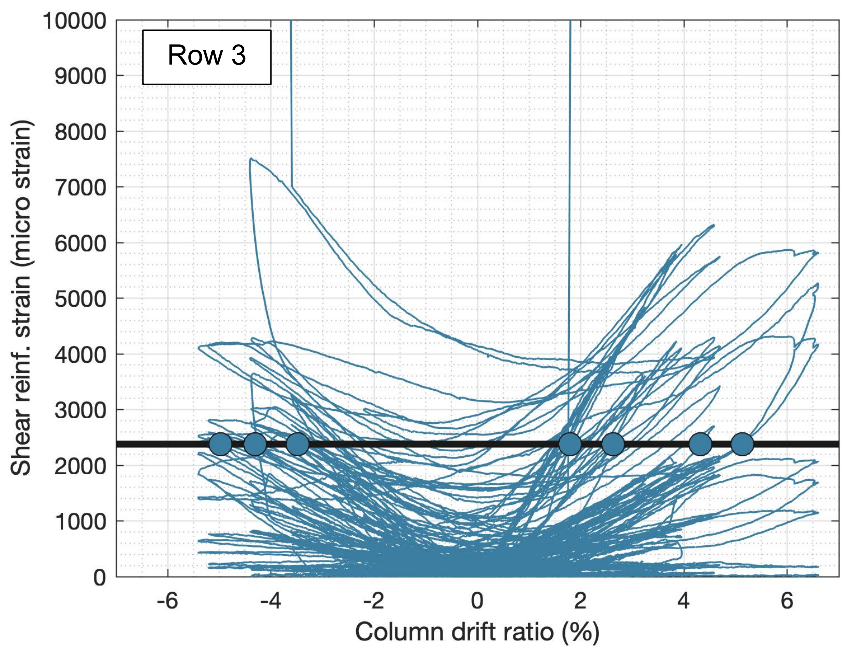

Figure 5-27. Load versus column drift ratio and shear reinforcing strain versus column drift ratio for <u>Row 3</u>. The first yield of each reinforcing bar is shown as a yellow circle. Vertical black lines indicate the first yielding of any reinforcing bar in that row. Expected yield is shown as a horizontal black line

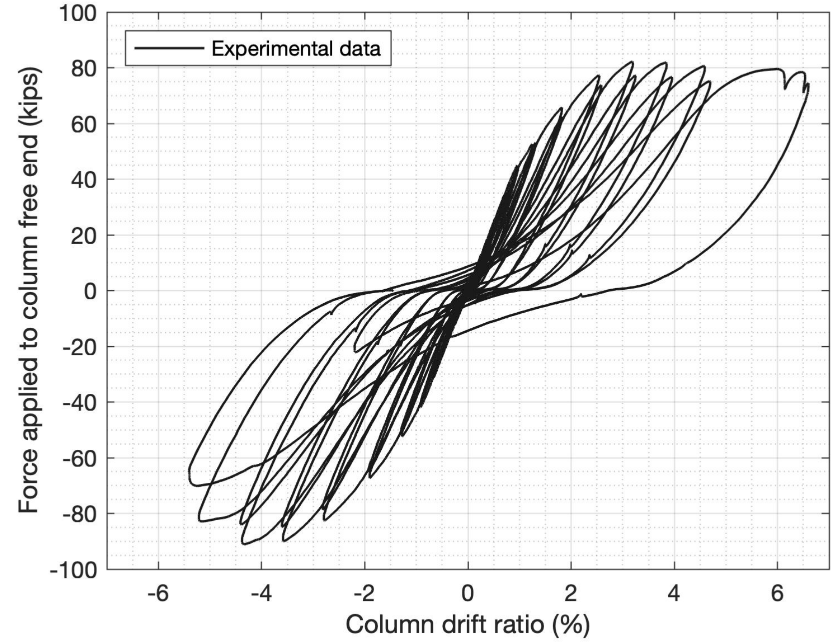

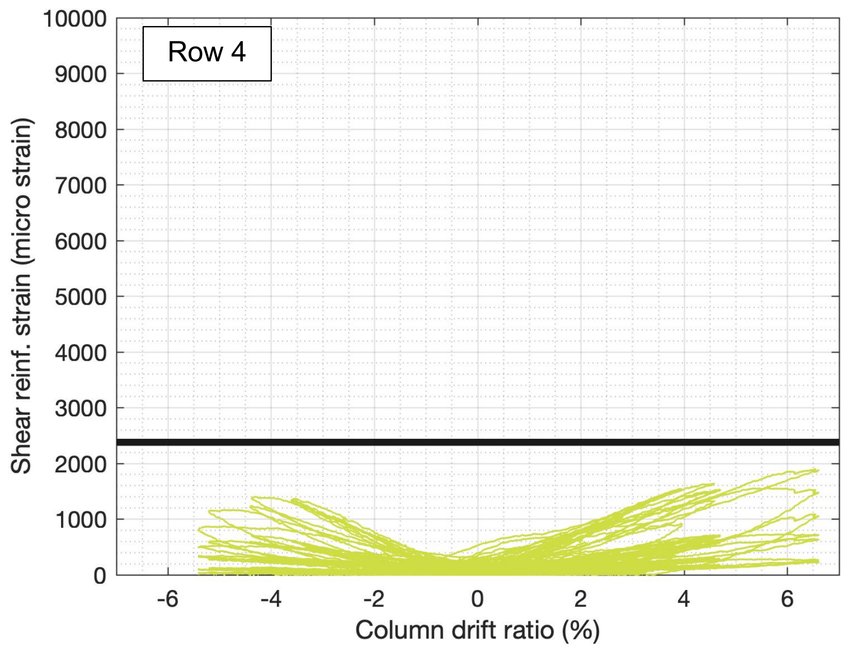

Figure 5-28. Load versus column drift ratio and shear reinforcing strain versus column drift ratio for Row 4. The first yield of each reinforcing bar is shown as a yellow circle. Vertical black lines indicate the first yielding of any reinforcing bar in that row. Expected yield is shown as a horizontal black line

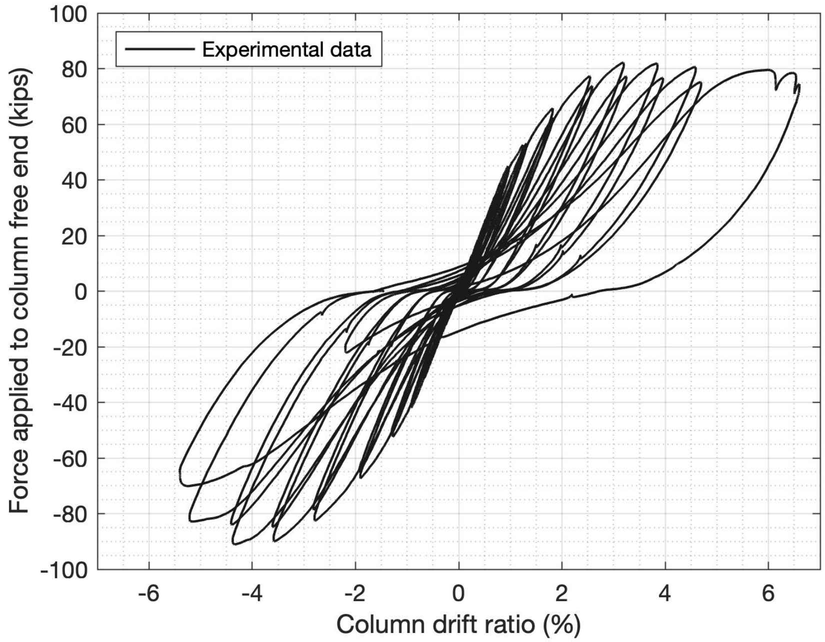

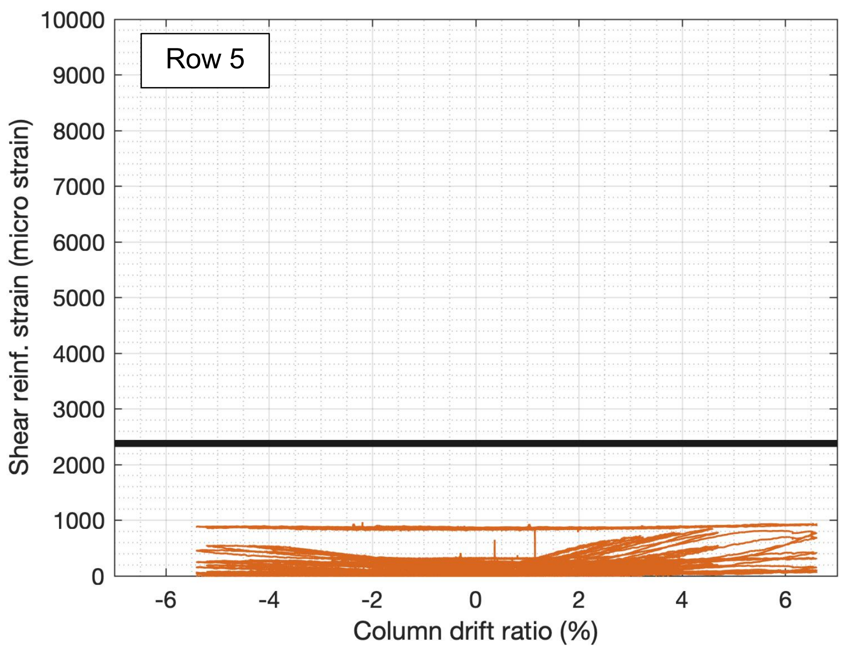

Figure 5-29. Load versus column drift ratio and shear reinforcing strain versus column drift ratio for <u>Row 5</u>. The first yield of each reinforcing bar is shown as a yellow circle. Vertical black lines indicate the first yielding of any reinforcing bar in that row. Expected yield is shown as a horizontal black line

Design Guide 1 by AISC (Base Plate and Anchor Rod Design, 2006) was used to proportion the specimen and estimate anchor forces from the loads placed on the column. This document recommends assuming a uniform bearing pressure below the base plate as seen in Figure 5-30. To verify this design assumption, the anchor forces obtained through this procedure are compared with the experimental anchor group forces as measured by load cells on the anchors. Figure 5-31 compares the theoretical and experimental anchor loads. The measured loads are consistently larger than the theoretically calculated loads. At peak load, the measured forces are about 20% higher than the theoretical forces. The discrepancy increases as the load cycles increase. This trend was also observed in M01 (Worsfold, 2019). These observations imply that the resultant of the bearing pressure is closer to the anchor group in tension than what is predicted by the AISC uniform pressure model. Improved models could decrease the value of the bearing pressure or assume the pressure distribution is not uniform.

An infinitely flexible base plate would place the compression resultant force below the column compression flange (15.2” from tension anchors). A rigid base plate would place the compression resultant at the far edge of the base plate (21.25” from tension anchors). Following the AISC procedure, at peak anchor force, the horizontal distance from the tension anchors to the compression resultant is near 20”.

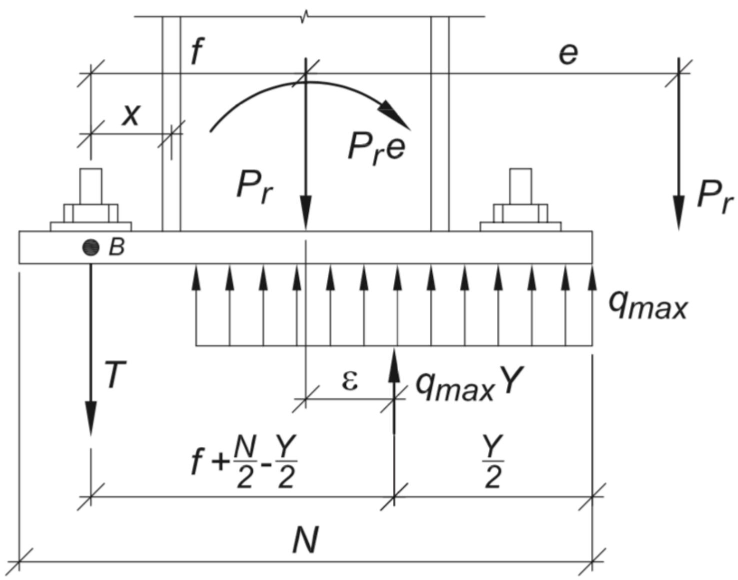

Figure 5-30. Assumed free body diagram for a base plate with large moment (AISC, 2006)

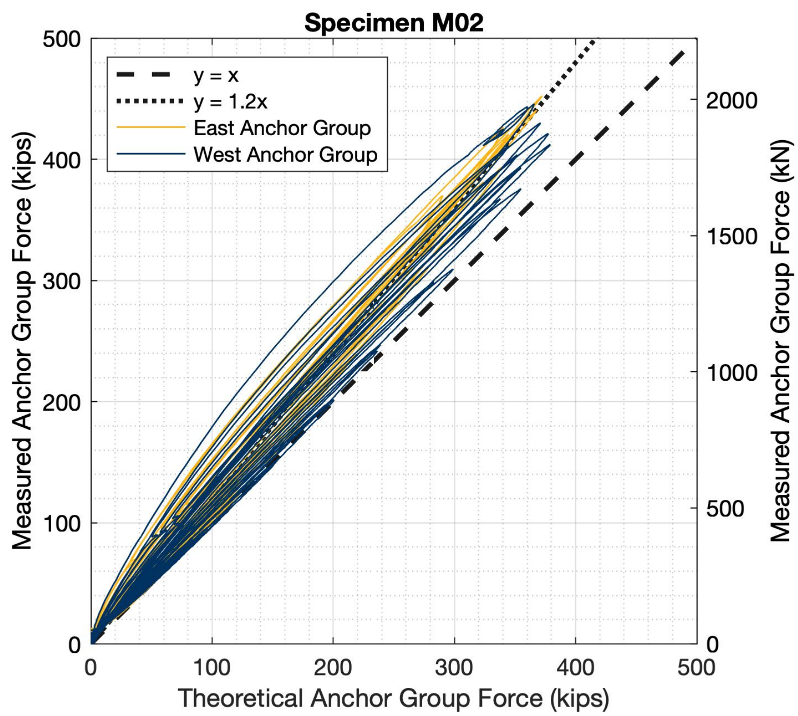

Figure 5-31. Comparison between the theoretical (AISC Design Guide 1) and the measured anchor group forces, measured loads from load cells on anchors

A row of linear potentiometers was placed along the top surface of the slab to measure vertical displacements (see arrangement of potentiometers in Figure 4-6). The row spans the longitudinal direction of the slab. Deflections due to self-weight are not included as the reference position of the instruments is the deformed shape of the simply supported slab under self-weight. The row of instruments is 19.5 in. from the slab centerline. During load cycle eight, the specimen began to leave the elastic range and the slab deformed with a double-curvature shape as can be seen in Figure 5-32. The double-curvature shape is flips when loading in the opposite directions. This shape is consistent with what would be expected from elastic beam theory.

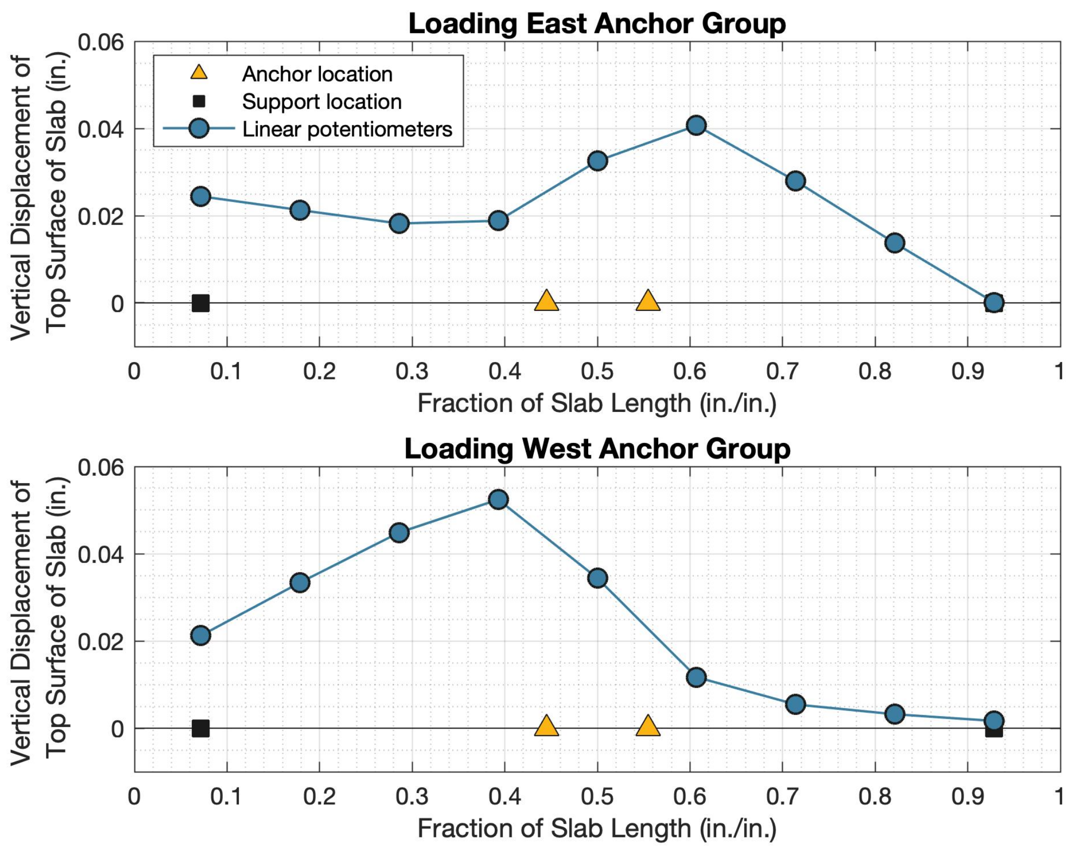

Figure 5-32. Vertical displacements of the top surface of the slab measured with a row of linear potentiometers at maximum positive and negative displacement for cycle eight (beginning to leave elastic range

Figure 5-33 shows the displacement measurements by the same instruments as described above, but for the first positive and negative peaks of cycle twelve. During this cycle the specimen is experiencing a yield plateau and the capacity has not yet dropped. The double-curvature shape is still clearly observed.

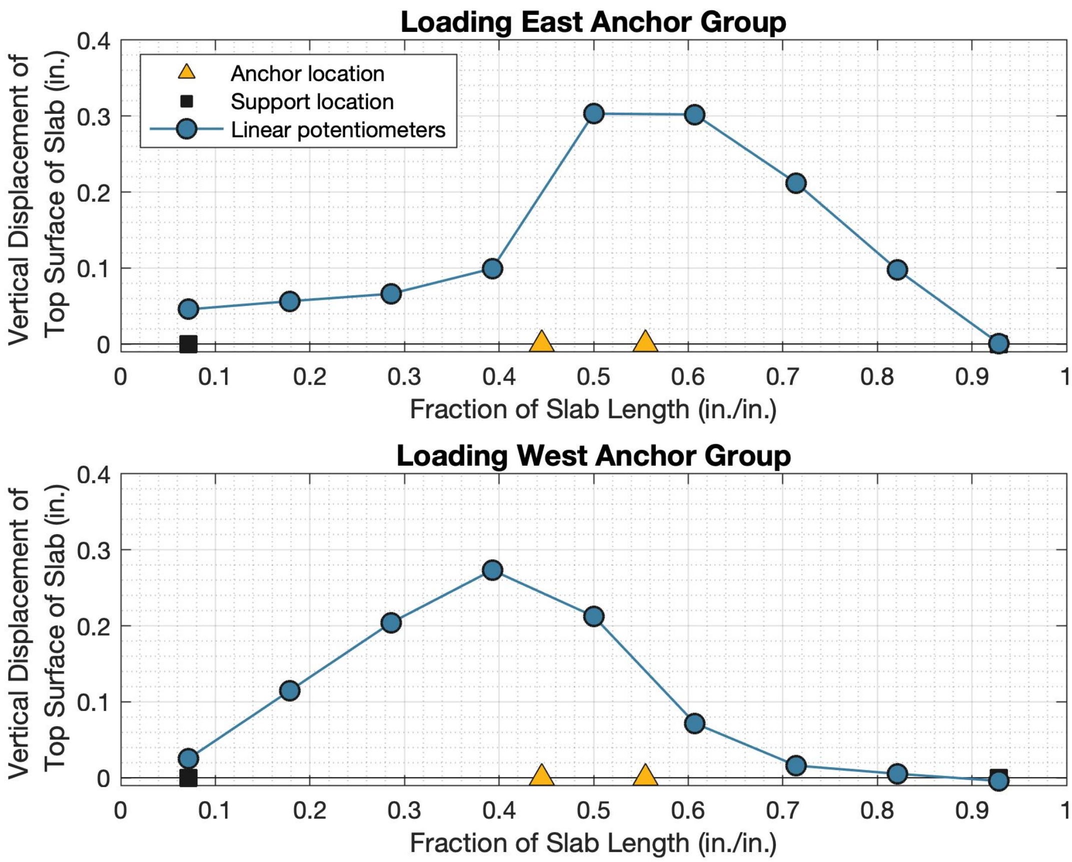

Figure 5-33. Vertical displacements of the top surface of the slab measured with a row of linear potentiometers at maximum positive and negative displacement for cycle twelve (during yield plateau)

Figure 5-34 shows the same displacement measurements by the instruments as described above. The first graph shows the maximum displacement during the whole test while the second graph shows the permanent deformation after the test was completed. Significant permanent displacement is observed. The area under the permanent displacement curve is larger along the right half (east side) of the specimen suggesting that the breakout cone volume was larger on this side. This was corroborated with in in situ crack pattern inspection (see Figure 5-4).

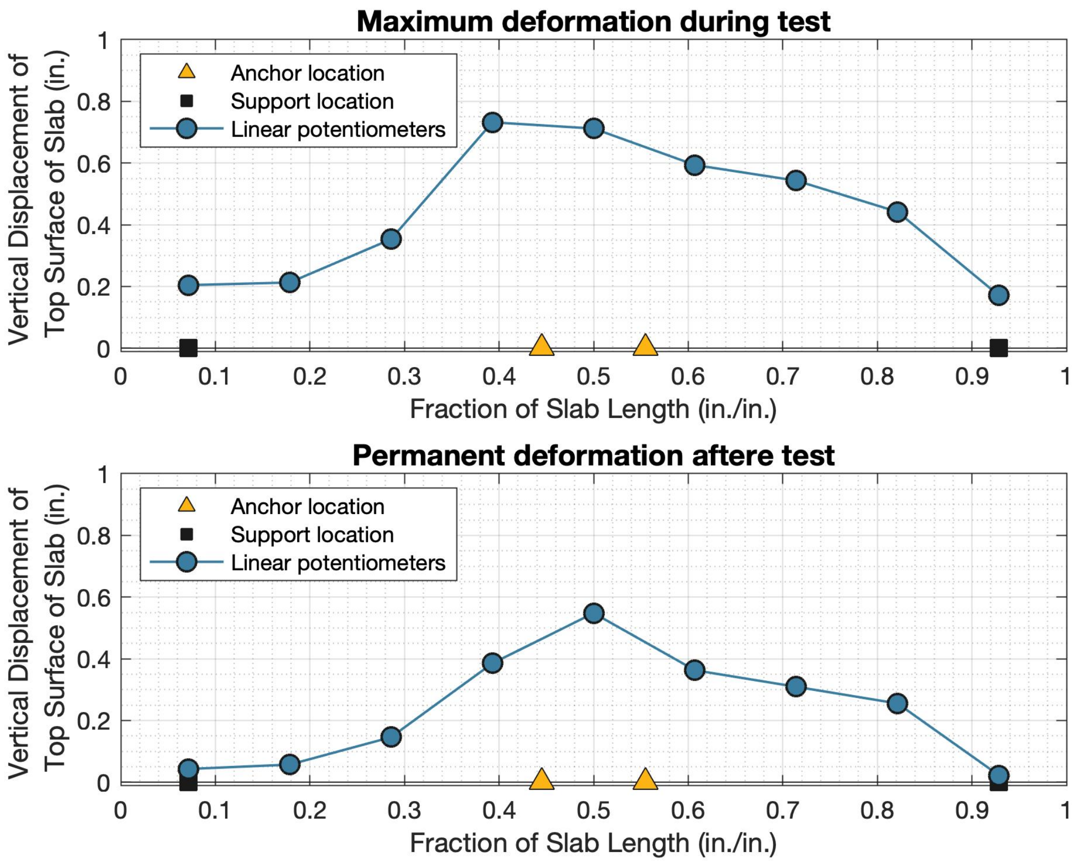

Figure 5-34. Vertical displacements of the top surface of the slab measured with a row of linear potentiometers showing maximum displacement during the test and permanent deformation after the test (permanent displacements)

A top and a bottom longitudinal reinforcing bar passing through the joint were instrumented with five strain gages each, 21 in. on center (see arrangement of strain gages in Figure 4-2). The instrumented bars were 4 in. from the slab centerline. Figure 5-35 plots the strains in these reinforcing bars at maximum positive and negative displacement for cycle eight. Strains due to self-weight are not included because the reference position of the instruments is the simply supported slab under self-weight. During this cycle the specimen is beginning to leave the elastic range. The top and bottom bars show an inverted double-curvature shape consistent with what would be expected from elastic beam theory. For loading in the opposite direction, the double-curvature shape is flipped. The strain gages in the middle of the specimen for the top and bottom bars do not follow this pattern as they show tensile strains for both loading directions. The strain gage in the middle of top bar shows a higher strain than others.

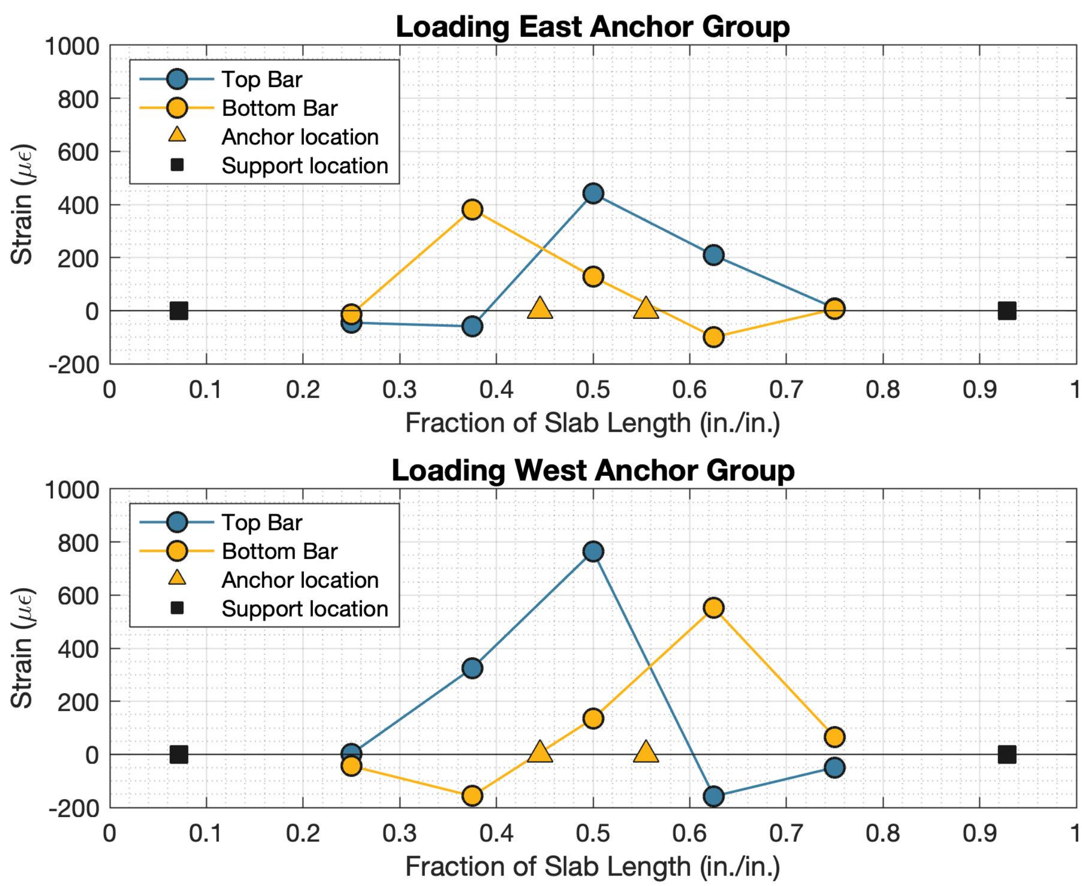

Figure 5-35. Strains in top and bottom longitudinal reinforcing bar at maximum positive and negative displacement for cycle eight (beginning to leave elastic range)

Figure 5-36 shows the strain measurements by the same instruments as described above, but for the first positive and negative peaks of cycle twelve. During this cycle the specimen is experiencing a yield plateau and the capacity has not yet dropped. In general, all strain gages experience tensile strains no matter the loading direction. Consistent with elastic beam theory, the portions of the slab with negative moment (tension on top) show higher tensile strains in the top reinforcing bar. Similarly, the segments with positive moment (tension on bottom) show higher tensile strains in the bottom bar. The double-curvature shape is not as visible as clearly as in the previous load step (Figure 5-35). The three middle gages of the bottom reinforcing bar show an approximately uniform tensile strain no matter the loading direction. The top reinforcing bar shows relatively low tensile strains except for the gages just outside the joint on the side of the slab where the anchors are being loaded in tension. The strains in this gage exceed the expected yield strain for A706 G60 reinforcing bars. As described in Chapter 3, the slab reinforcement was designed to resist moments corresponding to the expected column yield. However, to avoid excessive inelastic strains in case the moment capacity was underestimated, the Gr60 reinforcement was substituted for high strength reinforcement. This means that the steel has not yielded.

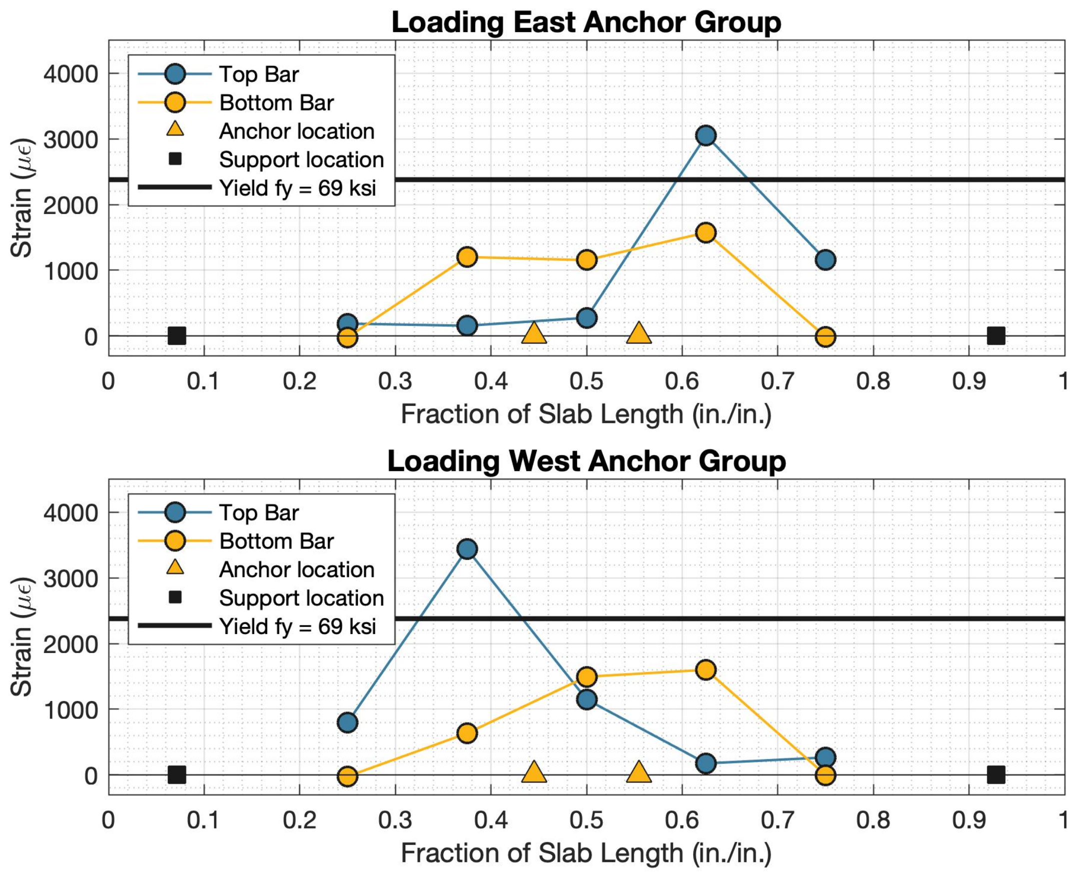

Figure 5-36. Strains in top and bottom longitudinal reinforcing bar at maximum positive and negative displacement for cycle twelve (yield plateau before strength degradation)

Figure 5-37 shows the maximum and minimum strain measured by each strain gage during the whole test. The middle strain gage of the top bar (T3) was damaged at the end of cycle 12. For this gage, the strain range shown is what was sensed before it failed. No strain gage exceeded 4480 με, which is approximately the yielding strain of reinforcement with fy = 130 ksi. During the whole test, no gage experienced significant compressive strains. Figure 5-38 shows the permanent strains in the gages after the test ended. The middle strain gage of the top bar (T3) is not shown.

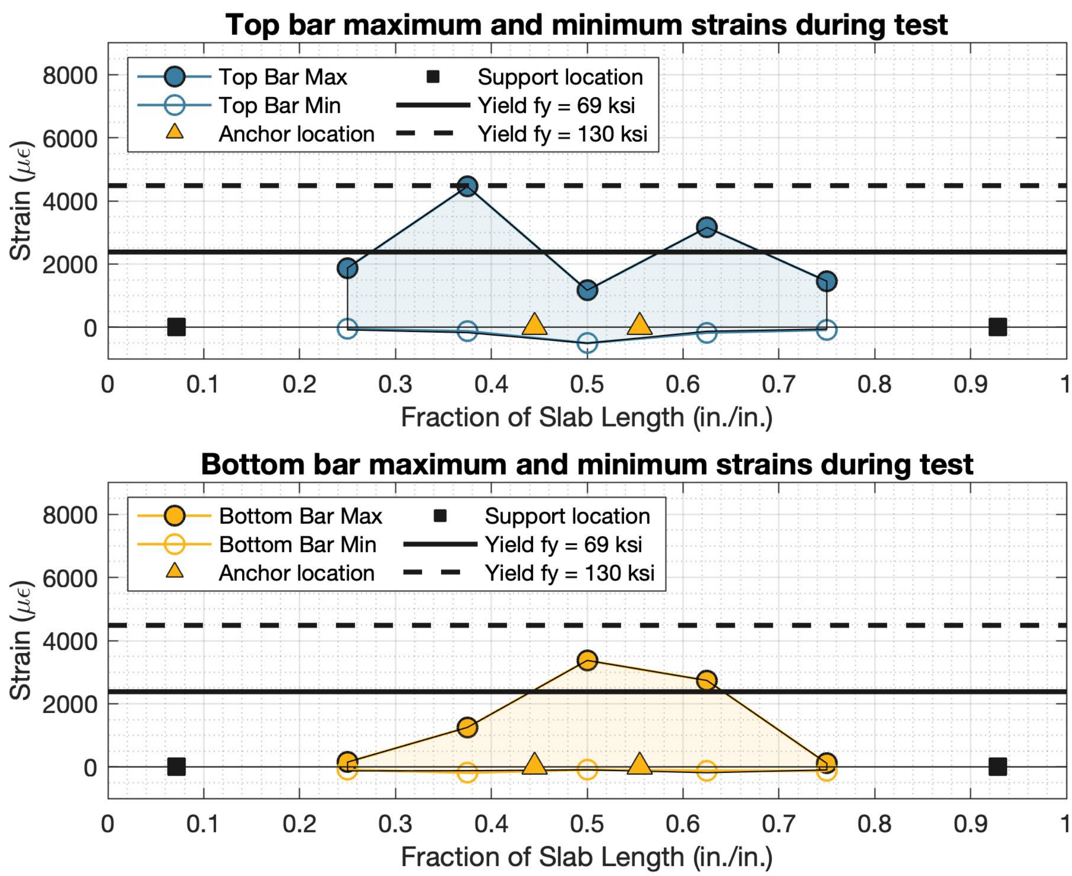

Figure 5-37. Strain range of top and bottom reinforcing bars during whole test. Note: the middle strain gage of the top bar (T3) was damaged at the end of cycle 12. The strain range shown is what was sensed before instrument failure

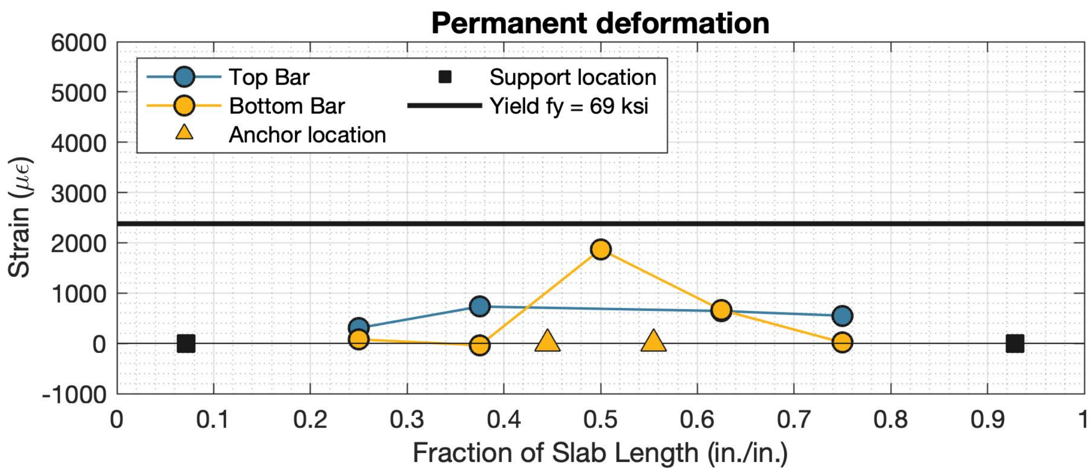

Figure 5-38. Permanent strains in gages after the test ended. Note: the middle strain gage of the top bar (T3) was damaged at the end of cycle 12 so it is not shown

5.4 SPECIMEN SLIDING, ELONGATION AND SUPPORT UPLIFT

To prevent sliding during the test, the specimen was prestressed to the laboratory floor with nine 1-3/4" 150 ksi Williams Rods prestressed to 140 kips each. Linear potentiometers were placed on the east and west faces of the slab and the concrete supports along the slab longitudinal center line at mid height (see section 4.1) to detect any sliding movement of the specimen relative to the laboratory floor. Figure 5-39 plots the horizontal displacement of the east and west supports as well as the east and west faces of the slab. Positive sliding represents movement towards the east. No sliding is observed, but the specimen experienced dilation when loaded in both directions. The specimen longitudinal dilation is calculated as the difference between the east and west face displacements and is shown in Figure 5-40. The maximum dilation was approximately 0.12 in. and occurred at maximum displacement in both loading directions. Permanent dilation was observed after the test of approximately 0.06 in..

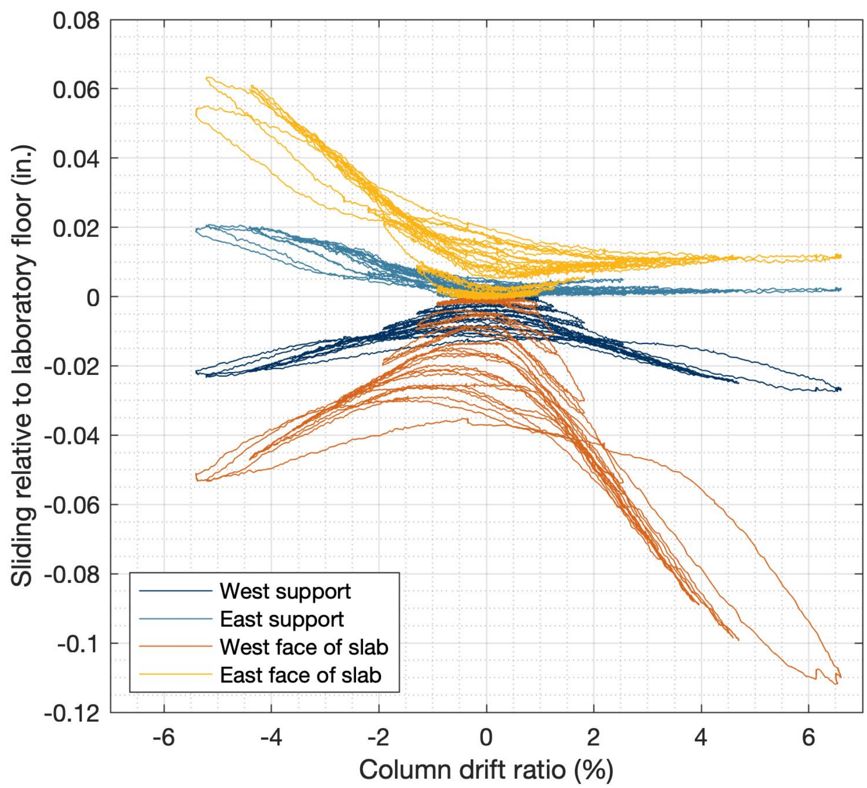

Figure 5-39. Horizontal displacement of east and west faces of specimen and support measured along the slab centerline in the direction of loading relative to the laboratory floor, positive sliding is movement towards the east

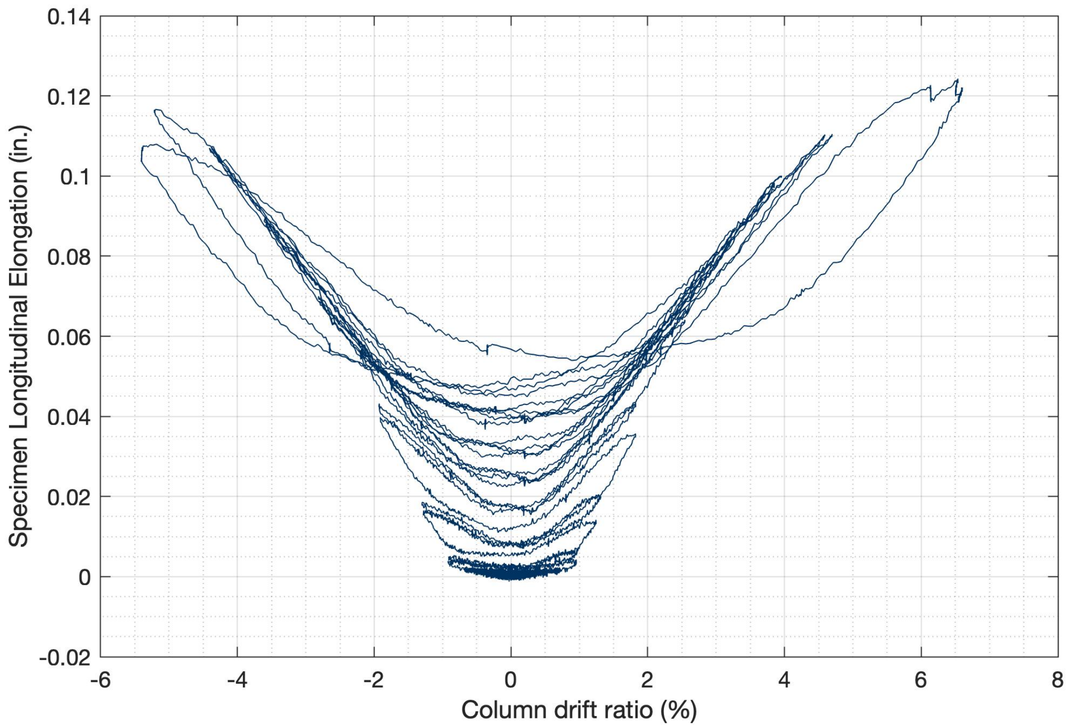

Figure 5-40. Slab longitudinal elongation during testing

Linear potentiometers were placed in a vertical position on the top surface of the slab above the concrete supports as described in section 4.1 to measure specimen uplift at the supports. Figure 5-41 plots the uplift of both support with a positive measurement indicating uplift. The magnitude of the displacements is small indicating that the prestressed supports were effective in preventing both uplift of the specimen during testing.

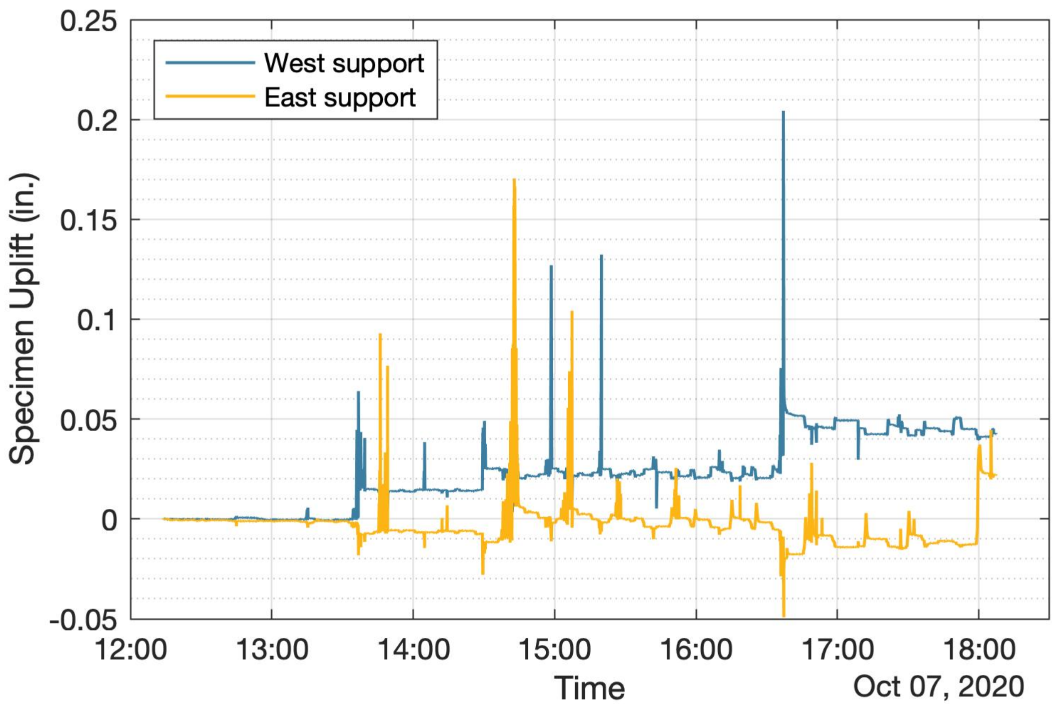

Figure 5-41. Specimen uplift at west and east supports versus time

6 DISCUSSION

A column-foundation connection was tested at UC Berkeley's Structural Laboratory. The column was a steel-wide-flange section with a base plate attached to the concrete foundation with cast-in-place anchors. The specimen was loaded quasi-statically in a cyclic manner with increasing displacements until failure. The specimen provided two data points, one per failure of each anchor group on the east and west sides. All four anchor groups failed in a concrete breakout mode, without indications of other failure modes such as flexure, one-way shear, or joint shear. The presence of shear reinforcing did not preclude the breakout failure mode.

Table 6-1 shows the median anchor group forces for multiple failure criteria. The table also shows the experimentally observed failure loads.

Table 6-1. Median anchor group forces per failure mode and experimental results

Failure Mode	Anchor Force (kip)
Breakout (Uncracked)	189
Breakout Secondary East (Uncracked)	324
Breakout Secondary West (Uncracked)	594
Beam-Column Joint	414
East Anchor Group	452
West Anchor Group	446

Specimen M02 incorporated an 8-in. by 8-in. [203 mm by 203 mm] shear reinforcing grid of #4G60 [Ø13 mm G420] bars with a 180-degree hook on one side and a head on the other. Both ends engaged longitudinal reinforcing. After controlling for concrete strength, the addition of shear reinforcing in specimen M02 increased the breakout force by 72% and displacement capacity by a factor of 3 on average compared to specimen M01 tested previously. The increased peak force is comparable to the calculated beam-column joint strength. The strength increase is consistent with the strut-and-tie model developed by (Kupfer H, 2003) for column-foundation connections which suggests tension ties outside the joint are required for equilibrium. Contrary to current assumptions in ACI 318-19 and EN 1992-4 design equations, relatively small amounts of shear reinforcing can improve the connection behavior. Most shear bars near the anchors developed strains well beyond the nominal yield strain (>3%) even though they were not developed on both sides of the potential breakout cone as would be required for ACI 318-19 anchor reinforcement. This observation suggests that anchoring shear reinforcing bars following the requirements for anchoring transverse reinforcement (ACI 318-19 Sec. 25.7.1.3) may be sufficient to develop the nominal yield stress.

The specimens exhibited pinched hysteresis loops (see Figure 5-7), indicating a non-ductile concrete breakout failure. Increasing the breakout failure strength may allow the designer to provide an alternate more ductile failure mode (for example, anchor or column yielding).

For the east anchor group of specimen M02, the east face of the failure cone is located beyond the outer perimeter of the shear reinforcing bars (see Figure 5-4). If one assumes the shear reinforcement bars form part of the anchor group, the calculated strength of this larger secondary breakout cone increases by a factor of 1.72 due to the increased group factor. This strength increase is almost exactly that observed between specimen M01 and M02 (72%). The calculated increase in strength for the secondary breakout cone on the west side is about 3.14 due to the larger reinforced area. This secondary breakout failure cone was observed on the west side but did not govern.

The additional rows of shear reinforcing on the west side of test specimen M02 did not increase the load capacity but did increase displacement capacity from a drift ratio of about 4% to about 6% and prevented the formation of a secondary breakout cone initiating where the shear reinforcing ended. The shear reinforcing beyond 0.75hef from the anchor centerline does not seem to increase anchor force, consistent with Eurocode provisions for supplementary reinforcement.

The specimen did not showed substantial cracking along the bottom surface, suggesting that the confining provided by soil may not have been critical to the concrete breakout failure mode which governed. The influence of soil support should be investigated further.

The failure cones were asymmetric with a steeper slope towards the interior of the joint (see Figure 5-4). This cone geometry is attributed to suppression of the unconstrained breakout surface because of flexural compression at the opposite side of the joint.

ACI 318-19 commentary Sec. R25.4.4.2c suggests that breakout failure can be precluded in a joint by keeping anchorage length greater than or equal to 1/1.5 times the effective depth of the member introducing the anchor force into the joint. However, breakout failure occurred even though this recommendation was satisfied.

With additional shear reinforcing, the breakout failure load of specimen M02 became comparable to the beam-column joint strength. The experiments did not test whether further additions of shear reinforcement would result in further increases in strength or whether strength would be limited by beam-column joint shear strength. The formation of a secondary failure cone beyond the outer perimeter of the shear reinforcing, analogous to the requirement for two-way slabs with shear reinforcement, should also be considered in design.

Crack patterns on the surface of the specimen, as well as posthumous interior exploration, revealed breakout cones for both anchor groups. Evidence of beam-column joint failure was not observed. This failure mode would have involved concrete deterioration and joint dilation which. Evidence of a strut-and-tie type failure was not observed. Tie failure would have involved the failure of anchors or longitudinal reinforcing bars. Node failure would have involved the crushing of concrete at the anchor head bearing surface or along the base plate bearing surface. Strut failure would have involved the splitting or crushing of struts.

Breakout failure does not seem to be precluded by placing the anchors a distance of d/1.5 into the concrete as suggested in the commentary of ACI 318-14 section R25.4.4.2c.

Current ACI breakout equations underpredicted the connection strength as it does not consider the effect of distributed shear reinforcing.

Breakout failures are generally expected to be brittle, but Figure 5-7 shows some ductility. An average ductility value of 1.62 was calculated (see Table 5-3).

Figure 5-7 and Figure 5-13 show relaxation of the specimen when the loading was paused, particularly during the final load cycles. The test was paused at about 50% of the peak displacement to minimize softening.

The initial prestressing force in the anchors was lost as the cyclic loading progressed (see Figure 5-13). The anchors were not re-stressed during the test.

Figure 5-11 and Figure 5-12 show that during the elastic loading cycles, the column free end displacement was due mostly to the elastic deflection of the column and the anchor elongation. As the cycling loading progressed and damage spread in the concrete, the slab rotation became the dominant contributor to the column free end deflection. Also, at the instant breakout failure occurred, the slab rotated suddenly and the column unloaded.

The AISC uniform bearing pressure model for the design of base plates from Design Guide 1, under predicts the peak anchor group force by about 20% (see Figure 5-31). The lever arm between the loaded anchors and the resultant of the bearing pressure is shorter than what is obtained using the AISC uniform pressure model.

Section 5.4 shows that the specimen supports performed as designed. The specimen sliding, elongation, and uplift were all less than 0.025in., which is considered acceptable.

As the specimen design intended, none of the instrumented reinforcing bars from the top or bottom meshes yielded.

Before breakout failure, the top surface of the slab deflected in a double curvature shape as would be expected from traditional elastic beam theory (see Figure 5-32).

7 CONCLUSIONS

A full-scale test specimen of an interior steel-column-to-concrete-foundation connection with cast-in-place anchor bolts was constructed and tested. The test specimen provided two data points corresponding to the peak forces of each anchor group. The connection was tested under incrementally increasing cyclic lateral loading resulting in moment transfer from the column to the foundation element. The anchor groups failed in a brittle concrete breakout mechanism due to tensile force transfer from the anchor bolts to the foundation. This observation challenges the preconceived notion held by some designers that breakout failures will not govern the behavior of large-scale connections, provided they have adequate capacity to transfer the moment by an alternative mechanism such as joint shear. The pinched hysteresis loops are indicative of concrete failure. There was no evidence of failure or distress associated with other potential force-limiting mechanisms.

Breakout failure governed even though the anchorage length was greater than 1/1.5 times the effective depth of the member introducing the anchor force into the joint. This observation runs contrary to ACI 318-19 commentary Sec. R25.4.4.2. ACI 318 should consider revised guidance or new code requirements emphasizing the importance of checking breakout failures in addition to checking joint shear strength. A good practice would be to check both breakout strength and beam-column joint shear strength and use the lower value as the limit for design.

The addition of a distributed grid of shear reinforcing in the breakout cone region can increase the breakout strength and displacement capacity. Increasing the breakout strength may allow the designer to provide a more desirable ductile failure mode like anchor yielding. Even though only the shear reinforcing within 0.75 hef of the anchors seems capable of increasing the breakout strength, additional rows can increase displacement capacity and prevent secondary breakout failure cones beyond the last row of shear reinforcement. ACI 318 and the Eurocodes should consider including provisions that combine the strength of concrete and shear reinforcement for the concrete breakout failure mode.

8 REFERENCES

ACI Committee 318. (2014). *Building Code Requirements for Structural Concrete and Commentary (ACI 318-14).* Farmington Hills, MI: American Concrete Institute.

ACI Committee 349. (2013). *Code Requirements for Nuclear Safety Related Concrete Structures.* Farmington Hills, MI: American Concrete Institute.

ACI Committee 374. (n.d.). *ACI 374, Performance-Based Seismic Design of Concrete Buildings.*

AISC. (2006). *Design Guide 1: Base Plate and Anchor Rod Design.*

ASTM. (2014). *ASTM C469, Standard Test Method for Static Modulus of Elasticity and Poisson's Ratio of Concrete in Compression.*

ASTM. (2017). ASTM A370 - 17, Standard Test Methods and Definitions for Mechanical Testing of Steel Products. In *ASTM International.* West Conshohocken, PA.

ASTM. (2017). *ASTM C496, Standard Test Method for Splitting Tensile Strength of Cylindrical Concrete Specimens.*

ASTM. (2018). ASTM C39 / C39M - 18, Standard Test Method for Compressive Strength of Cylindrical Concrete Specimens. In *ASTM International.* West Conshohocken, PA.

Caltrans. (2016). *Memo to Design MTD 20-7, Seismic Design of Slab Bridges.* CA, Sacramento: California Department of Transportation.

Eligehausen, R., & Balogh, T. (1995). Behaviour of Fasteners Loaded in Tension in Cracked Reinforced Concrete. *ACI-Structural Journal, 92*(3), 365-379.

Eligehausen, R., & Mallee, R. (2000). *Befestigungstechnik im Beton- und Mauerwerkbau.* Berlin, Germany: Ernst & Sohn.

Eligehausen, R., & Sawade, G. (1989). *A Fracture Mechanics based Description of the Pull-Out Behaviour of headed Studs embedded in Concrete.* (L. Elfgren, Ed.) London: Chapman and Hall.

Eligehausen, R., Bouska, P., Cervenka, V., & Pukl, R. (1992). Size Effect of the Concrete Cone Failure Load of Anchor Bolts. In Z. P. Bazant (Ed.), *Fracture Mechanics of Concrete Structures* (pp. 517-525). London, New York: Elsevier Applied Science.

Eligehausen, R., Fuch, W., Ick, U., Mallee, R., Reuter, M., Schimmelpfenning, K., & Schomal, B. (1992). Behaviour of headed anchors under concentrical tension. *Bauingeneiur, 68*, 183-196.

Eligehausen, R., Mallée, R., & Silva, J. F. (2006). *Anchorage in Concrete Construction.* Berlin: Ernst & Sohn.

FEMA-461. (2007). *InterimTesting Protocols for Determining the Seismic Performance Characteristics of Structural and Nonstructural Components.*

Fuchs, W., Eligehausen, R., & Breen, J. (1995). Concrete Capacity Design (CCD) Approach for Fastening to Concrete. *ACI Structural Journal*, 73-94.

Herzog, M. (2015). *Beitrag zur Vereinheitlichung der Bemessung im Stahlbetonbau und in der Befestigungstechnik (Contribution to the standardization of design in reinforced concrete construction and fastening technology).* Stuttgart, Germany: Institut für Werkstoffe im Bauwesen der Universität Stuttgart.

Joint ACI-ASCE Committee 352. (2002). *Recommendations for Design of Beam-Column Connections in Monolithic Reinforced Concrete Structures.* American Concrete Institute.

Kupfer H, M. F. (2003). Hauptaufsatze-Nachtraglich verankerte gerade Bewehrungsstabe bei Rahmenknoten (Anchorage of post installed straight bars for frame node connections). *Julius Springer*, 24-37.

Mahrenholtz, C., Akguzel, U., Eligehausen, R., & Pampanin, S. (2014, September - October). New Design Methodology for Seismic Column-to-Foundation Anchorage Connections. *ACI Structural Journal*.

Moehle, J. P. (2015). *Seismic Design of Reinforced Concrete Buildings* (1st ed.). McGraw-Hill Education.

Nilforoush, R., Nilsson, M., & Elfgren, L. (2017). Experimental Evalua- tions of Influence of Member Thickness, Anchor-Head Size, and Reinforce- ment on the Tensile Capacity of Headed Anchors in Uncracked Concrete. *Journal of Structural Engineering*.

Nilforoush, R., Nilsson, M., Elfgren, L., Ozbolt, J., Hofmann, J., & Eligehausen, R. (2017). Influence of Surface Reinforcement, Member Thickness and Cracked Concrete on Tensile Capacity of Anchor Bolts. *ACI Structural Journal*, 1543-1556.

Nilforoush, R., Nilsson, M., Elfgren, L., Ozbolt, J., Hofmann, J., & Eligehausen, R. (2017). Tensile Capacity of Anchor Bolts in Uncracked Concrete: Influence of Member Thickness and Anchor's Head Size. *ACI Structural Journal*, 1519-1530.

Ožbolt, J., Eligehausen, R., Periskic, G., & and Mayer, U. (2007). 3D FE Analysis of Anchor Bolts with Large EMbedments. *Engineering Fracutre Mechanics, 74*(1-2), 168-178.

Ozbolt, J., Eligehausen, R., & Periskic, G. (2007). 3D FE Analysis of Anchor Bolts with Large Embedments. *Engineering Fracture Mechanics, 74*(1-2), 168-178.

Papadopoulos, V. M.-D. (2018, September). Development of headed bars in slab-column joints of reinforced concrete slab bridges. *ACI-Structural Journal, 115*(5), 1393-1406.

Rehm, G., Eligehausen, R., & Mallee, R. (1988). *Befestigungstechnik (Fixing technology).* Berlin, Germany: Ernst & Sohn.

RILEM TC. (1985). FMC 1 Determination of fracture energy of mortar and concrete by menas of three-point bend tests on notched beams. *RILEM Recommendations for the Testing and Use of Constructions Materials*, 99-101.

Wight, J., & MacGregor, J. (2009). *Reinforced Concrete.* New Jersey: Pearson Prentice Hall.

Worsfold, B. a. (2019). *Laboratory Tests of Column-Foundation Moment Transfer Connections with Headed Anchors* (Vols. UCB/SEMM-2019/01). Structural Engineering, Mechanics, and Materials (SEMM).

APPENDIX A. MATERIAL PROPERTIES

A.1 Concrete Compressive Strength ASTM-C39

Table A- 1 and Figure A- 1 summarize the results of compressive strength tests performed according to ASTM-C39. The column-foundation test specimen was tested on day 34.

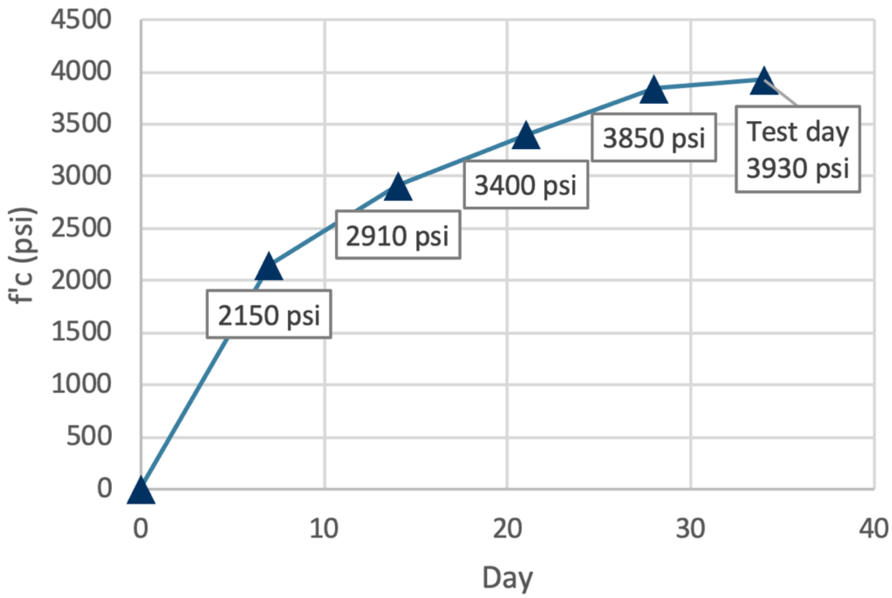

Figure A- 1. Concrete compressive strength growth

Table A- 1. Concrete compressive strength results

Date	Days since cast	f'c (psi)	Average f'c (psi)
10-Sep-20	7	2110	2150
		2190	
17-Sep-20	14	2930	2910
		2890	
24-Sep-20	21	3350	3400
		3450	
01-Oct-20	28	3870	3850
		3830	
07-Oct-20	34	3990	3930
		3863	

A.2 Concrete Modulus of Elasticity and Stress-Strain Curve ASTM-C469

Two concrete cylinders were tested according to ASTM-C469 to determine the modulus of elasticity on testing day (34 days from casting) (Figure A- 2).

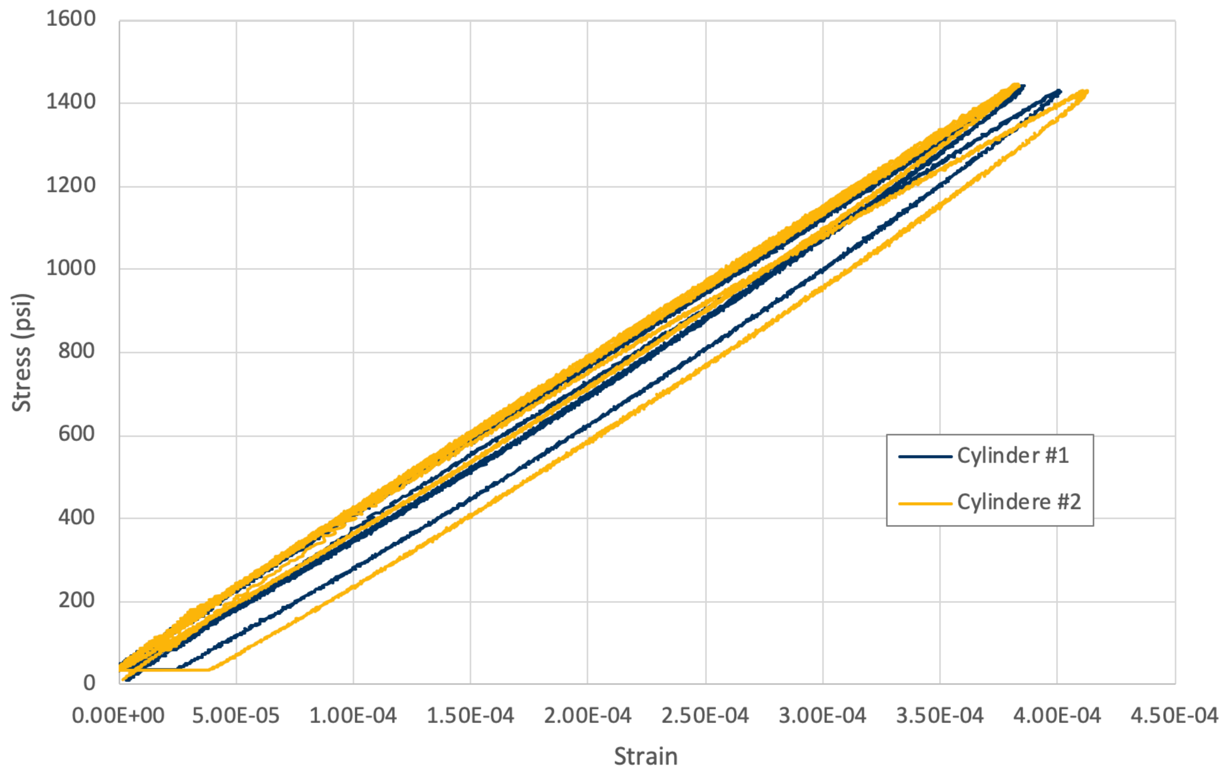

Figure A- 2. Concrete stress - strain results on test day (34 days from casting)

Table A- 2. Concrete modulus of elasticity test results

Specimen	1	2	Average
Initial Concrete Modulus of Elasticity E (psi)	3,590,000	3,620,000	3,610,000

A.3 Concrete Splitting Tensile Strength ASTM-C496

Splitting tensile strength tests on the concrete were performed on test day (34 days from casting) following the procedures of ASTM-C496-17. Results are shown in Table A- 3.

Table A- 3. Concrete splitting tensile strength results on test day (34 days from casting)

Specimen	Tensile Strength ft (psi)	Average ft (psi)
1	431	438
2	444	

A.4 Initial Concrete Fracture Energy

Initial concrete fracture energy (Gf) was determined following RELIM TC50-FMC-FMC1 recommendation. Multiple identical notched beams were tested in a simply supported condition, with a roller on each side and a ball on top as shown in Figure A- 3. Mid-span deflection was measured relative to cast-in pins on both sides of the beam with LVDTs. The load and displacement of the actuator was also recorded. Closed-loop loading was used such that the midspan deflection increased at 1 in / 50,000 s. After the peak load was reached, the loading was increased by a factor of 10 to 1 in / 5000 s until the load dropped to zero. Beams were wet cured until 7d when they were unmolded and placed in a lime bath. Beams were removed from the lime bath no more than 30 min before testing and were kept wet with burlap and spray bottles. The data was recorded at 10 Hz.

Figure A- 3. Concrete Fracture Energy test set-up

Figure A- 4, Table A- 4 and Table A- 5 summarize the chosen specimen geometry.

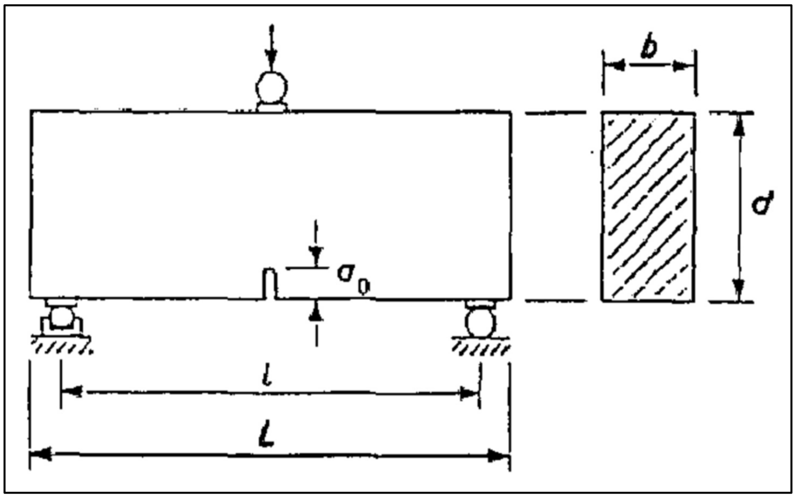

Figure A- 4. Fracture energy specimen geometry (RILEM TC, 1985)

Table A- 4. Fracture energy specimen geometry

d (in.)	b (in.)	L (in.)	l (in.)	a0 (in.)
6	6	21	18	1.8

Table A- 5. Geometric considerations and properties

da (in.)	0.75
d/da	8.0
b/da	8.0
L/d	3.5
S/d	3.0
a0/d	0.3

Figure A- 5 shows the load – deflection curves of five specimens. Figure A- 6 shows the displacement over time. The smoothness of these curves demonstrates that the closed loop loading system successfully produce uniform increase in displacement. Note the results for specimen 5 are not shown as this specimen was used for a trial test. Also, specimen 1 was loaded too quickly and is discarded.

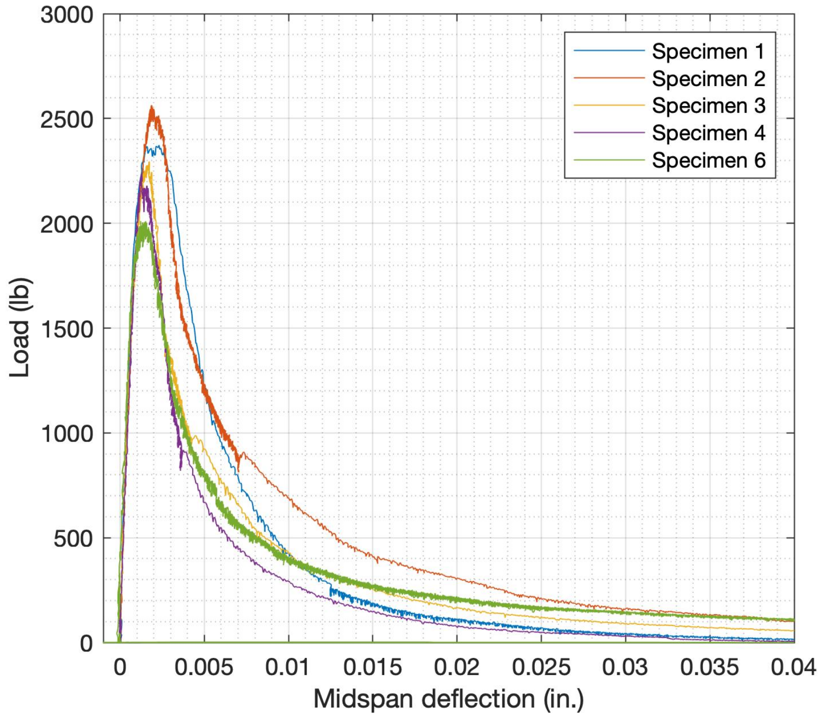

Figure A- 5. Midspan deflection – load graph for fracture energy beams

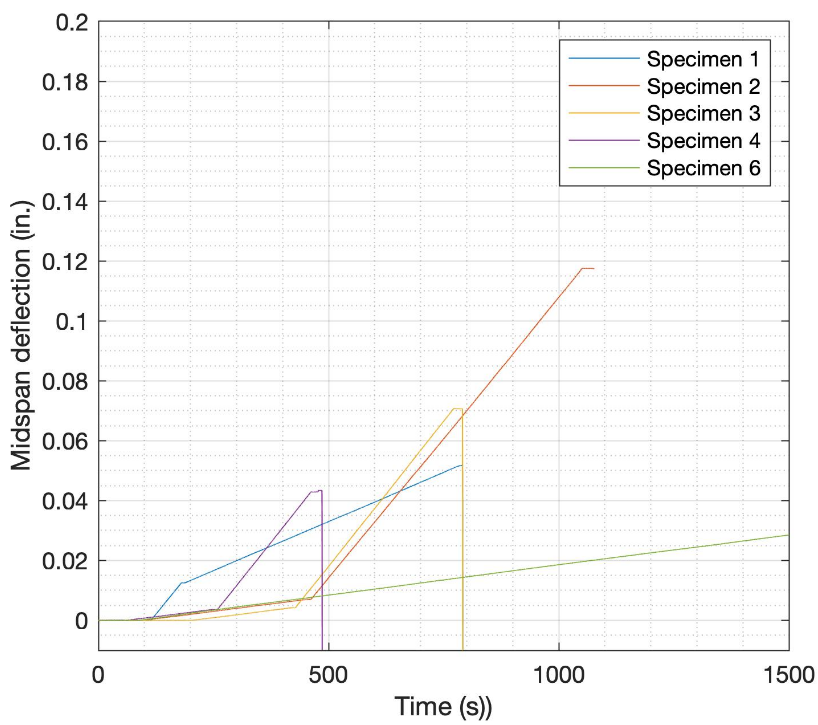

Figure A- 6. Midspan deflection over time for fracture energy beams

Table A- 6 summarizes the peak load and area under load - displacement curve for each specimen.

Table A- 6. Fracture energy weight and failure load

Specimen	Peak load (lb)	Time to peak (s)	W0 (lb-in)	δ_0 (in.)
1	2370	56	16.0	0.052
2	2560	181	24.3	0.120
3	2290	276	15.5	0.071
4	2240	122	11.4	0.043
6	2010	97	18.8	0.100

The initial fracture energy is shown in Table A- 7 and is calculated as shown below.

$$G_f = (W_0 + mg\delta_0)/A_{lig}$$

Table A- 7. Experimental initial fracture energy

Specimen	Gf (N/m)	Average Gf (N/m)
2	221	157
3	136	
4	97	
6	175	

For comparison, Table A- 8 shows the fracture energy as calculated with Model Code 1990 and 2010 equations.

Table A- 8. Initial fracture energy from experiment and code approximations

Method	Gf (N/m)
FMC1	157
MC 1990	71
MC 2010	132

A.5 Reinforcing Bar Properties ASTM-A370

Three types of reinforcing bars were used in the project: #4G60 A706 for shear reinforcing, #4G100 for longitudinal reinforcing in the North-South direction and #6G100 for the East-West longitudinal reinforcing. Two samples of each bar type were tested. The stress – strain curves are shown in Figure A- 7, Figure A- 8, and Figure A- 9. Summaries of the reinforcing bar properties are shown in Table A- 9. The #4G60 bars show no yield plateau which can be expected if the bars were straightened from a coiled spool.

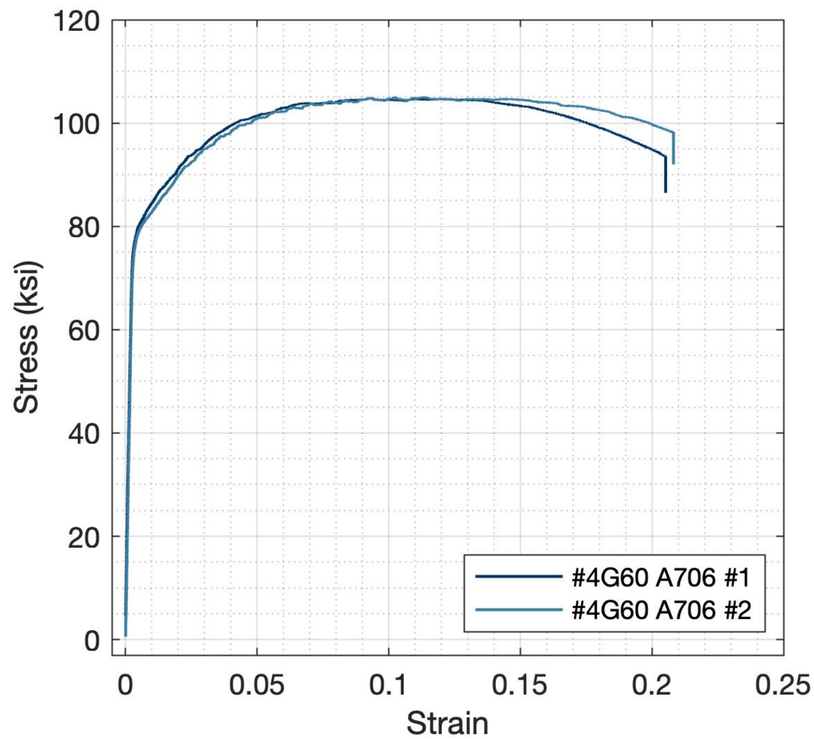

Figure A- 7. Stress - strain graph for shear reinforcing bars #4G60 A706

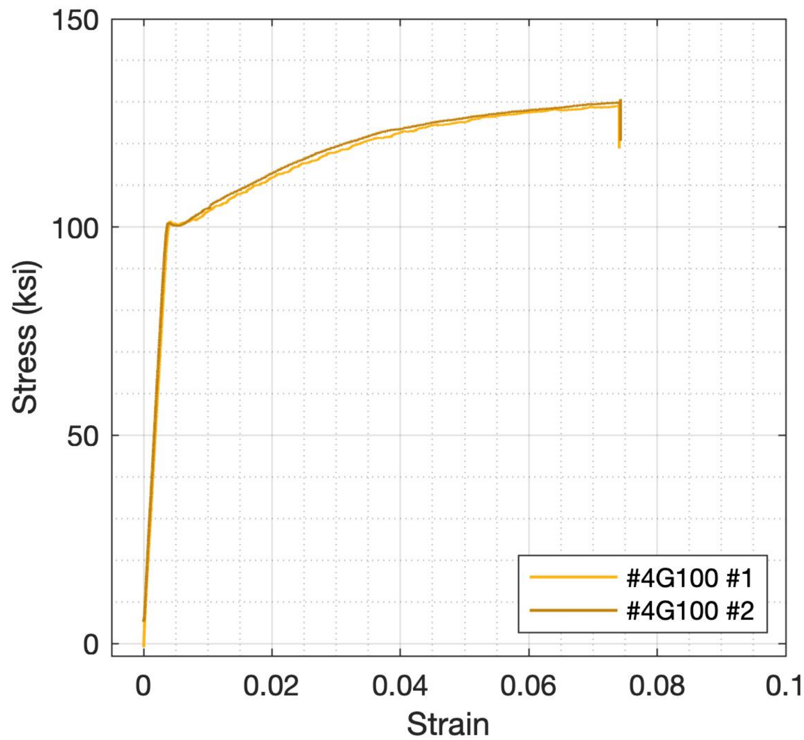

Figure A- 8. Stress - strain graph for longitudinal reinforcing bars #4G60 A706

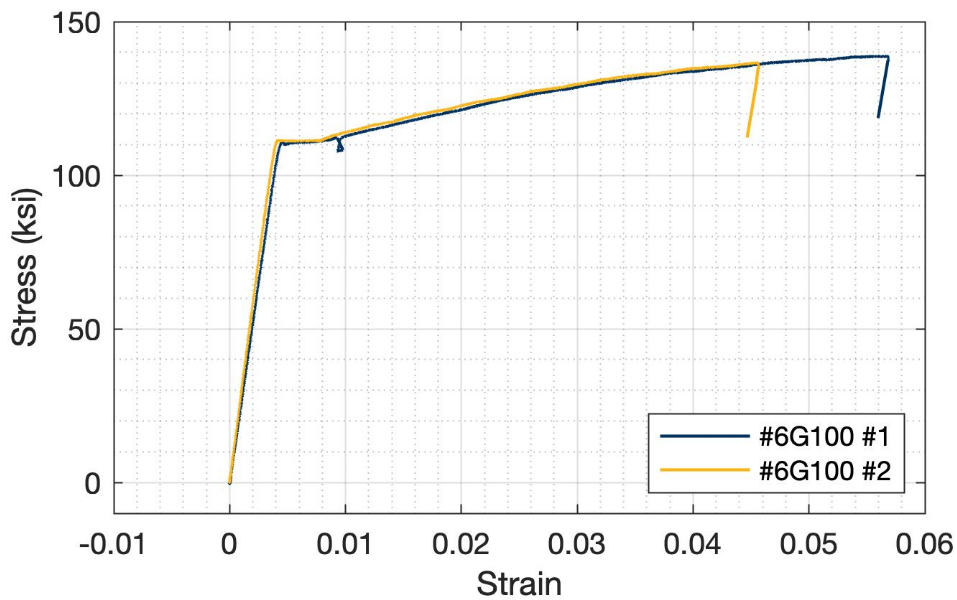

Figure A- 9. Stress - strain graph for longitudinal reinforcing bars #6G100

Table A- 9. Measured reinforcing bar properties

Bar	Specimen	Gague length (in)	Stopped test	σy (ksi)	εy	E (ksi)	σmax (ksi)	ε at σmax	ε rupture
#4G60 A706	1	2	Rupture	75.0	0.0028	27200	105	0.093	0.205
#4G60 A706	2	2	At necking	75.0	0.0033	27800	105	0.113	0.208
#4G100	1	8	Rupture	101	0.0040	26600	130	0.074	0.074
#4G100	2	8	Rupture	101	0.0038	27900	131	0.074	0.074
#6G100	1	2	Before rupture	110	0.0044	26200	139	0.0568	NA
#6G100	2	2	Before rupture	111	0.0041	28100	137	0.0456	NA

A.6 CONCRETE MIXTURE DESIGN

The concrete mixture was designed by Central Concrete as a 4000 psi mixture at 28 days with ¾" aggregate. Mixture details are shown in Figure A- 10. On casting day, not all the design water had been added into the mix resulting in a 3" slump. Once 30 gal of water had been added to the mix, the slump increased to a more workable 7.5" and the W/C ratio increased to the design value.

Date : **11/13/2017**
Mix Code : **347EG9E1** Description : **3IN LN 470LBS 3/4" 25FA 3-5SL**

Revision Number : 248 Creation Date : 09 Aug 2016 Customer :
Plant : OAKLAND PLANT (12) Created By : Kldiart Project :

Specifications

Consistence Class : 4.00 Max W/C : 1.00 Max Agg Size : 1
Strength Class : 3000 Min Cement : 471 lb Air Class : 2%
Grading Specification :

Material Type	Description	Supplier Source	Design Quantity	Specific Gravity	Volume ft3
Cement	990100 CEMENT ASTM C150 TYPE II/	Cemex-Victorville	353 lb	3.15	1.80
Fly Ash	990200 * FLY ASH	SRMG-Four Corners	118 lb	2.00	0.95
Coarse Aggregate	990301 3/4 GRAVEL	Cemex-Eliot	1675 lb	2.68	10.02
Fine Aggregate	990405 *ASTM C-33 SAND--ANGEL IS	Hanson-Oakland	1475 lb	2.62	9.02
Admixture	MASTER POZZOLITH 322N	BASF -Cleveland	19 lq oz	-	-
Water	990080 *WATER	Central Concrete-Central Concrete	33.0 gal	1.00	4.41
		Air Content	**3.00 %**	**--**	**0.81**
		Yield	**3896 lb**	**--**	**27.00**

Figure A- 10. Concrete mixture design 347EG9E1 by Central Concrete (Note: "Max Agg Size: 1" should read ¾")

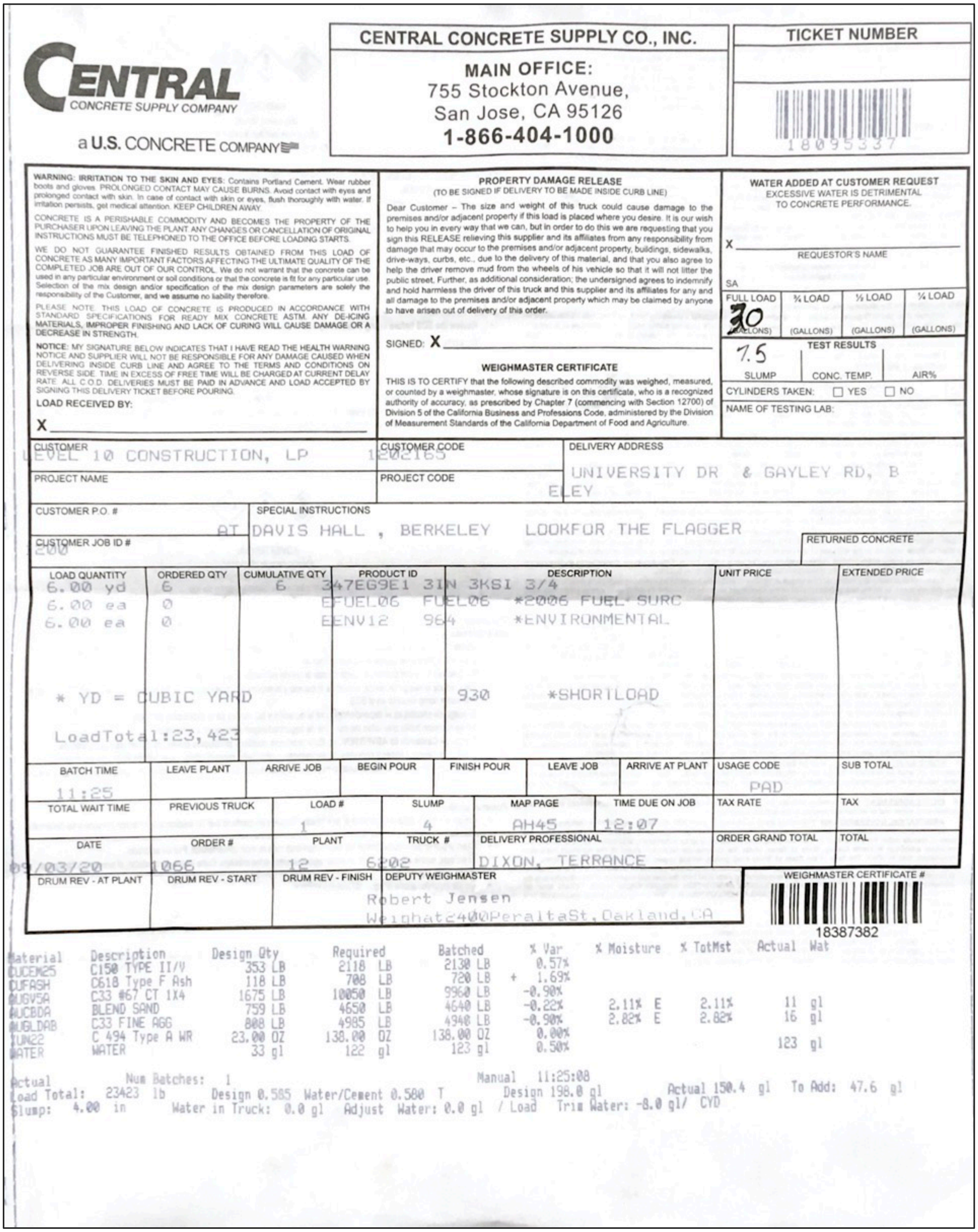
CENTRAL CONCRETE SUPPLY COMPANY

a U.S. CONCRETE COMPANY

CENTRAL CONCRETE SUPPLY CO., INC.

MAIN OFFICE:
755 Stockton Avenue,
San Jose, CA 95126
1-866-404-1000

TICKET NUMBER

18095337

WARNING: IRRITATION TO THE SKIN AND EYES: Contains Portland Cement. Wear rubber boots and gloves. PROLONGED CONTACT MAY CAUSE BURNS. Avoid contact with eyes and prolonged contact with skin. In case of contact with skin or eyes, flush thoroughly with water. If irritation persists, get medical attention. KEEP CHILDREN AWAY.

CONCRETE IS A PERISHABLE COMMODITY AND BECOMES THE PROPERTY OF THE PURCHASER UPON LEAVING THE PLANT. ANY CHANGES OR CANCELLATION OF ORIGINAL INSTRUCTIONS MUST BE TELEPHONED TO THE OFFICE BEFORE LOADING STARTS.

WE DO NOT GUARANTEE FINISHED RESULTS OBTAINED FROM THIS LOAD OF CONCRETE AS MANY IMPORTANT FACTORS AFFECTING THE ULTIMATE QUALITY OF THE COMPLETED JOB ARE OUT OF OUR CONTROL. We do not warrant that the concrete can be used in any particular environment or soil conditions or that the concrete is fit for any particular use. Selection of the mix design and/or specification of the mix design parameters are solely the responsibility of the Customer, and we assume no liability therefore.

PLEASE NOTE: THIS LOAD OF CONCRETE IS PRODUCED IN ACCORDANCE WITH STANDARD SPECIFICATIONS FOR READY MIX CONCRETE ASTM. ANY DE-ICING MATERIALS, IMPROPER FINISHING AND LACK OF CURING WILL CAUSE DAMAGE OR A DECREASE IN STRENGTH.

NOTICE: MY SIGNATURE BELOW INDICATES THAT I HAVE READ THE HEALTH WARNING NOTICE AND SUPPLIER WILL NOT BE RESPONSIBLE FOR ANY DAMAGE CAUSED WHEN DELIVERING INSIDE CURB LINE AND AGREE TO THE TERMS AND CONDITIONS ON REVERSE SIDE. TIME IN EXCESS OF FREE TIME WILL BE CHARGED AT CURRENT DELAY RATE. ALL C.O.D. DELIVERIES MUST BE PAID IN ADVANCE AND LOAD ACCEPTED BY SIGNING THIS DELIVERY TICKET BEFORE POURING.

LOAD RECEIVED BY:

X

PROPERTY DAMAGE RELEASE
(TO BE SIGNED IF DELIVERY TO BE MADE INSIDE CURB LINE)

Dear Customer – The size and weight of this truck could cause damage to the premises and/or adjacent property if this load is placed where you desire. It is our wish to help you in every way that we can, but in order to do this we are requesting that you sign this RELEASE relieving this supplier and its affiliates from any responsibility from damage that may occur to the premises and/or adjacent property, buildings, sidewalks, drive-ways, curbs, etc., due to the delivery of this material, and that you also agree to help the driver remove mud from the wheels of his vehicle so that it will not litter the public street. Further, as additional consideration; the undersigned agrees to indemnify and hold harmless the driver of this truck and this supplier and its affiliates for any and all damage to the premises and/or adjacent property which may be claimed by anyone to have arisen out of delivery of this order.

SIGNED: X

WEIGHMASTER CERTIFICATE

THIS IS TO CERTIFY that the following described commodity was weighed, measured, or counted by a weighmaster, whose signature is on this certificate, who is a recognized authority of accuracy, as prescribed by Chapter 7 (commencing with Section 12700) of Division 5 of the California Business and Professions Code, administered by the Division of Measurement Standards of the California Department of Food and Agriculture.

WATER ADDED AT CUSTOMER REQUEST
EXCESSIVE WATER IS DETRIMENTAL TO CONCRETE PERFORMANCE.

X
REQUESTOR'S NAME

SA

FULL LOAD	¾ LOAD	½ LOAD	¼ LOAD
30 (GALLONS)	(GALLONS)	(GALLONS)	(GALLONS)

TEST RESULTS

SLUMP	CONC. TEMP.	AIR%
7.5		

CYLINDERS TAKEN: ☐ YES ☐ NO

NAME OF TESTING LAB:

CUSTOMER: LEVEL 10 CONSTRUCTION, LP

CUSTOMER CODE: 1202165

DELIVERY ADDRESS: UNIVERSITY DR & GAYLEY RD, BERKELEY

PROJECT NAME:

PROJECT CODE:

CUSTOMER P.O. #:

SPECIAL INSTRUCTIONS: AT DAVIS HALL , BERKELEY LOOKFOR THE FLAGGER

CUSTOMER JOB ID #: 200

RETURNED CONCRETE

LOAD QUANTITY	ORDERED QTY	CUMULATIVE QTY	PRODUCT ID	DESCRIPTION	UNIT PRICE	EXTENDED PRICE
6.00 yd	6	6	347EG9E1	3IN 3KSI 3/4		
6.00 ea	0		EFUEL06	FUEL06 *2006 FUEL SURC		
6.00 ea	0		EENV12	964 *ENVIRONMENTAL		

* YD = CUBIC YARD 930 *SHORTLOAD

LoadTotal:23,423

BATCH TIME	LEAVE PLANT	ARRIVE JOB	BEGIN POUR	FINISH POUR	LEAVE JOB	ARRIVE AT PLANT	USAGE CODE	SUB TOTAL
11:25							PAD	

TOTAL WAIT TIME	PREVIOUS TRUCK	LOAD #	SLUMP	MAP PAGE	TIME DUE ON JOB	TAX RATE	TAX
		1	4	AH45	12:07		

DATE	ORDER #	PLANT	TRUCK #	DELIVERY PROFESSIONAL	ORDER GRAND TOTAL	TOTAL
09/03/20	1066	12	6202	DIXON, TERRANCE		

DRUM REV - AT PLANT	DRUM REV - START	DRUM REV - FINISH	DEPUTY WEIGHMASTER
			Robert Jensen Weighat2400PeraltaSt,Oakland,CA

WEIGHMASTER CERTIFICATE # 18387382

Material	Description	Design Qty	Required	Batched	% Var	% Moisture	% TotMst	Actual Wat
CUCEM25	C150 TYPE II/V	353 LB	2118 LB	2130 LB	0.57%			
CUFASH	C618 Type F Ash	118 LB	708 LB	720 LB	+ 1.69%			
AUGV5A	C33 #67 CT 1X4	1675 LB	10050 LB	9960 LB	-0.90%			
AUCBDA	BLEND SAND	759 LB	4650 LB	4640 LB	-0.22%	2.11% E	2.11%	11 gl
AUGLDAB	C33 FINE AGG	808 LB	4985 LB	4940 LB	-0.90%	2.82% E	2.82%	16 gl
IUN22	C 494 Type A WR	23.00 OZ	138.00 OZ	138.00 OZ	0.00%			
WATER	WATER	33 gl	122 gl	123 gl	0.50%			123 gl

Actual Num Batches: 1 Manual 11:25:08
Load Total: 23423 lb Design 0.585 Water/Cement 0.580 T Design 198.0 gl Actual 150.4 gl To Add: 47.6 gl
Slump: 4.00 in Water in Truck: 0.0 gl Adjust Water: 0.0 gl / Load Trim Water: -8.0 gl/ CYD

Figure A- 11. Concrete mixture batch ticket with actual weights

APPENDIX B. AS-BUILT SPECIMEN DRAWINGS

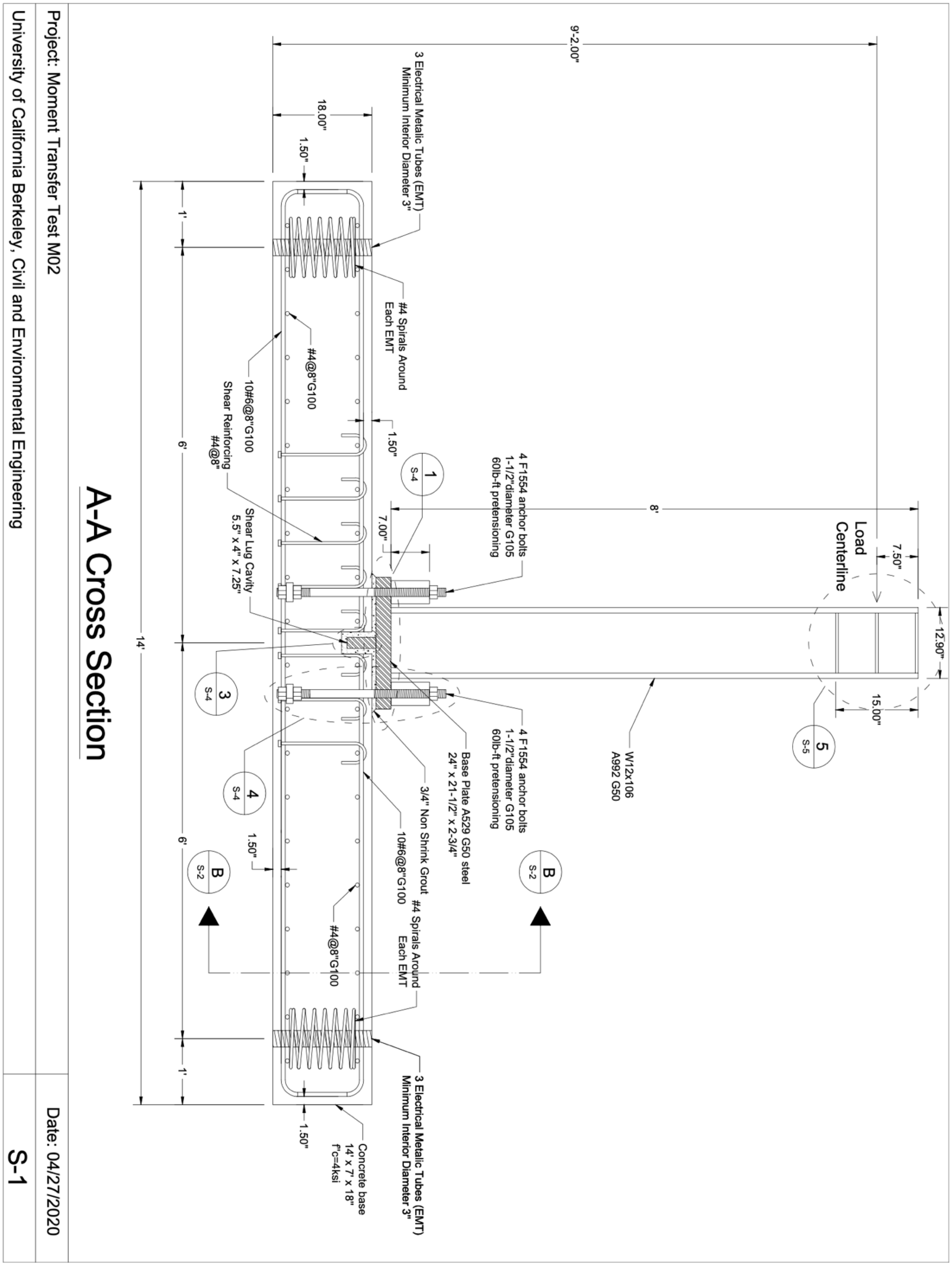
A-A Cross Section
Project: Moment Transfer Test M02
University of California Berkeley, Civil and Environmental Engineering
Date: 04/27/2020
S-1
9'-2.00"
3 Electrical Metalic Tubes (EMT) Minimum Interior Diameter 3"
18.00"
1.50"
1'
6'
14'
#4 Spirals Around Each EMT
#4@8"G100
10#6@8"G100
Shear Reinforcing #4@8"
1.50"
1
S-4
4 F1554 anchor bolts 1-1/2"diameter G105 60lb-ft pretensioning
8'
7.00"
Shear Lug Cavity 5.5" x 4" x 7.25"
Load Centerline
7.50"
12.90"
15.00"
5
S-5
W12x106 A992 G50
3
S-4
Base Plate A529 G50 steel 24" x 21-1/2" x 2-3/4"
3/4" Non Shrink Grout
4
S-4
B
S-2
Concrete base 14' x 7' x 18" f'c=4ksi

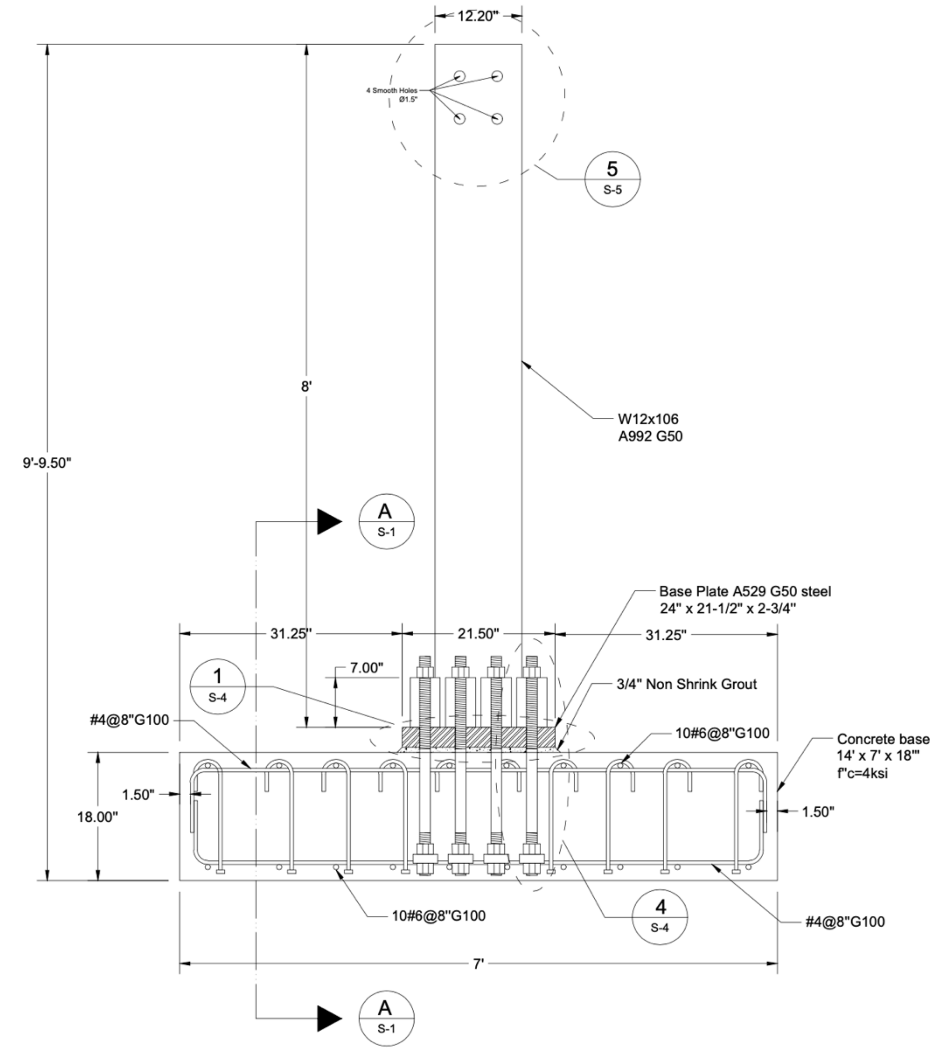

B-B Cross Section

Project: Moment Transfer Tes M02t	Date: 04/27/2020
University of California Berkeley, Civil and Environmental Engineering	S-2

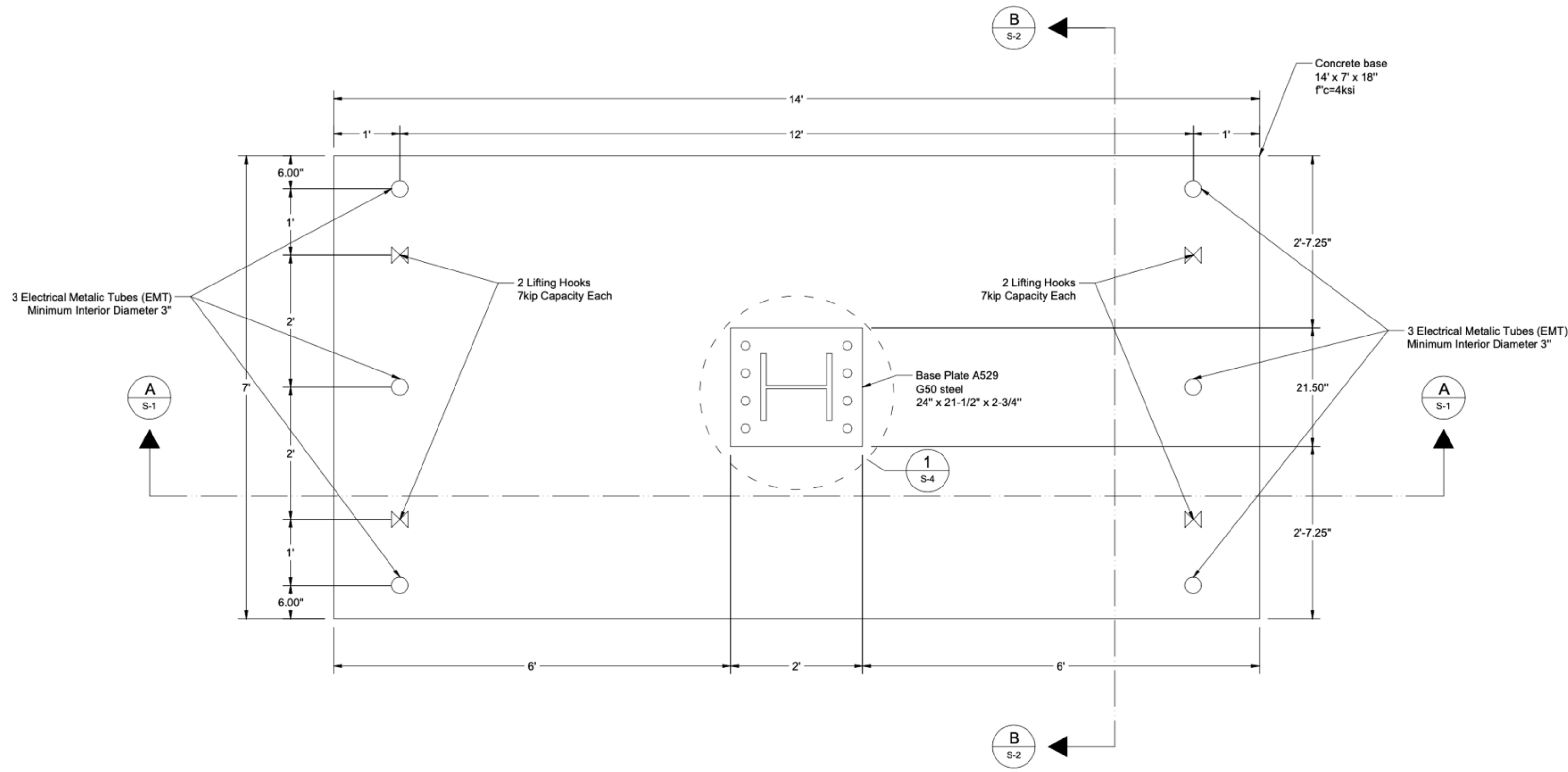

Plan View

Project: Moment Transfer Test M02	Date: 04/28/2020
University of California Berkeley, Civil and Environmental Engineering	S-3

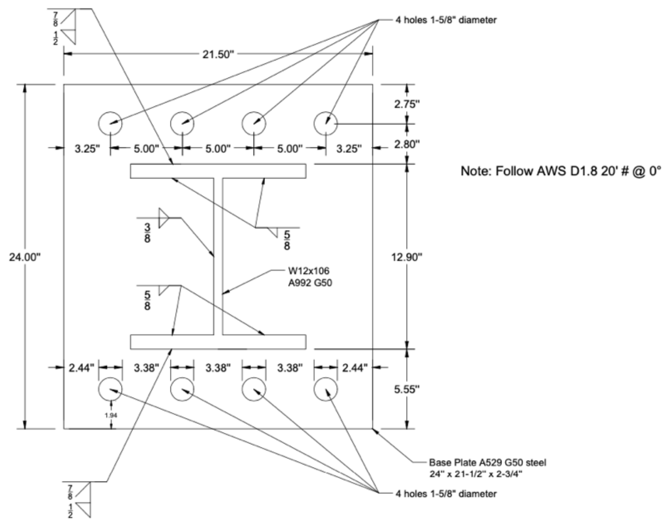

1 Base Plate

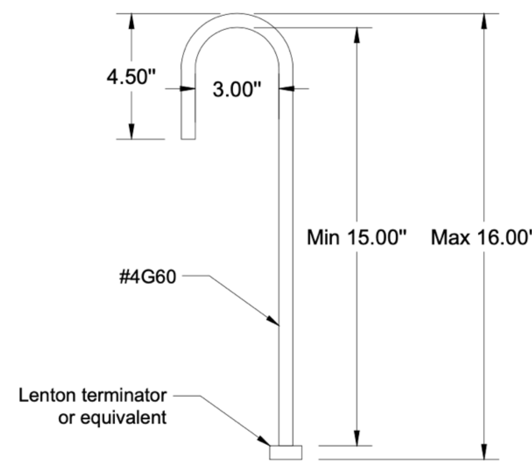

2 Shear Reinforcing

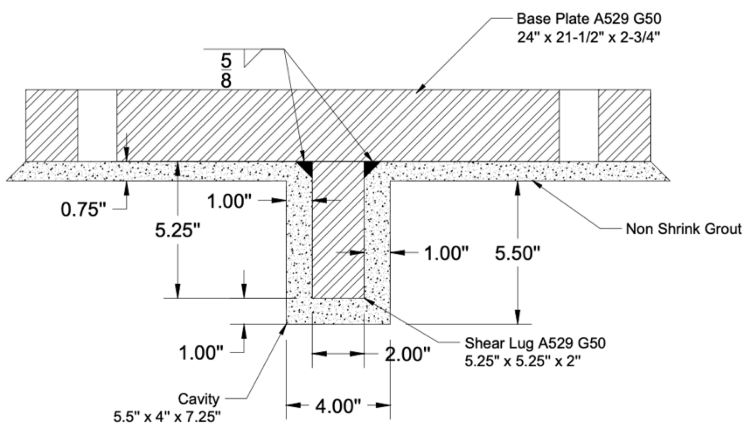

3 Shear Lug

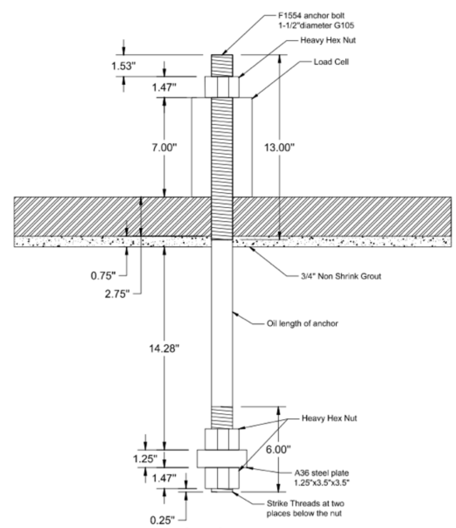

4 Anchors

Project: Moment Transfer Test M02	Date: 04/27/2020
University of California Berkeley, Civil and Environmental Engineering	S-4

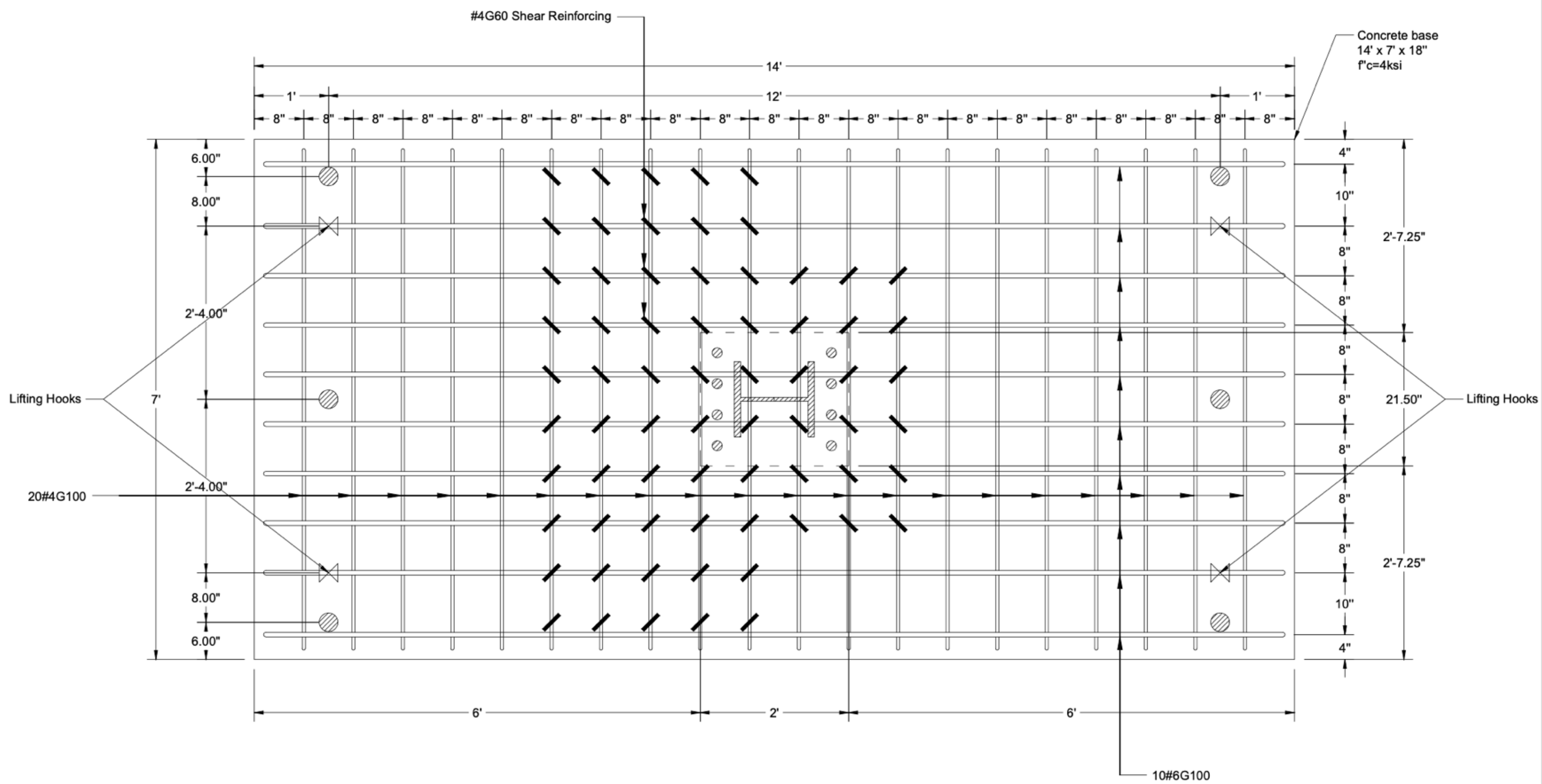

Plan View: Reinforcement Location

Project: Moment Transfer Test M02	Date: 04/27/2020
University of California Berkeley, Civil and Environmental Engineering	S-6

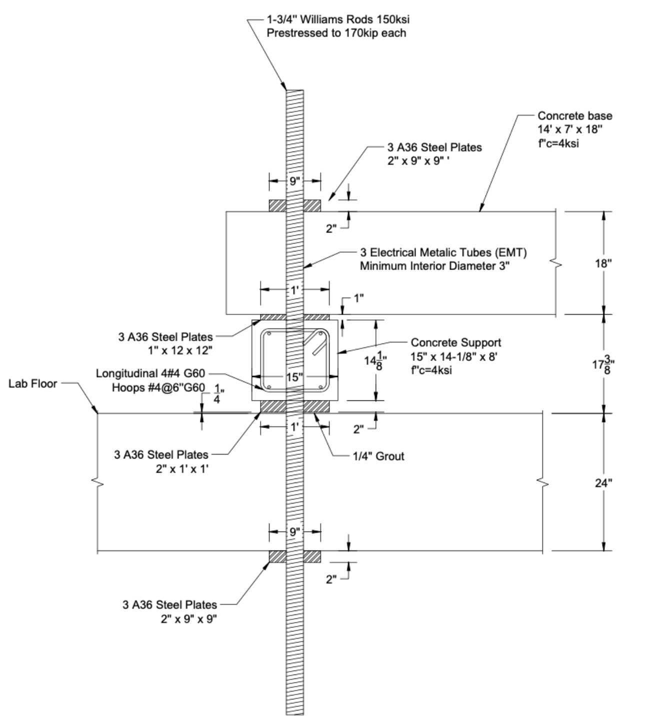

6 Support Type 1

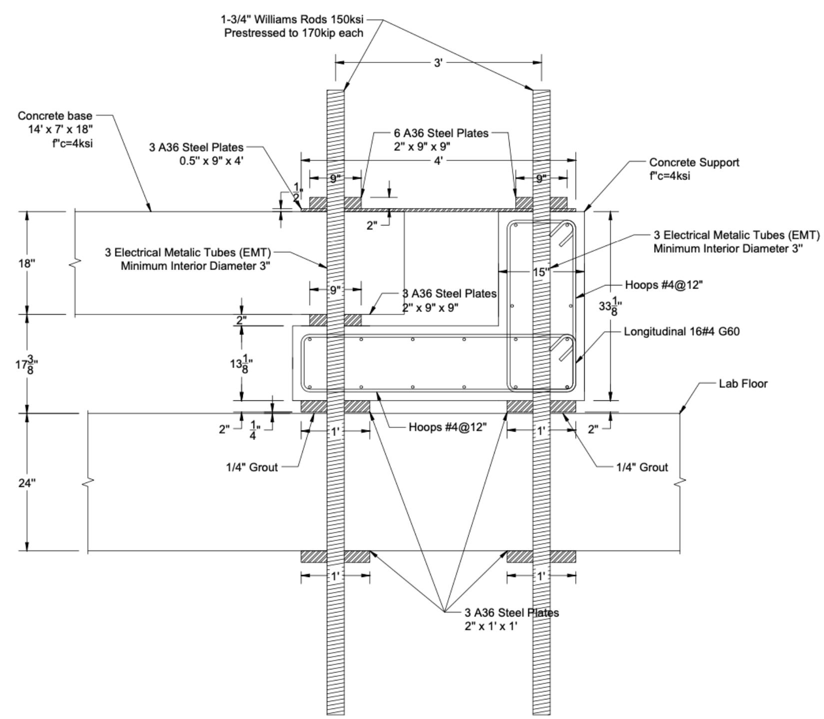

7 Support Type 2

Project: Moment Transfer Test M02	Date: 09/11/2020
University of California Berkeley, Civil and Environmental Engineering	S-7

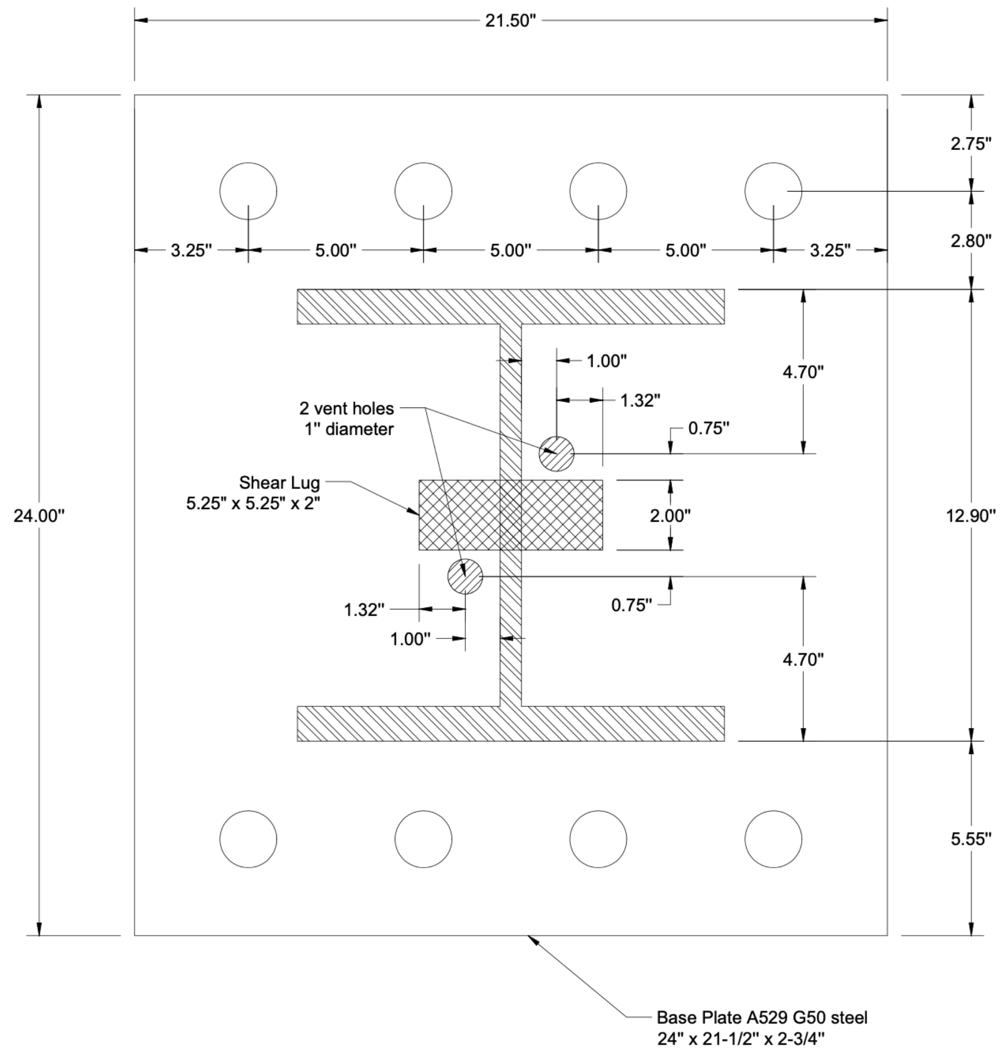

1 Base Plate

Project: Moment Transfer Test M02	Date: 07/02/2020
University of California Berkeley, Civil and Environmental Engineering	SD-12

APPENDIX C. ADDITIONAL SPECIMEN DESIGN CALCULATIONS

Detailed calculations of the specimen connection strengths are shown in section in the main body of the text. All other calculations of considered failure modes are shown below. Table C- 1 shows the factor of safety for all considered failure modes in increasing order.

Table C- 1. Summary of considered limit states and the factor of safety versus column yielding

Limit State	FS
Shear Lug	0.962
Tension Flange Welds	1.02
One Direction Shear	1.03
Anchor Rods Tension	1.06
Bearing on supports	1.09
Plate Thickness	1.09
Friction Sliding	1.56
Cantilever Tip Rods	1.80
Punching Shear	2.12
Shear Welds	2.15
Column Shear	2.50
Anchor Pryout	2.89
Anchor Rods Shear	3.74
Pullout	3.940
Web Local Yielding (point load)	8.51
Tension Plates	8.90
Web Crippling (point load)	12.5
Web Buckling	12.50
Slab Moment	20.70
Bolt Hole Bearing	23.7
Plate Shear Block	25.4

Note: Demand based on expected column yield, Capacities based on $\phi = 1$

Pullout

ACI 318-14 17.4.3 Crushing of concrete due to bearing on anchor head.

$N_p := 8 \cdot A_b \cdot f'c = 329.6 \text{ kips}$ Single anchor load that causes concrete crushing

$\psi cP := 1.4$ Cracked concrete

$nN_{pn} := nb \cdot \psi cP \cdot N_p = 1846 \text{ kips}$ Group load that causes concrete crushing

$FS := \dfrac{nN_{pn}}{468 \text{ kips}} = 3.94$ Factor of safety against column yielding

Bearing Stress

Calculate bearing stresses on nut at different failure loads.

$A_b = 10.5 \text{ in.}^2$

$\sigma_{brkt} := \dfrac{N_{cbg}}{nb \cdot A_b \cdot f'c} = 0.86$ Bearing stress on head at medain breakout as a multile of f'c

$\sigma_{bcj} := \dfrac{403 \text{ kip}}{nb \cdot A_b \cdot f'c} = 2.45$ Bearing stress on head when beam-column joine failure occurs as a multile of f'c.

$\sigma_{bcj} := \dfrac{370 \text{ kip}}{nb \cdot A_b \cdot f'c} = 2.25$ Bearing stress on head at peak load with 0.31% shear reinforcement ratio as a multile of f'c

Calculate bearing stresses on 3.5"x3.5" plate at different failure loads.

$A_{platewasher} := (3.5 \text{ in.})^2 - \pi \cdot (0.75 \text{ in.})^2 = 10.5 \text{ in.}^2$

$\sigma_{brkt} := \dfrac{N_{cbg}}{nb \cdot A_{platewasher} \cdot f'c} = 0.86$ Bearing stress on head at medain breakout as a multile of f'c

$\sigma_{bcj} := \dfrac{403 \text{ kip}}{nb \cdot A_{platewasher} \cdot f'c} = 2.45$ Bearing stress on head when beam-column joine failure occurs as a multile of f'c.

$\sigma_{bcj} := \dfrac{370 \text{ kip}}{nb \cdot A_{platewasher} \cdot f'c} = 2.25$ Bearing stress on head at peak load with 0.31% shear reinforcement ratio as a multile of f'c

Side-Face Blowout

ACI 318-14 17.4.4 For a single headed anchors with deep embedments close to an edge (h_{ef} > 2.5c_{a1}), side face blowout is not applicable.

Anchors in Shear

Concrete Breakout in Shear

ACI 318-14 17.5.2 **NOT APPLICABLE** because shear is transmited as compression through the slab to the supports.

Anchor Pryout

ACI 318-14 17.5.3

$k_{cp} := 2$

***k**cp* = **2.0** for ***h**ef* ≥ **2.5 in.**

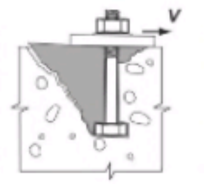

(ii) Concrete pryout for anchors far from a free edge

$N_{cpg} := N_{cbg} = 142 \text{ kips}$

$V_{cpg} := k_{cp} \cdot N_{cpg} = 285 \text{ kips}$ Compare to anchor rods as a group

$FS := \dfrac{V_{cpg}}{98.3 \text{ kips}} = 2.89$ Factor of safety against column yielding

M02 Desing:
Loads, Column, Base Plate and Anchor Rods

Assumptions

Base plate, anchor rods, punching shear and one direction shear are designed for the expected moment capacity of the column using fi of 1.
Shear lug and anchor rods are designed to resist all the shear individually.
Moment is calculated at the face of the joint

Notation

Input
Output
Condition Check

Data

$E := 29000 \text{ ksi}$
$f'c := 3700 \text{ psi}$

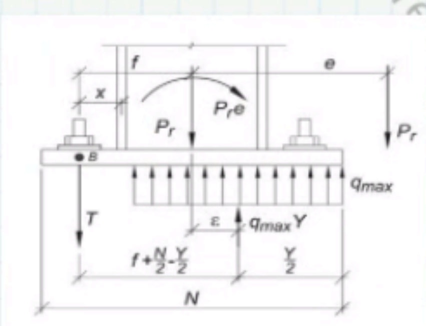

Fig. 3.4.1. Base plate with large moment.

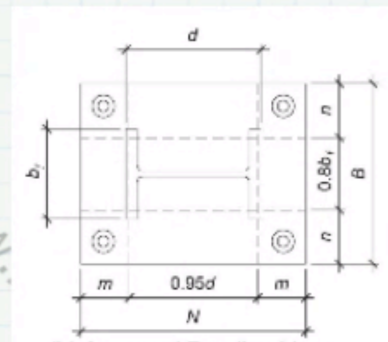

(b) Assumed Bending Lines

$B := 21.5 \text{ in.}$
$N := 24 \text{ in.}$

Column: W12x106 A529 G50

$bf := 12.2 \text{ in.}$
$d := 12.9 \text{ in.}$
$tf := 0.99 \text{ in.}$
$tw := 0.61 \text{ in.}$
$f := 9.25 \text{ in.}$

$x := f - \frac{d}{2} + \frac{tf}{2} = 3.3 \text{ in}$

$h := 15.9 \cdot tw = 9.7 \text{ in}$ $\qquad \frac{h}{tw} = 15.9$

$Fycol := 50000\ psi$

$Fucol := 65000\ psi$ Fucol is from 65-100ksi

$Zx := 164\ in.^3$

$Sx := 145\ in.^3$

$ry := 3.11\ in.$

$Ry := 1.2$ AISC-341-16 Table A3.1 Expected yield and rupture overstrength factors

$Rt := 1.2$

$\varphi_M := 1$

Expected Yield Moment

$My := Fycol \cdot Ry \cdot Sx = (8.7 \cdot 10^3)\ kips \cdot in.$

Expected Ultimate Moment

$Mu := Fycol \cdot Rt \cdot Zx = (9.8 \cdot 10^3)\ kips \cdot in.$

$Lp := 1.76 \cdot ry \cdot \sqrt{\frac{E}{Fycol \cdot Ry}} = 120\ in.$ Maximum length so lateral torsional buckling will not govern

Shear

$$\frac{\frac{h}{tw}}{2.24 \cdot \sqrt{\frac{E}{Fycol}}} = 0.295$$ Must be less than 1 for local buckling

$Cv := 1$

$Vn := 0.6\ Fycol \cdot (d \cdot tw)\ Cv = 236\ kips$

Loads

$Pu := 1\ kips$ Self weight of column and actuator. Some axial load is neccessary or equations do not work

$L := 92\ in.$ Vertical distance from force application to slab surface

$Vy := \frac{My}{L} = 94.6\ kips$ Lateral load that will yield the column

$$\frac{Vn}{Vy} = 2.5$$

Must be greater than 1

$$e := \frac{My}{Pu} = \left(8.7 \cdot 10^3\right)\ \text{in.}$$

Almost no axial load so excentricity is very large

Bearing capacity on concrete

ACI 318-14 22.8

A1<<A2 The base plate area is small compared to the concrete pedestal area. Factor of 2 included.

$$\varphi_{Bear} := 0.65$$

$$f_{pMax} := \varphi_{Bear} \cdot 0.85 \cdot f'c \cdot 2 = \left(4.09 \cdot 10^3\right)\ \text{psi}$$

$$q_{max} := \varphi_{Bear} \cdot 0.85 \cdot f'c \cdot 2 \cdot B = 87.9\ \frac{\text{kips}}{\text{in.}}$$

Minimum excentricity

Minimum excentricity so AISC Design Guide for plate, bearing, and bolts applies.

$$e_{min} := \frac{N}{2} - \frac{Pu}{\left(2 \cdot q_{max}\right)} = 12\ \text{in.}$$

$$\frac{e_{min}}{e} = 0.001$$

Must be less than 1

Base plate

Calculations based on ASCE Design Guide 1

$$\left(f + \frac{N}{2}\right)^2 = 452\ \text{in.}^2$$

$$2 \cdot Pu \cdot \frac{(e+f)}{q_{max}} = 198\ \text{in.}^2$$

$$\frac{\left(2 \cdot Pu \cdot \frac{(e+f)}{q_{max}}\right)}{\left(f + \frac{N}{2}\right)^2} = 0.439$$

Must be less than 1

$$Y1 := \left(f + \frac{N}{2}\right) - \sqrt{\left(f + \frac{N}{2}\right)^2 - 2 \cdot \frac{Pu \cdot (e+f)}{q_{max}}} = 5.33\ \text{in.}$$

$$Y2 := \left(f + \frac{N}{2}\right) + \sqrt{\left(f + \frac{N}{2}\right)^2 - 2 \cdot \frac{Pu \cdot (e+f)}{q_{max}}} = 37.2\ \text{in.}$$

$Y := Y1 = 5.33 \text{ in.}$ Choose realistic Y from Y1 and Y2

$T_{total} := q_{max} \cdot Y - Pu = 468 \text{ kips}$ Tension force in anchor group at column yield.

$z := f + \frac{N}{2} - \frac{Y}{2} = 18.6 \text{ in.}$ Internal lever arm

Base Plate Thickness

$Fy_{plate} := 50000 \text{ psi}$ Steel plate A529 G50

$Fu_{plate} := 70000 \text{ psi}$

$$n := \frac{(B - 0.8 \cdot bf)}{2} = 5.87 \text{ in.}$$

$$m := \frac{(N - 0.95 \cdot d)}{2} = 5.87 \text{ in.}$$

$$Maxmn := \max(m, n) = 5.87 \text{ in.}$$

$$x1 := 1.49 \cdot Maxmn \cdot \sqrt{\frac{f_{pMax}}{Fy_{plate}}} = 2.5 \text{ in.}$$

$$x2 := 2.11 \cdot \sqrt{\frac{f_{pMax} \cdot Y \cdot \left(Maxmn - \frac{Y}{2}\right)}{Fy_{plate}}} = 2.49 \text{ in.}$$

$$t_{pMin}1 := \text{if}(Y \geq Maxmn, x1, x2) = 2.49 \text{ in.}$$

$$t_{pMin}2 := 2.11 \cdot \sqrt{\frac{T_{total} \cdot x}{B \cdot Fy_{plate}}} = 2.53 \text{ in.}$$

$$t_{pMin} := \max\left(t_{pMin}1, t_{pMin}2\right) = 2.53 \text{ in.}$$

$tp := \left(2 + \frac{3}{4}\right) \text{ in.}$ $\frac{tp}{t_{pMin}} = 1.09$ Must be greater than 1

Welds

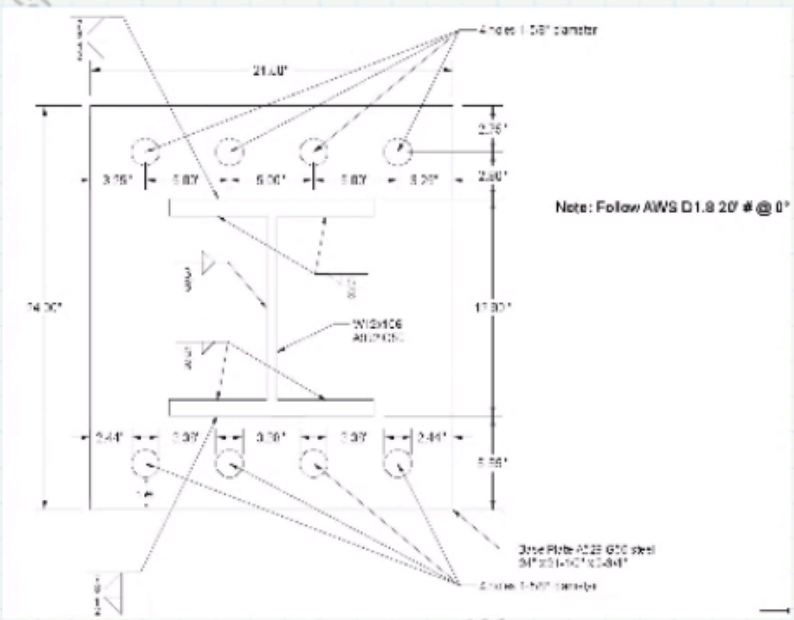

1. Tension Fillet Welds (tfw) on Flange

$F_{EXX} := 70000 \text{ psi}$ All welds 70,000 psi electrode

$w_{tfw} := \frac{9}{8} \text{ in.}$ 1/2in weld on one side and 5/8in on other side

$k1 := \left(1 + \frac{1}{8}\right) \text{ in.} = 1.13 \text{ in.}$

$Lw_{tfw} := bf - 2 \cdot k1 = 10 \text{ in.}$

$R_{n1} := 0.707 \cdot w_{tfw} \cdot Lw_{tfw} \cdot (0.6 \cdot F_{EXX} \cdot 1.5) = 499 \text{ kips}$

2. Tension Fillet Welds (tfw) on Flange, Base Metal

$Fy_{BM} := 50000 \text{ psi}$ Column steel properties

$Fu_{BM} := 65000 \text{ psi}$

$R_{n2A} := 0.6 \cdot Fy_{BM} \cdot Lw_{tfw} \cdot w_{tfw} = 336 \text{ kips}$

$R_{n2B} := 0.6 \cdot Fu_{BM} \cdot Lw_{tfw} \cdot w_{tfw} = 437 \text{ kip}$

$R_{n2} := min\left(R_{n2A}, R_{n2B}\right) = 336 \text{ kips}$

3. Partial Jont Penetration weld (PJP) on Flange

$w_{PJP} := \frac{7}{8} \text{ in.}$

$Lw_{PJP} := d = 12.9 \text{ in.}$

$R_{n3} := 0.6 \cdot F_{EXX} \cdot Lw_{PJP} \cdot \left(w_{PJP} - \frac{1}{8} \text{ in.}\right) = 406 \text{ kip}$

4. Partial Jont Penetration weld (PJP) on Flange, Base Metal

$R_{n4} := Fy_{BM} \cdot \left(w_{PJP} - \frac{1}{8} \text{ in.}\right) \cdot Lw_{PJP} = 484 \text{ kip}$

$R_{n5} := Fu_{BM} \cdot \left(w_{PJP} - \frac{1}{8} \text{ in.}\right) \cdot Lw_{PJP} = 629 \text{ kip}$

Flange Weld Summary

$R_n := min\left(R_{n1}, R_{n2}\right) + min\left(R_{n3}, R_{n4}, R_{n5}\right) = 742 \text{ kip}$

$P_{fw} := \frac{R_n \cdot (d - tf)}{L} = 96 \text{ kips}$

$Vu := Vy = 94.6 \text{ kip}$ Design for column yield

$\frac{P_{fw}}{Vu} = 1.02$ Must be greater than or equal to 1

1. Shear Weld

$$w_s := \frac{3}{8}\ \text{in.}$$

$$Lw_s := 2 \cdot \left(9 + \frac{1}{8}\right)\ \text{in.} = 18.3\ \text{in}$$

$$R_{ns1} := 0.6 \cdot F_{EXX} \cdot 0.707 \cdot w_s \cdot Lw_s = 203\ \text{kips}$$

2. Shear Weld - Base Metal

$$R_{ns2} := 0.6 \cdot Fy_{BM} \cdot w_s \cdot Lw_s = 205\ \text{kips}$$

Web Weld Summary

$$R_{ns} := min\left(R_{ns1}, R_{ns2}\right) = 203\ \text{kips}$$

$$\frac{R_{ns}}{Vu} = 2.15$$ Must be greater than 1

Anchor rods

$nb:=4$ Number of bolts resisting tension (bolts on one side)

$Tu:=\dfrac{T_{total}}{nb}=117\ \text{kips}$ Tension per anchor rod

$\phi Rn:=124\ \text{kips}$ Chose 4 anchor rods 1-1/2in F1554 G105

$\dfrac{\phi Rn}{Tu}=1.06$ Must be greater than 1

Table 3.1. ASTM F1554 Anchor Rod (rod only) Available Tensile Strength, kips

Rod Diameter, in.	Rod Area, A_g, in.^{2}	LRFD ϕR_n $\phi = 0.75$ Grade 36 kips	LRFD Grade 55 kips	LRFD Grade 105 kips	ASD R_n/Ω $\Omega = 2.00$ Grade 36 kips	ASD Grade 55 kips	ASD Grade 105 kips
5/8	0.307	10.0	12.9	21.6	6.68	8.63	14.4
3/4	0.442	14.4	18.6	31.1	9.60	12.4	20.7
7/8	0.601	19.6	25.4	42.3	13.1	16.9	28.2
1	0.785	25.6	33.1	55.2	17.1	22.1	36.8
1 1/8	0.994	32.4	41.9	69.9	21.6	28.0	46.6
1 1/4	1.23	40.0	51.8	86.3	26.7	34.5	57.5
1 1/2	1.77	57.7	74.6	124	38.4	49.7	82.8
1 3/4	2.41	78.5	102	169	52.3	67.6	113
2	3.14	103	133	221	68.3	88.4	147
2 1/4	3.98	130	168	280	86.5	112	186
2 1/2	4.91	160	207	345	107	138	230
2 3/4	5.94	194	251	418	129	167	278
3	7.07	231	298	497	154	199	331
3 1/4	8.30	271	350	583	180	233	389
3 1/2	9.62	314	406	677	209	271	451
3 3/4	11.0	360	466	777	240	311	518
4	12.6	410	530	884	273	353	589

Table from AISC Design Guide 1

Anchor Rods in Shear

As recommended by the Design Guide 1 AISC only half of the rods are assumed to resist shear.

$Vu=94.6\ \text{kips}$

$Fu_{rod}:=125000\ \text{psi}$

$Ab:=4\cdot 1.77\ \text{in.}^2=7.08\ \text{in.}^2$ Area of 4 bolts

$Vn:=0.4\cdot Fu_{rod}\cdot Ab=354\ \text{kips}$

$\dfrac{Vn}{Vu}=3.74$ Must be greater than 1

Minimum plate edge distance

$c_{min} := 1.25 \cdot 1.5\ \text{in.} = 1.88\ \text{in}$ 1-1/4 of the bolt diameter

$c_{actual} := 2.75\ \text{in.}$ From center to closest edge

$\frac{c_{actual}}{c_{min}} = 1.47$ Must be greater than 1

Minimum Anchor Rod Spacing

AISC J3.3

$db_{rod} := 1.5\ \text{in.}$

$spacing_{min} := \left(2 + \frac{2}{3}\right) \cdot db_{rod} = 4\ \text{in.}$

$spacing_{actual} := 5\ \text{in.}$ Center to center spacing of bolts

$\frac{spacing_{actual}}{spacing_{min}} = 1.25$ Must be greater than 1

Bolt Hole Bearing Strength

AISC J3.10

$lc := 1.94\ \text{in.}$ Dist from edge of hole to edge of plate

$Rn := min\left(1.5\ lc \cdot tp \cdot Fu_{plate}, 3\ db_{rod} \cdot tp \cdot Fu_{plate}\right) = 560\ \text{kips}$

$Rn \cdot nb = \left(2.24 \cdot 10^{3}\right)\ \text{kips}$

$\frac{Rn \cdot nb}{Vu} = 23.7$ Must be greater than 1

Plate Shear Block

AISC J4.3

$Agv := 2.75\ \text{in.} \cdot tp \cdot 2 = 15.1\ \text{in}^2$

$Anv := 1.94\ \text{in.} \cdot tp \cdot 2 = 10.7\ \text{in}^2$

$Ant := 3 \cdot 3.38\ \text{in.} \cdot tp = 27.9\ \text{in}^2$

$Rn_{SBlock1} := 0.6 \cdot Fu_{plate} \cdot Anv + 1 \cdot Fu_{plate} \cdot Ant = 2400\ \text{kips}$

$Rn_{SBlock2} := 0.6 \cdot Fy_{plate} \cdot Agv + 1 \cdot Fu_{plate} \cdot Ant = 2406\ \text{kips}$

$Rn_{SBlock} := min\left(Rn_{SBlock1}, Rn_{SBlock2}\right) = 2400\ \text{kips}$

$Rn_{SBlock} = \left(2.4 \cdot 10^3\right)\ \text{kips}$

$\dfrac{Rn_{SBlock}}{Vu} = 25.4$ Must be greaterthan 1

Shear Lug

AISC Design Guide 1 is used for shear lug design.

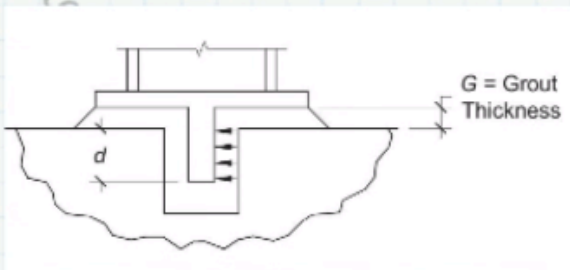

Lug Properties

$l := 5.25\ in.$

$G := 0.75\ in.$

$d := 4.5\ in.$

$h := G + d = 5.25\ in.$

$t := 2\ in.$

$F_{ylug} := 50000\ psi$

Weld

$t_w := \frac{5}{8}\ in.$

$F_{EXX} := 70000\ psi$

1. Bearing

$$A_{req} := \frac{Vu}{1.3 \cdot f'c} = 19.7\ in.^2$$

$$d_{req} := \frac{A_{req}}{l} = 3.74\ in.$$

$$\frac{d}{d_{req}} = 1.2$$

Must be greater than 1

2. Concrete Breakout

$A_v := 18\ \text{in.} \cdot 84\ \text{in.} - 12\ \text{in.} \cdot 2.5\ \text{in.} = (1.48 \cdot 10^3)\ \text{in}^2$ Projected area by 45 degree planes (AISC Design Guide 1 Fig 4.9.3)

$$V_{conc} := 4 \cdot \sqrt{\frac{f'c}{psi}} \cdot \frac{A_v}{\text{in.}^2} \cdot \frac{\text{kips}}{1000} = 361\ \text{kips}$$

$$\frac{V_{conc}}{Vu} = 3.81$$ Must be greater than 1

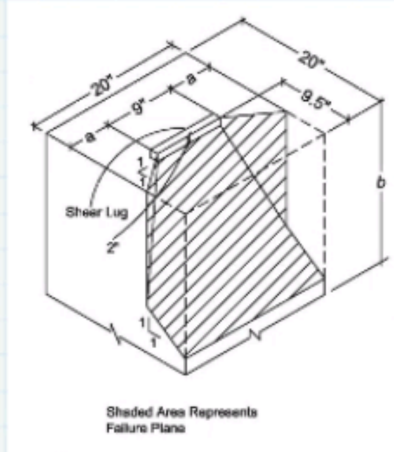

Fig. 4.9.3. Lug failure plane.

3. Lug Thickness

$$Mu_{lug} := Vu \cdot \left(G + \frac{d}{2}\right) = 284\ \text{kip} \cdot \text{in}$$ Cantilever model

$$t_{req} := \sqrt{\frac{Mu_{lug} \cdot 4}{F_{ylug} \cdot l}} = 2.079\ \text{in.}$$

$$\frac{t}{t_{req}} = 0.962$$ Must be less than 1

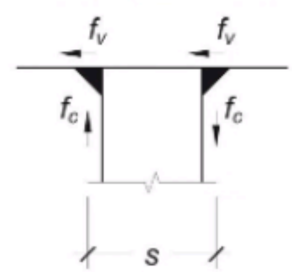

Fig. 4.9.4. Forces on shear lug welds.

4. Welds

$$s := t + 2 \cdot \frac{1}{3} \cdot t_w = 2.417\ \text{in.}$$

$$f_c := \frac{Mu_{lug}}{s \cdot l} = 22.4\ \frac{\text{kip}}{\text{in}}$$

$$f_v := \frac{Vu}{2 \cdot l} = 9.01\ \frac{\text{kips}}{\text{in.}}$$

$$f_r := \sqrt{{f_c}^2 + {f_v}^2} = 24.1\ \frac{\text{kips}}{\text{in.}}$$

$$R_n := 0.6 \cdot F_{EXX} \cdot 1.5 \cdot t_w \cdot 0.707 = 27.8\ \frac{\text{kips}}{\text{in.}}$$

$$\frac{R_n}{f_r} = 1.15$$

Must be greater than 1

Minimum safety factor for shear lug

$$a := min\left(\frac{d}{d_{req}}, \frac{V_{conc}}{Vu}, \frac{t}{t_{req}}, \frac{R_n}{f_r}\right) = 0.962$$

Shear Lug

ACI 318-19 Chap. 17.11

Lug Properties

$h_{ef} := 14.3\ \text{in.}$ $t_{sl} := 2\ \text{in.}$

$h_{sl} := 4.5\ \text{in.}$ $h_a := 18\ \text{in.}$

$c_{sl} := 9.25\ \text{in.}$

Weld

$t_w := \frac{5}{8}\ \text{in.}$

$F_{EXX} := 70000\ \text{psi}$

$F_{ylug} := 50000\ \text{psi}$

1. Geometry

$\frac{\left(\frac{h_{ef}}{h_{sl}}\right)}{2.5} = 1.271$ Must be greater than 1

$\frac{\left(\frac{h_{ef}}{c_{sl}}\right)}{2.5} = 0.618$ Must be greater than 1

2. Bearing strength

$t_{sl} := 2\ \text{in.}$ $b := 5.25\ \text{in.}$

$A_{ef\_sl} := 2 \cdot t_{sl} \cdot b = 21\ \text{in.}^2$

$Vu = 94.565\ \text{kip}$

$\psi_{brg\_sl} := 1$

$V_{brg\_sl} := 1.7 \cdot f'c \cdot A_{ef\_sl} \cdot \psi_{brg\_sl} = 132\ \text{kip}$

$\frac{V_{brg\_sl}}{Vu} = 1.397$ Must be greater than 1

3. Breakout strength shear perpendicular to edge

Not applicable

4. Breakout strength shear parallel to edge

$c_{a1} := 42\ in.$

$V_b := 9 \cdot \sqrt{\frac{f'c}{psi}} \cdot \left(\frac{c_{a1}}{in.}\right)^{1.5}\ lbf = 149\ kip$

$A_{vc} := 18\ in. \cdot (3 \cdot c_{a1} + t_{sl}) - t_{sl} \cdot h_{sl} = 2295\ in.^2$

$A_{vc0} := 4.5\left(\frac{c_{a1}}{in.}\right)^2\ in. \cdot in. = 7938\ in.^2$

$\frac{A_{vc}}{A_{vc0}} = 0.289$

$\psi_{ed\_V} := 1.0$

$\psi_{c\_V} := 1.2$

$\psi_{h\_V} := \sqrt{1.5\ \frac{c_{a1}}{h_a}} = 1.871$

$V_{cb\_sl} := 2\ \frac{A_{vc}}{A_{vc0}} \cdot \psi_{ed\_V} \cdot \psi_{c\_V} \cdot \psi_{h\_V} \cdot V_b = 193\ kip$

$\frac{V_{cb\_sl}}{Vu} = 2.046$ Must be greater than 1

M02 Design:
Punching Shear, One Direction Shear, Moment

Assumptions

Base plate, anchor rods, punching shear, one direction shear, and moment are designed for the expected column yielding.

Two-Way Shear

Notation

Input

Output

Condition Check

$f'c := 3930\ \text{psi}$ $\phi := 0.75$

$B := 21.5\ \text{in.}$ Base plate dimensions
$N := 24\ \text{in.}$

The critiacal section is taken a rectuangular area offset from the outer edge of the base plate a distance of d/2

$$d_{avg} := 18\ \text{in.} - 1.5\ \text{in.} - \frac{(0.5 + 0.75)}{2}\ \text{in.} = 15.9\ \text{in.}$$

Average d for both perpendicular direction of the slab.

$$b_o := 2\ (B + N + 2 \cdot d_{avg}) = 155\ \text{in.}$$

Perimeter of the critical section.

Two Way Shear Demand

Loads based on column yield.

$Pu := 2\ \text{kips}$
$Mu := 8700\ \text{kips} \cdot \text{in.}$

$c1 := N = 24\ \text{in.}$ Plate dimentions
$c2 := B = 21.5\ \text{in.}$

$b1 := c1 + d_{avg} = 39.9\ \text{in.}$
$b2 := c2 + d_{avg} = 37.4\ \text{in.}$

$$\gamma_f := \frac{1}{1 + \left(\frac{2}{3}\right)\sqrt{\frac{b1}{b2}}} = 0.592$$

ACI 318-14 8.4.2.3.2 Fraction of moment demant that will be resisted by moment in the slab.

$$\gamma_v := 1 - \gamma_f = 0.408$$

Fraction of moment demand that will be resisted by shear stress in the slab.

$$c := \frac{b1}{2} = 19.9\ \text{in.}$$

$$J_c := 2 \cdot \left(\frac{d_{avg} \cdot b1^3}{12} + \frac{b1 \cdot d_{avg}^{\ 3}}{12} + d_{avg} \cdot b2 \cdot \left(\frac{b1}{2} \right)^2 \right) = \left(6.66 \cdot 10^5\right) \text{ in}^4$$

$$vu := \frac{Pu}{b_o \cdot d_{avg}} + \gamma_v \cdot Mu \cdot \frac{c}{J_c} = 107 \text{ psi}$$

$$v_{u\_max} := \phi \cdot 6 \cdot \sqrt{\frac{f'c}{\text{psi}}} \text{ psi} = 282 \text{ psi}$$ Max shear for two-way members with shear reinf

$$\frac{v_{u\_max}}{vu} = 2.64$$ Must be greater than 1.

Two Way Shear Capacity Case 1: No shear reinforcement

If concrete can resist two-way shear at critical region near column, it can resist that load at other critical sections.

$$\beta := \frac{N}{B} = 1.12$$ Ratio of longer to shorter side of column

$$\lambda_s := \sqrt{\frac{2}{\left(1 + \frac{\left(\frac{d_{avg}}{\text{in.}}\right)}{10}\right)}} = 0.879$$ Size effect factor

$$\alpha_s := 40$$ For interior columns

$$vc1 := 4 \cdot \lambda_s \cdot \sqrt{\frac{f'c}{\text{psi}}} \text{ psi} = 220 \text{ psi}$$

$$vc2 := \left(2 + \frac{4}{\beta}\right) \cdot \lambda_s \cdot \sqrt{\frac{f'c}{\text{psi}}} \text{ psi} = 308 \text{ psi}$$

$$vc3 := \left(2 + \frac{\alpha_s \cdot d_{avg}}{b_o}\right) \cdot \lambda_s \cdot \sqrt{\frac{f'c}{\text{psi}}} \text{ psi} = 337 \text{ psi}$$

$$vc := \min(vc1, vc2, vc3) = 220 \text{ psi}$$

$$\frac{vc}{vu} = 2.06$$ Must be greater than 1.

Two Way Shear Capacity Case 2: #4@8"grid

$\beta := \frac{N}{B} = 1.12$ Ratio of longer to shorter side of column

$\lambda_s := \sqrt{\frac{2}{\left(1 + \frac{\left(\frac{d_{avg}}{in.}\right)}{10}\right)}} = 0.879$ Size effect factor

$\alpha_s := 40$ For interior columns

$vc := 2 \cdot \lambda_s \cdot \sqrt{\frac{f'c}{psi}}\ psi = 110\ psi$ vc for two-way member with stirrups is half of vc without stirrups.

Conditions for vs ACI 22.6.7.1

$\frac{d_{avg}}{6\ in.} = 2.65$ Must be greater than 1.

$d_b := 0.5\ in.$ Diameter of candy cane bars

$\frac{d_{avg}}{16\ d_b} = 1.98$ Must be greater than 1.

$A_v := 12 \cdot 0.2\ in.^2 = 2.4\ in.^2$ Sum of area of all legs on peripheral line not more than hef/2 from base plate.

$f_{yt} := 60\ ksi$

$s := 8\ in.$ Spacing

$vs := \frac{A_v \cdot f_{yt}}{b_o \cdot s} = 117\ psi$

$vn := vc + vs = 227\ psi$

$\frac{vn}{vu} = 2.12$ Must be greater than 1.

One Direction Shear

$b_{w\_ef} := 21.5\ in + 2 \cdot 1.5 \cdot 18\ in = 75.5\ in$ Not full slab is effective

No shear reinf present

$Nu := -47.3\ kip$ Tensile load in slab at column yield

$\lambda_s = 0.879$ Size effect factor

$\rho_w := \dfrac{10 \cdot 0.44\ in.^2}{b_{w\_ef} \cdot d_{avg}} = 0.0037$ Tensile reinforcing ratio

$A_g := 18\ in. \cdot b_{w\_ef} = 9.4\ ft^2$

$N_{axial} := \max\left(\dfrac{Nu}{6 \cdot A_g}, -0.05\ f'c\right) = -5.8\ psi$ Max limit on axial term

$$V_{c1} := \left(8 \cdot \lambda_s \cdot \rho_w^{\frac{1}{3}} \cdot \sqrt{\frac{f'c}{psi}} + N_{axial} \cdot \left(\frac{in.^2}{lbf}\right)\right) \left(\frac{b_{w\_ef}}{in.} \cdot \frac{d_{avg}}{in.}\right) \frac{kips}{1000} = 74.6\ kip$$

$$V_{c2} := \left(5 \cdot \sqrt{\frac{f'c}{psi}}\right) \left(\frac{b_{w\_ef}}{in.} \cdot \frac{d_{avg}}{in.}\right) \frac{kips}{1000} = 376\ kip$$

$V_c := min(V_{c1}, V_{c2}) = 74.6\ kip$

$V_u := 72.3\ kips$ From column expeced yield

$\dfrac{V_c}{V_u} = 1.031$ Must be greater than 1

Moment Capacity

The ultimate capacity of the slab is checked against the expected yield capacity of the column.

$f_y := 100 \text{ ksi}$ Nominal yield stress G100

$A_s := 10 \cdot 0.44 \text{ in}^2 = 4.4 \text{ in}^2$ 10#6G100 are selected.

$b_w := 82 \text{ in.}$

$$a := \frac{A_s \cdot f_y}{b_w \cdot 0.85 \cdot f'c} = 1.61 \text{ in}$$

$$d := 18 \text{ in.} - 1.5 \text{ in.} - .75 \frac{\text{in.}}{2} = 16.1 \text{ in.}$$

$$M_n := A_s \cdot f_y \cdot \left(d - \frac{a}{2}\right) = \left(6.74 \cdot 10^3\right) \text{ kips} \cdot \text{in.}$$

$M_u := 326 \text{ kips} \cdot \text{in.}$ From expected column yield

$\phi_M := 0.9$

$\frac{M_n}{M_u} = 20.7$ Must be greater than 1

Transverse Steel

Minimum steel is used.

$$A_{smin} := \max\left(0.0018 \cdot \frac{60}{100}, 0.0014\right) \cdot 18 \text{ in.} \cdot 8 \text{ in.} = 0.2 \text{ in.}^2$$ ACI318-14 7.6.1.1

4@8G100 are selected.

Moment Anchorage Test Specimen:
Prestressed Anchors, Rebar Hooks, Deflections, Point Load, Actuators

Assumptions

Designed for Expeceted moment of the column.

Notation

Input

Output

Condition Check

Data

$f'c := 3700 \text{ psi}$

150ksi Williams rod 1-3/4in diameter ASTM A722-07

Structural Properties	
Yield Stress	**Ultimate Stress**
120 KSI (827 MPa)	150 KSI (1034 MPa)
Elongation in 20 bar diameters	**Reduction of Area**
4%	20% min.

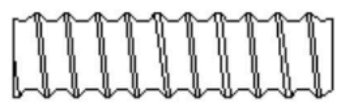

Unique Thread Form

R71 150 KSI All-Thread-Bar - ASTM A722*

Nominal Bar Diameter & Pitch	Minimum Net Area Thru Threads	Minimum Ultimate Strength	Prestressing Force			Nominal Weight	Approx. Thread Major Dia.	Part Number
			0.80f pu A	0.70f pu A	0.60f pu A			
1" - 4 (26 mm)	0.85 in^2 (549 mm^2)	128 kips (567 kN)	102 kips (454 kN)	89.3 kips (397 kN)	76.5 kips (340 kN)	3.09 lbs./ft. (4.6 Kg/M)	1-1/8" (28.6 mm)	R71-08
1-1/4" - 4 (32 mm)	1.25 in^2 (807 mm^2)	188 kips (834 kN)	150 kips (667 kN)	131 kips (584 kN)	113 kips (500 kN)	4.51 lbs./ft. (6.71 Kg/M)	1-7/16" (36.5 mm)	R71-10
1-3/8" - 4 (36 mm)	1.58 in^2 (1019 mm^2)	237 kips (1054 kN)	190 kips (843 kN)	166 kips (738 kN)	142 kips (633 kN)	5.71 lbs./ft. (8.50 Kg/M)	1-9/16" (39.7 mm)	R71-11
1-3/4" - 3-1/2 (46 mm)	2.60 in^2 (1664 mm^2)	390 kips (1734 kN)	312 kips (1388 kN)	273 kips (1214 kN)	234 kips (1041 kN)	9.06 lbs./ft. (13.5 Kg/M)	2" (50.8 mm)	R71-14
2-1/4"" - 3-1/2 (57 mm) **	4.08 in^2 (2632 mm^2)	613 kips (2727 kN)	490 kips (2181 kN)	429 kips (1909 kN)	368 kips (1636 kN)	14.1 lbs./ft. (20.8 Kg/M)	2-1/2" (63.5 mm)	R71-18
2-1/2" - 3 (65 mm)	5.19 in^2 (3350 mm^2)	778 kips (3457 kN)	622 kips (2766 kN)	545 kips (2422 kN)	467 kips (2074 kN)	18.2 lbs./ft. (27.1 Kg/M)	2-3/4" (69.9 mm)	R71-20
3" - 3 (75 mm)	6.85 in^2 (4419 mm^2)	1027 kips (4568 kN)	822 kips (3656 kN)	719 kips (3198 kN)	616 kips (2740 kN)	24.1 lbs./ft. (35.8 Kg/M)	3-1/8" (79.4 mm)	R71-24

** The 2-1/4" diameter bar is not covered under ASTM A722.

- ACI 355.1R section 3.2.5.1 indicates an ultimate strength in shear has a range of .6 to .7 of the ultimate tensile strength. Designers should provide adequate safety factors for safe shear strengths based on the condition of use.
- Per PTI recommendations for anchoring, anchors should be designed so that:
- The design load is not more than 60% of the specified minimum tensile strength of the prestressing steel.
- The lock-off load should not exceed 70% of the specified minimum tensile strength of the prestressing steel.
- The maximum test load should not exceed 80% of the specified minimum tensile strength of the prestressing steel.

Lateral Friction Resistance

Lateral load will be resisted by between the slab and the laboratory strong floor that are prestressed together with nine Williams rods.

$PT := 170 \text{ kips}$ Pretensioning force per bar

$L := 9 \text{ in.}$ Length of square metal plate

$\mu := 0.1$ Friction coefficient steel plate - concrete lab floor

$P := 9\ (PT) + 5.5 \text{ kips} = \left(1.54 \cdot 10^3\right) \text{ kips}$ Total prestressing force of nine bars plus self weight

$Fr := \mu \cdot P = 154 \text{ kips}$

$Vu := 98.3 \text{ kips}$ Lateral load that must be resisted at limit state of column yielding.

$$FS := \frac{Fr}{Vu} = 1.56$$

Bearing Pressure

Based on ACI 318-14 22.8 Bearing pressure.
See image below for load combinations

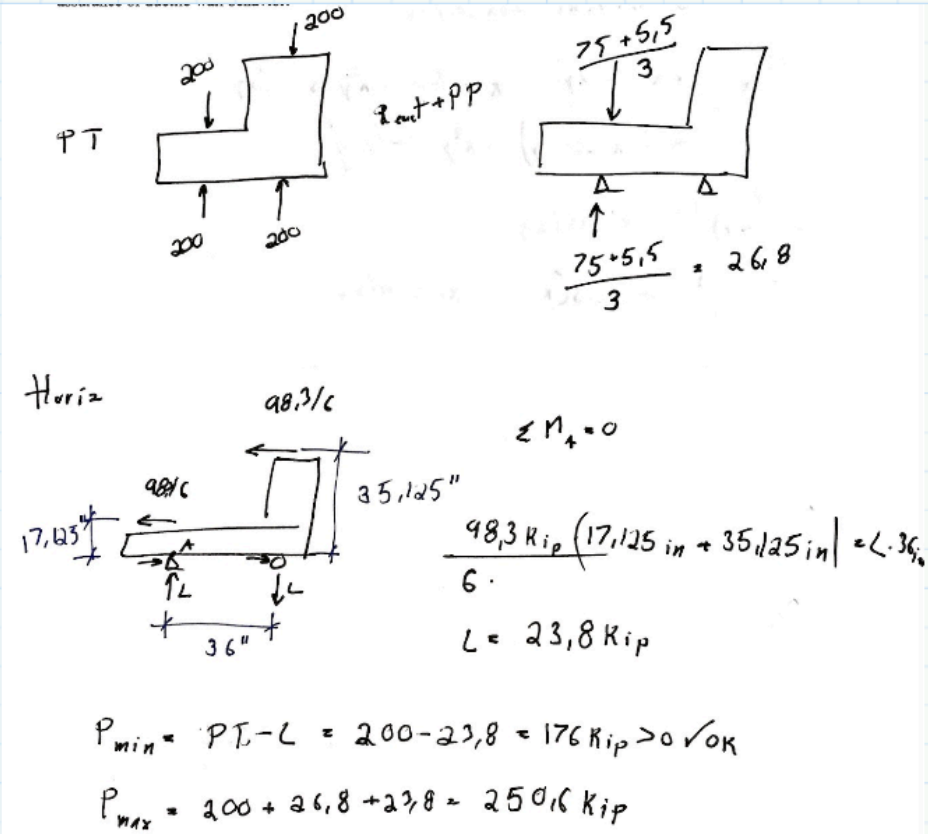

$Pu := (250.6\ \text{kips} - 30\ \text{kips})$

Prestressing force and reaction at column yield limit state (minus 30 because I prestressed to 170 kips)

$A_1 := L^2 - (\pi \cdot 1.5\ \text{in.}^2) = 76\ \text{in.}^2$

Load area

$C := 1$

C taken as 1 because the load cannot spread at 45 degrees through the element to a larger bearing surface on the other side.

$\phi B_n := C \cdot 0.85 \cdot f'c \cdot A_1 = 240\ \text{kips}$

$\dfrac{\phi B_n}{Pu} = 1.09$

Must be geater than 1

Also, minimum preasure is larger than zero meaning contact is not lost.

Tension Plates

$$Tu := \frac{Vu}{6} = 16.4 \text{ kips}$$

$t := 0.5 \text{ in.}$ Plate thickness

$b := 9 \text{ in.}$ Plte width

$fy_{pl} := 36000 \text{ psi}$ A36 steel

$fu_{pl} := 58000 \text{ psi}$

Yield

$$A_{npl} := t\ b = 4.5 \text{ in.}^2$$

$$Tn1 := 0.9 \cdot A_{npl} \cdot fy_{pl} = 146 \text{ kip}$$

Fracture

$$A_{epl} := A_{npl} - t \cdot 2 \text{ in.} = 3.5 \text{ in.}^2$$

$$Tn2 := fu_{pl} \cdot A_{epl} = 203 \text{ kips}$$

$$Tn := min(Tn1, Tn2) = 146 \text{ kip}$$

$\frac{Tn}{Tu} = 8.9$ Must be greater than 1

Point Load Web Failure

Beam Dimentions
W12x106

$Fyw := 50000 \text{ psi}$ Beam minimum yield stress

$d := 12.9 \text{ in.}$ Beam height

$tw := 0.61 \text{ in.}$ Web thickness

$bf := 12.2 \text{ in.}$ Flange width

$k1 := \left(1 + \frac{1}{8}\right) \text{ in.}$ Dist from cneterline to end of curved part of web

$tf := 0.99 \text{ in.}$ Flange thickness

$h := 15.9 \cdot tw = 9.7 \text{ in.}$

<u>Web Local Yielding</u>
AISC J10.2

$$k := \frac{(bf - 2\ k1)}{2} = 4.98 \text{ in.}$$

$lb := 15 \text{ in.}$ Bearing length

$$Rn := Fyw \cdot tw \cdot (2.5 \cdot k + lb) = 837 \text{ kip}$$

$$\frac{Rn}{Vu} = 8.51$$ Must be greater than 1

Web Crippling
AISC J10.3

Point of load application is more than d/2 from end of beam.

$$Rn := 0.8 \cdot tw^2 \cdot \left(1 + 3 \cdot \frac{lb}{d} \cdot \left(\frac{tw}{tf}\right)^{1.5}\right) \cdot \sqrt{\frac{(E \cdot Fyw \cdot tf)}{tw}} = \left(1.23 \cdot 10^3\right)\ \text{kips}$$

$$\frac{Rn}{Vu} = 12.5$$ Must be greater than 1

Web Sideways Buckling
AISC J10.4

Compression flange is not restrained

$Lb := 88.2\ \text{in.}$ Length of laterally unrestrained column

$$\frac{\left(\frac{h}{tw}\right)}{\left(\frac{Lb}{bf}\right)} = 2.2$$

$$\frac{\left(\frac{\left(\frac{h}{tw}\right)}{\left(\frac{Lb}{bf}\right)}\right)}{1.7} = 1.29$$ Must be greater than 1

Web sideways buckling does not govern.

Cantilever Tip Rods

$F_{yrod} := 36000\ \text{psi}$

$d_{rod} := 1.25\ \text{in.}$

$$Ty := \pi \cdot \left(\frac{d_{rod}}{2}\right)^2 \cdot F_{yrod} = 44.2\ \text{kips}$$

$4 \cdot Ty = 177\ \text{kip}$

$\frac{4 \cdot Ty}{Vu} = 1.8$ Must be greater than 1

APPENDIX D. CHANNEL LIST

Table D- 1. Channel list for moment transfer test M02

Number	Address	Type	Name	Description	Unit
1	0-2-0	Load Cell	LC-N	South Actuator	Force
2	0-2-1	Disp. Transducer	Disp-N		Disp
3	0-2-2	Load Cell	LC-S	North Actuator	Force
4	0-2-3	Disp. Transducer	Disp-S		Disp
5	0-2-4	String Potentiometer	WP1	Column Disp (E-W)	Disp
6	0-2-5	String Potentiometer	WP2	Column Disp (N-S)	Disp
7	0-2-6			NA	
8	0-2-7			NA	
9	0-3-0	Strain Gauge	T1	Top longitudinal strain gages from West to East #6G100	Strain
10	0-3-1	Strain Gauge	T2		Strain
11	0-3-2	Strain Gauge	T3		Strain
12	0-3-3	Strain Gauge	T4		Strain
13	0-3-4	Strain Gauge	T5		Strain
14	0-3-5	Strain Gauge	B1	Bottom longitudinal strain gages from West to East #6G100	Strain
15	0-3-6	Strain Gauge	B2		Strain
16	0-3-7	Strain Gauge	B3		Strain
17	0-4-0	Strain Gauge	B4		Strain
18	0-4-1	Strain Gauge	B5		Strain
19	0-4-2	Strain Gauge	A1N	Anchor strain gages (A - (Anchor #) - (North or South)	Strain
20	0-4-3	Strain Gauge	A1S		Strain
21	0-5-0	Strain Gauge	A2N		Strain
22	0-4-5	Strain Gauge	A2S		Strain
23	0-4-6	Strain Gauge	A3N		Strain
24	0-4-7	Strain Gauge	A3S		Strain
25	0-6-0	Strain Gauge	A4N		Strain
26	0-6-1	Strain Gauge	A4S		Strain
27	0-6-2	Strain Gauge	A5N		Strain
28	0-6-3	Strain Gauge	A5S		Strain
29	0-6-4	Strain Gauge	A6N		Strain
30	0-6-5	Strain Gauge	A6S		Strain

Number	Address	Type	Name	Description	Unit
31	0-6-6	Strain Gauge	A7N	Anchor strain gages (A - (Anchor #) - (North or South)	Strain
32	0-6-7	Strain Gauge	A7S		Strain
33	0-7-0	Strain Gauge	A8N		Strain
34	0-7-1	Strain Gauge	A8S		Strain
35	0-7-2	Strain Gauge	1R1	Shear reinf. Strain gages ((Ring #) - R (bar # counterclockwise))	Strain
36	0-7-3	Strain Gauge	1R2		Strain
37	0-7-4	Strain Gauge	2R1		Strain
38	0-7-5	Strain Gauge	2R2		Strain
39	0-7-6	Strain Gauge	2R3		Strain
40	0-7-7	Strain Gauge	2R4		Strain
41	0-8-0	Strain Gauge	2R5		Strain
42	0-8-1	Strain Gauge	2R6		Strain
43	0-8-2	Strain Gauge	3R1		Strain
44	0-8-3	Strain Gauge	3R2		Strain
45	0-8-4	Strain Gauge	3R3		Strain
46	0-8-5	Strain Gauge	3R4		Strain
47	0-8-6	Strain Gauge	3R5		Strain
48	0-8-7	Strain Gauge	3R6		Strain
49	0-9-0	Strain Gauge	3R7		Strain
50	0-9-1	Strain Gauge	3R8		Strain
51	0-9-2	Strain Gauge	3R9		Strain
52	0-9-3	Strain Gauge	3R10		Strain
53	0-9-4	Strain Gauge	4R1		Strain
54	0-9-5	Strain Gauge	4R2		Strain
55	0-9-6	Strain Gauge	4R3		Strain
56	0-9-7	Strain Gauge	4R4		Strain
57	0-10-0	Strain Gauge	4R5		Strain
58	0-10-1	Strain Gauge	4R6		Strain
59	0-10-2	Strain Gauge	4R7		Strain
60	0-10-3	Strain Gauge	5R1		Strain
61	0-10-4	Strain Gauge	5R2		Strain
62	0-10-5	Strain Gauge	5R3		Strain
63	0-10-6	Strain Gauge	5R4		Strain
64	0-10-7	Strain Gauge	5R5		Strain
65	0-11-0	Strain Gauge	5R6		Strain
66	0-11-1	Strain Gauge	5R7		Strain
67	0-11-2	Strain Gauge	5R8		Strain
68	0-11-3	Strain Gauge	5R9		Strain

Number	Address	Type	Name	Description	Unit
69	0-11-4			NA	
70	0-11-5			NA	
71	0-11-6			NA	
72	0-11-7			NA	
73	0-12-0	Linear Potentiometer	N1	Base plate vertical disp - West	Disp
74	0-12-1	Linear Potentiometer	N2	Base plate vertical disp - East	Disp
75	0-12-2	Linear Potentiometer	N3	Top surface W-E	Disp
76	0-12-3	Linear Potentiometer	N4	Top surface W-E and N-S	Disp
77	0-12-4	Linear Potentiometer	N5		Disp
78	0-12-5	Linear Potentiometer	N6		Disp
79	0-12-6	Linear Potentiometer	N7		Disp
80	0-12-7	Linear Potentiometer	N8		Disp
81	0-13-0	Linear Potentiometer	N9		Disp
82	0-13-1	Linear Potentiometer	N10		Disp
83	0-13-2	Linear Potentiometer	N11		Disp
84	0-13-3	Linear Potentiometer	N12		Disp
85	0-13-4	Linear Potentiometer	N13		Disp
86	0-13-5	Linear Potentiometer	N14	Sliding on West side, small support relative to floor	Disp
87	0-13-6	Linear Potentiometer	N15	Sliding on West side, specimen relative to floor	Disp
88	0-13-7	Linear Potentiometer	N16	Sliding on East side, large support relative to floor	Disp
89	0-14-0	Linear Potentiometer	N17	Siding East side, specimen relative large support	Disp
90	0-14-1			NA	
91	0-14-2			NA	
92	0-14-3			NA	
93	0-14-4			NA	
94	0-14-5			NA	
95	0-14-6			NA	

Number	Address	Type	Name	Description	Unit
96	0-14-7			NA	
97	0-15-0	Load Cell	LC1	Load cell on anchors (Number from North to South then West to East)	Force
98	0-15-1	Load Cell	LC2		Force
99	0-15-2	Load Cell	LC3		Force
100	0-15-3	Load Cell	LC4		Force
101	0-15-4	Load Cell	LC5		Force
102	0-15-5	Load Cell	LC6		Force
103	0-15-6	Load Cell	LC7		Force
104	0-15-7	Load Cell	LC8		Force

APPENDIX E. INSTRUMENTATION

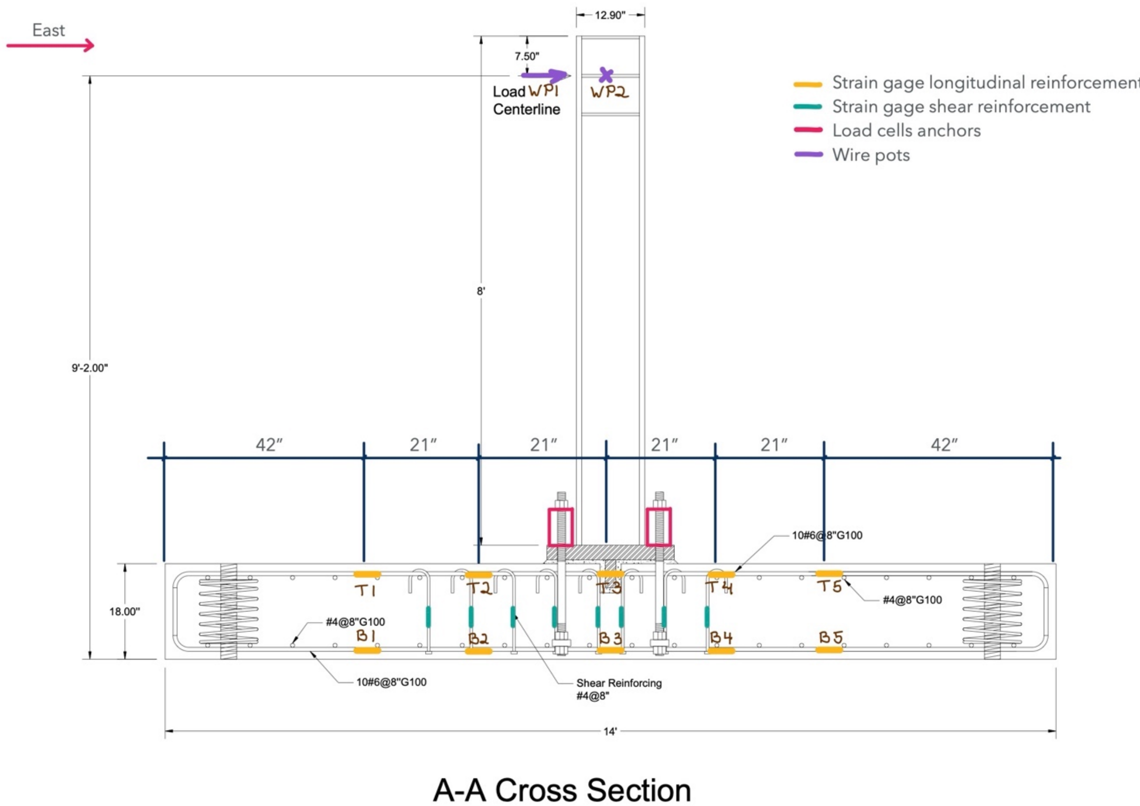

Figure E- 1. Instrumentation elevation view cut A-A

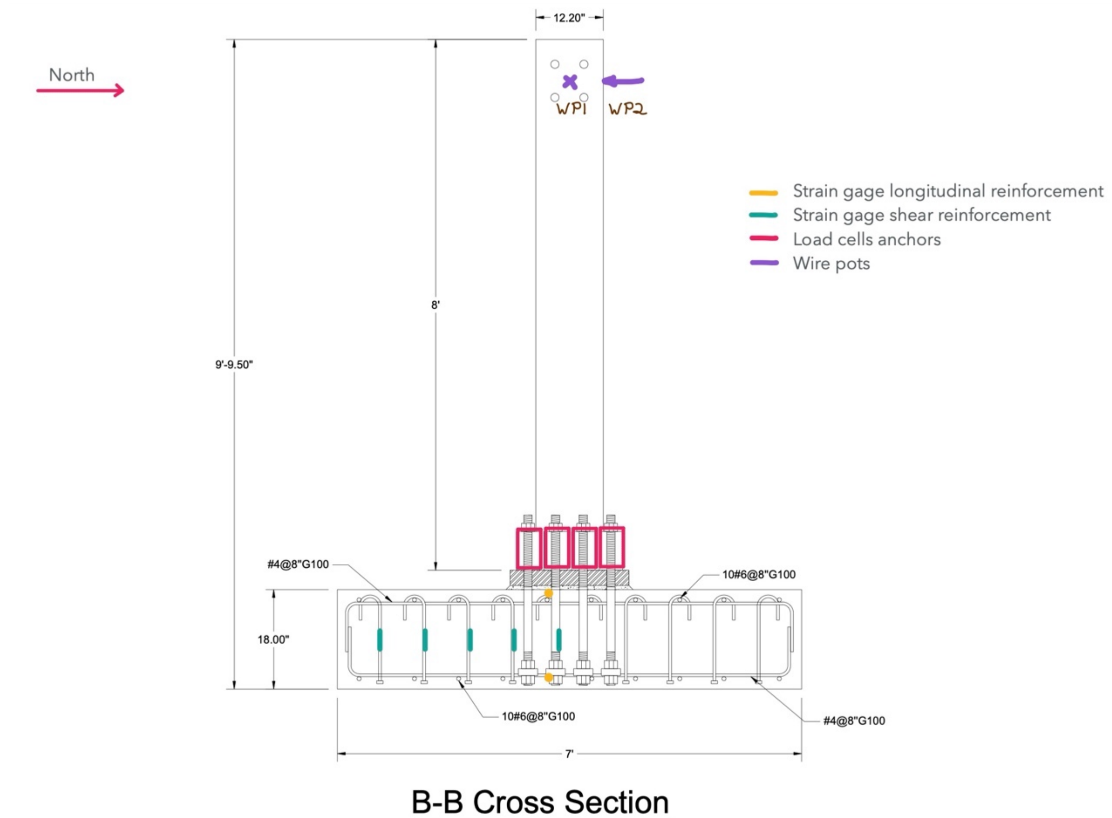

Figure E- 2. Instrumentation elevation view cut B-B

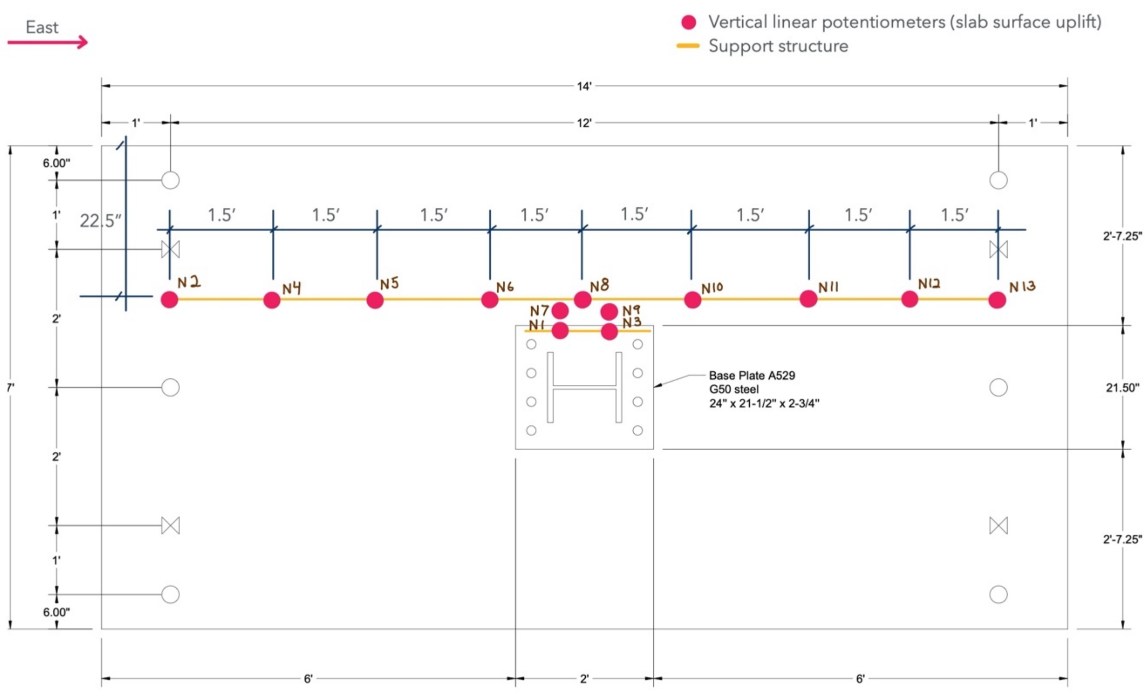

Figure E- 3. Plan view linear potentiometers

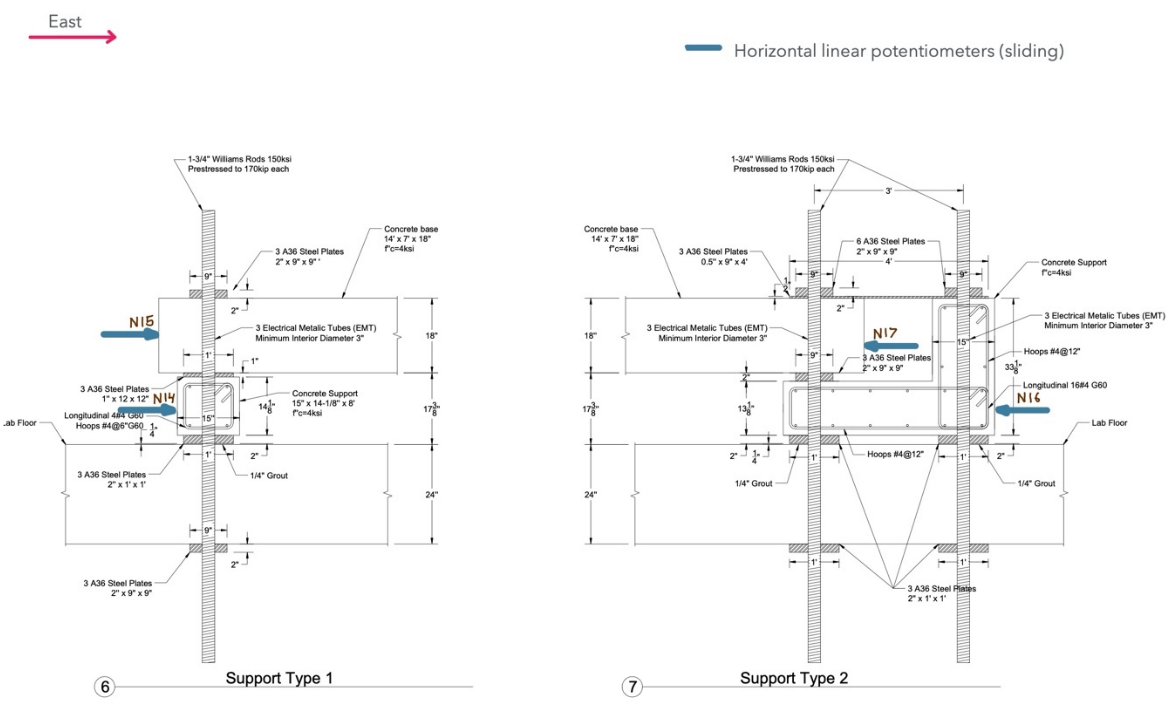

Figure E- 4. Elevation view linear potentiometers

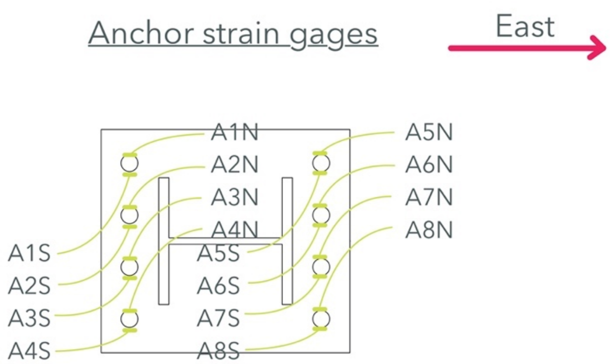

Figure E- 5. Strain gages on anchors

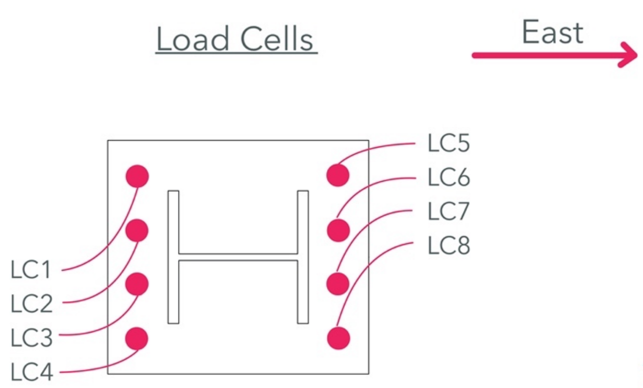

Figure E- 6. Anchor load cells

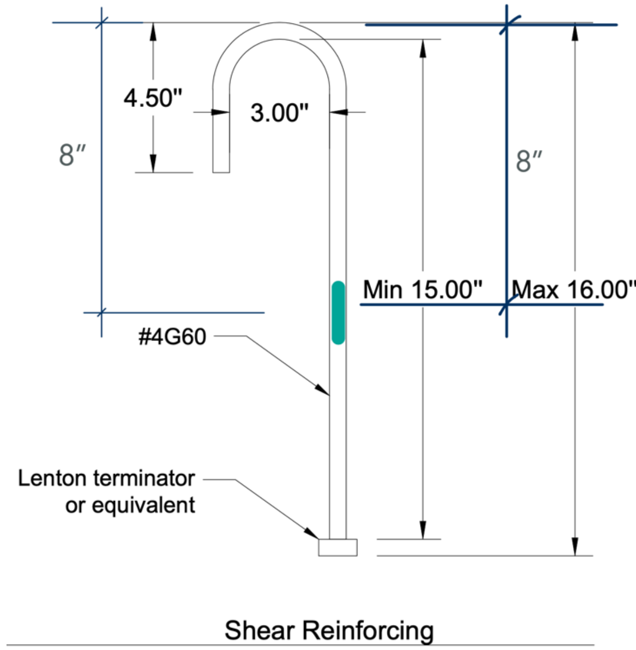

Figure E- 7. Strain gages location on shear reinforcing

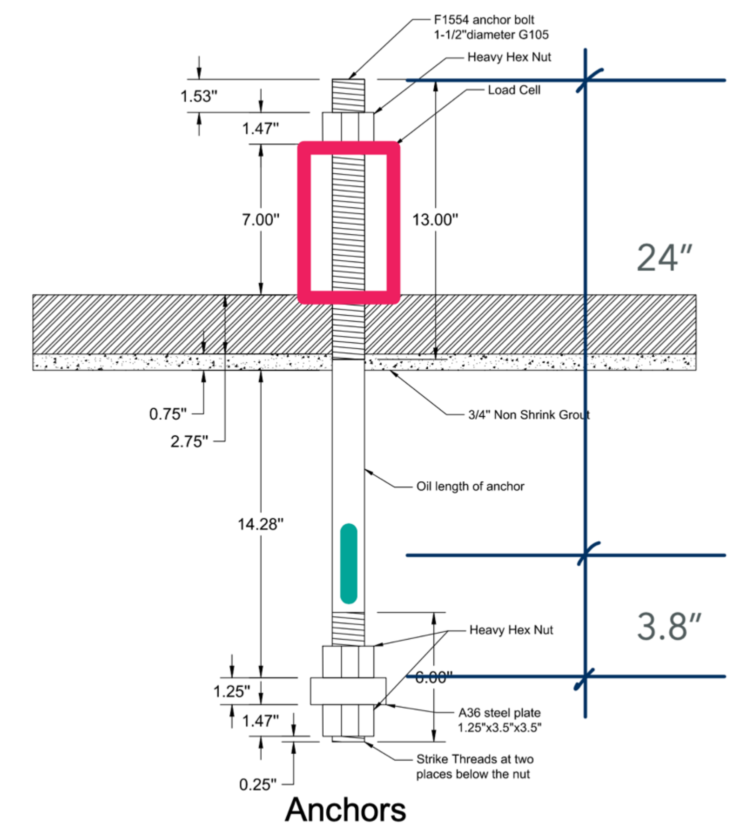

Figure E- 8. Strain gages location on anchors

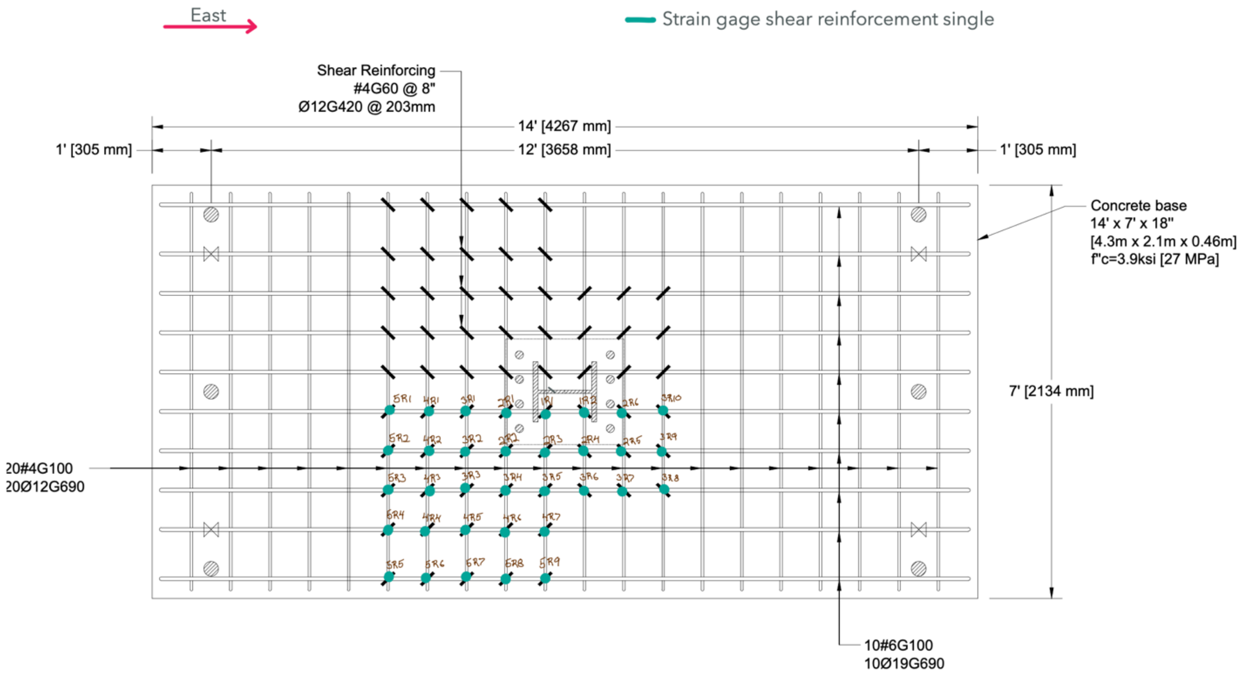

Figure E- 9. Strain gages on shear reinforcing

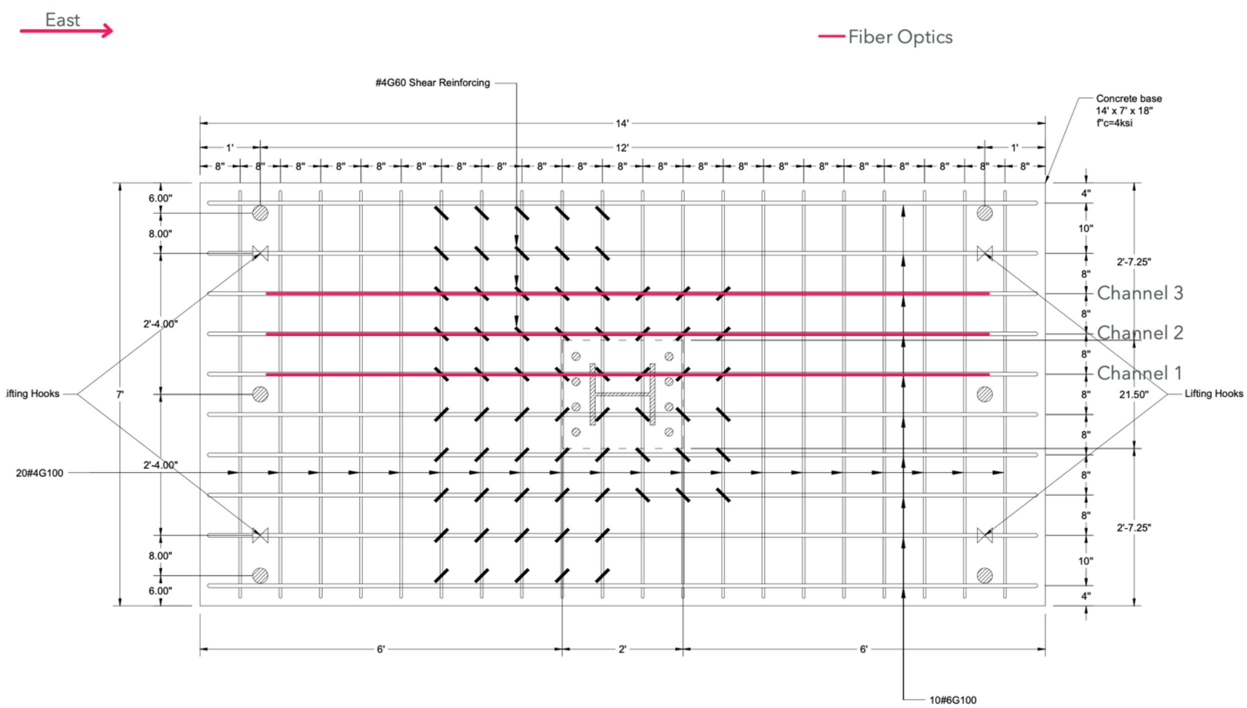

Figure E- 10. Fiber optics cable placement

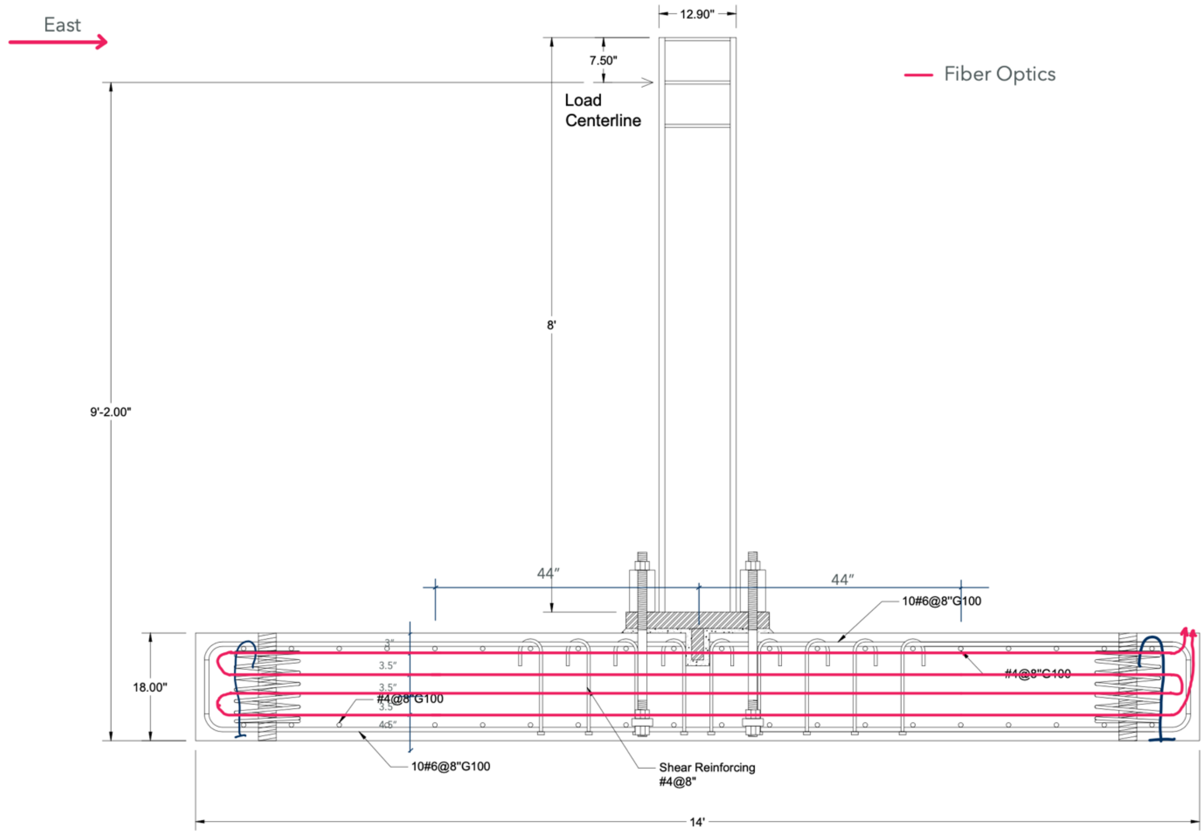

Figure E- 11. Fiber optics cable placement

APPENDIX F. PHOTOGRAPHS

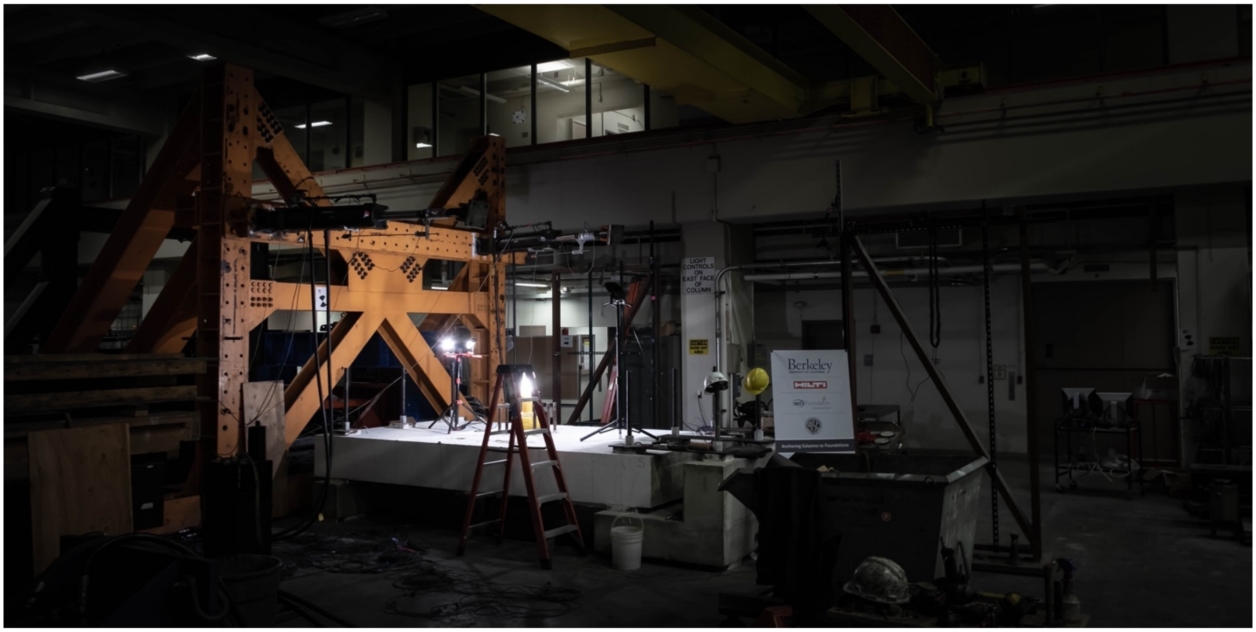

Figure F- 1. Specimen **M02 post test**

Figure F- 2. Strain gages on anchors

Figure F- 3. Anchor fixture

Figure F- 4. Anchor fixture

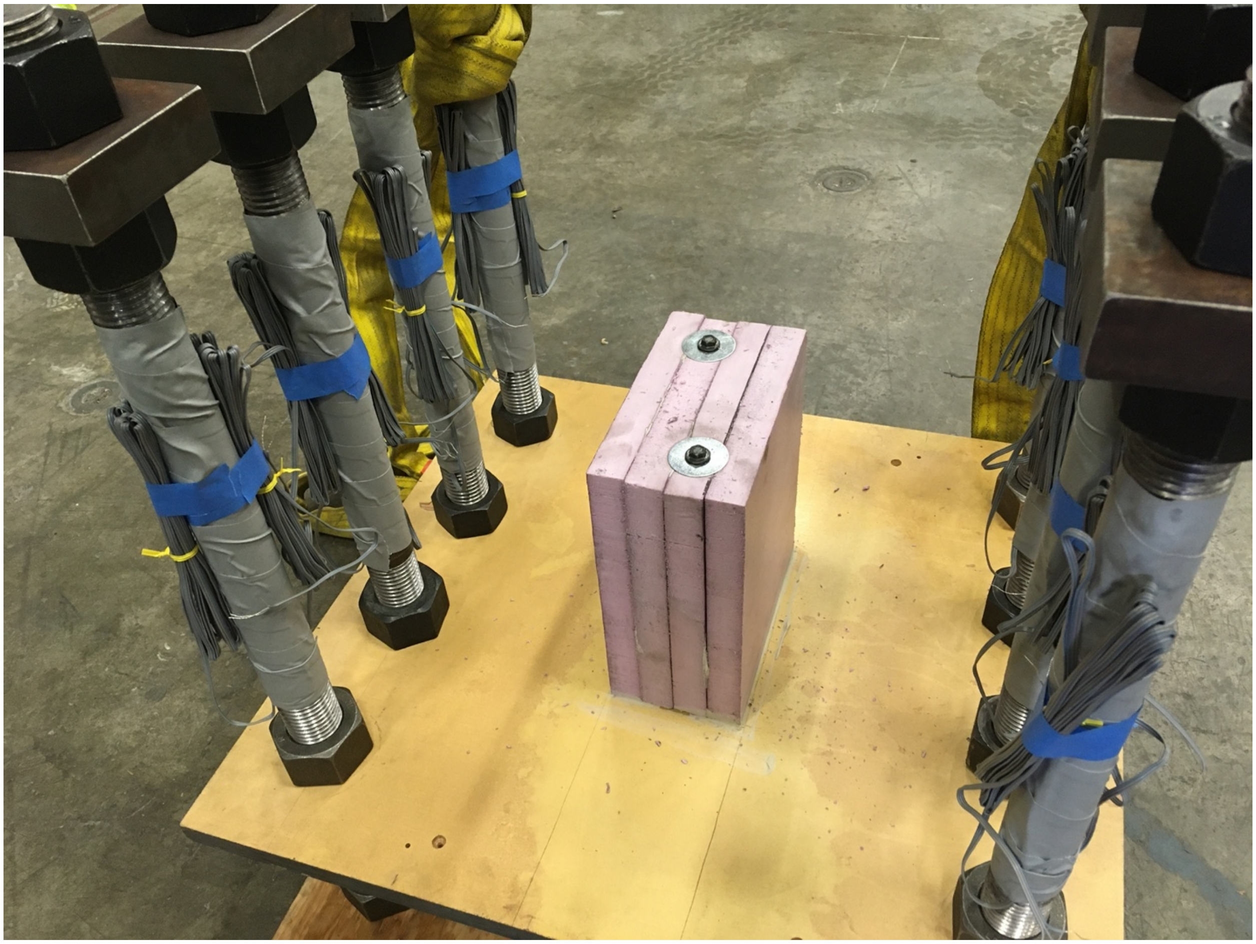

Figure F- 5. Anchor fixture showing foam mold for shear lug hole

Figure F- 6. Strain gages on shear reinfrocement

Figure F- 7. Strain gages on reinfrocement

Figure F- 8. Form building

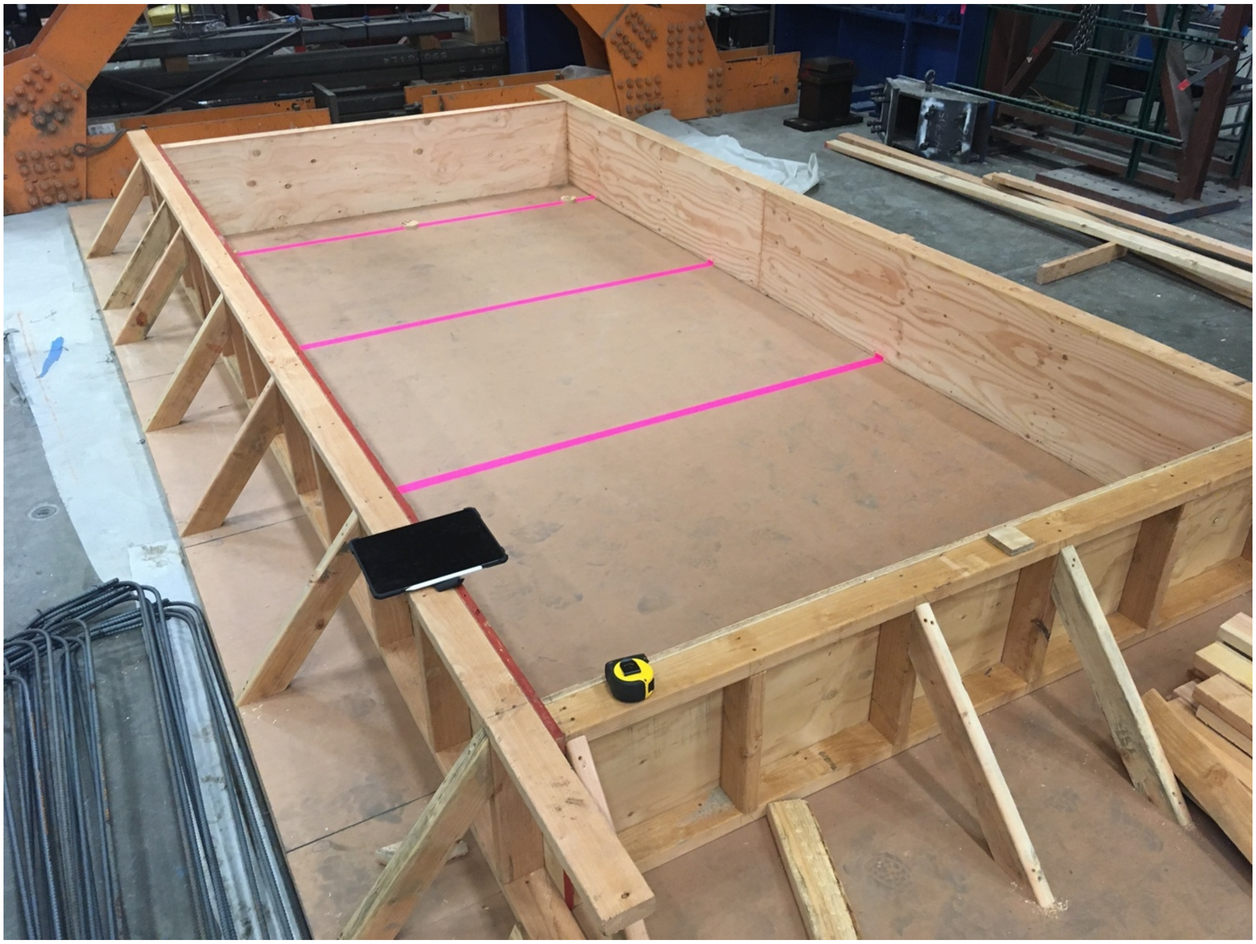

Figure F- 9. Form building

Figure F- 10. Cage building

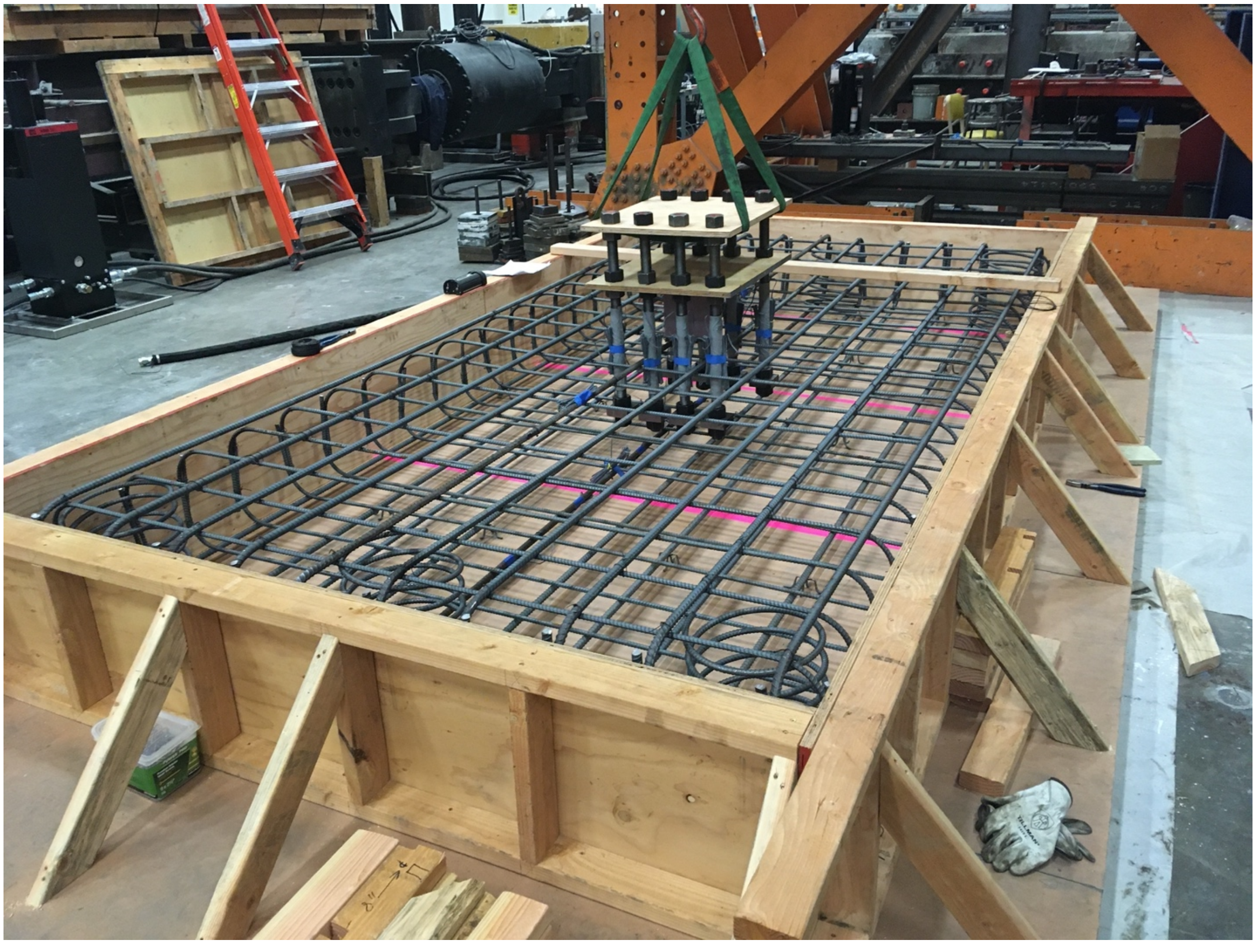

Figure F- 11. Cage building and anchor fixture

Figure F- 12. Cage building and anchor fixture

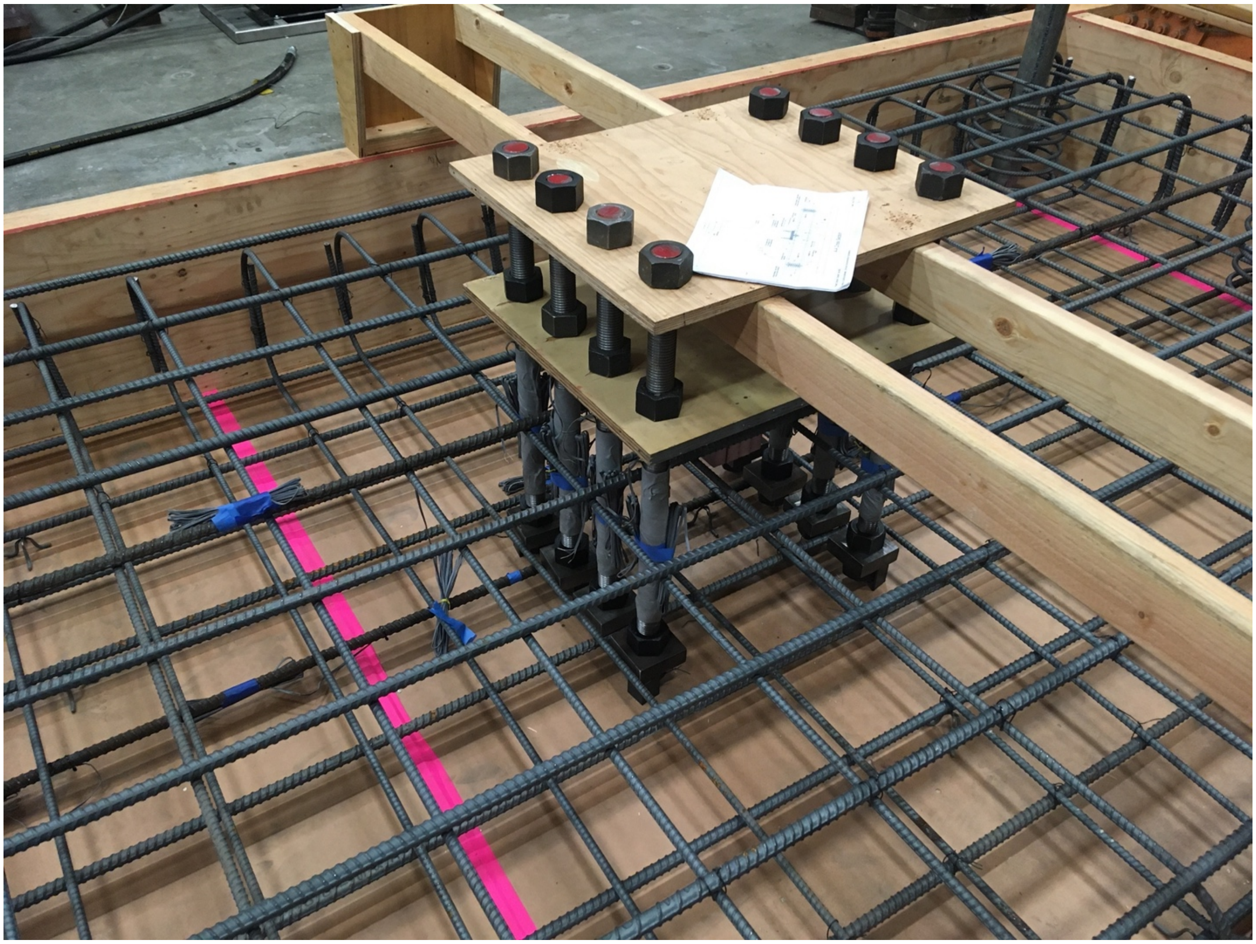

Figure F- 13. Cage building and anchor fixture

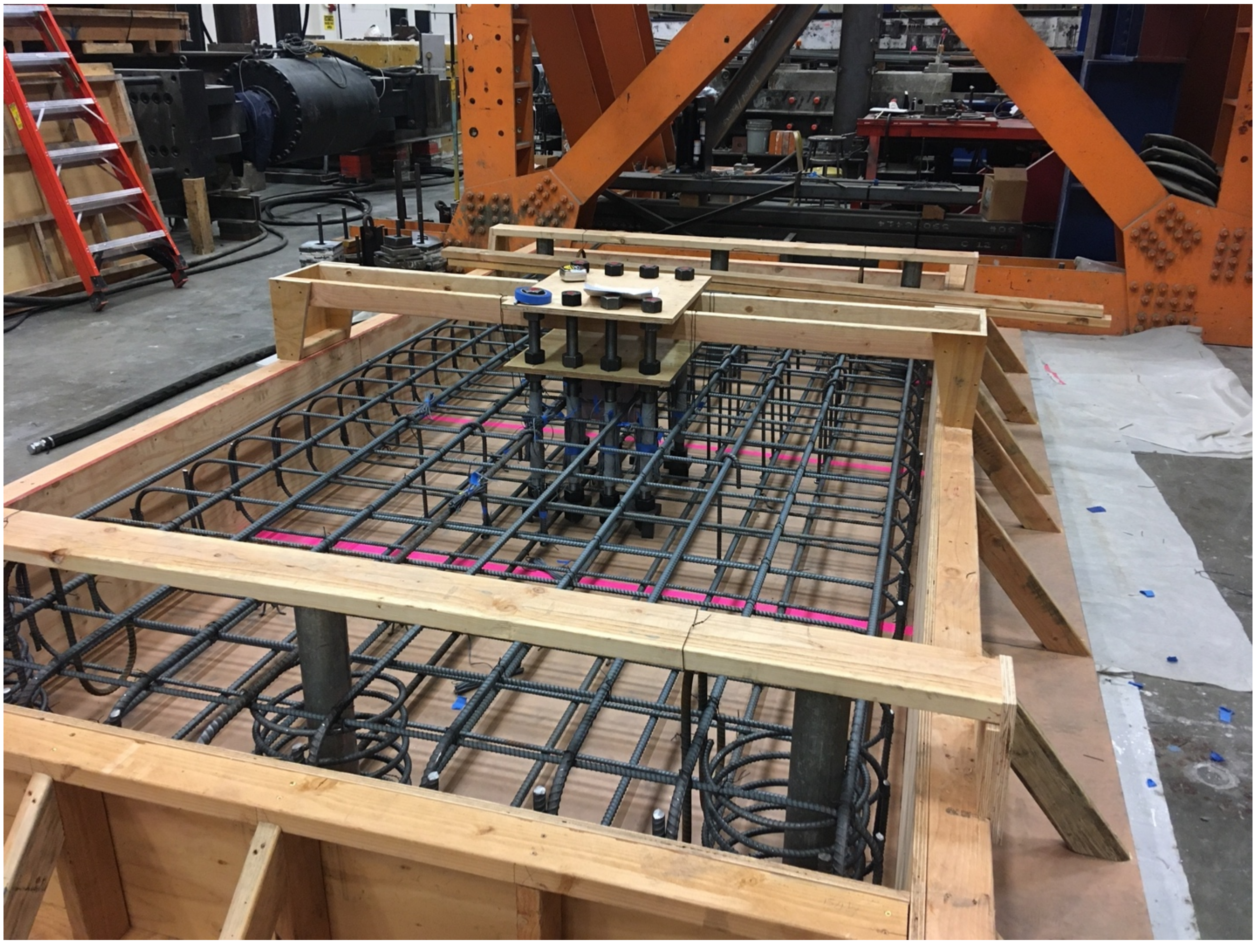

Figure F- 14. Cage building and anchor fixture

Figure F- 15. Placement of fiber optics cables

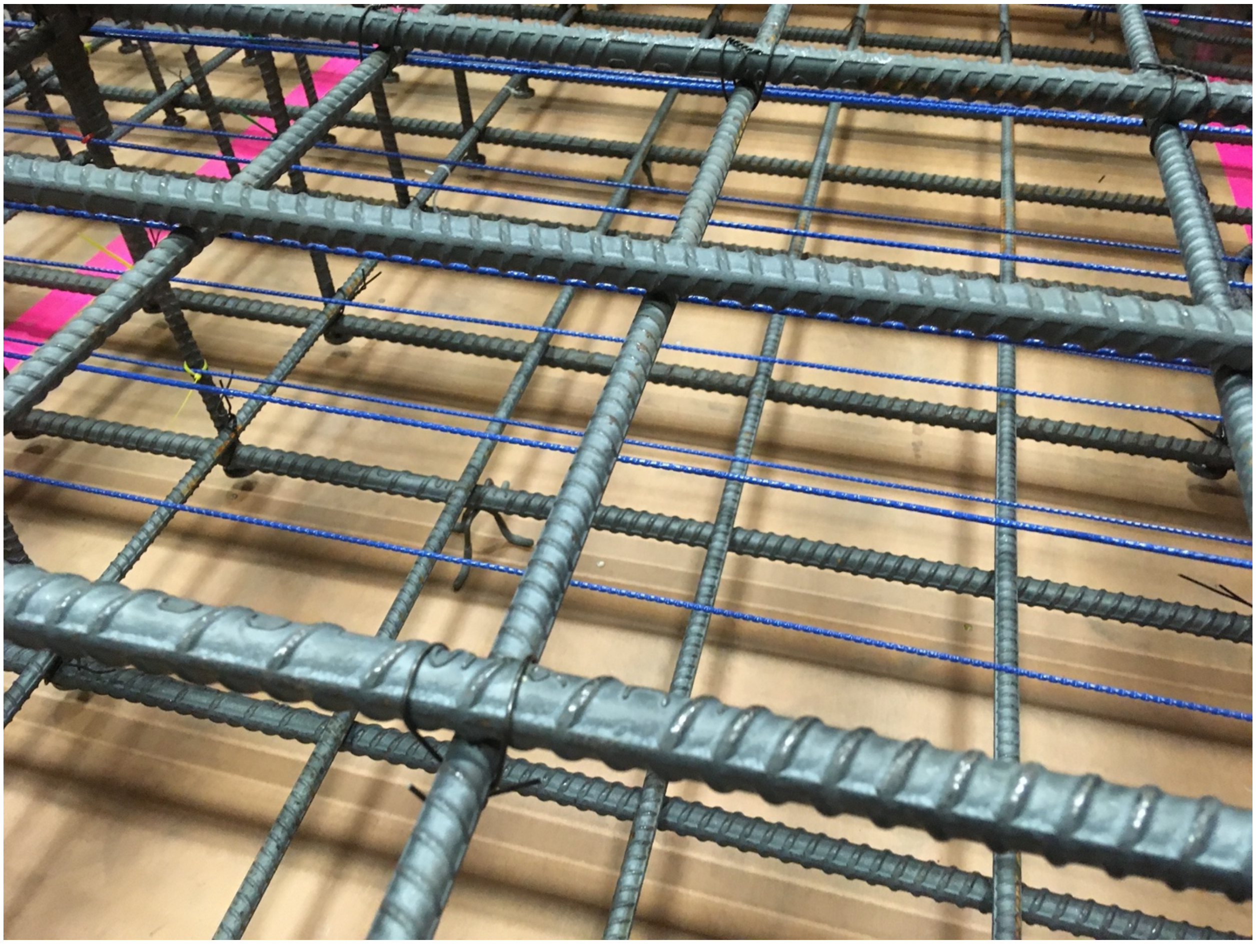

Figure F- 16. Placement of fiber optics cables

Figure F- 17. Placement of fiber optics cables

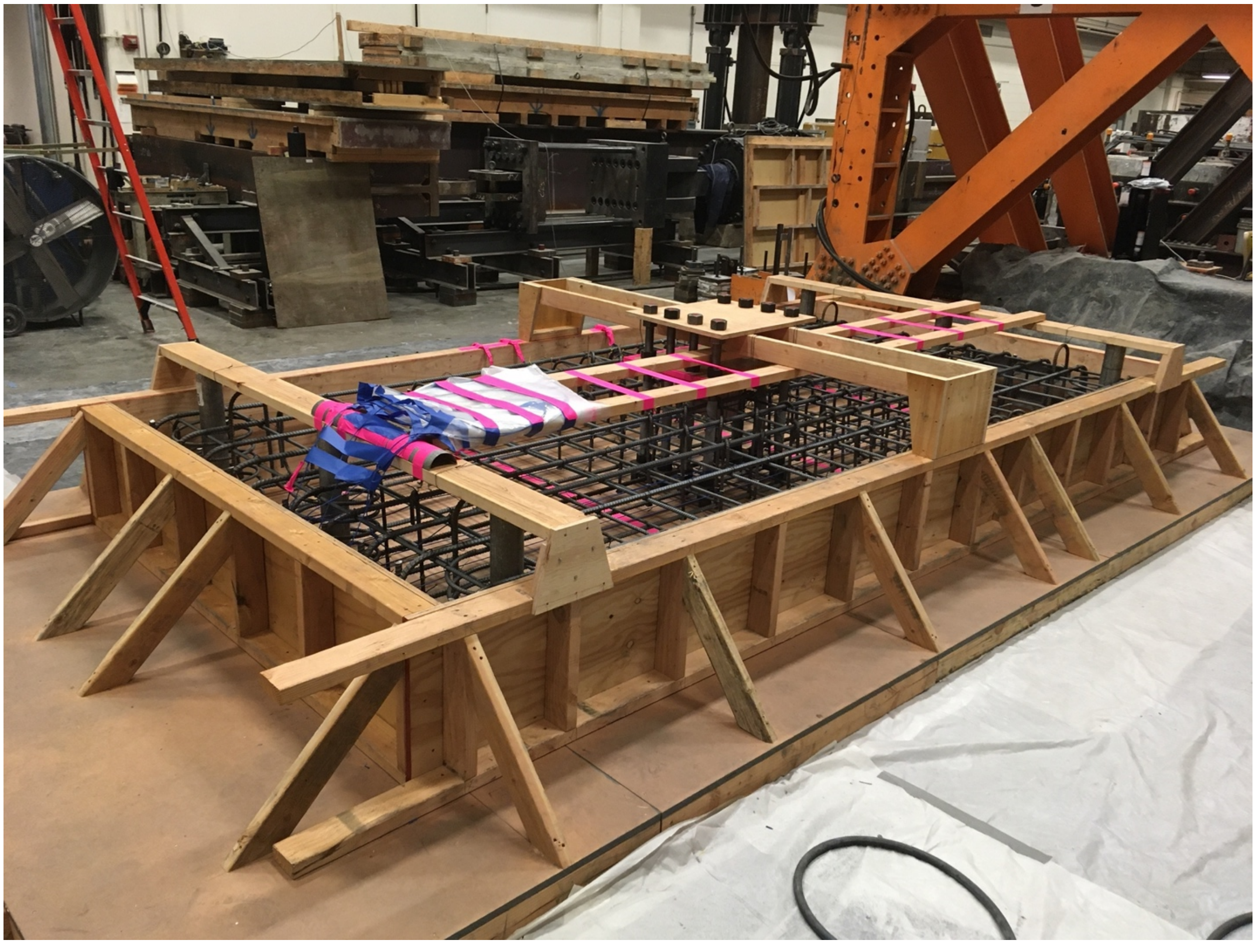

Figure F- 18. Form before casting concrete

Figure F- 19. Fracture energy forms before casting concrete

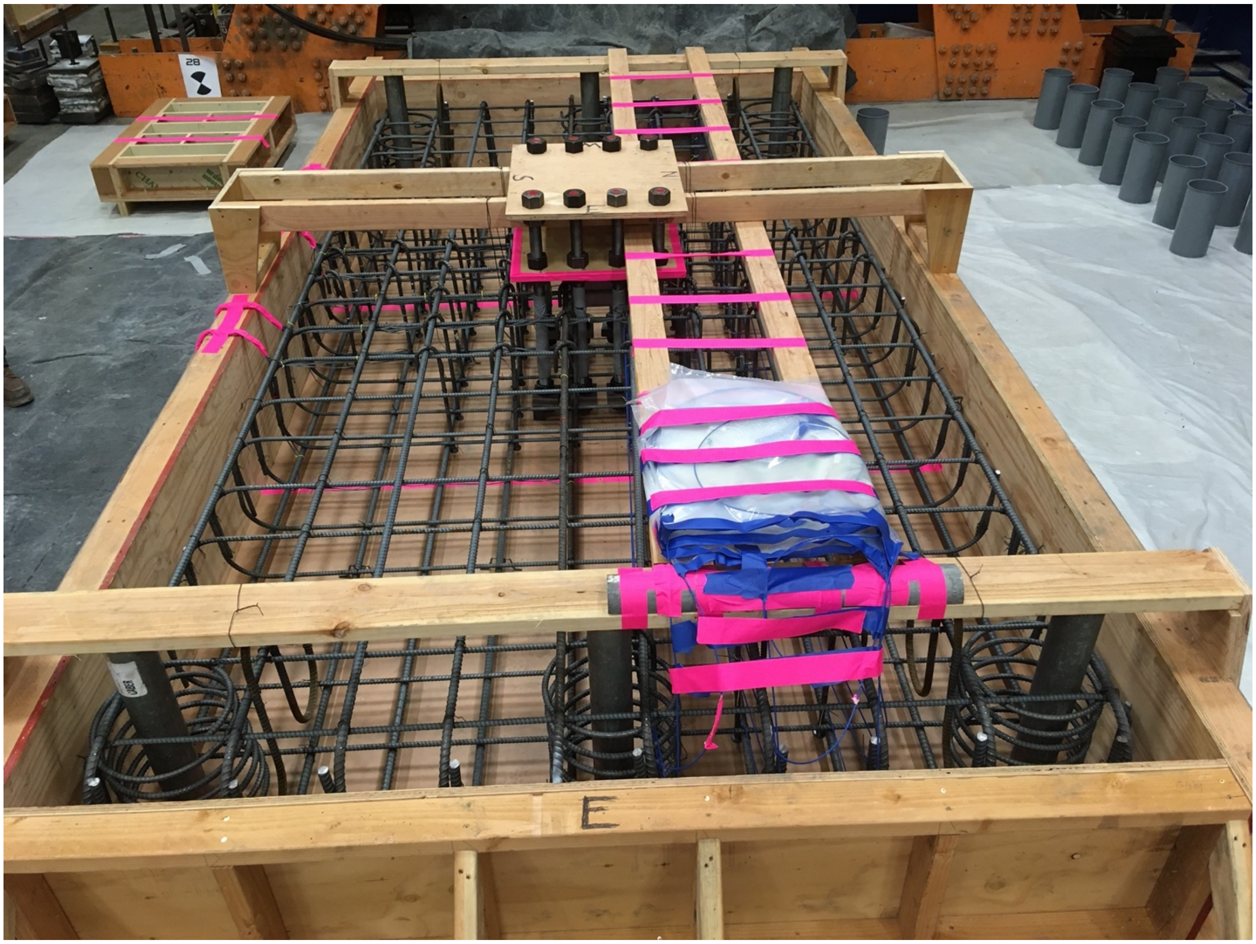

Figure F- 20. Form before casting concrete

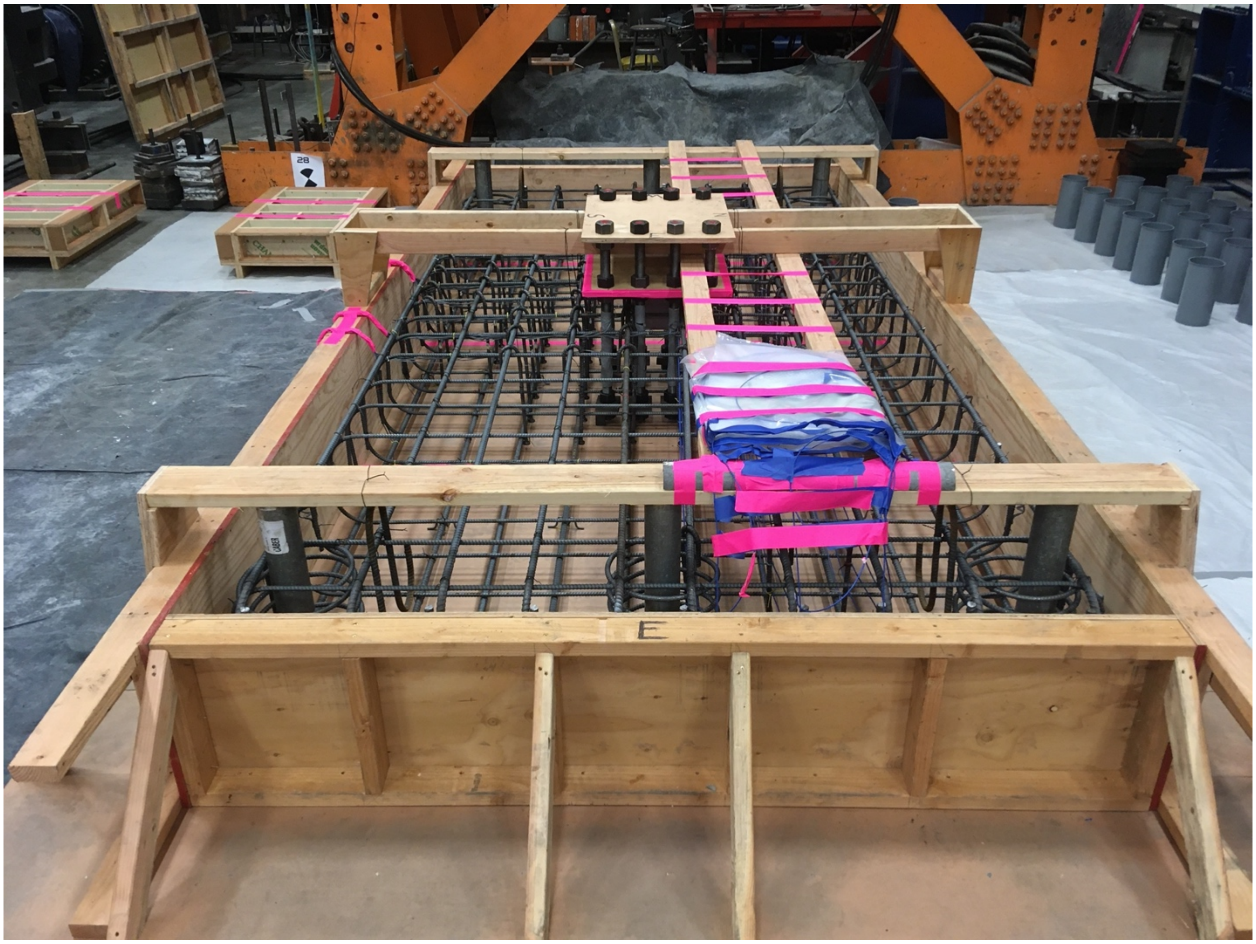

Figure F- 21. Form before casting concrete

Figure F- 22. Form before casting concrete

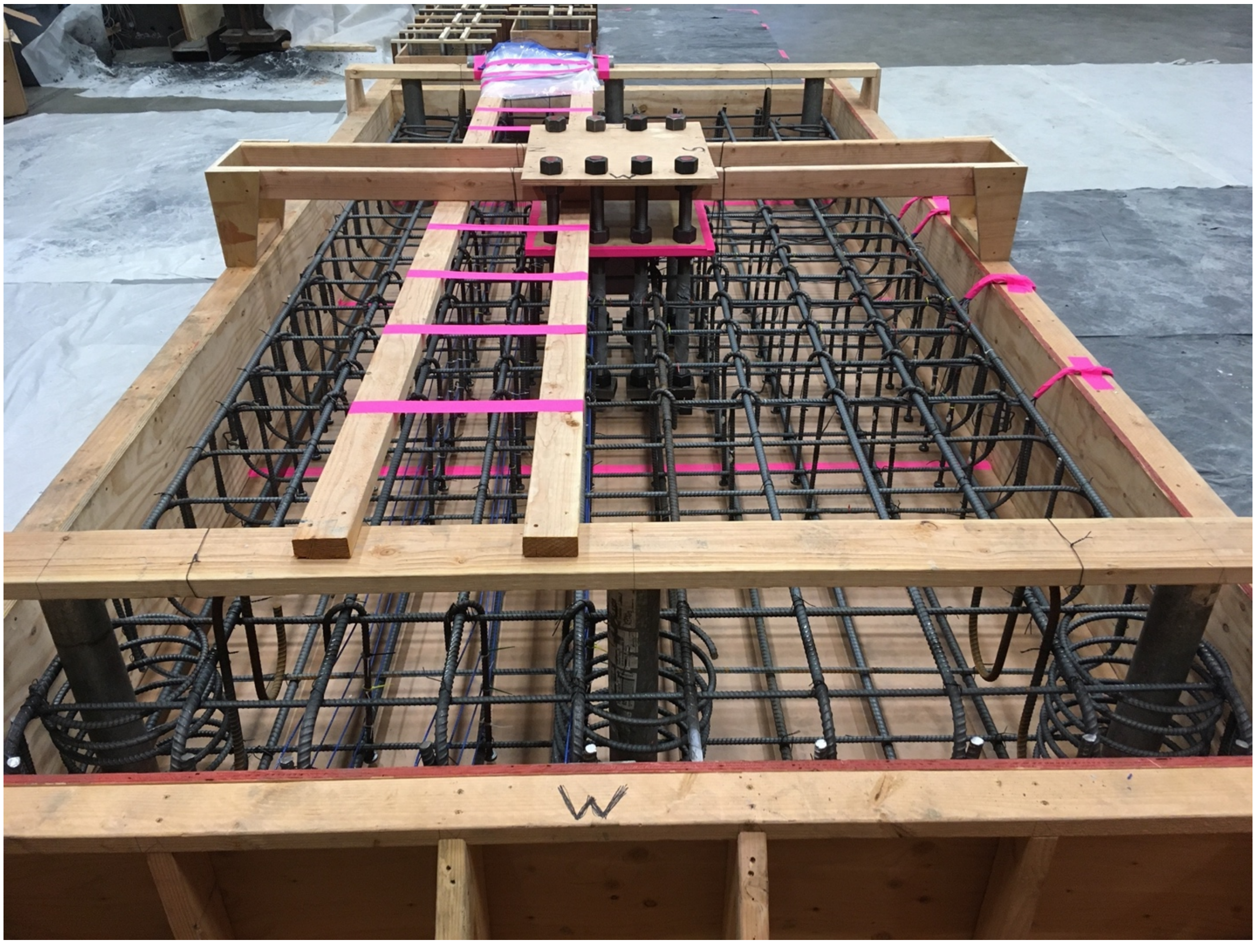

Figure F- 23. Form before casting concrete

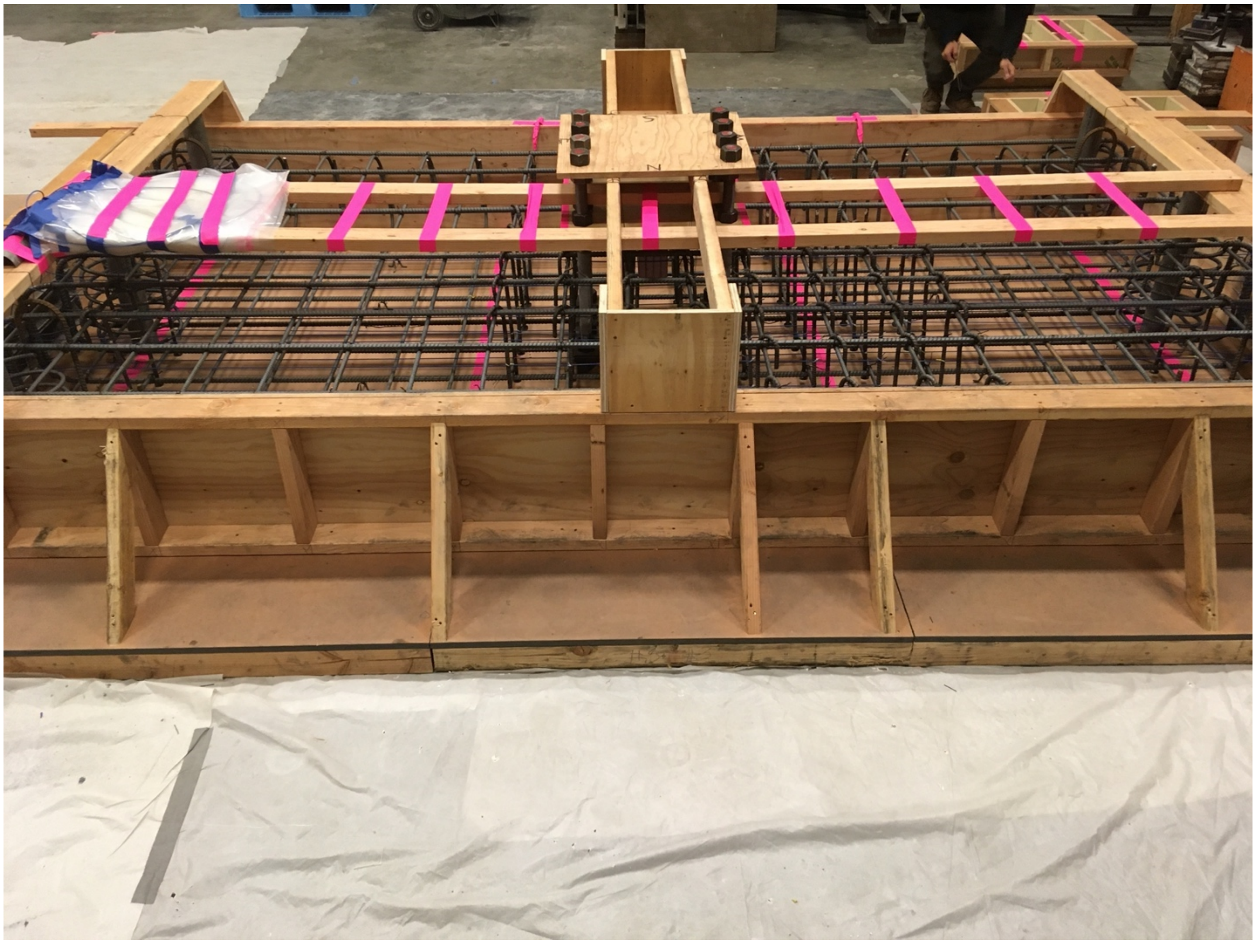

Figure F- 24. Form before casting concrete

Figure F- 25. Form before casting concrete

Figure F- 26. Form before casting concrete

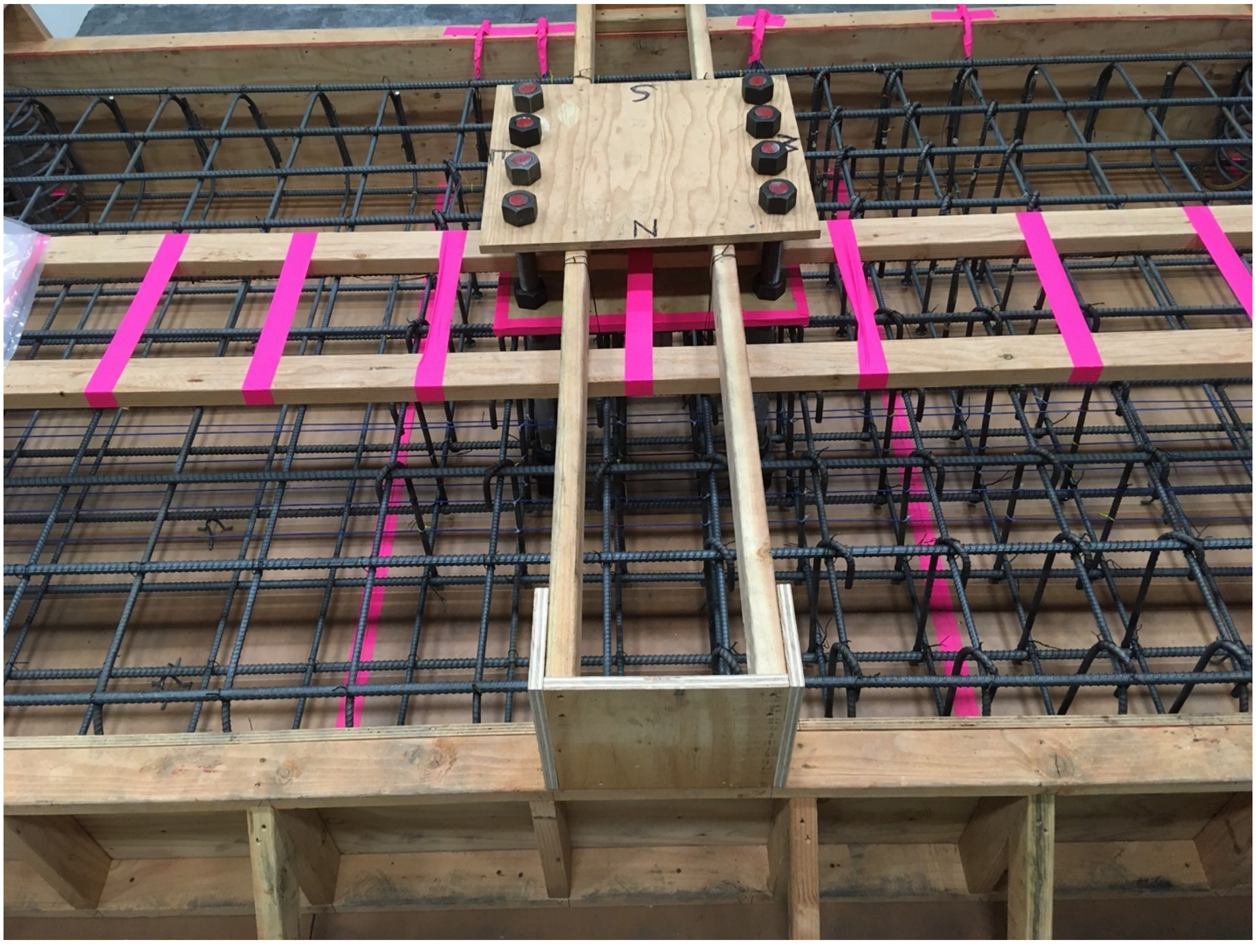

Figure F- 27. Form before casting concrete

Figure F- 28. Form before casting concrete

Figure F- 29. Form before casting concrete

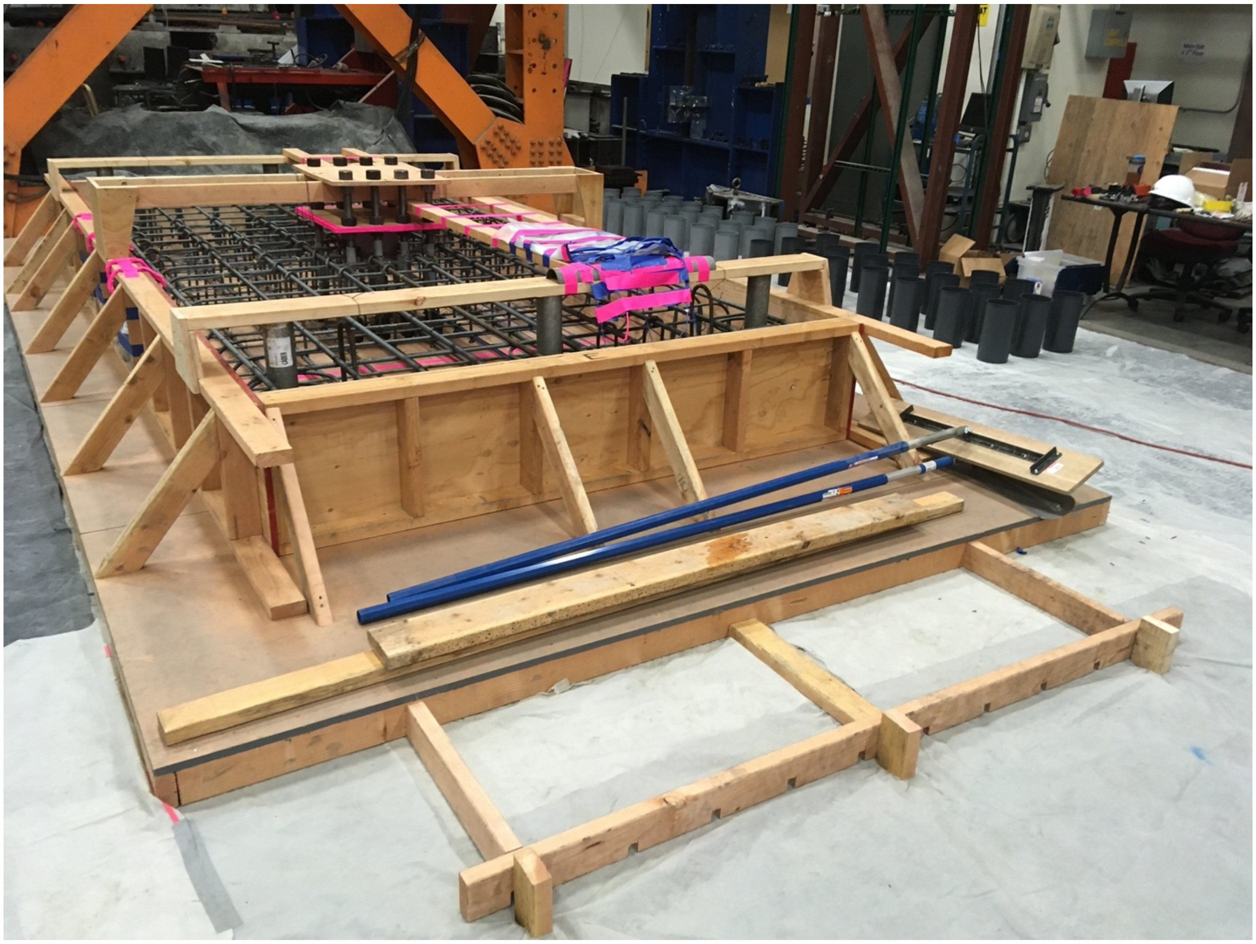

Figure F- 30. Form before casting concrete

Figure F- 31. Form before casting concrete

Figure F- 32. Concrete slump test

Figure F- 33. Casting concrete

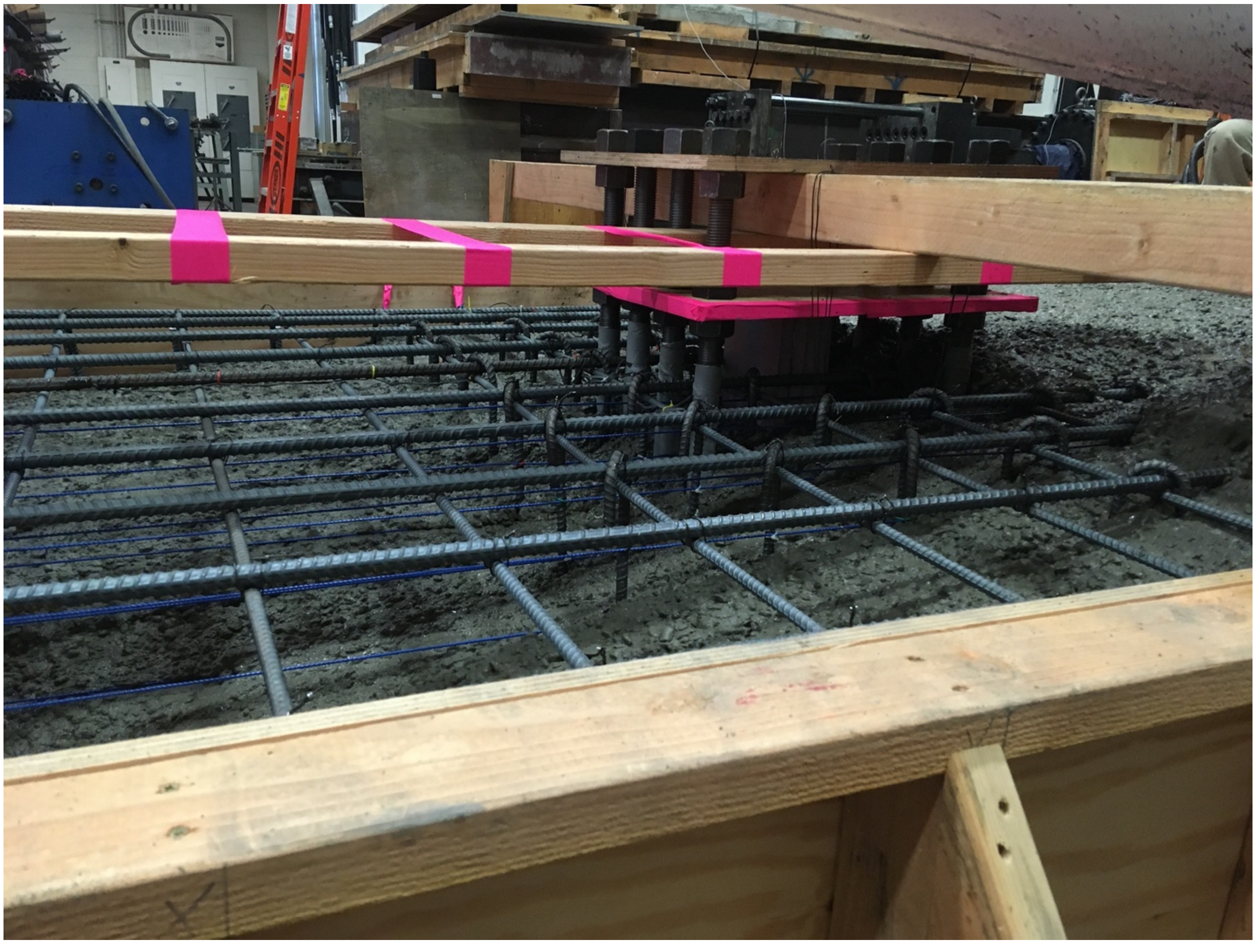

Figure F- 34. Casting concrete

Figure F- 35. Casting concrete

Figure F- 36. Casting concrete

Figure F- 37. Casting concrete

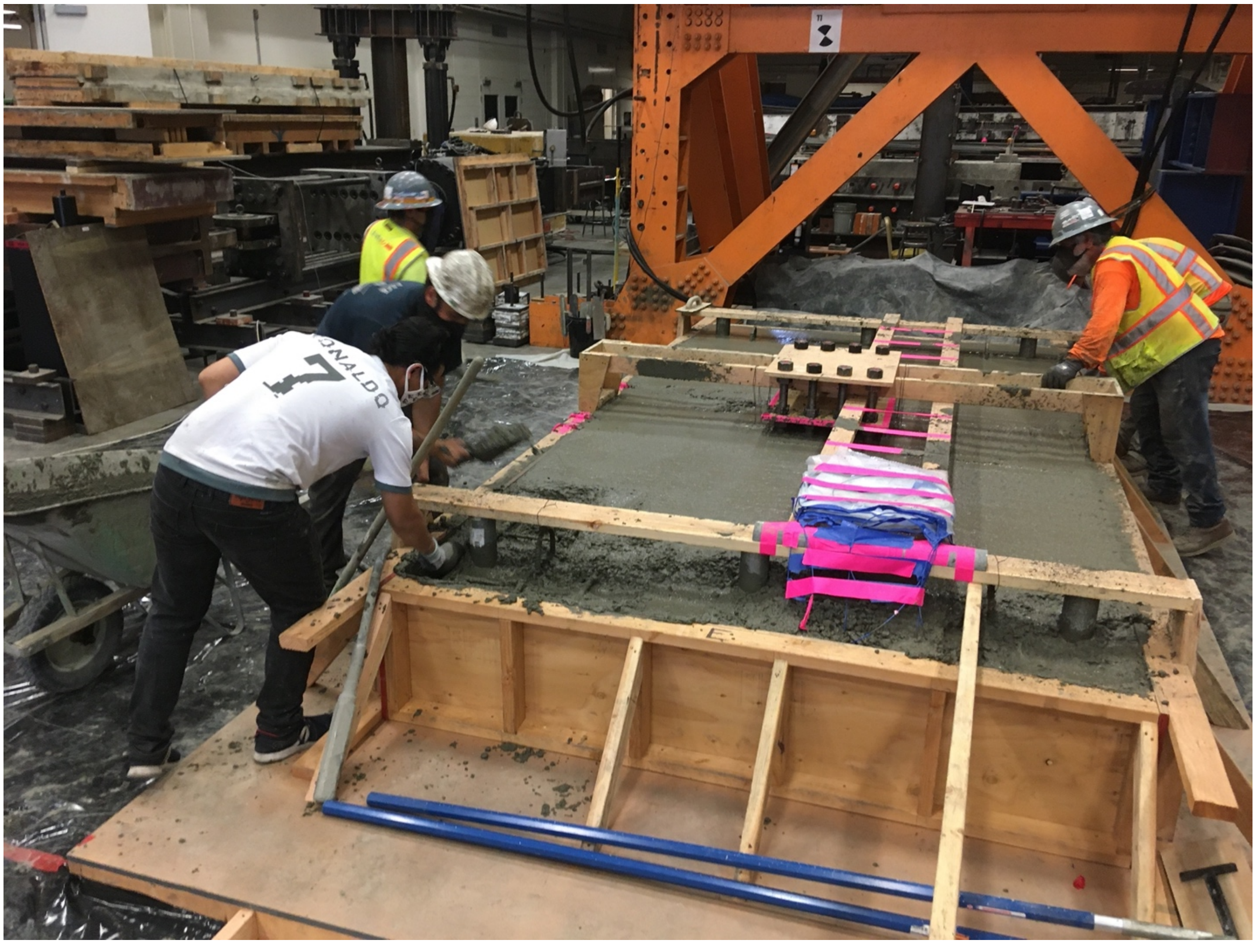

Figure F- 38. Casting concrete

Figure F- 39. Casting concrete

Figure F- 40. Casting concrete

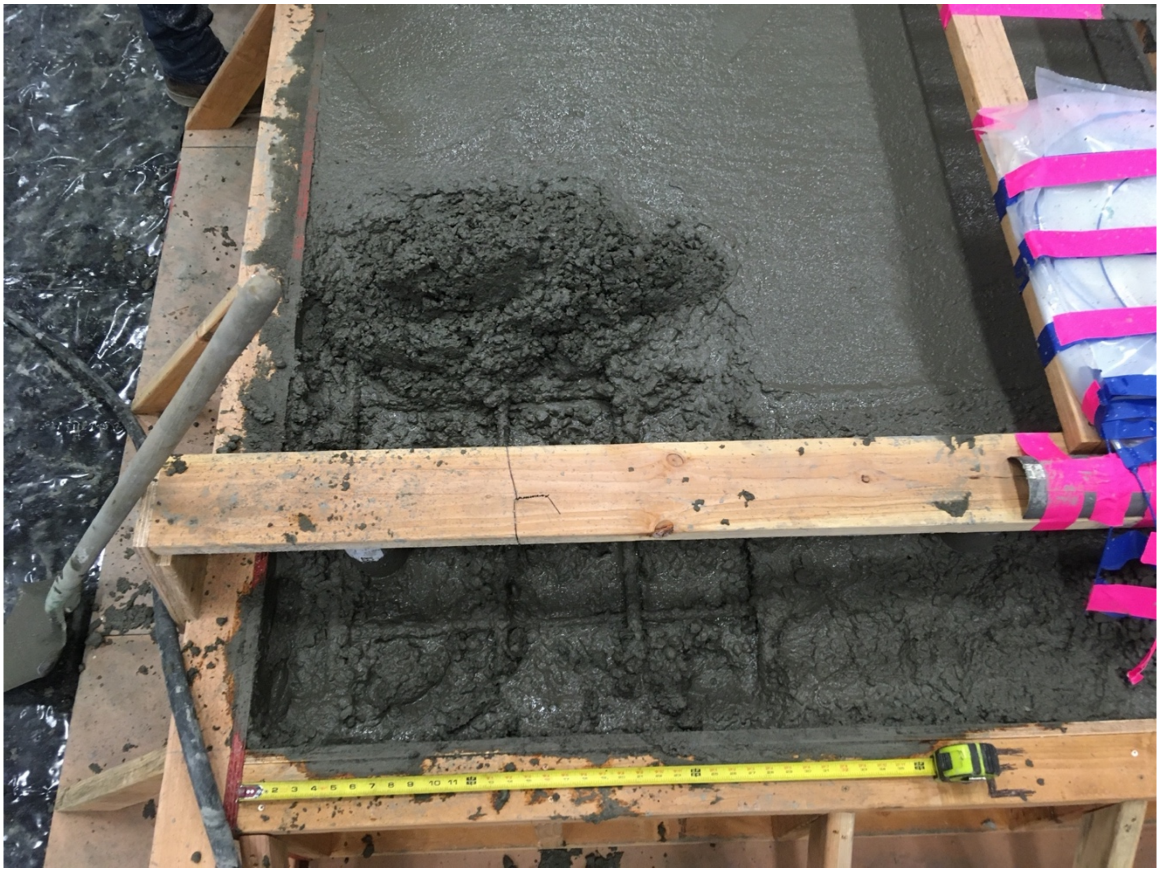

Figure F- 41. Casting concrete

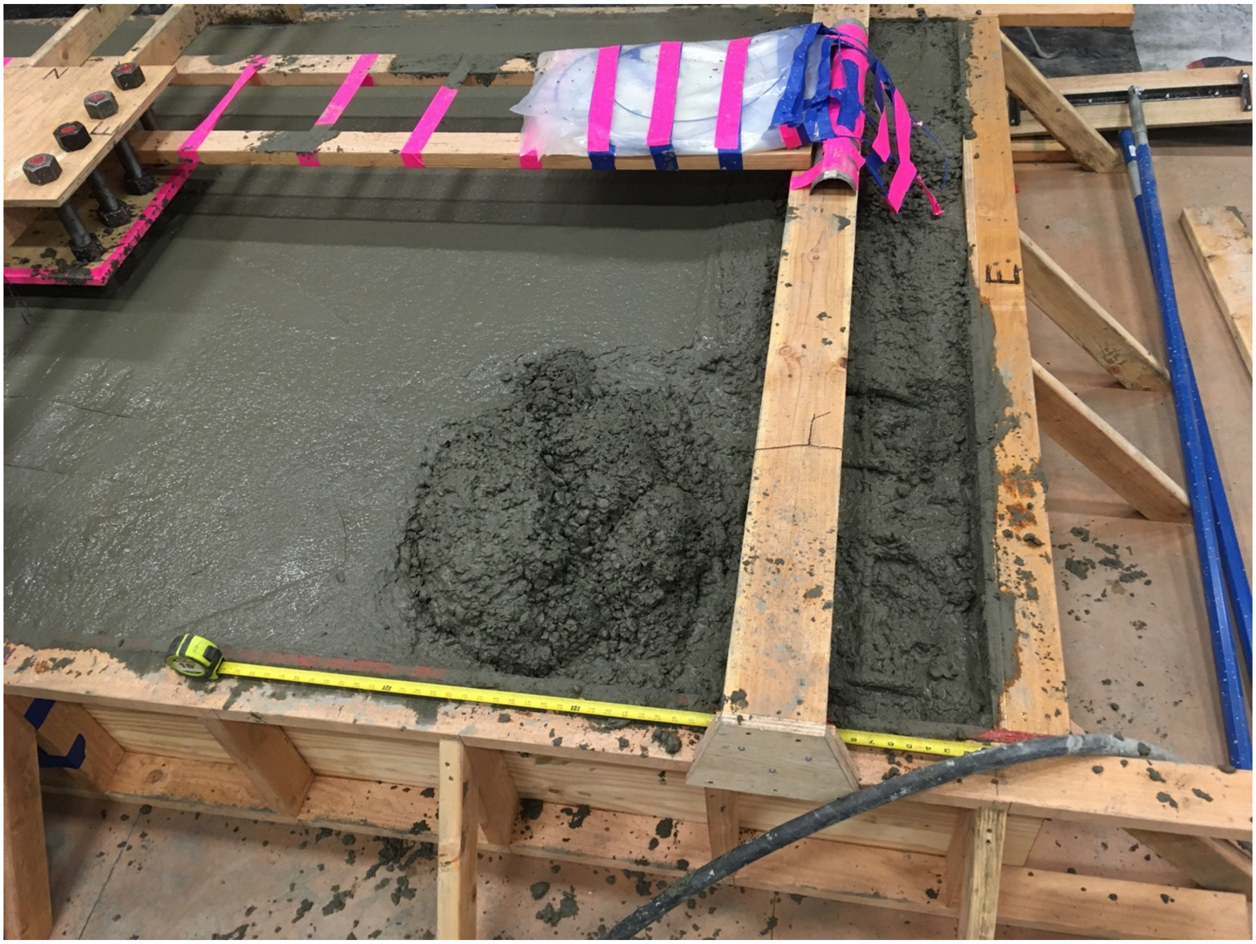

Figure F- 42. Casting concrete

Figure F- 43. Casting concrete

Figure F- 44. Casting concrete

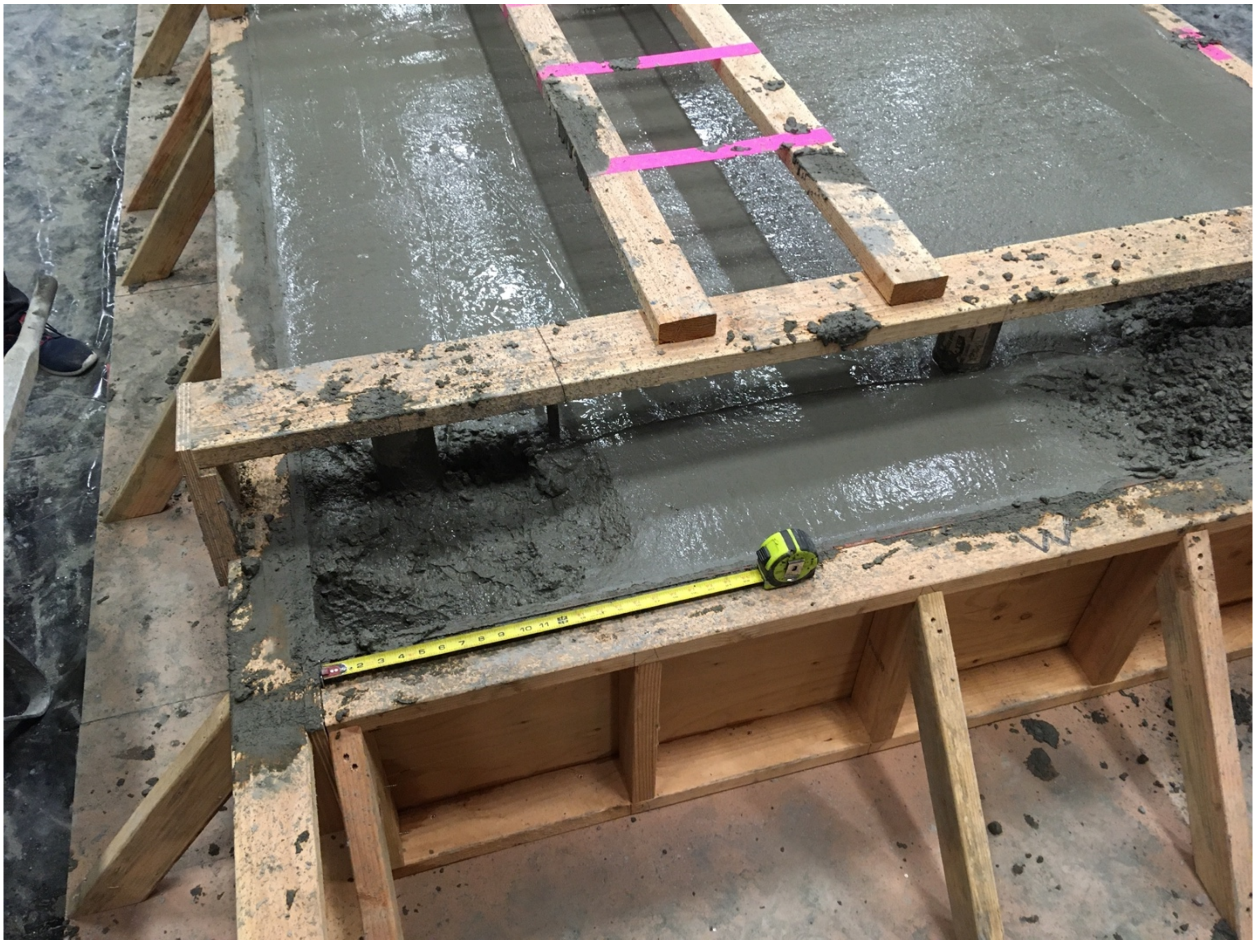

Figure F- 45. Casting concrete

Figure F- 46. Casting concrete

Figure F- 47. Casting concrete

Figure F- 48. Curing specimen with burlap

Figure F- 49. Curing specimen and cylinders with burlap and plastic

Figure F- 50. Removing plywood anchor molds

Figure F- 51. Fracture energy beams in fog room

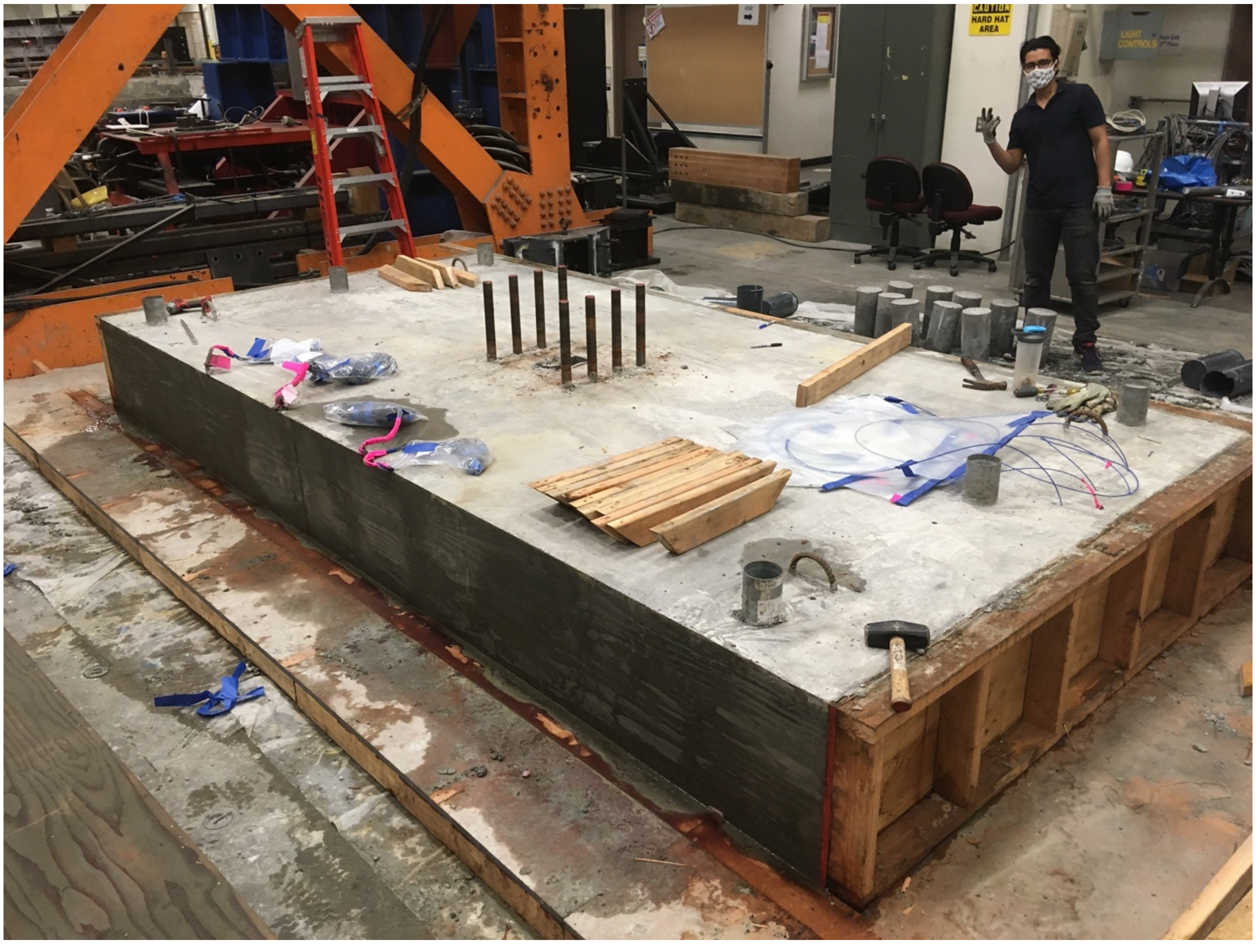

Figure F- 52. Removing formwork

Figure F- 53. Moving specimen with crane

Figure F- 54. Moving specimen with crane

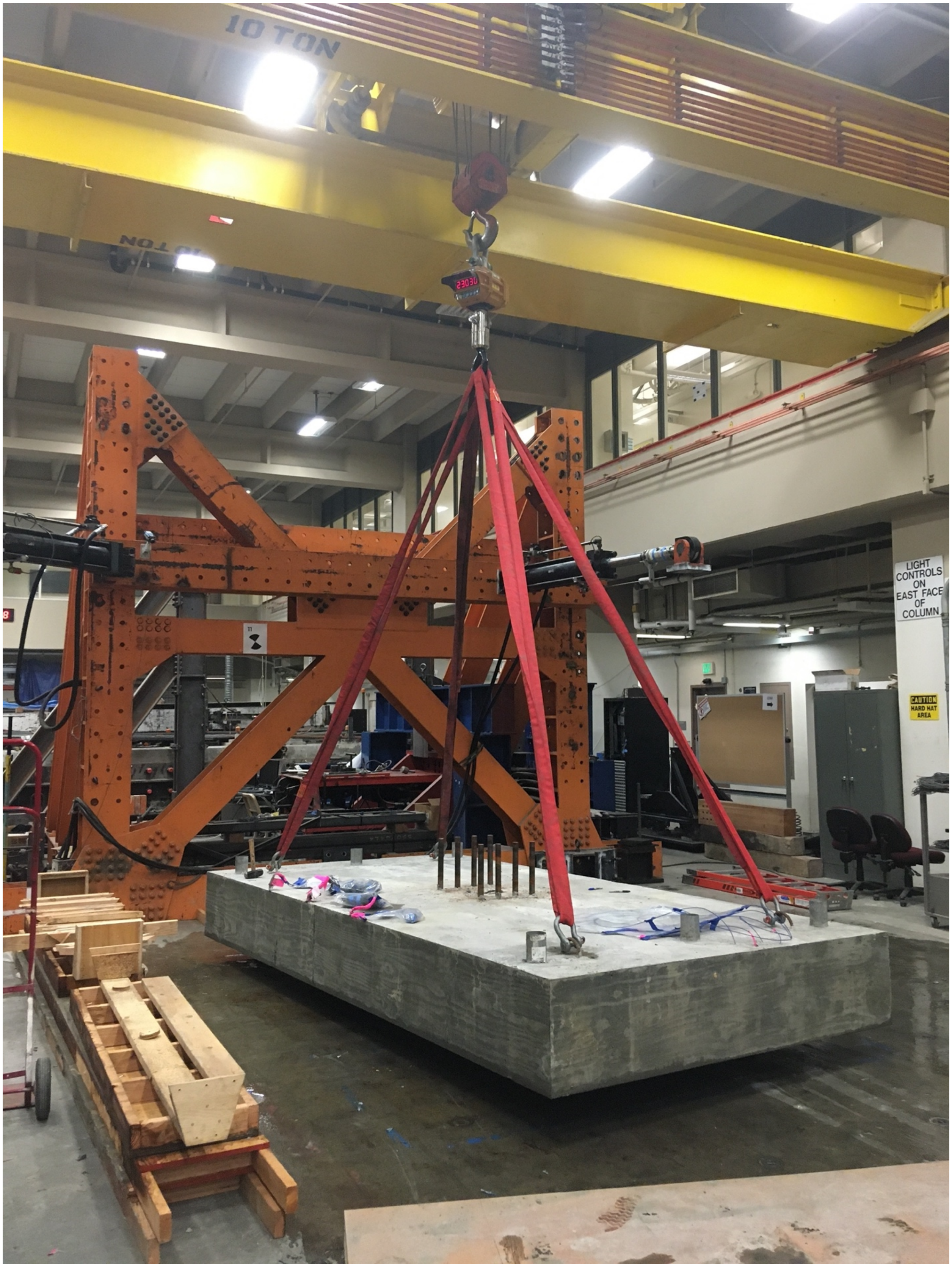

Figure F- 55. Moving specimen with crane

Figure F- 56. Moving specimen with crane

Figure F- 57. Specimen placed on concrete supports

Figure F- 58. Specimen placed on concrete supports

Figure F- 59. Fracture energy beams in lime pool in fog room

Figure F- 60. Hole left by foam mold for shear lug

Figure F- 61. Column hydrostoned to specimen

Figure F- 62. Column hydrostoned to specimen

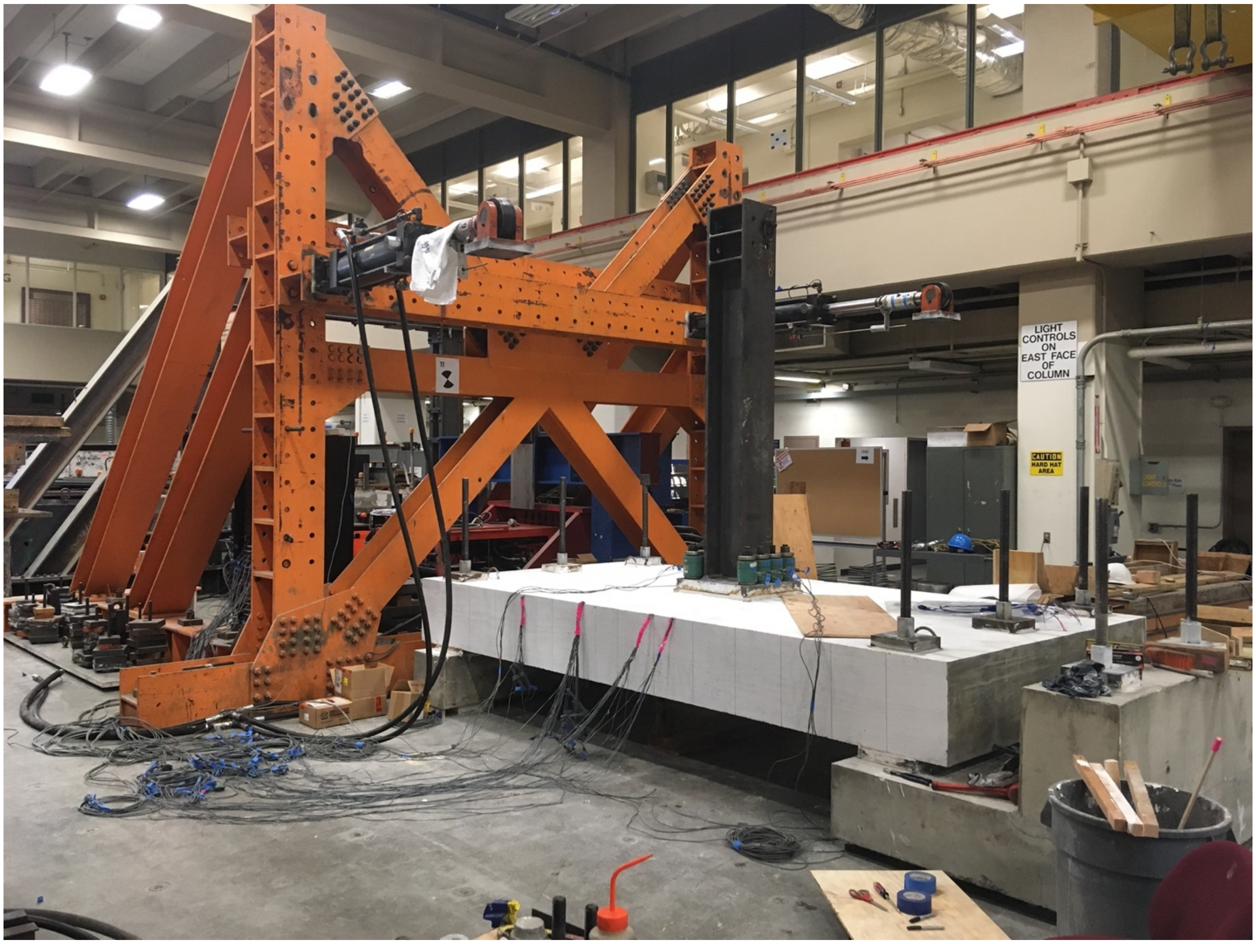

Figure F- 63. Column hydrostoned to specimen and anchor load cells in place

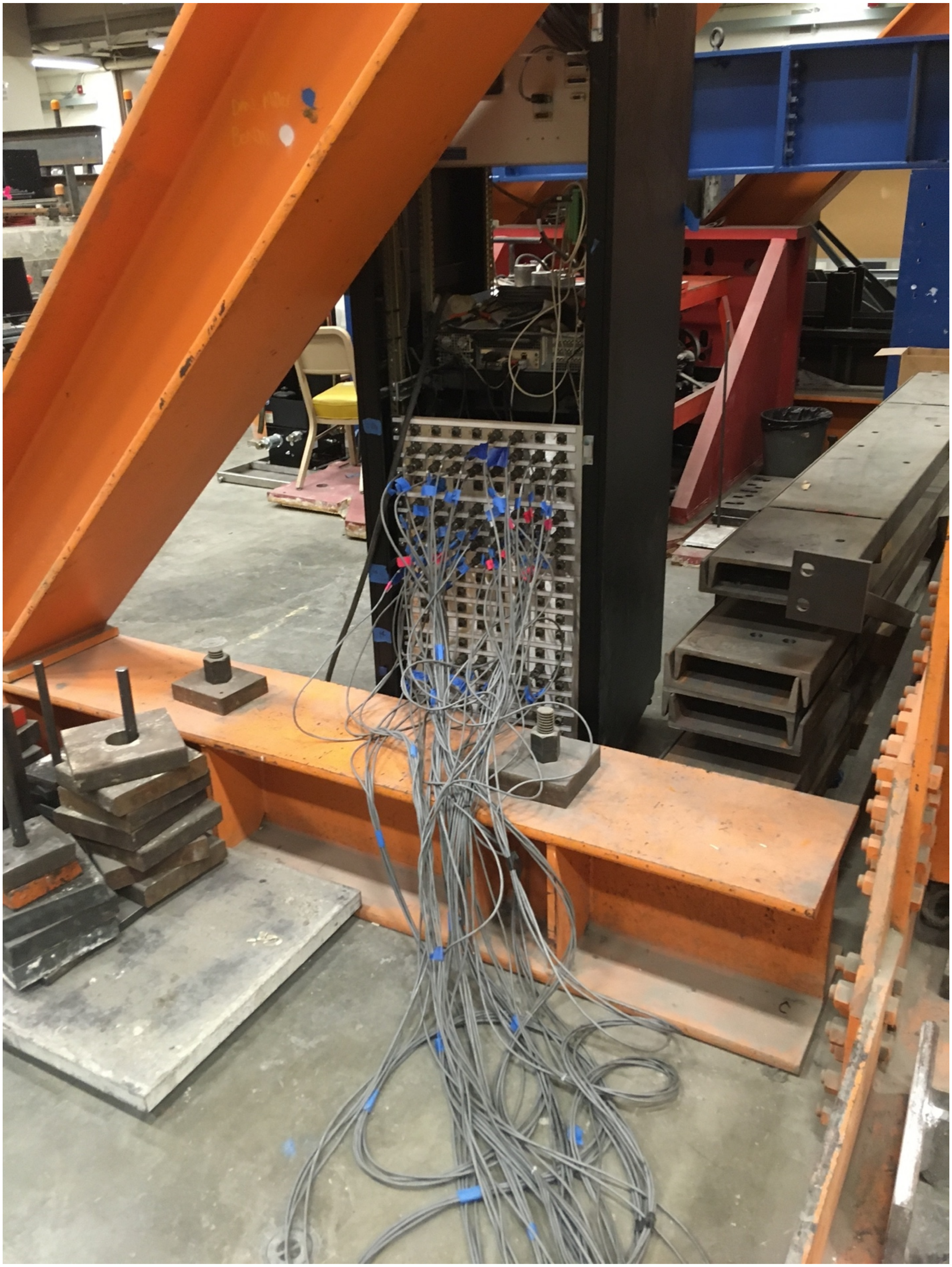

Figure F- 64. Connecting instruments to data acquisition system

Figure F- 65. Modification to column-actuator attachment

Figure F- 66. Modification to column-actuator attachment

Figure F- 67. Modification to column-actuator attachment

Figure F- 68. Modification to column-actuator attachment

Figure F- 69. Instrumentation frame to attach linear potentiometers to measure vertical displacements

Figure F- 70. Camera placement

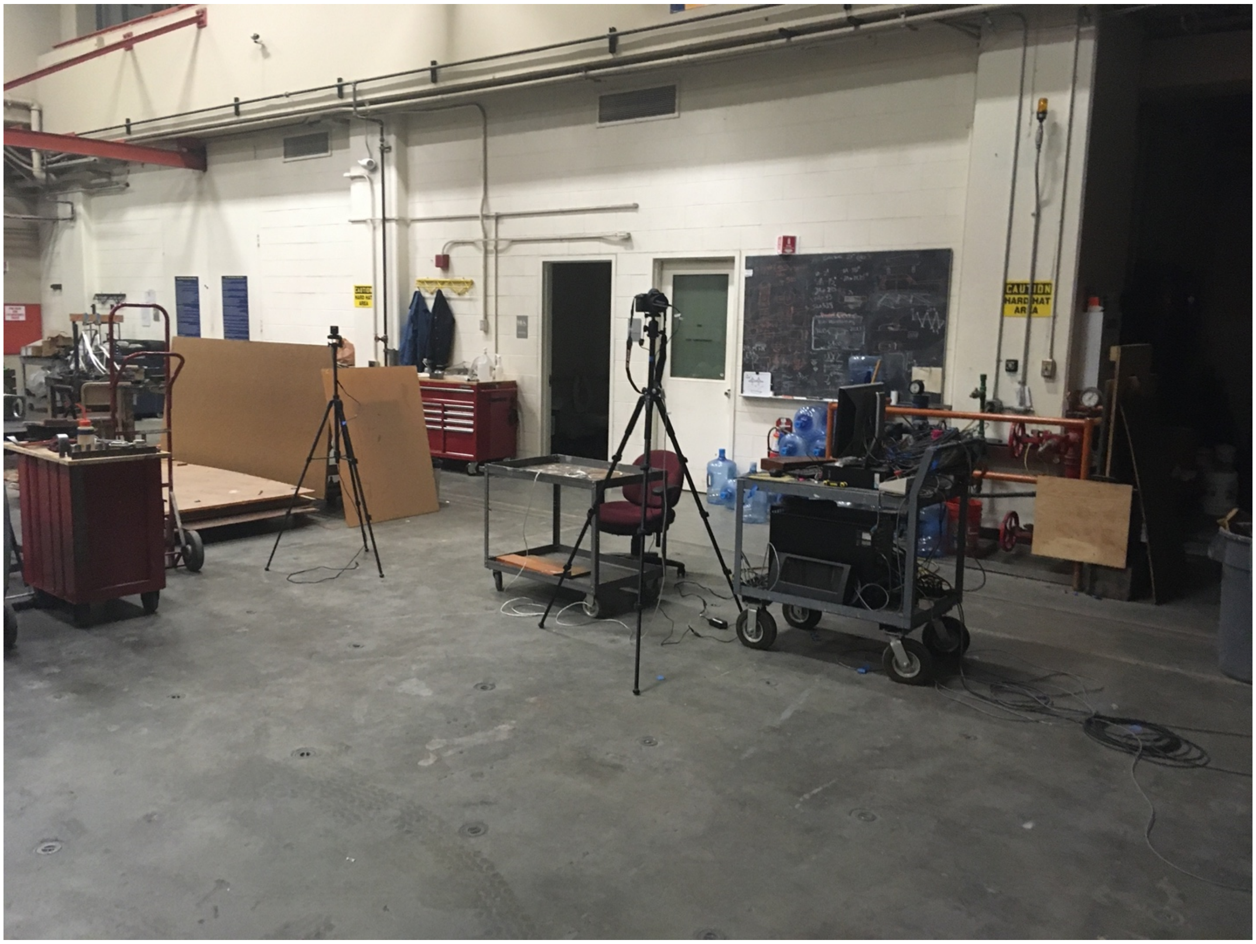

Figure F- 71. Camera placement

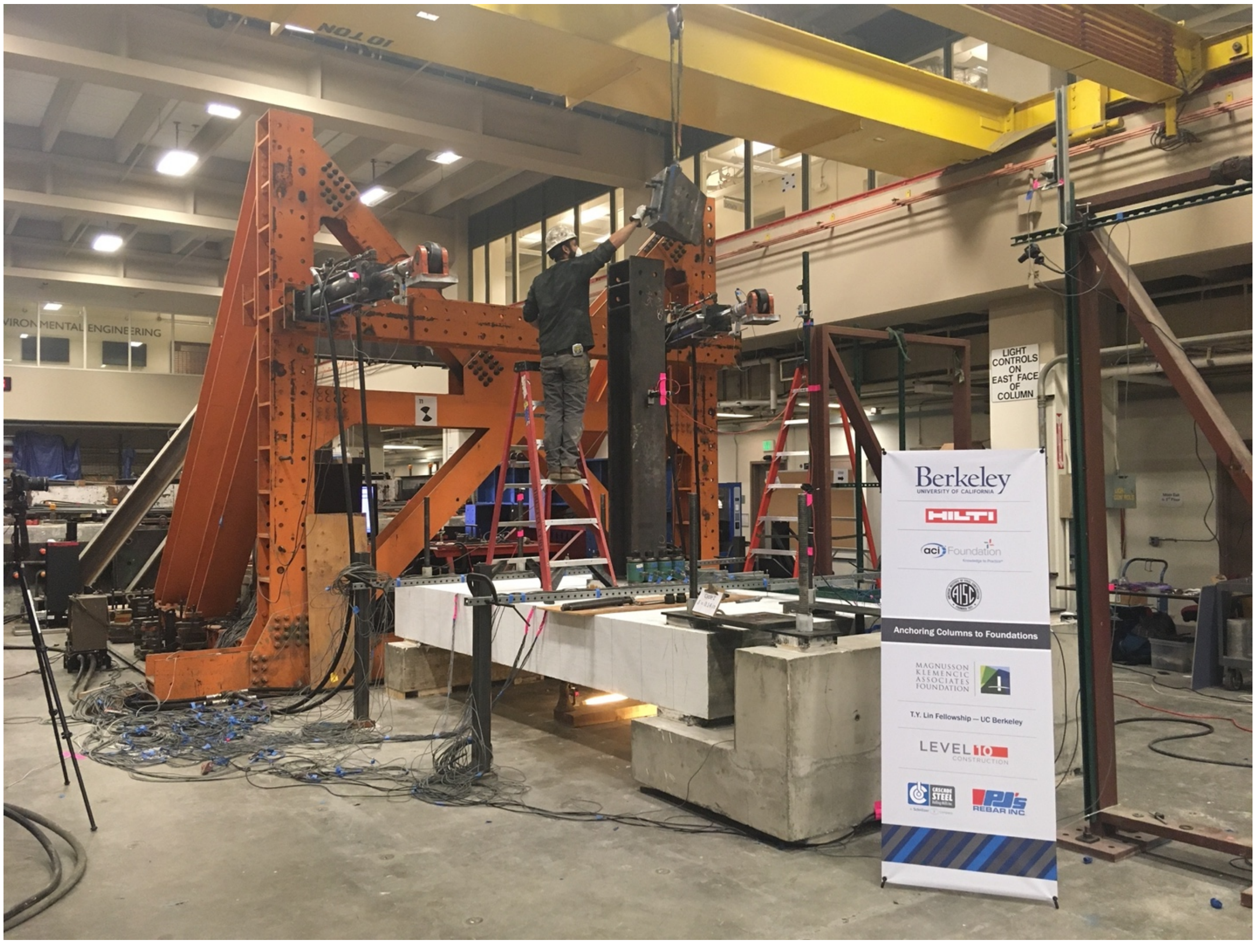

Figure F- 72. Attaching actuators on test day

Figure F- 73. Base plate during test

Figure F- 74. Documenting cracks during test

Figure F- 75. Slab plan view after removing column

Figure F- 76. Yielding of washers on top of anchor load cells post test

Figure F- 77. Cutting cross sections

Figure F- 78. Cutting cross sections

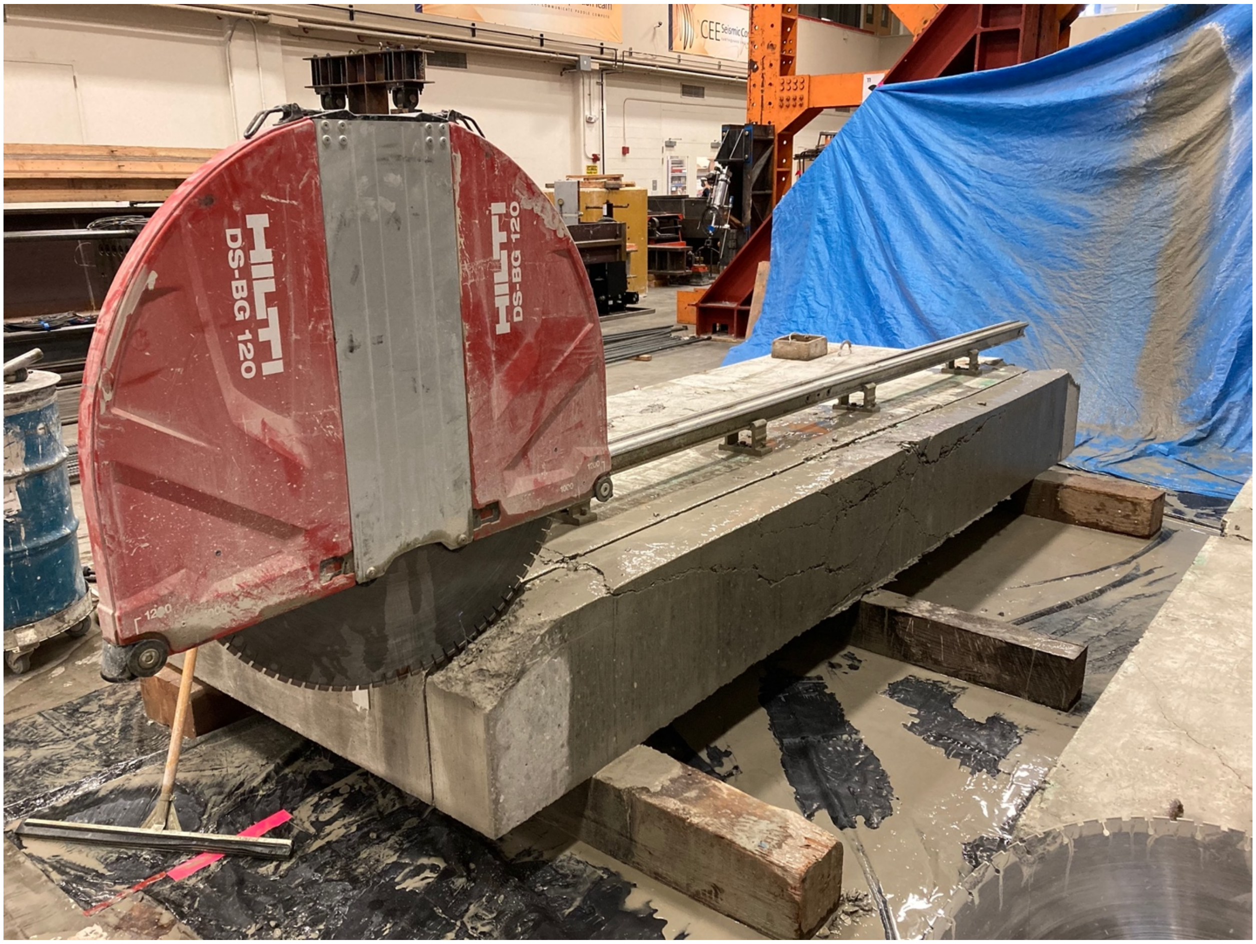

Figure F- 79. Cutting cross sections

Figure F- 80. Cutting cross sections

Figure F- 81. Cutting cross sections

Figure F- 82. Cutting cross sections

Figure F- 83. Testing shear reinfrocing bars with 2” gage extensometer

Figure F- 84. Fracture energy tests

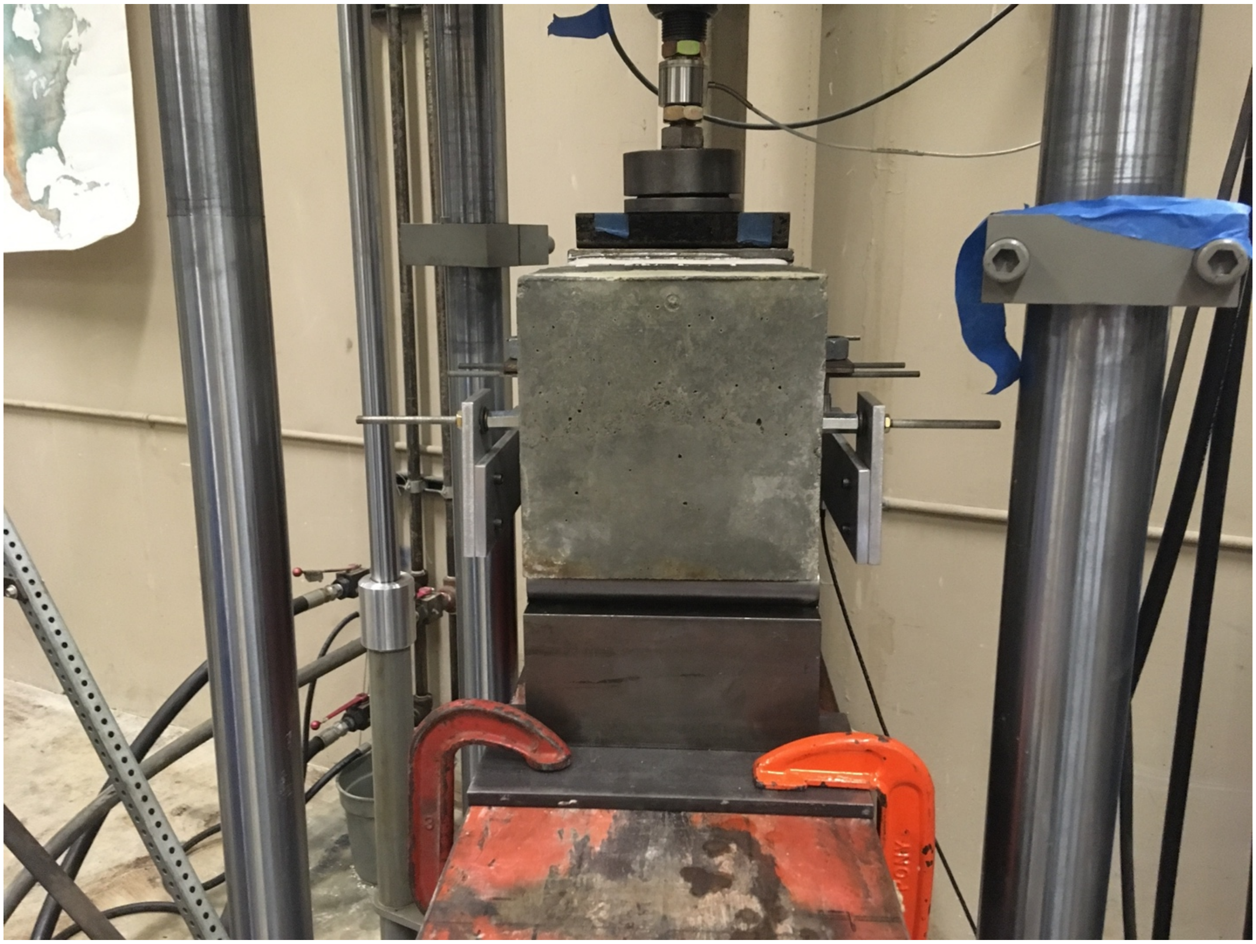

Figure F- 85. Fracture energy tests

Figure F- 86. Fracture energy tests

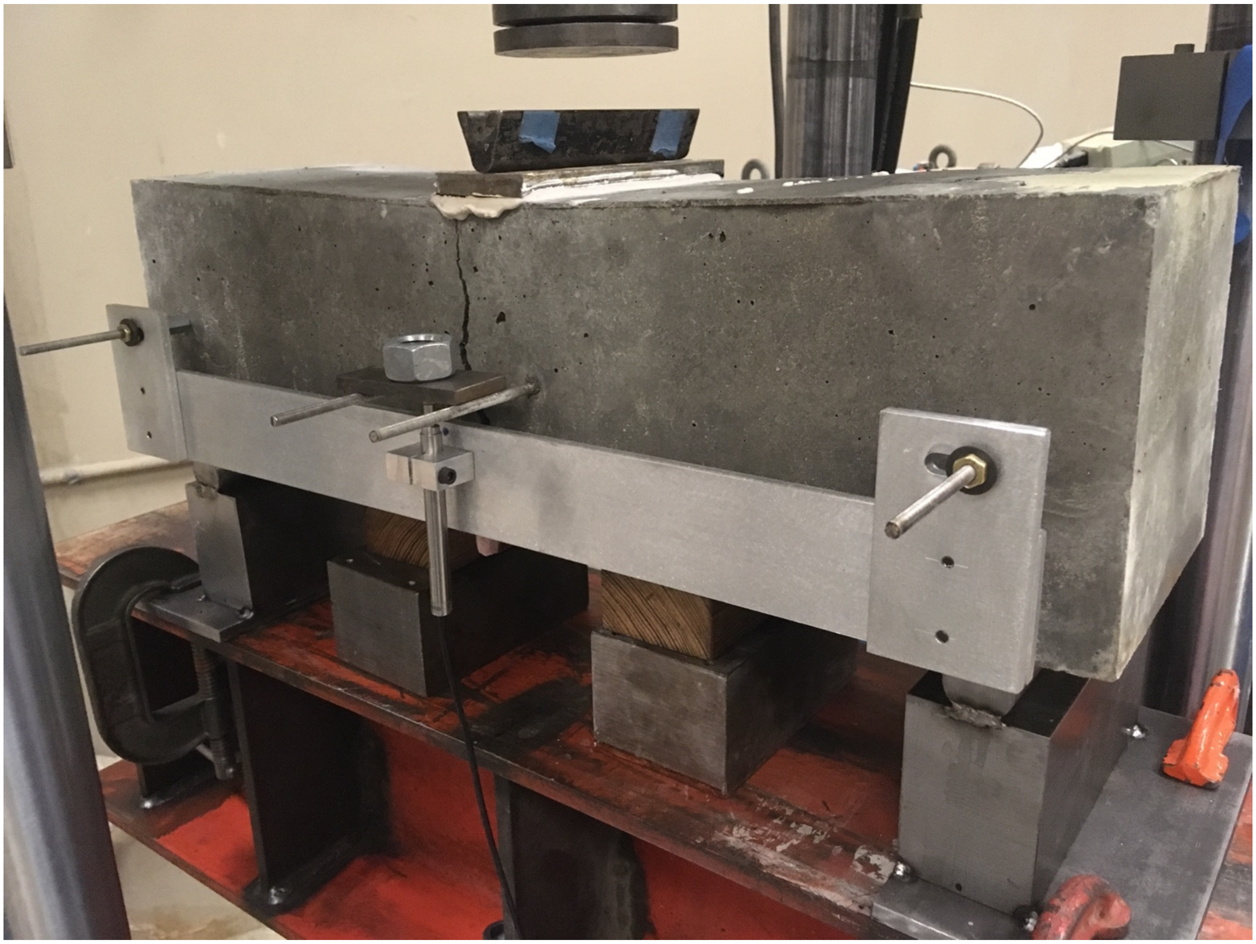

Figure F- 87. Fracture energy tests

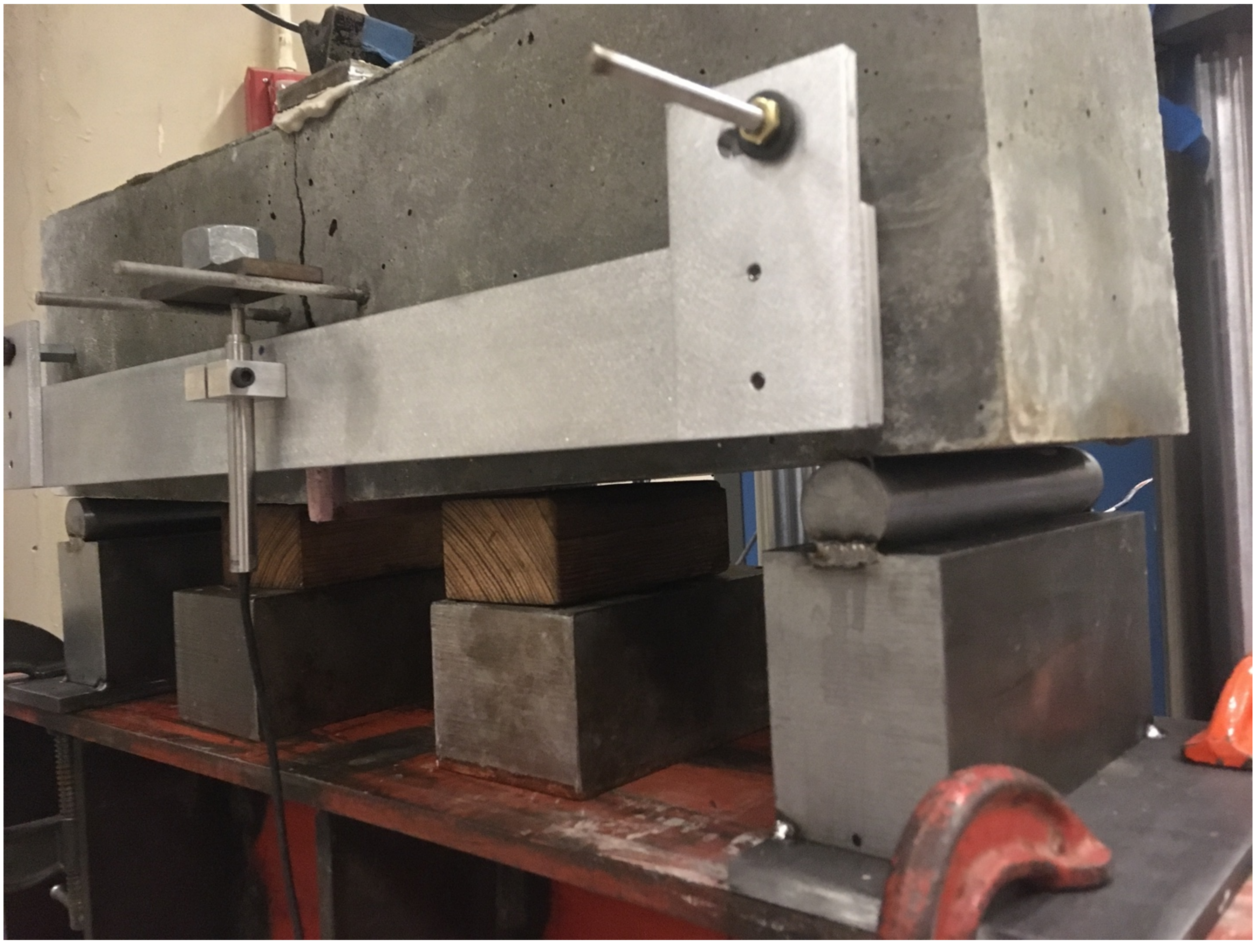

Figure F- 88. Fracture energy tests

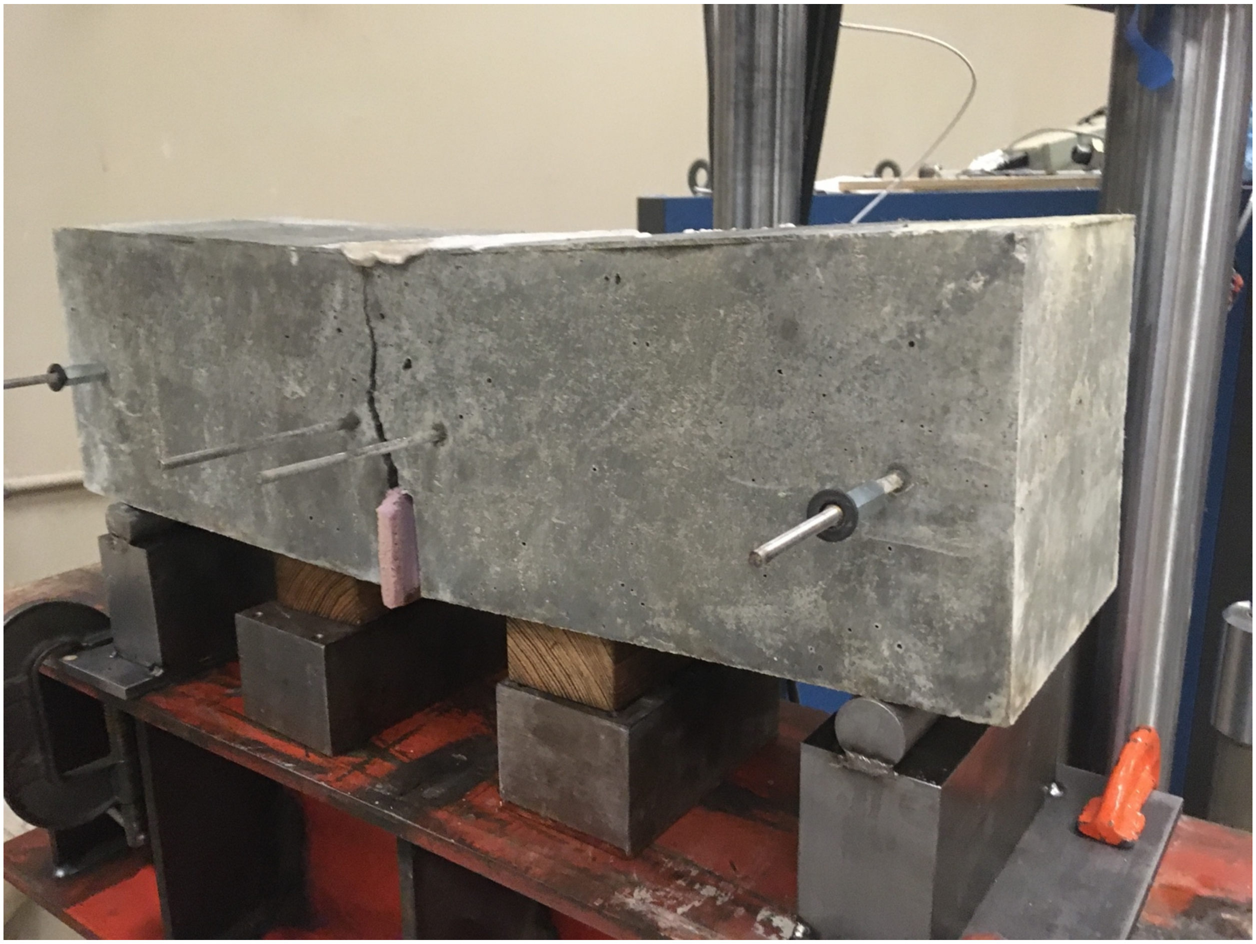

Figure F- 89. Fracture energy tests

Figure F- 90. Fracture energy tests

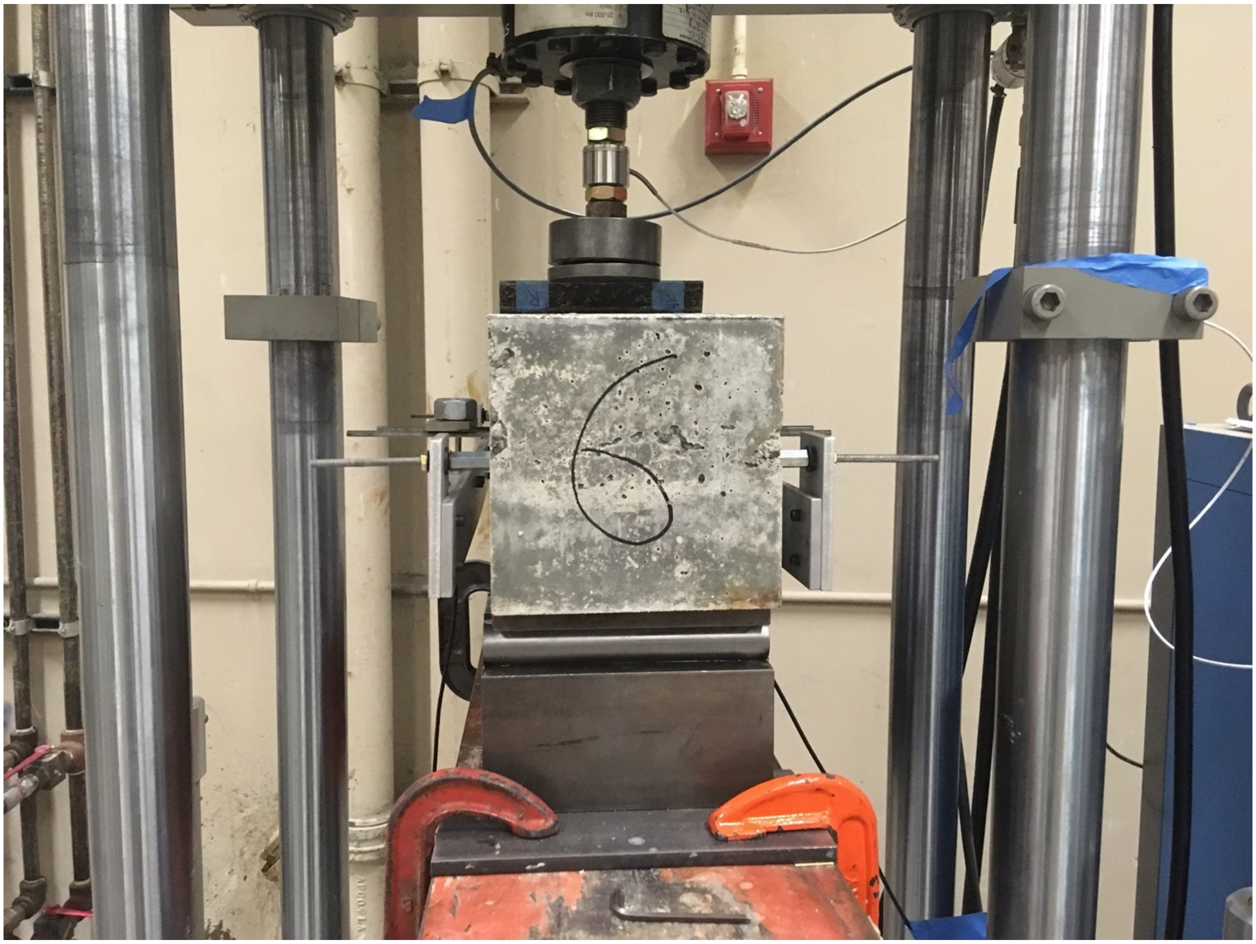

Figure F- 91. Fracture energy tests


Figure F- 92. Fracture energy tests